

AD-A204 353

④

CR-88.013

September 1988

An Investigation Conducted By

SYNTEK Engineering & Computer Systems, Inc.

Marietta, GA 30067

Sponsored by

Naval Facilities Engineering Command

NCEL

Contract Report

Determination of the Best Ground Penetrating Radar Source Signal Type for the Accurate Location of Underground Utilities

ABSTRACT This investigation was to determine the best ground-penetrating radar (GPR) source signal applicable for locating underground utilities and other construction obstacles. Four types of GPR systems were tested: two time-domain short-pulse radars, one swept frequency FM-CW system, and one stepped FM system. The performance of the systems were compared by examining their time-domain or simulated time-domain responses. The detection problem was modeled analytically to evaluate the expected performance of the GPR systems. Tests were conducted in a scale model tank with two soils of differing dielectric properties. Specially designed shielded triangular-sheet dipole antennas were used for comparison tests. It is concluded that a frequency-domain GPR based on a stepped frequency design provides the highest performance capabilities. The general performance of a full-scale version of such a GPR was demonstrated in an outdoor test field containing buried plastic and metal pipes.

**BEST
AVAILABLE COPY**

DTIC
SELECTED
DEC 06 1988
S E D

NAVAL CIVIL ENGINEERING LABORATORY, PORT HUENEME, CALIFORNIA 93043

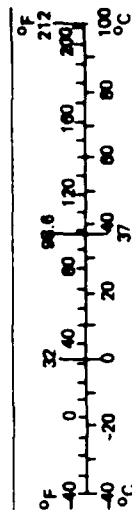
Approved for public release; distribution is unlimited.

88 12 5 077

METRIC CONVERSION FACTORS

Approximate Conversions to Metric Measures				Approximate Conversions from Metric Measures			
Symbol	When You Know	Multiply by	To Find	Symbol	When You Know	Multiply by	To Find
LENGTH				LENGTH			
in	inches	*2.5	centimeters	mm	millimeters	0.04	inches
ft	feet	30	centimeters	cm	centimeters	0.4	inches
yd	yards	0.9	meters	m	meters	3.3	feet
mi	miles	1.6	kilometers	km	kilometers	1.1	yards
AREA				AREA			
in ²	square inches	6.5	square centimeters	cm ²	square centimeters	0.16	square inches
ft ²	square feet	0.09	square meters	m ²	square meters	1.2	square yards
yd ²	square yards	0.8	square meters	km ²	square kilometers	0.4	square miles
mi ²	square miles	2.6	square kilometers	ha	hectares (10,000 m ²)	2.5	acres
MASS (weight)				MASS (weight)			
oz	ounces	28	grams	g	grams	0.035	ounces
lb	pounds	0.45	kilograms	kg	kilograms	2.2	pounds
	short tons	0.9	tonnes	t	tonnes (1,000 kg)	1.1	short tons
	(2,000 lb)						
VOLUME				VOLUME			
tsp	teaspoons	5	milliliters	ml	milliliters	0.03	fluid ounces
Tbsp	tablespoons	15	milliliters	l	liters	2.1	pints
fl oz	fluid ounces	30	milliliters	l	liters	1.06	quarts
c	cups	0.24	liters	l	liters	0.26	gallons
pt	pints	0.47	liters	m ³	cubic meters	35	cubic feet
qt	quarts	0.95	liters	m ³	cubic meters	1.3	cubic yards
gal	gallons	3.8	liters				
ft ³	cubic feet	0.03	cubic meters	°C	Celsius temperature	9/5 (then add 32)	Fahrenheit temperature
yd ³	cubic yards	0.76	cubic meters				
TEMPERATURE (exact)				TEMPERATURE (exact)			
°F	Fahrenheit temperature	5/9 (after subtracting 32)	Celsius temperature	°C	Celsius temperature	9/5 (then add 32)	Fahrenheit temperature

*1 in = 2.54 (exactly). For other exact conversions and more detailed tables, see NBS Misc. Publ. 286, Units of Weights and Measures, Price \$2.25, SD Catalog No. C13.10.286.



DISCLAIMER NOTICE

**THIS DOCUMENT IS BEST QUALITY
PRACTICABLE. THE COPY FURNISHED
TO DTIC CONTAINED A SIGNIFICANT
NUMBER OF PAGES WHICH DO NOT
REPRODUCE LEGIBLY.**

Unclassified

SECURITY CLASSIFICATION OF THIS PAGE (When Data Entered)

REPORT DOCUMENTATION PAGE		READ INSTRUCTIONS BEFORE COMPLETING FORM
1. REPORT NUMBER CR 88.013	2. GOVT ACCESSION NO.	3. RECIPIENT'S CATALOG NUMBER
4. TITLE (and Subtitle) Determination of the Best Ground Penetrating Radar Source Signal Type for the Accurate Location of Underground Utilities		5. TYPE OF REPORT & PERIOD COVERED Final Dec 1986 - Jun 1988
6. AUTHOR(s) W.E. Thain		7. CONTRACT OR GRANT NUMBER(s) N62474-87-C-3056
8. PERFORMING ORGANIZATION NAME AND ADDRESS SYNTEK Engrg & Computer Systems, Inc. 1351-K Dividend Drive Marietta, GA 30067		9. PROGRAM ELEMENT PROJECT TASK AREA & WORK UNIT NUMBERS YM33F60-001-08-04-010
10. CONTROLLING OFFICE NAME AND ADDRESS Naval Civil Engineering Laboratory Port Hueneme, CA 93043-5003		11. REPORT DATE Sep 1988
12. MONITORING AGENCY NAME & ADDRESS (if different from Controlling Office) Naval Facilities Engineering Command 200 Stovall Street Alexandria, VA 22332-2300		13. NUMBER OF PAGES 150
		14. SECURITY CLASS (of this report) Unclassified
15. DISTRIBUTION STATEMENT (of this Report) Approved for public release; distribution is unlimited.		16. DECLASSIFICATION/DOWNGRADING SCHEDULE
17. DISTRIBUTION STATEMENT (of the abstract entered in Block 20, if different from Report)		
18. SUPPLEMENTARY NOTES		
19. KEY WORDS (Continue on reverse side if necessary and identify by block number) ground penetrating radar, GPR, source signal, GPR design, underground surveys, utility lines, obstacles		
20. ABSTRACT (Continue on reverse side if necessary and identify by block number) This investigation was to determine the best ground-penetrating radar (GPR) source signal applicable for locating underground utilities and other construction obstacles. Four types of GPR systems were tested: two time-domain short-pulse radars, one swept frequency FM-CW system, and one stepped-FM system. The		

DD FORM 1473 EDITION OF 1 NOV 85 IS OBSOLETE

Unclassified

SECURITY CLASSIFICATION OF THIS PAGE (When Data Entered)

Unclassified

SECURITY CLASSIFICATION OF THIS PAGE (When Data Entered)

performance of the systems were compared by examining their time-domain or simulated time-domain responses. The detection problem was modeled analytically to evaluate the expected performance of the GPR systems. Tests were conducted in a scale-model tank with two soils of differing dielectric properties. Specially designed shielded triangular-sheet dipole antennas were used for comparison tests. It is concluded that a frequency-domain GPR based on a stepped-frequency design provides the highest performance capabilities. The general performance of a full-scale version of such a GPR was demonstrated in an outdoor test field containing buried plastic and metal pipes.

Accession For	
NTIS GRA&I	<input checked="" type="checkbox"/>
DTIC TAB	<input checked="" type="checkbox"/>
Unannounced	<input type="checkbox"/>
Justification	
By	
Distribution/	
Availability Codes	
Dist	Avail and/or Special
A-1	



Unclassified

SECURITY CLASSIFICATION OF THIS PAGE (When Data Entered)

TABLE OF CONTENTS

SECTION 1:	INTRODUCTION	1
SECTION 2:	SUMMARY OF WORK PERFORMED	3
SECTION 3:	DESCRIPTION OF THE GROUND PENETRATION PROBLEM ..	7
3.1	SOIL DIELECTRIC PROPERTIES	7
3.1.1	ELECTROMAGNETIC PROPAGATION IN SOIL	8
3.1.2	DETERMINING SOIL PARAMETERS	11
3.1.3	EFFECTS OF SOIL PARAMETERS ON GPR SYSTEM PERFORMANCE	15
3.2	THE TARGET IDENTIFICATION PROBLEM	17
3.3	DESIGNING THE GPR SYSTEM	19
3.3.1	GPR BANDWIDTH AND RESOLUTION	19
3.3.2	GPR TRANSMITTER POWER CONSIDERATIONS	22
3.3.3	GPR ANTENNA CHARACTERISTICS	23
3.3.4	REDUCING INTERNAL CLUTTER IN A GPR SYSTEM	25
SECTION 4:	MODELING THE PIPE DETECTION PROBLEM	26
4.1	SUBSURFACE TARGET DETECTION MODEL	26
4.2	EXAMPLE CALCULATION USING THE NBS MODEL	29
SECTION 5:	DESIGN OF THE SCALE-MODEL TEST TANK	34
5.1	DESCRIPTION OF THE GPR SCALE-MODEL CHARACTERISTICS ..	34
5.2	THE LIQUID-DIELECTRIC SOIL MODEL	35
5.3	THE SOIL-DIELECTRIC MODEL	37
SECTION 6:	DESCRIPTION OF THE GPR SYSTEMS TESTED	41
6.1	THE GAR SHORT-PULSE RADAR SYSTEM	41
6.2	THE GSSI SHORT-PULSE RADAR SYSTEM	46
6.3	THE FREQUENCY-DOMAIN GPR SYSTEMS USING THE HP 8510 NETWORK ANALYZER	47
6.3.1	HP 8510 NETWORK ANALYZER CAPABILITIES	49
6.3.1.1	SCATTERING PARAMETER MEASUREMENTS WITH THE HP 8510	49
6.3.1.2	HP 8510 TIME-DOMAIN MEASUREMENT MODE	52
6.3.1.2.1	TIME-DOMAIN PULSE SYNTHESIS WITH WEIGHTING FUNCTIONS	52

TABLE OF CONTENTS

6.3.1.2.2	EFFECT OF THE NUMBER OF FREQUENCY MEASUREMENT POINTS SELECTED	56
6.3.1.3	DIFFERENCES BETWEEN THE HP 8510 SWEPT- FREQUENCY AND STEPPED-FREQUENCY MEASUREMENT MODES	57
6.3.2	SUMMARY OF NETWORK ANALYZER CONFIGURATIONS AND SPECIFICATIONS FOR SOIL-MODEL TANK MEASUREMENTS	58
6.4	ANTENNAS USED FOR THE GPR SOIL-MODEL TESTS	59
6.4.1	TEM HORN ANTENNA	59
6.4.2	TRIANGULAR-SHEET DIPOLE ANTENNA	60
6.4.3	QUALITATIVE COMPARISONS BETWEEN THE TEM HORN ANTENNAS AND THE TRIANGULAR-SHEET BOW-TIE ANTENNAS	61
SECTION 7: DESCRIPTION OF THE MEASUREMENTS USING THE CANDIDATE GPR SYSTEMS		64
7.1	DESCRIPTION OF THE PHASE 1 AND PHASE 2 SCALE-MODEL GPR MEASUREMENTS USING THE SOIL-MODEL TANK	64
7.2	FULL-SCALE GPR FIELD MEASUREMENTS	71
SECTION 8: MEASUREMENT RESULTS		75
8.1	PHASE 1 SCALE-MODEL GPR MEASUREMENTS (CLAY SHALE) .	75
8.1.1	SIGNAL-TO-CLUTTER MEASUREMENTS	76
8.1.2	GPR MEASUREMENT OF THE RELATIVE DIELECTRIC CONSTANT OF THE PHASE 1 SOIL-MODEL TEST TANK..	77
8.1.3	PHASE 1 SOIL-MODEL TANK TARGET MEASUREMENTS...	80
8.2	PHASE 2 SCALE-MODEL GPR MEASUREMENTS (CLAY SCHIST)	102
8.2.1	GPR MEASUREMENT OF THE RELATIVE DIELECTRIC CONSTANT OF THE PHASE 2 SOIL-MODEL TEST TANK.	102
8.2.2	PHASE 2 SOIL-MODEL TANK TARGET MEASUREMENTS..	104
8.3	FULL-SCALE GPR MEASUREMENTS WITH HP 8510	129
SECTION 9: SELECTION OF THE OPTIMUM GPR SOURCE SIGNAL BASED ON THE PHASE 1 AND PHASE 2 SOIL-MODEL TANK MEASUREMENTS		136
9.1	EVALUATION OF THE EFFECTIVENESS OF THE SCALE-MODEL TESTS	136
9.2	DETERMINATION OF THE OPTIMUM GPR SOURCE SIGNAL ...	139
9.2.1	EVALUATION OF THE GPR SYSTEMS TESTED	139

TABLE OF CONTENTS

9.2.2	SELECTION OF THE OPTIMUM GPR SYSTEM	142
9.3	THE MAXIMUM PERFORMANCE GPR	142
SECTION 10:	REFERENCES	147

APPENDICES

APPENDIX A	MEASURED ELECTROMAGNETIC PROPERTIES OF VARIOUS SOIL TYPES	A-1
APPENDIX B	MEASURED ELECTROMAGNETIC PROPERTIES OF THE CLAY SHALE AND CLAY SCHIST USED IN THE SOIL MODEL PIT	B-1
APPENDIX C	HP8510 NETWORK ANALYZER SYSTEM OVERVIEW - EXCERPT FROM THE HP8510 MANUAL	C-1
APPENDIX D	HP8510 NETWORK ANALYZER TIME DOMAIN MEASUREMENTS - EXCERPT FROM THE HP8510 MANUAL	D-1

SECTION 1

INTRODUCTION

This technical report summarizes the work performed on NCEL contract number N62474-87-C-3056, "Determination of the Best Ground-Penetrating Radar Source Signal Type for Accurate Location of Underground Utilities." The report is divided into several sections describing the work performed on the program and the results obtained.

There are many applications today for ground-penetrating radar (GPR) systems with varying requirements. These applications encompass utility pipe detection, subsurface highway surveys, archaeological surveys, mine shaft detection, and more. Many GPR systems have been developed to meet these needs. The designs of the GPR systems are as varied as their applications.

Each application requires that the GPR provide information about the subsurface target(s) of interest and that the signal from the desired target(s) be distinguishable from other signals, for example, from those generated by the surrounding media. Thus, the potential GPR user identifies system performance requirements such as depth penetration, target resolution, range accuracy, measurement speed, power consumption, and the GPR physical dimensions. These performance requirements translate into the radar system design parameters of bandwidth, pulse width, resolution, range accuracy, maximum range, pulse repetition frequency (PRF), required radiated power levels, permitted radiated power levels, measurement scan speeds, etc.

All radar designs, whether or not they are used for GPR applications, incorporate well-established signal processing techniques. Most of the basic radar parameters are determined by using Fourier Transform analysis. Thus, radar system designers must approach their design requirements by considering time-domain and frequency-domain fundamentals. The two domains are linked; and the solution to a given problem may be approached from either domain. Consequently, GPR systems

have been built using time-domain techniques, frequency-domain techniques, and combinations of both.

Most of the time-domain GPR systems use baseband pulsers with pulse widths and power levels determined by the design requirements. However, optimum pulse shapes are difficult to generate. These time-domain systems often use simple, broadband sampling receivers which produce low-frequency output waveforms that are easily recorded and displayed. Many different signal-processing techniques have been applied to time-domain GPR output data to enhance target detection and identification.

Frequency-domain GPR systems typically use RF frequency-modulation techniques. These systems are usually larger and more expensive than their time-domain counterparts. However, the frequency-domain systems offer more flexibility in RF bandwidth selection. Furthermore, receivers and transmitters can be designed that yield better overall system clutter and noise performance than their time-domain counterparts. Output data from the frequency-domain radars must usually undergo complex signal processing before it can be easily interpreted by the operator.

The purpose of this GPR signal source evaluation program was to identify which type of GPR system provided the best performance, based on the criteria of depth penetration, resolution, and signal-to-clutter performance. GAR tested two pulsed GPR systems, as well as a FM-CW based GPR system, and a stepped FM-based system to determine which technology yielded the best results. Each of the systems was tested on a scale-model test tank containing homogeneous soil with known buried targets and probes. Two different soil types were modeled with the tank to simulate a medium-loss environment and a low-loss environment.

SECTION 2

SUMMARY OF WORK PERFORMED

Early work on the program involved the specification of the candidate scale-model GPR source signal types, the design of a suitable soil scale-model tank for testing the GPR systems, the analytical modeling of the GPR pipe detection problem, and the fabrication of antennas to be used for testing the candidate GPR systems. The remainder of the program work included soil-tank measurements with each of the candidate GPR systems, the examination of the corresponding data collected from these measurements, and the evaluation of the performance obtained from each of the candidate systems. A recommendation based on this evaluation was made which specified the optimum GPR source signal for accurate utility location. Finally, a full-scale version of the GPR system producing the best scale-model performance was qualitatively tested on an outdoor pipe test field at the GAR facility.

Four types of GPR systems were selected for testing. Two systems were time-domain short-pulse radars; one was a swept-frequency FM-CW system, and one was a stepped-FM system. All four systems represent radar technology that had been applied to GPR problems in the past. One of the short-pulse radar systems is built by Gulf Applied Research (GAR) and utilizes a one-nanosecond monocycle pulser and an equivalent-time sampling receiver. The other short-pulse radar is built by Geophysical Survey Systems, Inc. (GSSI) and uses a balanced, one-nanosecond unipolar pulser and an equivalent-time sampling receiver. The two frequency-domain systems were simulated using a Hewlett-Packard 8510 network analyzer. The network analyzer was operated in its time-domain mode with synthesized one-nanosecond unipolar pulses. Thus, the performance of all four systems could be appropriately compared by examining their time-domain, or simulated time-domain responses. Functional descriptions of the candidate GPR systems are included in Section 6.

The pipe target detection problem was modeled analytically in order to evaluate the expected performance of GPR systems. An approximate analytical model based on the radar range equation was used. The model accounted for antenna parameters

soil parameters, and the pipe target parameters. The analysis predicted that high signal losses were expected for deeply buried targets in moderately lossy soil. The predicted signal loss was higher than expected. GAR concluded that the approximations used in the analytical model may have introduced some error into the calculations. Actual results obtained while testing the GPR systems on the soil-model tank indicated that the analytical model indeed produced pessimistic results.

We concluded that accurate measurements of the GPR antenna pattern in the soil, and of the radar cross sections of various pipe targets, would facilitate the improvement of the analytical model. Some of the results from the GPR tests in this program could be used to improve the analytical model. However, an extensive measurement program to establish an accurate analytical model was beyond the scope of this program.

GAR elected to build a scale-model soil environment containing buried pipe and plate targets for the purpose of testing the candidate GPR systems. This was done because a full-scale testing area with buried targets would be difficult to construct and maintain. The design of the scale-model soil tank is discussed in Section 5. Some of the important concepts and factors influencing the design of the scale-model tank are outlined below.

Essentially, scaling allows the reduction of all dimensions of the full-scale environment by the corresponding scale factor. This includes all target dimensions, burial depths, and the pulse widths of the GPR transmitter signals. Therefore, the dimensions of the test facility and the GPR antennas were reduced by the scale factor. The electromagnetic loss characteristic of the dielectric material used in the model tank was scaled higher than the loss characteristic of soil in the full-scale environment. This was done to maintain the same total soil loss over the scale-model target burial depth that would occur with the actual target burial depth in the full-scale environment.

GAR initially considered construction of a soil scale-model tank using a liquid dielectric. A liquid dielectric offered several advantages over a soil dielectric. The dielectric properties of the liquid could be accurately controlled, targets could be easily inserted or removed from

the liquid, and the electromagnetic effects of the tank boundaries could be removed from the GPR test data. Despite these advantages, a liquid soil-model tank would have been costly to build and maintain. Also, there was a significant technical risk that the liquid dielectric properties could not be maintained with satisfactory homogeneity in a large volume tank, such as the one that would have been required for the GPR tests.

The cost and logistical problems associated with constructing and maintaining a liquid scale-model dielectric prompted GAR to use homogeneous soils as scale-model dielectric materials instead. GAR located commercial sources of two lossy clay soils and used these soils as the scale-model dielectrics. These clays exhibited high enough attenuation factors to allow them to be used as scaled dielectrics.

GAR filled the soil-model tank with one of the clays and buried various plastic pipes, metal pipes, and metal plates in the clay at different depths. After measurements were made with the first clay soil, the tank was emptied and re-filled with the other clay. The same targets were buried in the same locations as they were with the original clay, and measurements were then made with the new soil. Using two different materials in the test tank allowed the prediction of GPR performance in two full-scale environments. This approach also facilitates the extrapolation of the results obtained to other, similar soil types.

Antennas were specially designed to be used for the tests of the candidate GPR systems. Accurate comparisons between the GPR systems were possible only if the same antennas were used for each of them. GAR designed and built a pair of TEM horn antennas and a pair of shielded triangular-sheet dipole antennas to be used with the radars. The performance of each pair of antennas was evaluated and the best pair was used for the GPR comparison tests. Section 3.3.3 establishes the design requirements of GPR antennas and Section 6.4 describes the two types of antennas constructed by GAR for the tests.

The TEM antennas had more desirable pulse performance characteristics than the dipole antennas. Therefore, considerable care was taken in their fabrication. In addition, the TEM horns were designed and built very carefully in an

attempt to minimize the effects of clutter signals on the received target signals. However, we discovered during the tests of the two types of antennas that the dipole antennas provided noticeably better signal-to-clutter performance than the TEM horns. Since the signal-to-clutter ratio was the dominant limitation in target detectability, the triangular-sheet dipoles were used for the subsequent GPR comparison tests.

The four candidate GPR sources were tested with the two clay model environments. The triangular-sheet dipole antennas were used with all of the systems except the GSSI radar. The antennas could not be used with the GSSI radar because it had a single integrated receiver, transmitter, and antenna assembly. Target signal return amplitudes were measured from the pipe targets and the performances of the radars were compared. The measurement results are presented in Section 8.

Section 8 also presents the results of measurements using a full-scale version of the scale-model GPR system that gave the best performance in the scale-model tests. The system was tested on an outdoor pipe test field containing buried plastic and metal pipes. Qualitative data from the full-scale measurements demonstrated the general performance characteristics of that GPR system.

A recommendation for a high-performance GPR based on an evaluation of the measurement results is given in Section 9. After reviewing the results, GAR felt that a single, fixed RF bandwidth GPR is not flexible enough to meet all of the requirements of resolution and deep penetration. Several RF bandwidths are required. The frequency-domain systems provide more performance flexibility than the time-domain pulsed GPR systems at the expense of higher cost and complexity. If the receiver dynamic range and system-generated-clutter performance are used as evaluation criteria, a pulsed, time-domain GPR cannot typically match the capabilities of a frequency-domain GPR that utilizes a synthesized signal source. Reducing clutter and maximizing dynamic range are critical in order to distinguish desired target signals from clutter returns.

SECTION 3

DESCRIPTION OF THE GROUND PENETRATION PROBLEM

Ground-penetrating radars are designed to operate in a considerably different environment than more conventional radars. The GPR must operate with a medium that is electromagnetically inhomogeneous and lossy. Furthermore, the electromagnetic properties of the soil containing the targets are usually unknown or are known only near the surface. These properties may vary on a daily basis with varying moisture content.

An ideal ground-penetrating radar system should be able to detect targets buried at any desired depth, and resolve multiple targets if they are closely spaced. However, the relative dielectric constant and attenuation properties of the soil generate severe limitations on one's ability to construct a GPR system that provides such ideal performance. The GPR design goals usually represent a compromise between such desired ideal performance and the best performance achievable under given conditions. For example, a high resolution GPR typically is not capable of great depth penetration. In addition, most GPR systems have maximum range capabilities of a few meters or less. Although the radar designer is typically not able to achieve ideal performance, he can in practice approach optimum performance, that is, the best performance obtainable with available technology under existing conditions.

3.1 SOIL DIELECTRIC PROPERTIES

The dielectric properties of the soil affect the performance of a GPR more than any other factor. These soil properties vary with geographical location, as well as with depth from the surface. The attenuation, conductivity, relative dielectric constant, loss tangent, and permeability are interrelated factors that determine the way electromagnetic energy propagates through the soil. The effects that these soil characteristics have on the performance requirements of a GPR are explained below.

3.1.1 ELECTROMAGNETIC PROPAGATION IN SOIL

The propagation characteristics of an electromagnetic wave in any medium are determined largely by the propagation constant of the medium. The propagation constant includes the effects of attenuation, conductivity, and the relative dielectric constant. The following description of electromagnetic wave propagation in soil illustrates the effects of these factors.

To simplify the description of electromagnetic wave propagation in soil, or any other medium, it is helpful to make several assumptions. Let us assume that the soil medium is infinite in spatial extent, linear, homogeneous, isotropic, and electromagnetically source-free. Assume also that the electromagnetic field energy propagating in the ground has a transverse electromagnetic field structure (the TEM mode), has a sinusoidal variation with time, and operates as a plane wave.

Under these assumptions, Maxwell's equations may be expressed as:

$$\nabla^2 \mathbf{E} - \gamma^2 \mathbf{E} = 0 \quad (3.1)$$

$$\nabla^2 \mathbf{H} - \gamma^2 \mathbf{H} = 0 \quad (3.2)$$

$$\nabla \cdot \mathbf{H} = 0 \quad (3.3)$$

$$\nabla \cdot \mathbf{E} = 0 \quad (3.4)$$

$$\gamma = (j\omega\mu(\sigma + j\omega\epsilon))^{1/2} \quad (3.5)$$

Here, \mathbf{E} and \mathbf{H} are vector, sinusoidal representations of the electric and magnetic field components of the electromagnetic wave. The scalar quantity γ is the complex propagation constant, determined by characteristics of the medium. It is described in detail later. The term μ is the permeability of the medium, σ is the conductivity, and ϵ is the dielectric constant.

Assume that a rectangular coordinate system is established having x, y, and z axes, with the positive z direction being the direction of propagation of the electromagnetic wave into the ground. This assumption yields solutions of Maxwell's equations of the form:

$$E_x = E_x^+ e^{-\gamma z} \quad (3.6)$$

$$E_y = E_y^+ e^{-\gamma z} \quad (3.7)$$

$$H_x = H_x^+ e^{-\gamma z} \quad (3.8)$$

$$H_y = H_y^+ e^{-\gamma z} \quad (3.9)$$

Where E_x , E_y , H_x , and H_y are scalar components of the vectors E and H in the x and y directions. The + sign on the E and H field components indicates that the wave is traveling in the positive z direction. Solutions also exist for waves traveling in the negative z direction, but they are neglected here for simplicity. Equations (3.6) through (3.9) describe the form of the electromagnetic plane-wave components in the soil with the parameters established above.

The complex variable γ in the exponent of Equations (3.6) through (3.9) is of great interest in predicting the performance of a GPR. This term is defined in Equation (3.5) and contains all of the electromagnetic parameters of the medium through which the wave propagates. In Equation (3.5), $\gamma = j\omega\sqrt{\mu\epsilon}$, where f is the frequency of the propagating sinusoidal electromagnetic energy. Also, $j = (-1)^{1/2}$ and denotes an imaginary number.

Often, γ is expressed in terms of its real and imaginary parts as in Equation (3.10) below:

$$\gamma = \alpha + j\beta \quad (3.10)$$

Solving Equation (3.5) for its real and imaginary parts produces two roots; however, only the solution yielding a positive imaginary part is valid for real media. The quantity α is the attenuation factor and β is the phase propagation factor.

Once the quantities μ , σ , and ϵ are determined for a given medium, the attenuation and phase factors in Equation (3.10) are known. Solving for α and β yields:

$$\alpha = \omega \sqrt{\mu \epsilon} \left\{ \frac{1}{2} \left[\sqrt{1 + (\sigma/\omega \epsilon)^2} - 1 \right] \right\}^{1/2} \quad (3.11)$$

$$\beta = \omega \sqrt{\mu \epsilon} \left\{ \frac{1}{2} \left[\sqrt{1 + (\sigma/\omega \epsilon)^2} + 1 \right] \right\}^{1/2} \quad (3.12)$$

Often the electromagnetic soil attenuation characteristic is expressed in dB/meter. This method of expressing the soil attenuation addresses power loss and is computed as follows:

$$\text{Attenuation (dB/meter)} = 20 \log_{10} e^{\alpha} . \quad (3.13)$$

Other quantities used to characterize dielectric media and soil are derived from γ , μ , σ , and ϵ . These quantities are the relative dielectric constant, the relative permeability, the loss tangent, and the intrinsic impedance. The definitions of these quantities are given below:

$$\text{Relative Dielectric Const. } \epsilon_r = \epsilon / \epsilon_0 \quad (3.14)$$

$$\text{Relative Permeability } \mu_r = \mu / \mu_0 \quad (3.15)$$

$$\text{Loss Tangent } \delta = \sigma / \omega \epsilon \quad (3.16)$$

$$\text{Intrinsic Impedance } \eta = (j\omega \mu / (\sigma + j\omega \epsilon))^{1/2} \quad (3.17)$$

Here, ϵ_0 and μ_0 are the permittivity and permeability of free space, respectively. For most soils, $\mu_r=1$.

The intrinsic impedance relates the amplitudes of the E and H field components by the equation:

$$|\eta| = |E| / |H| \quad (3.18)$$

In this report, the most commonly used terms to describe soil characteristics will be α , the attenuation in dB/m, and ϵ_r .

3.1.2 DETERMINING SOIL PARAMETERS

One of the most challenging problems confronting any GPR designer is to design the radar to operate in a soil environment that is quite diverse. The designer must address the most demanding environment and tailor his design to meet those requirements. The worst soils often exhibit high relative dielectric constants coupled with high loss characteristics. These lossy soils impose stringent requirements on maintaining high signal-to-clutter and signal-to-noise ratios in the radar.

Soil characteristics vary greatly with geographical location. Figure 3.1 is a map of the United States indicating the different soil types that may be found in different geographical areas¹. The map is generalized and does not show the range of soil types that occur even within the areas indicated.

Table 3.1 is a list of common materials, including soils, with their approximate relative dielectric constants. The relative dielectric constants range from 1 for air to 81 for water. The relative dielectric constant determines the speed of electromagnetic energy in that medium. That speed is inversely proportional to the square root of the dielectric constant for the medium. This relationship is given by:

$$\text{Speed in medium} = c / \sqrt{\epsilon_r} = v, \quad (3.19)$$

where c is the speed of light in a vacuum.

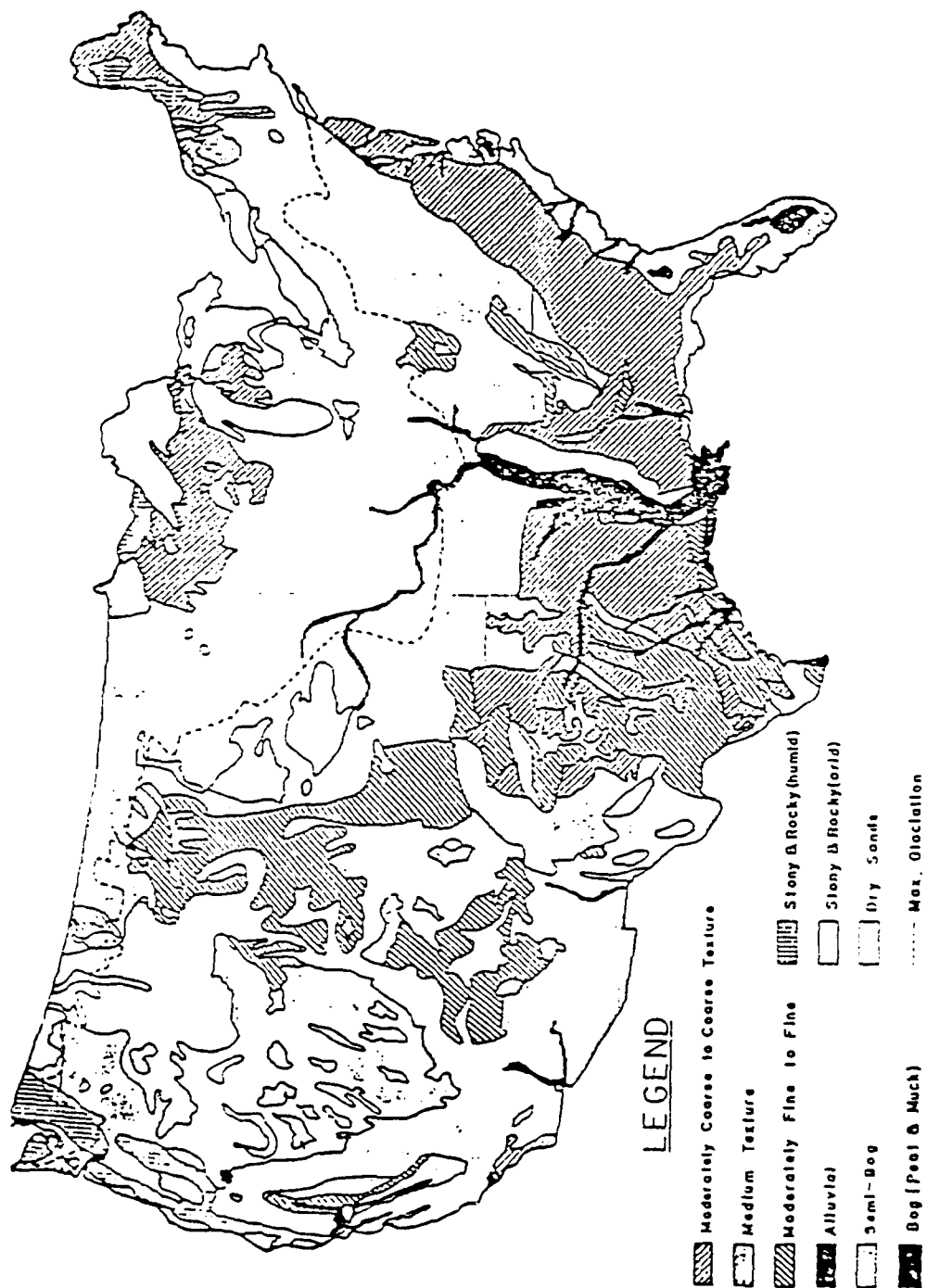


Figure 3.1: Soil texture association of United States soil.

TABLE 3-1. TYPICAL RELATIVE DIELECTRIC CONSTANTS FOR SELECTED MATERIALS.

Material	ϵ_r
Air	1
Pure Water	81
Seawater	81
Freshwater ice	4
Seawater ice	6
Snow (firm)	1.4
Sand (dry)	5
Sand (saturated)	30
Clay (saturated)	10
Granite (dry)	5
Granite (wet)	7
Limestone (dry)	7
Limestone (wet)	8
Shale (wet)	7
Sandstone (wet)	6
Soil - sandy dry	2-4
sandy wet	20-25
loamy dry	2-6
loamy wet	15-20
clay dry	2-6
clay wet	10-20
Permafrost	6-13
Strong concrete - dry	5-9
soaked 20 hrs	10-15
Cracked concrete - dry	4-5
soaked 20 hrs	13-20
Asphalt	12-16

For example, assume that an electromagnetic wave is propagating through a soil with a relative dielectric constant of 16. Since the speed of light in a vacuum is approximately 3×10^8 meters/second, the speed of the wave in the soil is $3 \times 10^8 / (16)^{1/2}$, or 7.5×10^7 meters/second.

Since the speed of electromagnetic energy in a medium is inversely proportional to the square root of the relative dielectric constant of that medium, the wavelength of the energy is also inversely proportional to this quantity. This derives from the relationship between frequency (f), wavelength (λ), and speed (ν) of electromagnetic energy:

$$f\lambda = \nu \quad (3.20)$$

The variation in speed and wavelength with respect to the relative dielectric constant of the medium implies that range accuracy and resolution are medium-dependent. The impact of this observation on the operation of a GPR is discussed in the next section.

In order to evaluate GPR performance in a given soil, one must know all of the important soil parameters in addition to the dielectric constant. Unfortunately, all of these parameters, including the dielectric constant, are frequency-dependent. To measure the parameters accurately with respect to frequency, a soil sample must be taken and measured.

Typical test equipment for making soil parameter measurements at radio frequencies (RF) includes a test cell and a microwave network analyzer. The test cell is usually a section of RF transmission line that is filled with the soil sample. The propagation characteristics of the RF energy in the test cell filled with the sample are measured with the network analyzer. Since the propagation characteristics of the unfilled test cell are known, the soil parameters can be determined by comparing the results of the measurements with the filled and unfilled test cells.

Appendix A contains plots of the measured parameters of various soil samples. All of the measurements were performed by Dr. Glenn Smith of the Georgia Institute of Technology.

School of Electrical Engineering. Dr. Smith used a Hewlett-Packard 8408 network analyzer and a calibrated, open-circuit test cell.

The first group of measurements were made with a sample of clay soil taken near the Gulf Applied Research facility in Marietta, Georgia. The moisture content of the clay was varied and a set of measurement curves was generated. The curves indicate the variations in relative dielectric constant and attenuation with respect to moisture content.

As the clay moisture content increases, so does the relative dielectric constant and the attenuation of the energy as it travels through a given depth of soil. One should note that, in the frequency range of the measurements, the attenuation for a given moisture content increases with frequency. This is true for typical soils. Also, note that the attenuation-per-meter curves are for one-way travel through the soil. Thus, if a target is located one meter below the surface, this one meter represents the one-way travel distance. However, the radar energy actually travels two meters as it travels from the transmitter antenna to the target and back to the receiver antenna.

The next group of measurements was made with a sample of sand. At low to moderate moisture contents, the sand has a low relative dielectric constant and low attenuation. The characteristics of the sand are considerably different than those of the clay discussed above.

The last group of measurements in Appendix A was made from several samples of soil taken in Japan. The locations where the soil samples were taken are unknown. No attempt was made to vary the moisture content of the soil samples. Nevertheless, the variation in the soil parameters on a sample-to-sample basis is remarkable.

3.1.3 EFFECTS OF SOIL PARAMETERS ON GPR SYSTEM PERFORMANCE

The properties of the soil greatly affect the performance of a GPR. The relative dielectric constant of the soil determines the maximum depth resolution possible for a given bandwidth. Depth resolution is defined as the capability of

distinguishing two targets that are closely spaced in range (time). The resolution of any radar system is related to its RF bandwidth, or equivalently, to its RF pulse width. As the relative dielectric constant of the soil increases, the resolution of a GPR with a given RF bandwidth improves.

The resolution capabilities of a GPR are easiest to visualize if a pulse-based, time-domain system is considered. Nonetheless, a frequency-domain GPR, such as one that uses continuous frequency modulation, has resolution capabilities based on its RF bandwidth as well.

Resolution for a pulse radar is usually defined as half of the pulse length in the medium. A GPR that generates a one-nanosecond pulse in air has a pulse length of 0.3 meter. This gives the GPR a resolution of $0.3/2 = 0.15$ meter in air. In a soil with a dielectric constant of 16, the resolution improves to $0.15/(16)^{1/2} = 0.0375$ meter.

Not only will the relative dielectric constant affect the GPR resolution, this constant must be known exactly in order to measure the target depth accurately. Although the time difference between the surface return and a subsurface target return can be accurately measured with the GPR, a knowledge of the speed of the RF energy is required to determine the corresponding depth of the target. Without a knowledge of the soil relative dielectric constant, the speed of the RF energy in the soil is unknown.

Fortunately, in many GPR applications, precise depth accuracy is not required. An experienced operator can often estimate the relative dielectric constant of the soil well enough for the purposes of most field operations. In practice, it is usually possible to obtain soil samples for the purpose of measuring the dielectric constant in regions near the surface. The dielectric constant of the surface sample can sometimes be used as a reasonable approximation of the dielectric constant of deeper soil.

The soil attenuation characteristics can affect the GPR resolution and depth penetration. The attenuation curves usually show increasing loss-per-meter with increasing frequency. This means that soil acts like a lowpass filter for the RF energy passing through it. Removing some of the high

frequency energy from an RF pulse has the effect of slowing the rise time of the pulse and widening it as well. The degree to which this occurs depends on the severity of the attenuation curves for a particular soil. As a GPR pulse widens on its passage through lossy soil, the effective resolution of the GPR decreases. Thus, one finds that most GPR systems designed for deeper penetration (and corresponding poorer resolution) use wider pulses than those designed for shallow penetration and higher resolution.

The depth penetration capability of a given GPR is primarily dependent on the attenuation characteristics of the soil. As RF energy passes through the soil, it encounters targets that reflect a portion of the energy. The energy is attenuated as it travels through the soil toward the target as well as back to the surface from the target. The amount of attenuation due to the soil parameters is based on the attenuation curves for that particular soil. Unfortunately, the attenuation is not linear with depth and it is usually measured in decibels-per-meter (dB/m).

For example, assume that an RF pulse passes through soil with a 20 dB/m attenuation characteristic and that this attenuation is uniform with respect to frequency. Thus, energy traveling through one meter of soil is attenuated 20 dB. This means that the pulse power level after one meter is 0.01 times the power level as the pulse enters the soil. If the pulse travels two meters, it is attenuated 40 dB and the corresponding power level at that point is 0.0001 times the original power level.

3.2 THE TARGET IDENTIFICATION PROBLEM

The main purpose of a GPR is to detect subsurface buried objects, or targets. These targets can be utility pipes, tunnels, cavities, buried cables, etc. Signal returns from the GPR are typically processed and displayed to identify the returns from desired targets. However, the signals received by the GPR do not necessarily represent returns from desired targets.

The RF energy transmitted from the antenna system can encounter many interfaces and objects. When the propagating RF energy impinges on an interface or object, a portion of the energy is reflected back toward the source. The rest of the energy either scatters in other directions or passes through the object or interface. The amount of energy reflected back toward the source is determined by the size and shape of the interface as well as by the difference between the relative dielectric constants of the materials at the interface.

Reflections from undesired targets are often referred to as clutter. However, clutter is not restricted to undesired target returns. Clutter also refers to any undesired signals that appear in the receiver that are coherent with the transmitted signal. This can include connector reflections in the RF circuitry, multiple bounces in the antenna, and noise coupling from the transmitter to the receiver over the power supply lines.

Clutter has the tendency to mask, or interfere with, the returns from desired targets. With most broadband GPR systems, the internally generated or "system" clutter (not related to false targets) limits the detectability of a desired target. One refers to such a system as being "clutter-limited," as opposed to a "noise-limited" system, in which target detectability is limited by the thermal noise level.

If the target signal level falls below the clutter level, it becomes more difficult, if not impossible, to reliably detect the target. Fortunately, certain signal processing techniques can reduce the effects of the clutter. Such techniques for GPR systems can be quite diverse. Most of them are developed from techniques used with conventional radar systems. Examples of these techniques are clutter subtraction, time-domain synthetic aperture processing², various types of digital filter processing³, and probabilistic target discrimination⁴. These techniques vary in implementation, complexity, and speed. The selection of the specific technique to use in a given case is dependent upon the application of interest.

In brief, the task of identifying a desired target becomes one of distinguishing its signal return from the returns of undesired targets, system clutter, and system noise.

Furthermore, the need to satisfy this requirement is independent of the type of RF modulation used by the GPR. In essence, this is a key performance criterion of any GPR system.

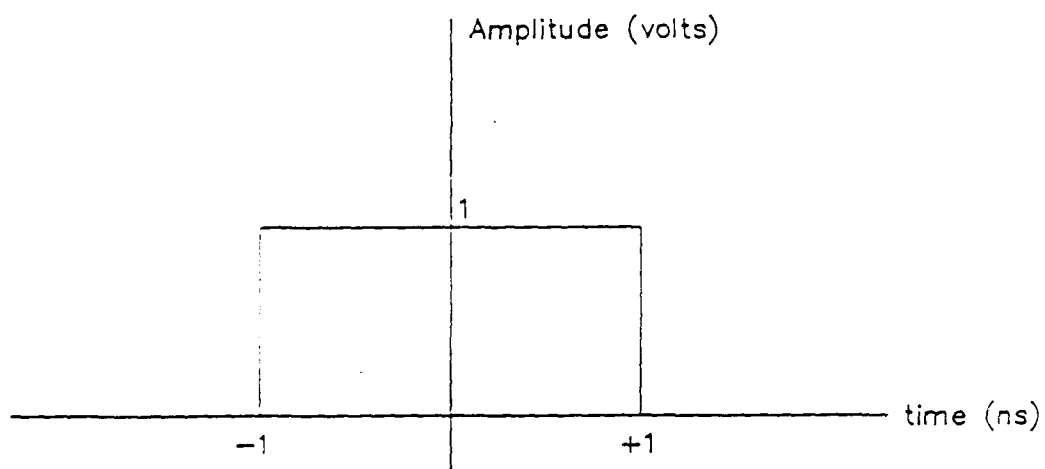
3.3 DESIGNING THE GPR SYSTEM

This section presents some of the design considerations that influence the development of a GPR system. The design goals are usually based on the required penetration depth, target resolution, RF power radiation limits, the GPR system size, and the system cost. These requirements must always be referenced to some specific soil parameters. This section focuses on the relationship between GPR resolution and bandwidth, as well as on RF power requirements, general antenna design considerations, and the elimination of system-generated clutter.

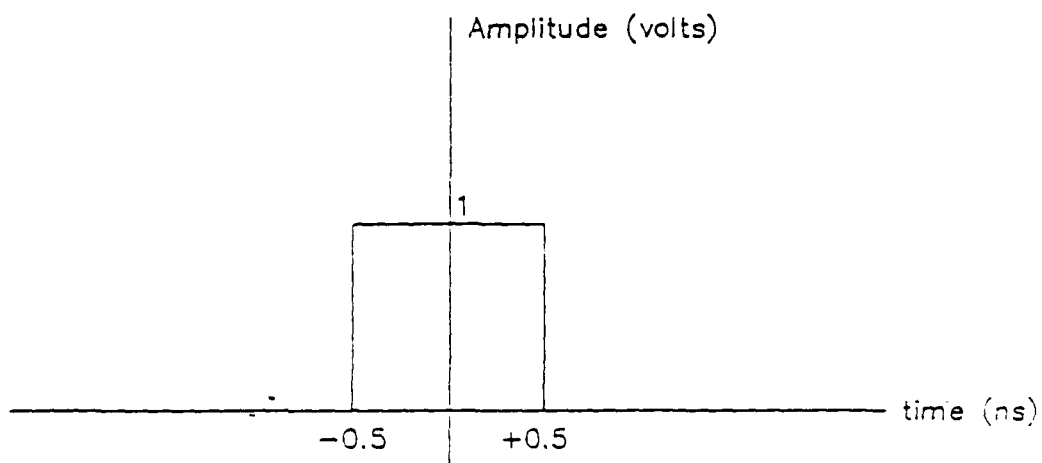
3.3.1 GPR BANDWIDTH AND RESOLUTION

The penetration depth and resolution specifications determine the RF bandwidth required for a GPR. The bandwidth may be developed using a direct time-domain pulse; or by using a frequency-domain system, such as FM-CW or stepped-FM. The frequency-domain systems provide the most flexibility in tailoring the RF bandwidth, since generating optimum time-domain pulses directly is difficult. With frequency-domain systems, the frequency components can be individually phase- and amplitude-modulated to achieve beneficial system characteristics. This is not as easy to accomplish with pulse radars.

Due to the soil attenuation characteristics, good depth penetration requires the use of low-frequency RF energy. In contrast, high resolution requires high-frequency energy. Figure 3.2 plots two rectangular pulses. The rectangular pulses each have normalized amplitudes of one volt. Figure 3.3a is the frequency spectrum of the two-nanosecond pulse from Figure 3.2a and Figure 3.3b is the spectrum of the higher-resolution one-nanosecond pulse. Note that the bandwidths of the pulses are inversely proportional to their pulse widths. The rectangular pulse shapes were selected purely as an example.



(A)



(B)

Figure 3.2: Plot of (a) 2ns rectangular pulse and (b) 1ns rectangular pulse.

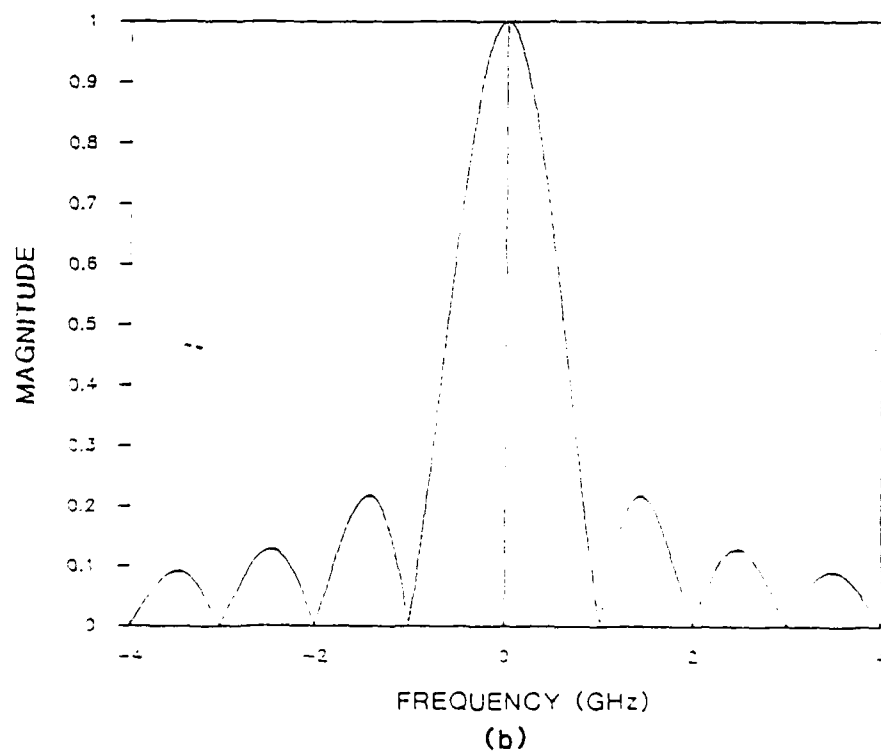
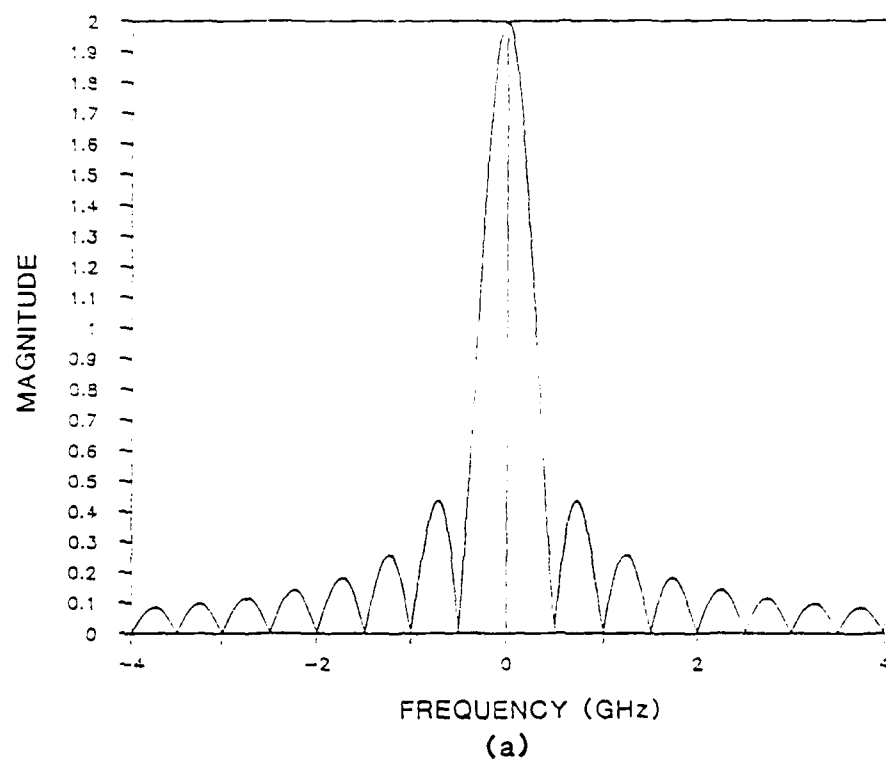


Figure 3.3: Plot of the frequency spectra of (a) 2ns rectangular pulse and (b) 1ns rectangular pulse

and do not necessarily represent optimum pulse shapes for a GPR design.

Since the soil acts as a lowpass filter to electromagnetic energy, a compromise will exist in the GPR design between resolution and depth penetration. In fact, with increasing depth penetration, a GPR with a given RF bandwidth will have better resolution at shallow depths than it will at deeper depths. For this reason, many GPR systems utilize different RF bandwidths and antennas depending on their application.

3.3.2 GPR TRANSMITTER POWER CONSIDERATIONS

Once the GPR RF frequency range has been selected, the transmitter power requirement must be identified. The power requirement is a function of the desired depth penetration, the soil attenuation, the target radar cross section, the efficiency of the antennas, the receiver noise level, and the applicable regulations regarding RF energy emissions. The GPR designer must estimate the expected signal level from a buried target given a reference power level. If the estimate indicates that the signal level will fall below the minimum detectable receiver signal, then the power transmitted must be increased. The limits on the maximum radiated power are usually regulated by governmental agencies and are based on safety and RF interference requirements.

Unfortunately, merely increasing the GPR transmitter power does not necessarily mean that signals from deeper subsurface targets will be identifiable at the receiver. The system-generated clutter usually proves to be the limiting factor. The clutter will increase linearly with increasing transmitter power, as will the desired target returns. Therefore, if a target signal is masked by an internally-generated clutter signal when a low-power transmitter is used, increasing its power will increase the clutter signal as well, so that the target signal will still be masked.

The internally-generated clutter often appears in fixed time positions within the receiver output signal range window. Thus, this type of clutter does not always interfere with the target return signal. If the receiver window is positioned

optimally in time, or the internal clutter is moved away from the receiver time window, then the GPR will usually benefit from increased transmitter power. The optimal positioning of the internal clutter is not always possible, however.

The reader should note that soils have one-way power attenuation characteristics that are on the order of tens of decibels per meter. To increase the transmitter output power 10 dB, the output signal voltage must increase by a factor of 3.16. To increase it by 20 dB, the output voltage must be 10 times higher. Large increases in transmitter power can place heavy demands on the transmitter design, especially for short-pulse systems. This is because higher-power transmitters usually require electronic components that can withstand larger power supply voltages and currents. Such components typically cannot produce pulses as narrow as the ones produced by lower-power devices.

3.3.3 GPR ANTENNA CHARACTERISTICS

One of the key elements in a GPR design is the selection of a proper antenna. A GPR can use a single antenna for both transmitting and receiving (monostatic configuration), or one antenna for transmitting and a separate antenna for receiving (bistatic configuration). In any case, the antenna(s) used must provide a good RF match to the transmitter and receiver and should be as efficient as possible. In addition, the antenna size and radiation pattern may be important considerations for particular GPR applications.

Typical GPR applications require relatively broadband RF systems. The antenna must have the capability of radiating as much of the transmitter output energy as possible. Thus, the RF bandwidth of the GPR must match the radiation bandwidth of the antenna. Or, equivalently, the antenna must be designed to match the RF bandwidth of the transmitter.

Broadband antennas act much like highpass or bandpass filters. They cannot radiate energy below their low-frequency cutoff. Therefore, if the RF frequency band of the GPR is such that it extends below the low-frequency cutoff of the antenna, that portion of the energy below the cutoff will not be

radiated. A similar situation exists at the antenna upper cutoff frequency.

One desires that the transmitting antenna absorb the energy that it cannot radiate. Otherwise, the antenna will present a high reflection coefficient for the frequencies outside its efficient-radiation band. Any reflected energy from the antenna input will propagate back toward the source. This can be disastrous, especially for a monostatic system, because the reflected energy will contribute to the internal system clutter and can mask weak targets if it should appear in the receiver window.

An additional requirement for the antenna is that it be non-dispersive. This implies that the group delay for the frequencies in the antenna passband is constant. If a pulse system uses an antenna with a constant group delay and a bandwidth that is wide enough for the RF frequency range, the radiated and received pulses will not ring or stretch appreciably. This will maintain a minimum pulse resolution cell. These benefits are also desirable for CW systems.

However, one can measure the antenna characteristics on a discrete-frequency basis and correct for certain antenna distortions, whether in amplitude or phase. Unfortunately, these corrections are not always easily performed. The best approach to minimizing antenna-related distortion problems is with careful antenna design, thereby eliminating as much waveform pre-processing or post-processing as possible.

The antenna propagation and radiation characteristics are related to the length and shape of the antenna. For a given antenna with a known radiation bandwidth, doubling its length will reduce the low-frequency cutoff by a factor of two. Thus, antennas for GPR systems that are designed for deep penetration are usually larger than those used with high-resolution GPR systems. This is because soils typically attenuate high RF frequencies more than low RF frequencies. Therefore, deep-penetrating GPR systems have transmitter bandwidths concentrated at lower frequencies. Such concentration at lower frequencies creates larger pulse widths in time-domain systems. In contrast, the high-resolution GPR systems require a relatively large RF bandwidths, which is equivalent to a narrow pulse.

The antenna size also affects its radiation pattern. Many antennas have radiation patterns that can be approximated as though originating from apertures. Larger antennas approximate larger apertures. For a given frequency of electromagnetic energy being radiated, the radiation pattern from a small aperture will be broader than that from a large aperture. Also, for a given aperture size, the radiation pattern will be broad for low frequencies and narrow for high frequencies. This implies that the antenna radiation pattern will not be constant over the typical bandwidths of GPR systems. This phenomenon will affect system resolution at target angles off-boresight from the antenna.

3.3.4 REDUCING INTERNAL CLUTTER IN A GPR SYSTEM

Internal clutter in a GPR system is minimized by careful design and construction practices. A critical factor affecting the clutter levels is the design of the transmitter and receiver transmission systems. All RF components should be matched as well as possible to the transmission lines (usually 50 ohm coaxial cables) to eliminate reflection points. This includes antennas, transmitters, samplers, RF amplifiers, mixers, etc. Any reflections should be absorbed or moved in time with RF delay lines to keep them out of the receiver range window. Any discontinuities in the transmission lines, such as connectors, will contribute to the reflections.

Clutter may also enter the transmitter and receiver systems through the power supply lines for the system components. For example, a transmitter pulser can place high-frequency noise on its power supplies and ground plane. If this power supply noise is not filtered or removed by other techniques, it can enter the receiver section through the supply lines. This type of noise can easily add significant clutter to the receiver output.

SECTION 4

MODELING THE PIPE DETECTION PROBLEM

The initial approach to determining the optimum GPR signal source required detailed investigation of the problem of subsurface pipe detection. GAR performed an approximate analysis to estimate the maximum depth capability of a GPR in a known environment. The analytical model selected was flexible enough to include effects of soil attenuation, antenna parameters, surface reflection loss, wave diffraction at the surface with variable antenna height, and the target radar cross section. The model did not include the effects of clutter, whether generated internally or externally. GAR adjusted the model to simplify the computations. The dominating factors controlling the signal propagation and attenuation were retained in the analysis. These factors included the antenna gain-bandwidth product, the soil attenuation characteristics, the transmission coefficient at the air/soil interface, and the radar cross section of the pipe.

4.1 SUBSURFACE TARGET DETECTION MODEL

The model selected was developed by the National Bureau of Standards (NBS) as part of a research project for the U.S. Department of the Interior, Bureau of Mines⁵. This section describes that model and the approximations used by GAR to simplify the pipe target analysis. The basis for the model is the radar range equation. The model estimates the received signal power as a function of GPR system parameters, soil parameters, and target parameters. The model accounts for only one RF frequency at a time; thus, the model should be evaluated for all of the discrete frequencies in the RF frequency band of interest. The radar equation is given below:

$$S = \frac{PG_s}{4\pi R^2} \frac{\sigma}{4\pi R^2} \frac{\lambda^2 G_t}{4\pi} |C_d D e^{-4\alpha R}|, \quad (4.1)$$

where

- S = received signal power,
- P = transmitter output power,
- G_1, G_2 = gains of the transmit and receive antennas, respectively
- σ = target radar cross section,
- λ_s = wavelength of electromagnetic energy in air,
- α = the attenuation factor of the complex propagation constant,
- I = two-way power transmission at the air/soil interface, accounting for dielectric differences,
- D = dispersion effect due to the medium resulting in pulse stretch and subsequent amplitude reduction,
- R = range from the radar antenna to the target,
- R_1 = the part of the range in the soil only,
- C_d = factor accounting for the two-way refraction at the air/soil interface.

In Equation (4.1), the left-most fraction is the power density at the target, and the second is the reflected power density at the receiver, based on the target radar cross section. These power densities assume a free space environment. The right-most fraction is the effective aperture of the receiving antenna. The remaining terms account for the losses associated with the soil and the air/soil interface.

Several simplifying assumptions were made for the GAR analysis using the model in Equation (4.1). First, the antenna and its phase center were assumed to be on the surface so that $R_1 = R$. Second, the factors C_d and D were neglected. Third, a monostatic GPR configuration was assumed, so $G_1 = G_2$. Fourth,

the soil was assumed to be homogeneous. The first two simplifications were instituted because detailed information concerning the antenna radiation pattern for each of the frequencies of interest was required if the factors C_d and D , as well as the antenna phase center were included in the analysis. This information was not available and it was felt that these parameters did not have the significant impact on the analysis that the remaining parameters had.

The radar cross section of a target is defined as the ratio of the power density of the scattered wave at the receiver to the power density of the incident wave at the target, multiplied by $4\pi R^2$, where R is the distance from the source to the target. For this analysis, a pipe target was assumed to be an infinitely long cylinder and the incident electromagnetic field was assumed to be polarized parallel to the pipe axis. The NBS radar cross section model of an infinite cylinder assumed that the distance from the source to the cylinder was very large with respect to the wavelength of the electromagnetic energy, so that there was plane-wave incidence at the cylinder.

Equation (4.2) gives the radar cross section for the cylinder at plane wave incidence:

$$\sigma_{\text{prt}} = 8R |P|^2 / k \quad (4.2)$$

where, P is given by:

$$P = - \sum_{n=0}^{\infty} (-1)^n e_n J_n(ka) \left[\frac{\cos n\phi}{H_n^{(2)}(ka)} \right] \quad (4.3)$$

Here, $e_n=1$ for $n=0$ and $e_n=2$ otherwise, J_n are Bessel functions, $H_n^{(2)}$ are Hankel functions, $k=(\omega^2\mu_0\epsilon_0\epsilon^*)^{1/2}$, and a is the cylinder radius.

For regions where $ka < 0.05$, the solution for Equation (4.3) may be approximated by a Rayleigh function. For regions where $ka > 6$, Equation (4.3) may be approximated by a geometric optics solution. For the intermediate region of ka , the exact solution for Equation (4.3) is used for maximum accuracy.

The value of ka for most GPR applications falls into the intermediate region. However, to simplify the analysis considerably, at the risk of some tolerable inaccuracy, the GAR approach utilizes the geometric optics approximation for the radar cross section of the pipe using a monostatic radar. This radar cross section is given by:

$$\sigma_r \approx R\pi a \quad (4.4)$$

4.2 EXAMPLE CALCULATION USING THE NBS MODEL

The following example will illustrate the use of the NBS model for predicting the radar return from a buried pipe. The simplifying assumptions outlined in Section 4.1 will apply for this example. Although the accuracy of the model is compromised by the assumptions, the reader should keep in mind that the object of the assumptions was to allow a quick assessment of potential GPR performance in a given environment. Note that the radar range equation model that is used assumes a homogeneous soil and neglects the effects of clutter. Also, the assumptions are made that the GPR antenna system is monostatic and the antenna (and its phase center) is in contact with the ground surface.

The key element in the radar range equation model is the specification of the antenna parameters. GAR selected a TEM horn antenna for this application. This particular antenna is used by GAR for its RODARTM ground-penetrating radar system. The antenna was originally developed by R. Wohlers at Calspan, and its radiation characteristics in air are well documented⁶. The antenna has many of the desirable properties that a pulse GPR system requires. It has a low voltage standing wave ratio (VSWR); it is extremely broadband; it has good group delay properties; and it has low pulse stretch.

The antenna gain, in air, was measured for one of the Calspan TEM antennas and is given approximately by⁵:

$$G = 4\pi (L^2/\lambda^2) \sin \theta_0 \quad (4.5)$$

where L is the antenna length, θ_0 is equal to the angle between the two antenna plates divided by two, and λ is the wavelength

of the RF energy. The antenna under consideration had a length, L , of one meter and an angle between the plates of 11.6 degrees. The effective aperture of the antenna was measured in air⁶ and a plot of the measured effective aperture vs. frequency is shown in Figure 4.1.

The performance of the antenna in contact with the soil is different than its performance in air. Specifically, its gain and effective aperture increase somewhat when the antenna contacts the ground due to the larger dielectric constant of the soil. Also, the soil interface is in the near-field region of the antenna. Thus, it is difficult to evaluate the transmitted power density at the soil interface. For this reason, the parameters of the antenna measured in air, rather than those measured in the ground-contacting mode, are used in the radar range equation model.

The soil parameters selected for this example were obtained from a red clay soil found near the GAR facility in Marietta, Georgia. It was assumed that the clay had a moisture content of 20 percent by dry weight. The soil data are presented in Appendix A.

The RF frequency range for the example was chosen to be from 100 megahertz (MHz) to 300 MHz. This bandwidth is equivalent to about a five-nanosecond pulse width in the time-domain. The radar range equation was evaluated at 100 MHz, 200 MHz, and 300 MHz.

The subsurface target was selected to be a 12-inch diameter metal pipe buried at a depth of three meters (measured from the surface to the top of the pipe). The pipe was considered to be infinitely long. Its radar cross section was assumed to be described by the NBS model for a cylinder in the geometric optics region.

Equation (4.6) below is the modified NBS radar range equation that was used for the GAR evaluation. The equation expresses the ratio of received power to transmitted power as a function of the soil parameters, antenna parameters, and target parameters.

$$S/P = \frac{1}{4\pi R^2} \frac{\sigma}{4\pi R^2} G_1 A_1 I e^{-4\alpha R} \quad (4.6)$$

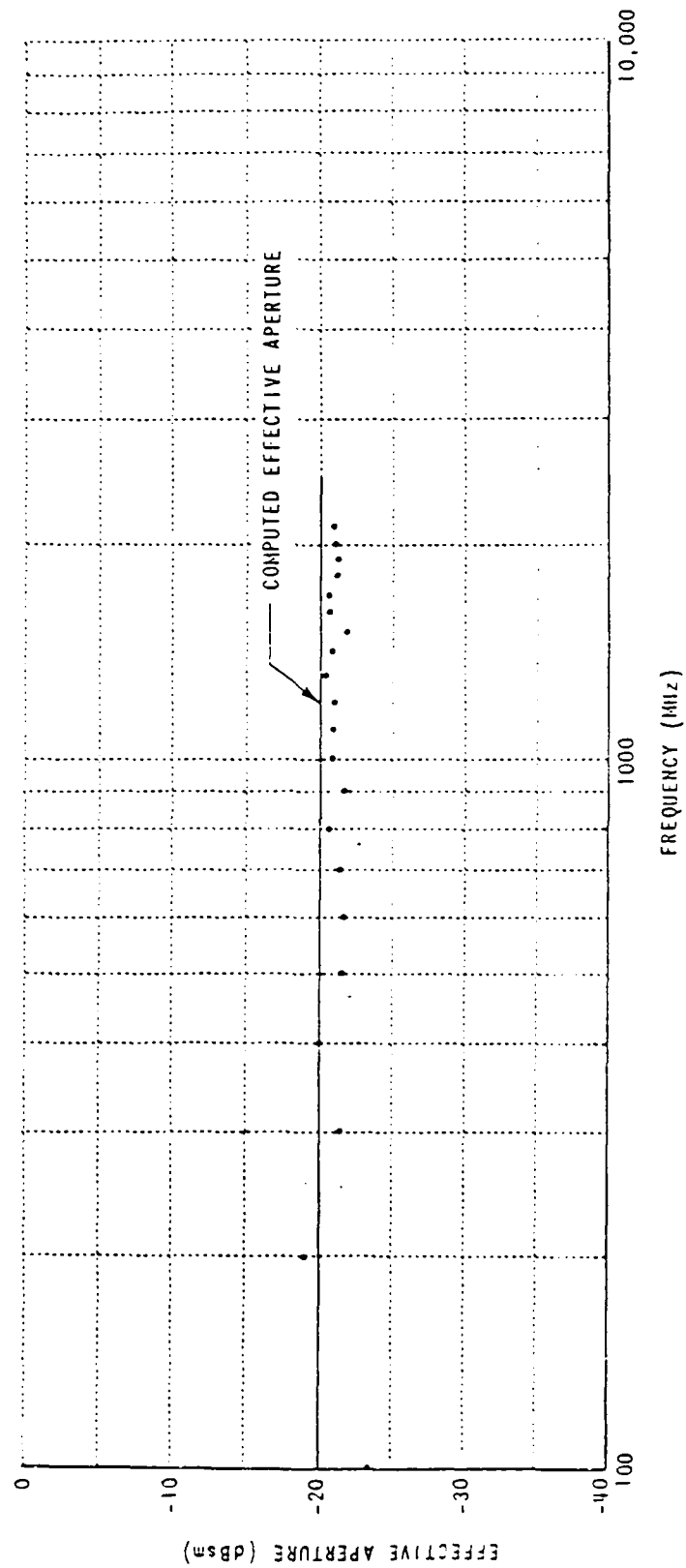


Figure 4.1: Plot of TEM horn antenna effective aperture.

where, $A_e = (\lambda_o^2 G_t)/4\pi$ is the effective receiving aperture of the antenna, and the factors C_d and D in Equation (4.1) have been neglected.

Table 4.1 summarizes the soil, antenna, and pipe parameters used in Equation (4.6) for the frequencies of 100 MHz, 200 MHz, and 300 MHz. The results obtained from Equation (4.6) for the S/P ratios reflect tremendous signal attenuation, extending from -142 dB at 100 MHz to -162 dB at 300 MHz.

We feel, however, that these calculations are somewhat pessimistic because the performance of the antenna near the soil interface is unknown, but is likely better than that assumed in the calculations. Thus, a more exact analytical approximation of the received target signal power would probably yield a more optimistic answer for the received power level. However, the results obtained based on our approximations lend insight into the performance requirements that must be imposed on a successful GPR system.

TABLE 4.1. RESULTS OF NUMERICAL ESTIMATION OF PIPE TARGET
DETECTION FOR FREQUENCIES OF 100 MHZ,
200 MHZ, AND 300 MHZ.

<u>Parameter</u>	FREQUENCY (MHz)		
	<u>100</u>	<u>200</u>	<u>300</u>
σ (m ²)	1.44	1.44	1.44
A_s (m ²)	0.01	0.01	0.01
G	0.014	0.058	0.130
α (Nepers)	1.15	1.50	1.73
I	0.426	0.458	0.458
ω (radians/s)	6.28×10^3	1.26×10^9	1.88×10^9
S/P	6.82×10^{-15}	4.55×10^{-16}	6.46×10^{-17}
S/P (dB)	-142	-153	-162

SECTION 5

DESIGN OF THE SCALE-MODEL TEST TANK

A soil test tank was required to test the various GPR signal source types. The test tank was designed to contain various pipe targets, metal plate targets, and electromagnetic field probes in order to test candidate GPR systems. The GPR system requirements provided by NCEL included the specification to detect and resolve plastic and metal pipes buried at depths of up to 20 feet. Care was taken to ensure that the dielectric medium in the test tank was homogeneous to obtain repeatable measurements and reduce the effects of random external clutter.

GAR decided to evaluate the GPR sources using a higher-frequency scale model than the operating frequency of a full-scale GPR. Such a scale model is much easier to use while making laboratory measurements than is a full-scale system because of its reduced size. However, the scale model provides measurement results that apply directly to the full-scale system.

5.1 DESCRIPTION OF THE GPR SCALE-MODEL CHARACTERISTICS

To create a high-frequency scale model for a GPR, the radar environment, as well as the radar system parameters, must be adjusted. All spatial dimensions are reduced by the scaling factor, resulting in a much smaller testing environment and a radar system that is more manageable. The target dimensions and burial depths are also reduced by the scale factor.

Several types of scale models are outlined in Antennas in Matter by King and Smith⁷. The one selected by GAR permits the use of the same relative dielectric constants in the model that are found in the full-scale environment. This means that air can be used as a dielectric in the model. Otherwise, if the dielectric constants were scaled, air could not be used in the model environment, since its dielectric constant would have to be scaled. The dielectric parameter that is scaled in the GAR model is the soil conductivity, and hence, its attenuation.

For example, assume that a full-scale GPR system is to be modeled using a scale factor of 5. Let the RF bandwidth of the full-scale GPR extend from 100 MHz to 300 MHz. Furthermore, assume that the full-scale soil parameters include a relative dielectric constant of 16 and an attenuation characteristic of 10 dB/m. The scale-model RF bandwidth would then extend from 500 MHz to 1500 MHz. The model-soil dielectric constant would remain at 16, but its attenuation characteristic would increase to 50 dB per meter.

GAR chose the scale-model soil tank dimensions to be six feet wide by eight feet long by four feet high. This corresponds to full scale dimensions of 30 feet by 40 feet by 20 feet. The targets were appropriately placed in the model soil to avoid boundary effects. They were also placed in such a manner as to avoid any interference with each other.

The scale factor selected for the model was five. This scale factor allowed GAR to use its one-nanosecond monocycle short-pulse radar to model a full-scale GPR system with a five-nanosecond pulse. A five-nanosecond pulse is of the duration that might be used for a GPR system designed for deep penetration and medium resolution.

GAR investigated two approaches to building a scale-model environment. One approach used a soil that had the required parameters of the model dielectric. The second approach used a liquid dielectric. The liquid dielectric used an emulsion of oil, water, and salt to achieve the required properties of the model dielectric. Dr. Glenn Smith of the Georgia Institute of Technology has previously investigated and used such liquid dielectrics as soil models.

5.2 THE LIQUID-DIELECTRIC SOIL MODEL

The liquid-dielectric model had three key advantages over a soil dielectric. First, the liquid tank has the potential of being more homogeneous than a soil dielectric. Second, the targets and their positions can be easily changed. Third, the effects of the liquid tank boundaries can be easily eliminated in any target measurements after a "baseline" measurement is made of a target-free tank. In general, eliminating the

boundary effects in a soil dielectric tank is not possible because the removal and insertion of the targets would disturb the soil, which could never be replaced in exactly the same configuration. Furthermore, a controlled clutter environment could easily be placed in the liquid-dielectric tank to examine the effects of external clutter on the GPR systems.

The emulsion created for use in the liquid tank could be made to model selected soil dielectrics. Dr. Smith uses a high-grade, light mineral oil, water, and salt as the emulsion ingredients. He has investigated many different combinations of emulsion ingredients and their ratios. The dielectric properties of these emulsions were measured and used to create sets of curves that allow the specification of a particular emulsion mix ratio to achieve a given liquid dielectric constant and loss characteristic.

The primary drawback in using a liquid tank with a large volume was the need to mix and maintain a homogeneous emulsion of the liquid dielectric. A tank with dimensions of six feet by eight feet by four feet holds over 1400 gallons of liquid. To correctly mix and maintain the emulsion, a shearing gear pump would be required that must operate at a high flow rate. The emulsion must be circulated very quickly during mixing to ensure a homogeneous mix. Furthermore, the emulsion must be re-circulated and mixed prior to each measurement to ensure its homogeneity and the accuracy of its dielectric properties.

At the time the GAR model-soil parameters were specified, Dr. Smith had not built a liquid-dielectric tank of such large dimensions. The cost and logistics of fabricating a large tank, purchasing the necessary pumps, and constructing a working model tank appeared to be quite formidable. In addition, there was a significant technical risk in making a large tank work properly as a model. GAR felt that the technical risks and the costs associated with the liquid tank precluded its use in the measurement program. GAR elected to construct a soil tank instead.

5.3 THE SOIL-DIELECTRIC MODEL

A model tank containing soil is much easier and less costly to construct and maintain than a corresponding liquid tank. However, any change in target placement once objects are buried is much more difficult with the soil tank. In addition, the effects of any inhomogeneities and of the tank boundaries are difficult to characterize and their effects on the target measurement are very difficult to remove.

In order to build the soil tank, GAR had to locate a source of homogeneous soil with electromagnetic properties suitable for use as a model soil. Thus, a local brick manufacturer was contacted and arrangements were made to test the properties of the clay soils that they used for the bricks. The brick manufacturer used two types of clays in the bricks, which were identified as a clay shale and a clay schist. Appendix B contains the measured characteristics of these clays. The GPR source evaluation and measurement program required the use of at least two soil dielectrics. This allowed evaluation of the performances of the GPR systems with different soil types. Therefore, the two clays from the brick manufacturer would satisfy this requirement.

The properties of the clay shale approximated those of actual clay with 20 percent moisture as given in Appendix A. The shale had an attenuation characteristic of 50 dB/m at 1 GHz. This attenuation scaled to 10 dB/m at 200 MHz. The schist had an attenuation characteristic of 33 dB/m at 1 GHz, which scaled to 6.6 dB/m at 200 MHz.

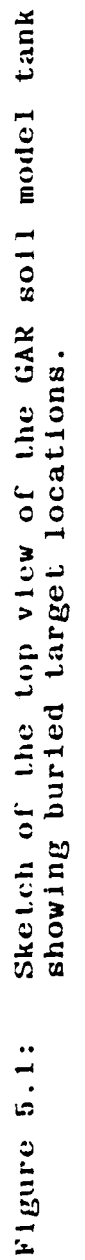
GAR decided to use the clay shale as the first soil in the soil-model tank. Sixteen targets were buried in a six-foot by eight-foot by four-foot high soil test tank. Thirteen pipes with diameters ranging from 0.88 inch to 6.63 inches were used. The pipe diameters increased with burial depth. Each pipe target was two-feet seven-inches long. For each metal pipe there was a corresponding PVC plastic pipe of similar diameter. The one exception was the 6.63 inch diameter metal pipe that was five-feet six-inches long and buried at a three-foot depth. No plastic pipe of a comparable size was buried in the model tank.

Figures 5.1 and 5.2 are sketches of a top view and a side view, respectively, of the soil-model tank. The sketches show the locations of the pipe targets. In general, one side of the tank was reserved for metal pipes and the other was reserved for plastic pipes. The exception to this was the 6.63 inch diameter pipe which extended across the entire tank. In addition to the 13 pipes, three metal plate targets of various sizes and burial depths were also included in the tank. Each of these plates had a half-loop H-field probe mounted on it. The probes had a 0.25 inch radius and used the plates as an image plane. The probes were included as sensors to detect any energy reaching them. The reader should note that energy reaching the loop probes was only subjected to one-way attenuation through the soil.

The targets in the soil tank were arranged to minimize potential electromagnetic interference between each other and the tank boundaries. The pipe diameters and burial depths were largest at the center of the tank. The shallow, smaller pipes were located at the tank edges.

During construction, care was taken to maintain soil homogeneity in the tank. This was accomplished by tamping the clay every six inches as the tank was filled. The tank was covered with a thin sheet of polyethylene plastic to minimize the evaporation of moisture from the model soil. If the moisture had evaporated from the soil tank, the electromagnetic soil properties would have been altered.

After the measurements were performed with the clay shale, the shale was removed and replaced with the clay schist. Target and probe locations were the same as they were with the clay-shale tank.



SECTION 6

DESCRIPTION OF THE GPR SYSTEMS TESTED

GAR tested four GPR systems representing time-domain and frequency-domain technologies. Two of the systems used short-pulse, time-domain techniques; and the other two systems used frequency-modulation techniques. The basic operations of the two time-domain radar systems were quite similar, and the operations of the two frequency-domain radars were also very similar. However, the time-domain radar systems functioned quite differently in concept from the frequency-domain radars.

One of the time-domain radar systems tested was built by GAR for the RODARTM highway-surveying short-pulse radar system, and the other was a Geophysical Survey Systems, Inc. (GSSI) short-pulse radar. Both FM systems were based on the HP 8510 microwave network analyzer. The radar systems used for the tests are described below.

Comparisons between the FM systems and the GAR short-pulse radar were made using antennas built by GAR specifically for this testing program. However, due to the use of an integrated transmitter, receiver, and antenna assembly in the GSSI system, this unit could not be used with the GAR-built antennas. Therefore, it was not possible to make direct comparisons between the GSSI radar and the others.

6.1 THE GAR SHORT-PULSE RADAR SYSTEM

The GAR short-pulse radar system used for the testing program included a transmitter pulser, equivalent-time sampling receiver, antenna, oscilloscope display, and chart recorder display. A block diagram of the GAR short-pulse radar is shown in Figure 6.1 and the system specifications are given in Table 6.1.

The radar uses a 15 MHz timing reference, from which all other timing signals are derived. These timing signals are developed on the radar timing board. The 15 MHz reference is divided down to a 5 MHz pulse repetition frequency (PRF) and a

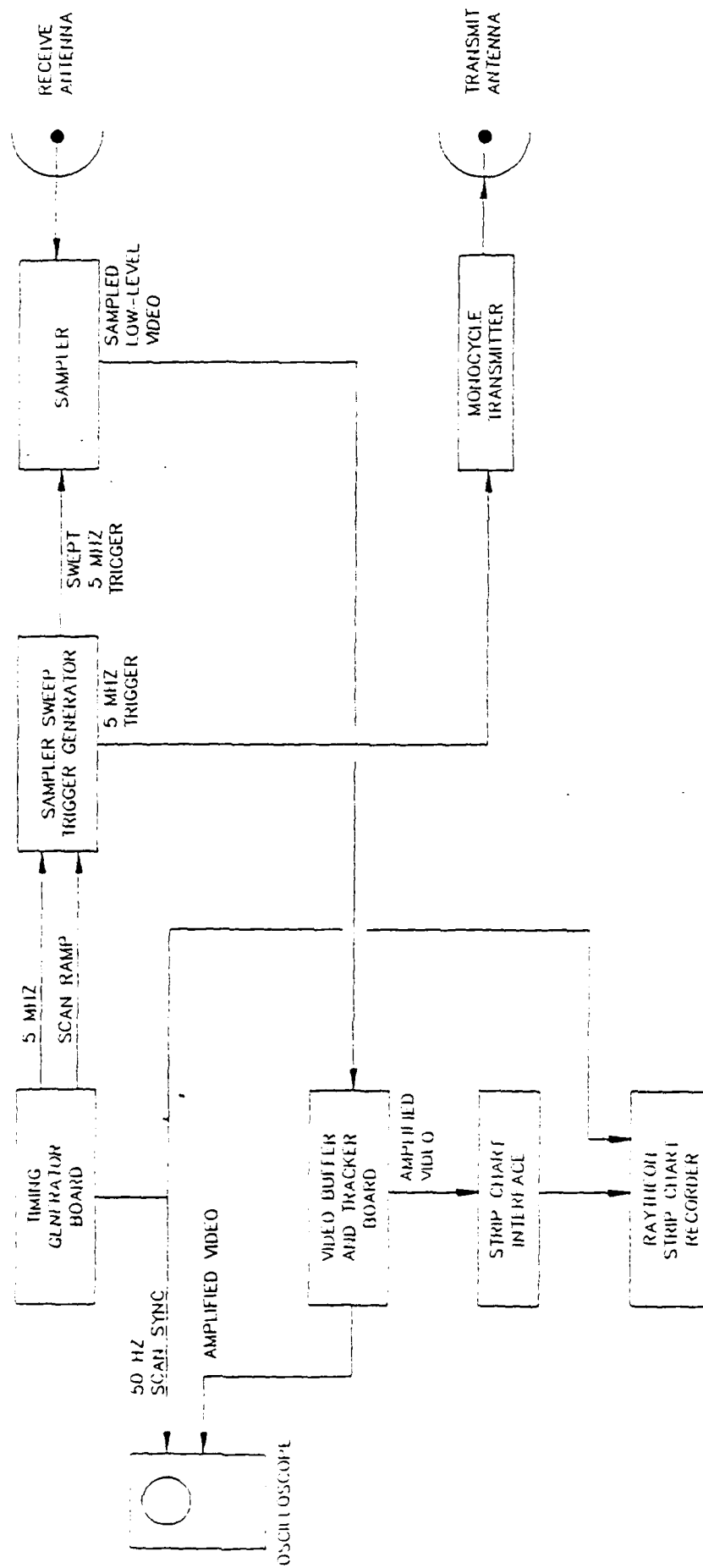


Figure 6.1: Block diagram of the GAR short pulse radar system.

TABLE 6.1. GAR SHORT-PULSE RADAR SYSTEM SPECIFICATIONS.

Transmitter

Pulse shape	Sine monocycle
Pulse repetition frequency (PRF)	5 MHz
Pulse width	1 nanosecond
Pulse amplitude	20 v peak-to-peak
Pulse peak power	8 watts
Pulse average power	40 mw (+16 dBm)

Sampler

Type	Single diode gate, 50 ohm terminated
Sample strobe width	400 picoseconds

Receiver

Type	Equivalent-time sampling
Frequency division ratio	500,000
Scan repetition frequency	50 Hz
Real-time receiver window width	36 nanoseconds
Minimum discernible signal	2 mV, terminated in 50 ohms
Dynamic range	60 dB

50 Hz scan frequency. The timing board generates a 50 Hz scan ramp that is used in the receiver, along with the 5 MHz PRF signal, to generate its sweeping sampler trigger signal.

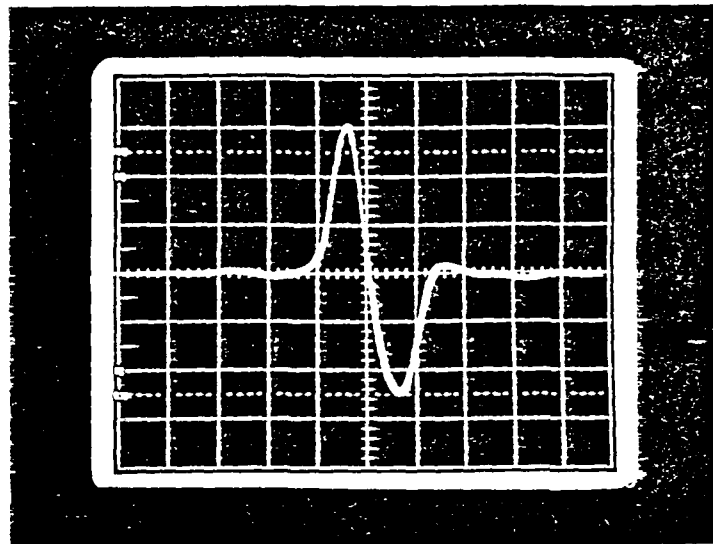
The GAR short-pulse radar uses a transmitter that generates a one-nanosecond pulse shaped as a single cycle of a sine wave. The transmitter operates at a PRF of 5 MHz and produces a power output of 8 watts peak and 40 milliwatts average. When specified in decibels referenced to a milliwatt (dBm), the power output is +39 dBm peak and +16 dBm average. The pulse has approximately a 20 volt amplitude into a 50 ohm load. The transmitter output waveform and frequency spectrum are shown in Figure 6.2.

The receiver is an equivalent-time sampling type that generates a low-frequency replica of the received RF waveform. An equivalent-time sampler does not sample a signal at the true Nyquist frequency, where the Nyquist frequency is defined as the minimum sampling frequency required to sample a waveform without aliasing. This frequency is equal to twice the highest frequency present in the waveform. Clearly, since the GAR short-pulse radar generates a one-nanosecond pulse, the true Nyquist frequency is in the GHz region.

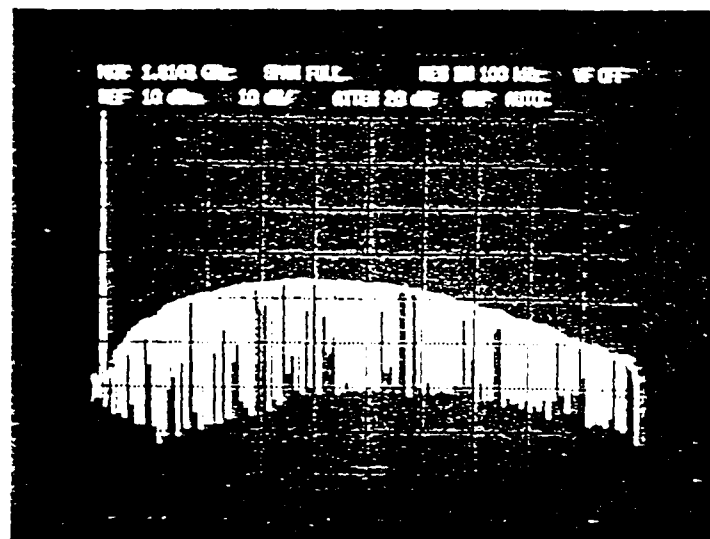
The sampling receiver implements a 500,000:1 frequency division ratio. The receiver output waveform occurs at a 50 Hz scan rate, or a 20 millisecond scan period. However, the actual sampled waveform duration is only 18 milliseconds, due to a 2 millisecond reset time for the receiver. The real-time window is set to 36 nanoseconds. Thus, a one-nanosecond pulse is converted to a 500 microsecond pulse by the equivalent-time receiver.

The equivalent-time sampling technique avoids the problems associated with an extremely high real-time sampling frequency by utilizing frequency division. The only requirement is that the sampled waveform be repetitive. For a short-pulse radar, this is equivalent to requiring that the received radar signal be stationary in time over a receiver scan period.

The sampler takes one sample during each period of the PRF, delaying it slightly each time relative to the previous one. Each successive sample modulates the charge on a sampling storage capacitor. The GAR short-pulse waveform is sampled



(A) MONOCYCLE TRANSMITTER OUTPUT WAVEFORM.
 VERTICAL SCALE = 3.55 VOLTS/DIV.
 HORIZONTAL SCALE = 500 PS/DIV.



(B) FREQUENCY SPECTRUM OF THE ABOVE PULSE.
 HORIZONTAL SCALE = 180 MHZ/DIV.

Figure 6.2: GAR short-pulse radar transmitter (a) output waveform and (b) its frequency spectrum.

once every period of the 5 MHz PRF for 18 milliseconds. Since, 90,000 periods of the PRF exist in the 18 millisecond sampled-waveform window, 90,000 samples are required to replicate a 36 nanosecond real-time window. The equivalent sample spacing of the receiver is approximately:

$$36 \text{ ns}/90,000 = 0.4 \text{ picosecond}, \quad (6.1)$$

which easily meets the Nyquist criterion.

The receiver RF sampler is a 50 ohm terminated, single-diode-gate sampler using a Schottky sampling diode. The sample strobe is nominally a 10 volt, 400 picosecond pulse. The maximum input level that the sampler can handle is 4 volts peak-to-peak. There is approximately a 6 dB conversion loss through the sampler. The minimum discernible signal at the sampler output is 2 millivolts. Therefore, the sampler dynamic range is 60 dB.

6.2 THE GSSI SHORT-PULSE RADAR SYSTEM

The GSSI short-pulse radar used for the tests with the soil-model test tank operates in a similar fashion as the GAR short-pulse radar. However, the specifications, timing functions, and operating modes for the GSSI radar system are not as well known by GAR personnel as those for the GAR short-pulse radar. During tests, the radar was operated with minimum use of its signal processing functions in order to make objective comparisons with the other GPR systems.

The GSSI radar uses a one-nanosecond transmitter pulse and an equivalent-time receiver. The transmitter pulser generates a balanced, one-nanosecond, unipolar impulse. It operates at a system PRF of approximately 50 kHz. Its peak power output is unknown, but is comparable to the GAR monocycle transmitter power output. Its average power output, however, is less than the GAR transmitter because it operates at a PRF that is 100 times lower.

The GSSI receiver is a balanced diode-bridge sampler that operates in an equivalent-time mode. It has an adjustable real-time window and an adjustable output waveform scan rate.

The radar was adjusted for the tests to operate with a scan frequency of 51.2 Hz (a 19.5 millisecond period). The equivalent-time frequency division ratio was adjusted to 500,000:1 to match the GAR system. The GSSI receiver has a reset time of about 400 microseconds. Therefore, the real-time window is 39 nanoseconds long. Based on a 50 kHz PRF, 977 samples are used to generate the replica waveform. This translates into a 40 picosecond equivalent-time sample spacing.

Figure 6.3 is a block diagram of the GSSI short-pulse GPR. The radar timing and control signals are generated in the control unit. Trigger signals are sent to the transmitter and sampling receiver through a cable. The sampler output waveform is sent by cable to the control unit for further processing. The receiver output waveform can be displayed on an oscilloscope and a strip chart recorder.

The transmitter and sampler are housed with their respective antennas in an integrated transducer enclosure. The radar operates in a bistatic mode using triangular-sheet bow-tie antennas. The exact construction of the receiver, transmitter, and antennas is not known because it is not possible to gain access to any of the components in the transducer.

6.3 THE FREQUENCY-DOMAIN GPR SYSTEMS USING THE HP 8510 NETWORK ANALYZER

This section gives an overview of the Hewlett-Packard 8510 network analyzer system and describes its application to the GPR signal source testing program. An explanation of all of the functions and capabilities of the HP 8510 is beyond the scope of this document. However, Appendix C contains an excerpt from the HP 8510 manual and provides a good introduction and system overview. Appendix C also contains a simplified block diagram of the network analyzer system. The present section only addresses those functions of the HP 8510 that are directly applicable to the GPR measurement program.

The HP 8510 was used in two modes for the GPR measurements. The first was a swept-frequency mode that used a synthesized sweeper in its linear frequency sweeping mode to

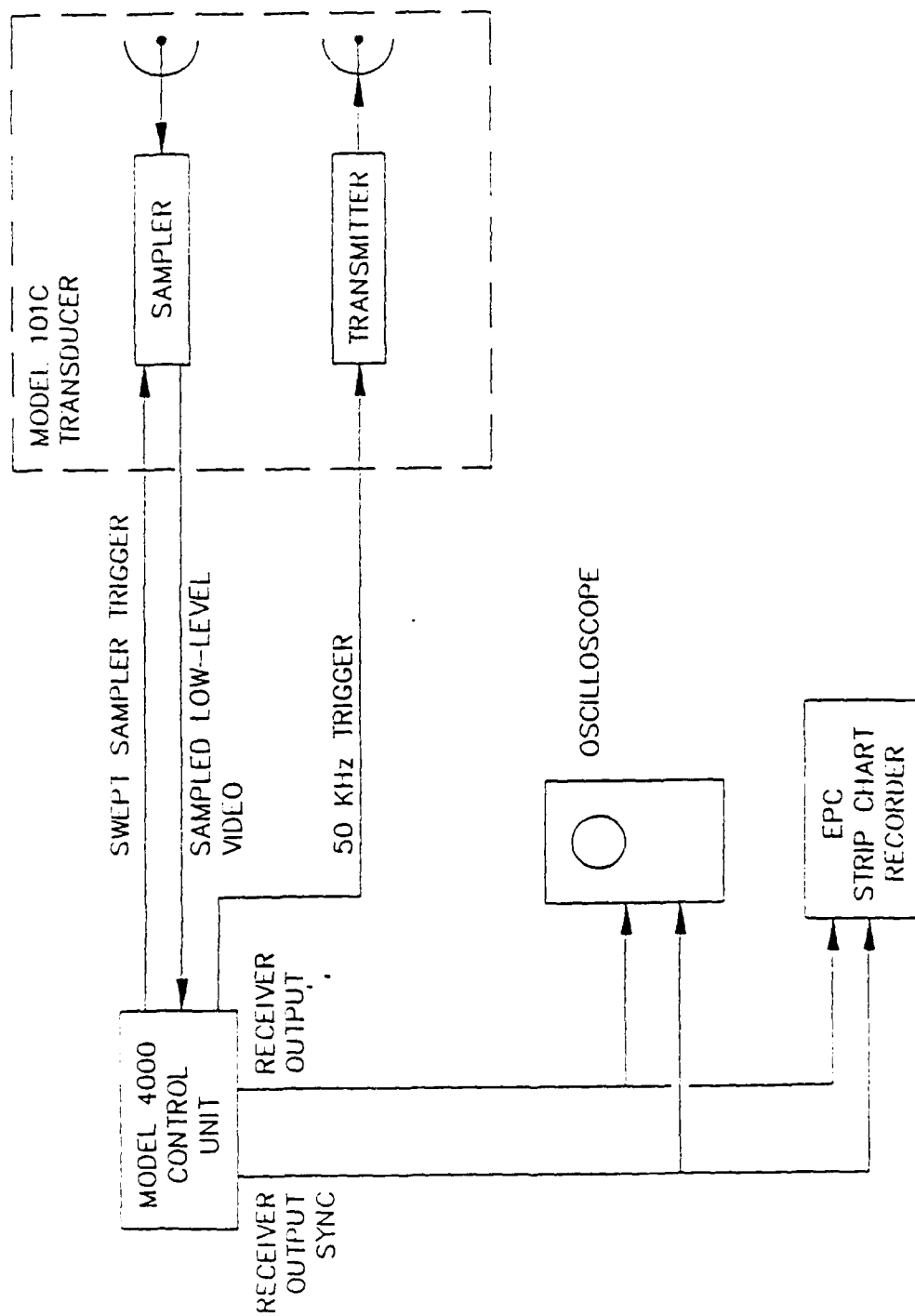


Figure 6.3: Block diagram of the GSST short-pulse radar.

generate the increasing-frequency sweep of RF signal frequencies required for the measurements. This mode represented a simulation of a swept FM-CW GPR system. The second mode of operation for the HP 8510 simulated a stepped-FM GPR by using a stepped-frequency signal source.

Section 6.3.1 below explains some of the common capabilities of the HP 8510 that were used in both the FM-CW and stepped-FM system tests. Section 6.3.1.3 describes the differences between the swept and stepped operating modes of the HP 8510.

6.3.1 HP 8510 NETWORK ANALYZER CAPABILITIES

The Hewlett-Packard 8510 network analyzer is a precision instrument used for making RF and microwave measurements of two-port networks. The 8510 measurement system includes the following four subsystems: a frequency source, a test set, a signal detector and analog-to-digital converter, and a microprocessor and display. The HP 8510 system configuration used by GAR for this program included an HP 8341A synthesized sweeper, an HP 8513A transmission test set, an HP 85102A IF detector, and an HP 85101A display processor. This HP 8510 configuration allows measurements to be made over the frequency range from 45 MHz to 20 GHz.

6.3.1.1 SCATTERING PARAMETER MEASUREMENTS WITH THE HP 8510

The HP 8510 is designed to make vector (signal amplitude and phase) scattering parameter (S-parameter) measurements of a two-port electrical network. Measurements of devices at RF and microwave frequencies primarily use S-parameters because S-parameters are well-suited to describing the performance of transmission line-based circuits and systems. The S-parameters are quite useful for characterizing networks at RF and microwave frequencies because they are directly related to the amount of power reflected at the test network ports and the amount of power transmitted through the device. The derivation and advanced applications of S-parameters are described in texts treating the subject of RF and microwave applications³.

The S-parameters are often normalized to impedances of 50 ohms. This implies that the network has an input impedance and output impedance of 50 ohms. Thus, any connecting transmission lines and test cables should have 50 ohm characteristic impedances as well. GPR test equipment configurations including the HP 8510 used 50 ohm coaxial cables to connect the antennas to the test set ports. Also, the antennas have nominal input impedances of 50 ohms.

The two-port network measurements using S-parameters are sub-divided into those related to transmission through the network (forward and reverse), and those related to reflections at the two network ports. Transmission measurements include insertion loss or gain, transmission coefficient, electrical delay, and group delay. Reflection measurements include return loss, voltage standing wave ratio (VSWR), reflection coefficient, and impedance.

The measurement quantities of primary interest in this testing program are the reflection coefficient, S_{11} , and the transmission coefficient, S_{21} . If 50 ohm impedance normalization is used, S_{11} is the ratio of the reflected voltage to the incident voltage at port one of the two-port network under test. The measurement of S_{11} requires that port two of the network be properly terminated while port one is being driven by a signal source with a 50 ohm driving impedance. S_{21} is the ratio of the voltage measured at port two of the network to the incident voltage at port one, with port one being driven by the signal source. The 50 ohm termination and driving impedance requirements apply to the S_{21} measurement as well.

If an antenna is connected to port one of the HP 8513A test set, the parameter S_{11} represents a measurement of the energy reflected by the antenna itself and any targets that reflect radiated energy back to the antenna. This configuration represents both a one-port network and a monostatic radar system.

If an antenna is also connected to port two of the test set, the parameter S_{21} represents the energy received at port two through the two-antenna network. The energy received at port two includes reflections from targets irradiated by the port one antenna. This configuration represents a two-port

network and a bistatic radar system. The measurements conducted with the soil-model tank were performed with a bistatic arrangement, measuring the S_{21} parameter.

When S_{11} and S_{21} measurements are made with the network analyzer, the RF frequency range of interest must be specified. Whether in a ramp mode or a stepped mode, the network analyzer adjusts the frequency of its signal source and makes S-parameter measurements at a number of individual frequencies throughout the specified bandwidth. The number of frequencies is selectable, with the available choices being 51, 101, 201, and 401. The effects of choosing a particular number of measurement frequencies are discussed later.

Once the frequency range, the number of frequency points, and the ramp or stepped mode are selected, the network analyzer requires calibration. Calibrating the network analyzer reduces measurement errors. The vector calibration identifies the measurement reference planes at the two network ports and corrects for any losses or phase aberrations up to the reference planes. Thus, the calibration procedure can be used to establish the reference planes for a S_{21} measurement at the ends of the antenna cables. The HP 8510 then corrects for any cable loss and phase effects.

The network analyzer calibration procedure requires measurements of known terminations at the reference planes before the test network is inserted for measurements. The standard terminations include a shielded open circuit, a short circuit, and a 50 ohm load (a 50 ohm sliding load termination is required if precise, high-frequency measurements are to be made). Once the standard terminations are measured and the network analyzer computes its vector correction factors, all subsequent measurements automatically apply the correction factors to the data. The HP 8510 uses an elaborate S-parameter error model to compute the correction factors, the details of which are beyond the scope of this document. However, the HP 8510 manual contains a complete description of the vector error-correction model.

6.3.1.2 HP 8510 TIME-DOMAIN MEASUREMENT MODE

The HP 8510 can display the results of its measurements in the frequency-domain or the time-domain. However, all of its measurements are made in the frequency-domain. The HP 8510 has a time-domain bandpass mode of operation that synthesizes an impulse function with a pulse width inversely proportional to the RF bandwidth specified for the measurement. A type of digital Fourier transform known as the Chirp-Z transform is used to transform measurements of S_{11} and S_{21} from a frequency-domain representation to a time-domain representation. Appendix D contains excerpts from the HP 8510 manual explaining the time-domain synthesis mode of operation.

6.3.1.2.1 TIME-DOMAIN PULSE SYNTHESIS WITH WEIGHTING FUNCTIONS

Once an RF bandwidth is selected for measurements, and the time-domain synthesis mode is selected, frequency-domain weighting functions are applied to adjust the sidelobe levels of the synthesized impulse. Three selectable weighting functions are provided which give maximum sidelobe levels of -13 dB, -43 dB, and -90 dB below the pulse main lobe. These weighting functions are identified as "minimum," "normal," and "maximum," respectively. For a given bandwidth, the cost of increased sidelobe suppression is an increased pulse width for the synthesized pulse.

Figures 6.4 through 6.6 are magnitude plots of one-nanosecond synthesized pulses generated by the network analyzer using the three frequency-domain weighting functions, or windows. The pulse in Figure 6.4 uses the minimum window with a 45 MHz to 1.2 GHz bandwidth; the pulse in Figure 6.5 uses the normal window with a 45 MHz to 2.0 GHz bandwidth; and the pulse in Figure 6.6 uses the maximum window with a 45 MHz to 2.8 GHz bandwidth. All of the plots use a one-nanosecond per division horizontal scale and the pulse magnitude is normalized to one unit, with a linear vertical scale. Note that more RF bandwidth is required to maintain a given pulse width with suppressed sidelobes.

All network analyzer measurements performed with the soil-model test tank used a one-nanosecond pulse having a 45 MHz to

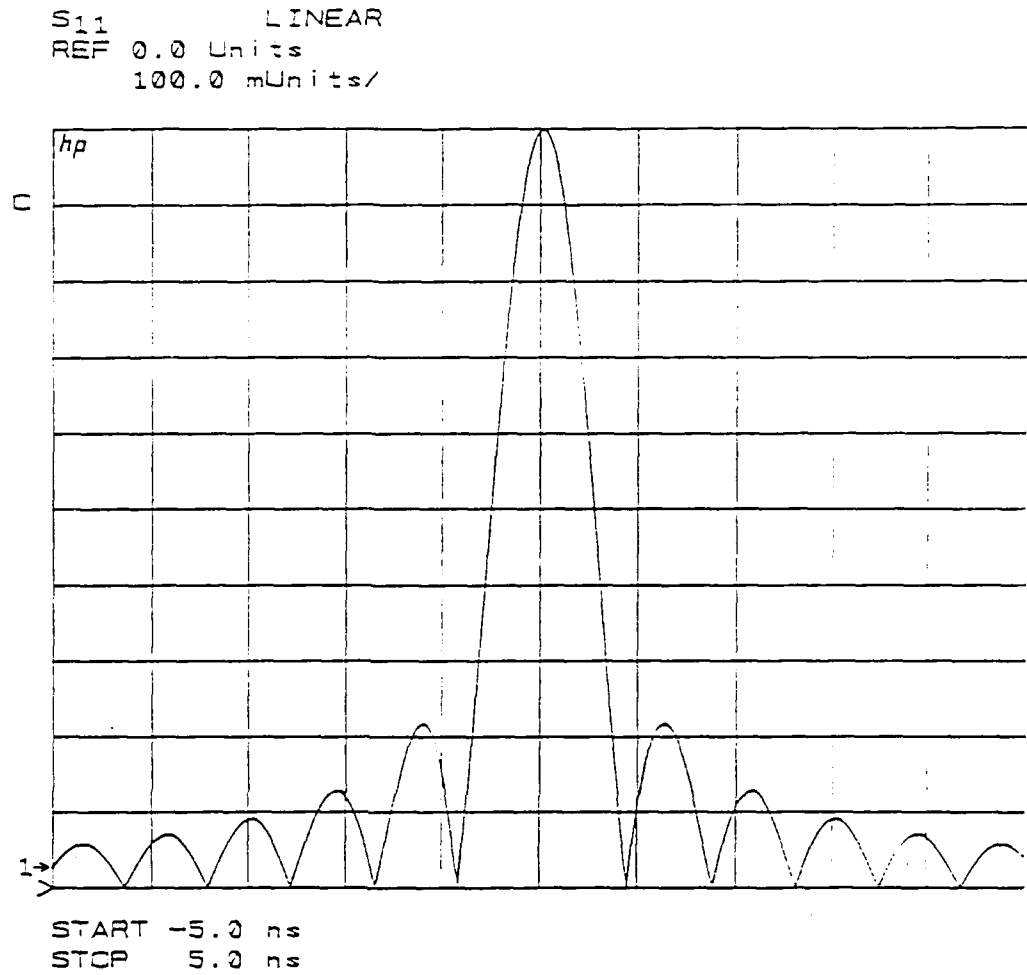


Figure 6.4: HP8510 plot of the magnitude of a 1ns pulse synthesized using the minimum weighting function and a 45MHz-1.2GHz bandwidth.

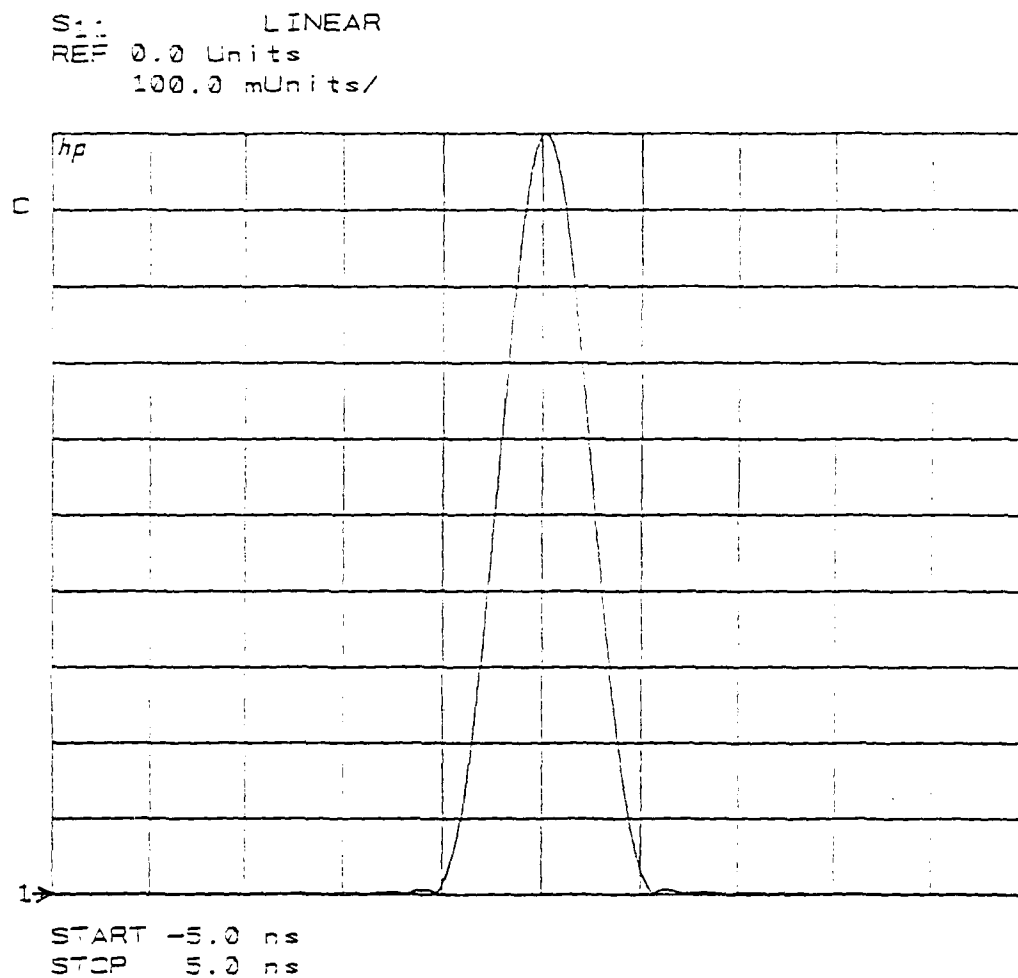


Figure 6.5: HP3310 plot of the magnitude of a 1ns pulse synthesized using the normal weighting function and a 45MHz-2.0GHz bandwidth.

S11 LINEAR
REF 0.0 Units
100.0 mUnits/

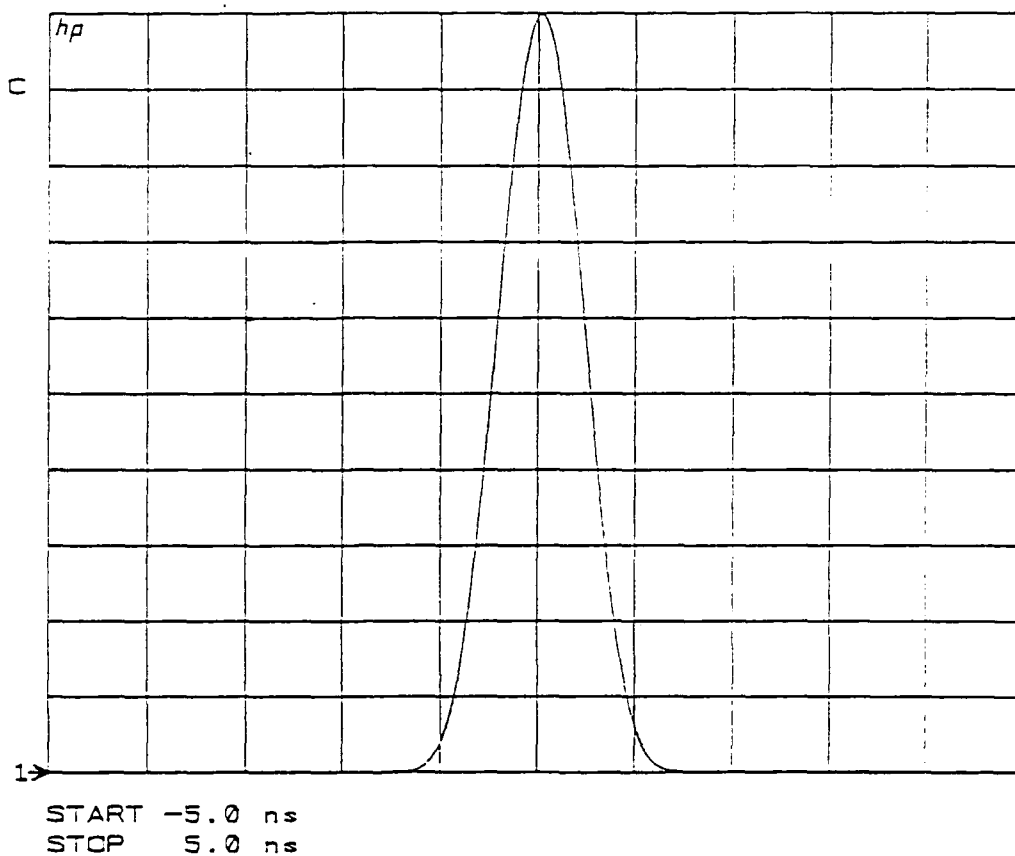


Figure 6.6: HP8510 plot of the magnitude of a 1ns pulse synthesized using the maximum weighting function and a 45MHz-2.8GHz bandwidth.

2.0 GHz bandwidth, and a normal window. The one-nanosecond pulse width was selected to permit a more accurate comparison of the network analyzer system performance with the performance obtained with the pulsed GPR systems. In addition, GAR felt that the bandwidth required for the maximum window was too great, and the bow-tie antennas used for the tests could not support the extended bandwidth. Also, the soil attenuation properties would cause greater attenuation of the higher frequencies, thus widening the pulse.

6.3.1.2.2 EFFECT OF THE NUMBER OF FREQUENCY MEASUREMENT POINTS SELECTED

As indicated earlier, the HP 8510 network analyzer performs its measurements at a finite number of points over the bandwidth specified by the user. The number of points is selectable from 51, 101, 201, and 401. When the network analyzer is operated in the time-domain bandpass mode, it generates the same number of measurement points as specified by the user during the HP 8510 calibration in the frequency-domain.

The number of measurement points and the bandwidth selected determine the unambiguous range in the time-domain mode. The unambiguous range is the maximum range time for which the time-domain waveform will not repeat. This is analogous to the reciprocal of the PRF for a time-domain pulse radar system. The unambiguous range for the network analyzer is equal to the reciprocal of the frequency spacing. For example, if 201 points are selected, and a frequency range of 45 MHz to 2.0 GHz is specified, the unambiguous range is $(201 - 1) / (2.0 \text{ GHz} - 45 \text{ MHz}) = 102.3$ nanoseconds, which corresponds to slightly more than 25 feet in soil with a dielectric constant of 16.

The selection of the number of measurement points also determines the range measurement accuracy of the network analyzer. For the GPR measurements, the range window was selected to be 36 nanoseconds long and the number of measurement points was selected to be 201. Using these quantities as an example, the range measurement accuracy is

given by $36 \text{ ns}/(201-1) = 180 \text{ picoseconds}$, which corresponds to about 0.5 inch in soil with a dielectric constant of 16.

Another important factor affected by the selection of the number of measurement points is the time required to complete a measurement over the specified bandwidth. Increasing the number of measurement points requires an increase in the measurement time. Therefore, doubling the number of points from 201 to 401 will require approximately twice the time to complete the measurement.

6.3.1.3 DIFFERENCES BETWEEN THE HP 8510 SWEPT-FREQUENCY AND STEPPED-FREQUENCY MEASUREMENT MODES

The HP 8510 network analyzer can perform its measurements over a specified frequency band by stepping its frequency source in discrete frequency steps, or by sweeping its source continuously. Stepping the source provides the highest measurement accuracy and dynamic range. In the stepped mode, the HP 8341A synthesizer is stepped and phase-locked to each measurement frequency. This reduces the phase noise effects and the frequency inaccuracies that appear in the swept mode.

When the swept mode is used, the synthesizer is locked to the start frequency and swept linearly to the stop frequency. However, the synthesizer is not locked to any other frequency besides the start frequency. The network analyzer in effect assumes that the synthesizer will be at certain frequency points at certain times during its sweep. It has no way to determine the exact frequency of the synthesizer. Thus, inaccuracies in determining the exact frequency of the synthesizer will exist as it is swept across the specified bandwidth. The primary advantage to the swept-frequency measurement mode is its speed. In the swept mode, the network analyzer produces a measurement on the order of 100 times faster than in the stepped mode.

6.3.2 SUMMARY OF NETWORK ANALYZER CONFIGURATIONS AND SPECIFICATIONS FOR SOIL-MODEL TANK MEASUREMENTS

All measurements performed with the network analyzer on the soil-model test tank used the HP 8510 time-domain bandpass mode. The time-domain range window for the shale clay measurements was set to 36 nanoseconds in duration. It was changed to 40 nanoseconds for the clay-schist measurements because the schist had a higher relative dielectric constant than the shale. The frequency range of 45 MHz to 2.0 GHz with 201 points was selected. A normal weighting function was used to synthesize a one-nanosecond pulse with maximum sidelobe levels of -43 dB.

The sweep time was set for 100 milliseconds. In the swept measurement mode, the 45 MHz to 2 GHz sweep takes place in 100 milliseconds. However, in the stepped measurement mode, a measurement takes approximately 100 times longer, or 10 seconds.

The measurements utilized a bistatic antenna configuration. Hence, the S_{21} scattering parameter was of primary interest. Recall that S_{21} measures the insertion loss of a two port network, which is essentially what a bistatic GPR does when it radiates energy from one antenna and receives energy at another.

The HP 8510 RF output power was set to +10 dBm (0.1 watt) average for all frequencies over the measurement range. At this power level, the network analyzer had approximately a 90 dB dynamic range. However, the full dynamic range capabilities of the network analyzer were not utilized. This was because the surface return signal from the S_{21} measurements with the GPR antennas was about 40 dB below the calibration signal level. Thus, the usable dynamic range was reduced by 40 dB.

The dynamic range might be improved at the expense of calibration accuracy by inserting a low-noise amplifier at port two (the receiver port) of the HP 8513A transmission test set. Unfortunately, calibrating the analyzer with the amplifier would require adding an attenuator in front of the amplifier during calibration to avoid overloading the port two input. The attenuator would then be removed during actual measurements. However, the vector calibration would then be

inaccurate. It was decided not to use an amplifier at the receiver port to maintain the accuracy of the calibration.

The network analyzer has the capability of performing trace averaging. Averaging traces reduces the noise effects, and hence increases the measurement dynamic range. The measurement time in the swept mode increases linearly with the number of averages, but in the stepped mode, at least 500 averages are required to lengthen the measurement time. It was decided not to utilize the averaging capabilities of the HP 8510 because the pulsed GPR systems tested did not have averaging as a built-in feature. Utilizing averaging for only the frequency-domain GPR systems would not allow an objective comparison between all of the tested radars.

6.4 ANTENNAS USED FOR THE GPR SOIL-MODEL TESTS

Two types of antennas were designed and built for testing the GPR systems. One type was a TEM horn similar to the ones used with the GAR RODARTM highway-survey GPR. The other was a triangular-sheet (bow-tie) dipole. Each of these antennas offered advantages over the other. Tests were performed with the two types of antennas to decide which type gave the best overall performance.

6.4.1 TEM HORN ANTENNA

The TEM horn has several performance capabilities that make it useful for GPR applications. It has broad bandwidth, low dispersion, and a low reflection coefficient. Such factors make it ideal for short-pulse radars, which require low pulse stretch and high bandwidth. Some of the considerations impacting the design of a TEM antenna for GPR applications are outlined in Section 3.3.3.

GAR spent considerable time constructing a pair of TEM horns for use in the tests. We used a design similar to the RODARTM antennas, except that a wider aperture and a different shape for the antenna foil plates were employed. The dimensions of the TEM antennas were selected for optimum operation with the one-nanosecond time-domain pulses that were

used with the test GPR systems. Furthermore, we decided to use an alternative fabrication technique for the test antennas in order to see if enhanced antenna clutter and reflection coefficient performance could be achieved.

Each antenna was fabricated with two 39-inch long brass foil plates that had varying width cross-sections along their lengths. The foil plates were adjusted into a wedge shape with the feed point at the narrow end. The foil plates were glued to two 0.75-inch thick foam boards and spaced with the proper wedge angle by additional foam side panels. The plates faced each other on the inside of the wedge. The intention was to have only air between the foil plates to minimize adverse performance anomalies that could result with other materials between the plates.

At the feed point, a coaxial connector made the transition to the parallel plate structure of the antenna. The tips of the antenna plates were attached to resistive cards that terminated the surface currents flowing on the plates. The antenna feed point and tip were tuned to reduce time-domain reflections. This tuning procedure was a time-consuming task requiring considerable patience.

The antennas were tested using both short-pulse time-domain reflectometry and HP 8510 frequency-domain tests to verify their performance. We found that the antennas had reflection waveform amplitudes that were about -36 dB down from the incident pulse amplitude. Their effective radiation bandwidth extended from 250 MHz to 2.0 GHz. However, time limitations did not allow formal and extensive antenna parameter and pattern tests to be performed.

6.4.2 TRIANGULAR-SHEET DIPOLE ANTENNA

The coplanar, triangular-sheet dipole antenna is a simple design that has been used extensively in GPR applications. It exhibits a moderately broadband response, and achieves it with a simple, compact structure. It does not, however, exhibit the wide bandwidth, low dispersion, or low reflection coefficient of the TEM horn.

These antennas are deployed with the two triangular sheets lying on the surface of the ground. If the antenna is electrostatically shielded on the back side, most of the radiated signal energy from the antenna couples into the ground. The close coupling of the dipole to the ground gives it a tremendous advantage over the TEM horn.

The length of the dipole arms is directly related to the radiation bandwidth of the antenna. Long triangular sheets can radiate lower frequency RF energy than short triangular sheets. Typically, each antenna arm must be at least $1/4$ wavelength long at the lowest desired RF frequency in order to radiate properly. Fortunately, when the bow-tie antenna is in direct contact with the ground, the dielectric constant of the soil acts to decrease the wavelength of the RF energy, and thus appears to make the antenna arms effectively longer. This implies that for a given RF bandwidth, the GPR bow-tie antenna dimensions can be reduced from the dimensions of an antenna designed to radiate in air.

GAR designed one pair of bow-tie antennas for the GPR tests. The antennas were designed to have a low-frequency cutoff of approximately 200 MHz when operated over soil with a relative dielectric constant of 16. The design parameters of the antenna were extracted from a report published by Brown and Woodward³. The bow-tie was built from brass shim stock and included a shield on the back to minimize clutter returns and maximize the energy coupled into the ground.

A sketch of the bow-tie antenna is shown in Figure 6.7. A coaxial cable feed is coupled to the two antenna leaves through a 50-ohm to 200-ohm balun transformer. Each of the antenna leaves has two 200-ohm resistors connecting the antenna foils to the antenna shield. These resistors help to absorb the energy that is not radiated or reflected by the antenna.

6.4.3 QUALITATIVE COMPARISONS BETWEEN THE TEM HORN ANTENNAS AND THE TRIANGULAR-SHEET BOW-TIE ANTENNAS

Qualitative tests were used to compare the performances of the TEM horns and the bow-tie antennas in order to determine which type of antenna to use for the GPR source tests. The

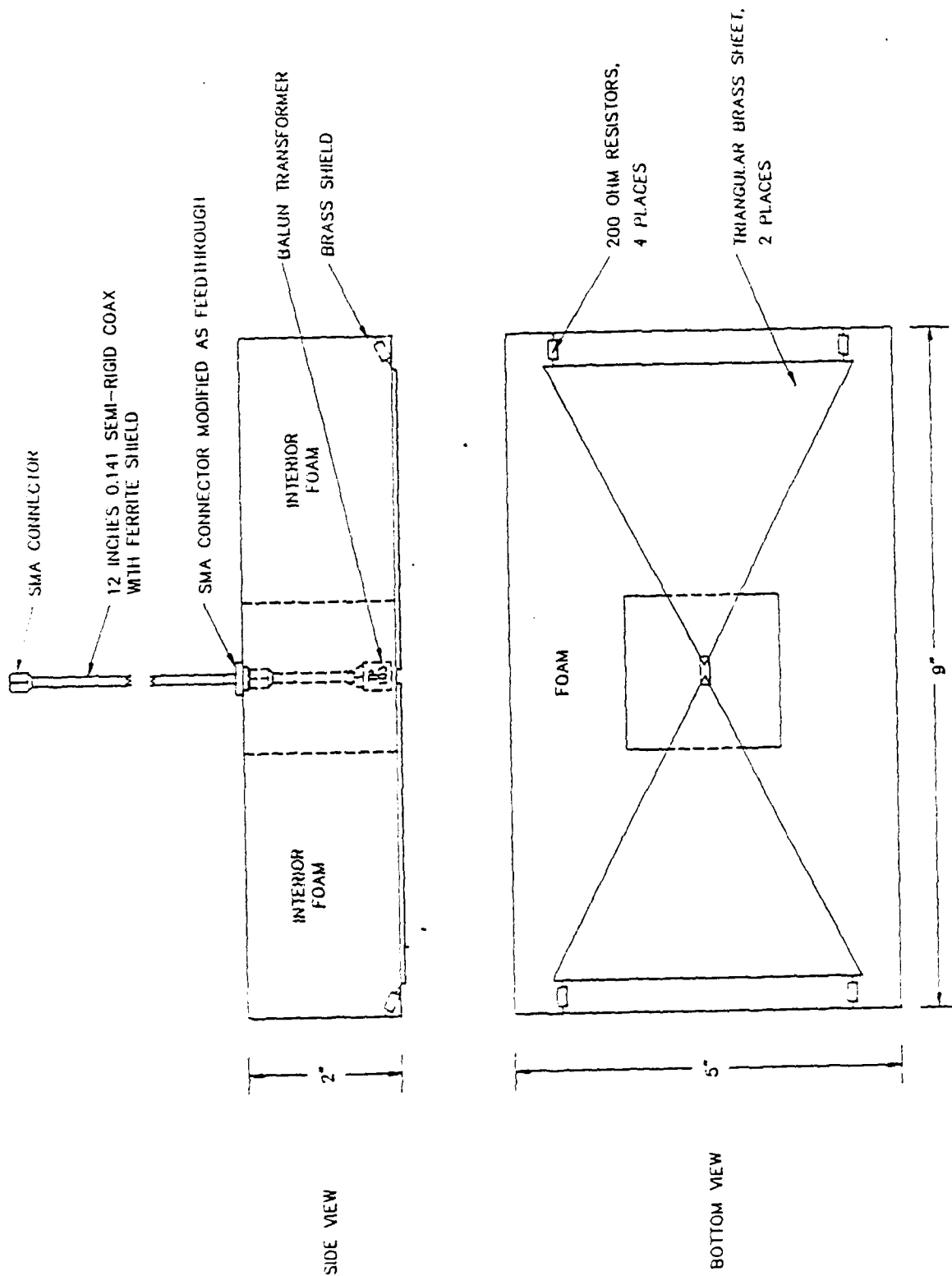


Figure 6.7: Sketch of triangular-sheet dipole antenna used for GPR tests with the soil model test tank.

antennas were tested in the ground-penetration mode on the soil-model tank using the responses from the buried targets and loop probes as the criteria of selection. No formal antenna pattern, VSWR, or pulse tests were performed. The antennas were tested in the bistatic and monostatic modes with both the GAR time-domain GPR and the HP 8510 network analyzer-based systems. The TEM horn antennas were tested in a ground-contact mode and an air-coupled mode. Most of the expected performance characteristics of the antennas were verified during the tests.

The TEM horns exhibited good bandwidth response and a low reflection coefficient in both the ground-contacting and air-coupled modes. The target returns and probe signals showed little pulse stretch. The response of the bow-tie antennas showed more pulse stretch and less bandwidth. The bow-tie antennas had a higher reflection coefficient than did the TEM horn antennas. The bow-tie antennas also coupled more energy into the ground than did the TEM horns. This was evidenced by the higher target return signals.

An unexpected result led to the selection of the bow-tie antennas for the subsequent GPR tests. Specifically, the bow-tie antennas had a signal-to-clutter ratio that was at least 10 dB larger than that of the horns. This phenomenon was probably due to the better antenna-to-ground energy coupling of the bow-tie antennas. In addition, the TEM horns radiate along their entire 39-inch structure and thus are susceptible to above-ground clutter.

SECTION 7

DESCRIPTION OF THE MEASUREMENTS USING THE CANDIDATE GPR SYSTEMS

The GPR measurement program was divided into three phases. Phases 1 and 2 involved scale-model measurements with the soil tank using two different clay dielectrics. Phase 3 consisted of full-scale GPR measurements using the HP 8510 in a stepped-frequency mode on an outdoor test field. The stepped-frequency system was chosen exclusively for the Phase 3 measurements because it showed the best performance of the four scale-model GPR systems tested.

7.1 DESCRIPTION OF THE PHASE 1 AND PHASE 2 SCALE-MODEL GPR MEASUREMENTS USING THE SOIL-MODEL TANK

Phase 1 involved soil-model tank measurements using clay shale as the model dielectric. The clay shale provided the most demanding of the two scale-model testing environments. This was because the shale had considerably higher loss characteristics than the clay schist used in the Phase 2 measurements. Phase 1 and Phase 2 measurements were conducted in a similar fashion. Figures 7.1 through 7.3 are photographs of some of the GPR equipment configurations used for the soil tank measurements.

When the target measurements were made, the bistatic antenna systems were placed directly over each of the pipes. The antennas were oriented in such a manner that the electric field polarization vector was parallel with the pipe axial dimension to ensure maximum signal return. Recall that the GSSI short-pulse radar required the use of its own antenna system, so the specially-constructed test antennas could not be used with it. This should be taken into account when comparing the results of the GSSI radar measurements with those from the other GPR systems.

The output data of each of the candidate GPR systems were presented in a time-domain format so that the results could easily be compared. Photographs were taken of the GPR time-domain displays. In the case of the HP 8510-based frequency-

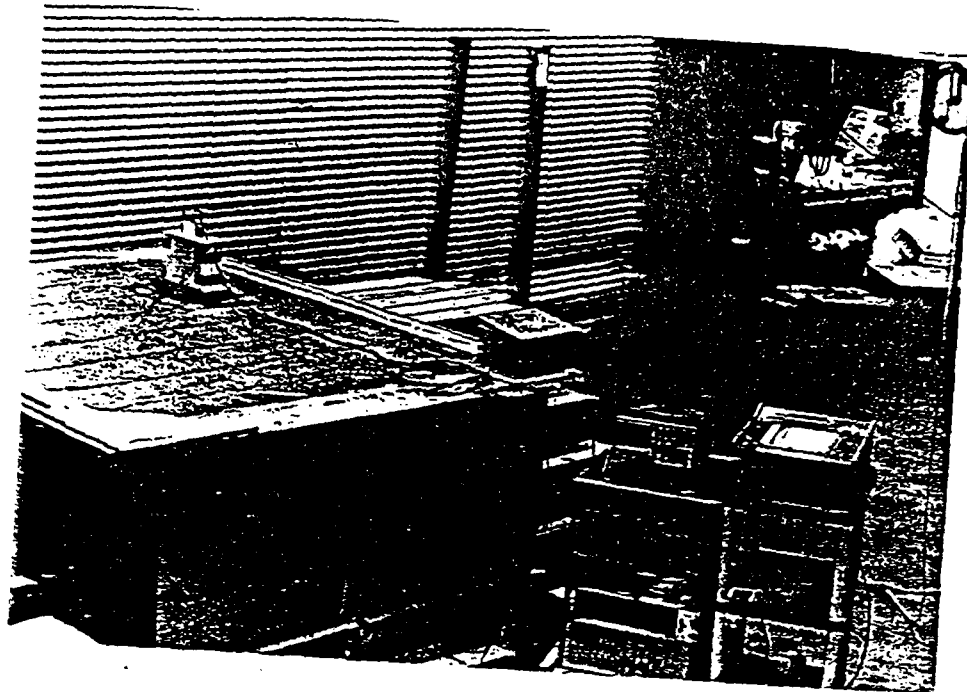


Figure 7.1: GAR short-pulse radar used for soil model tank test.

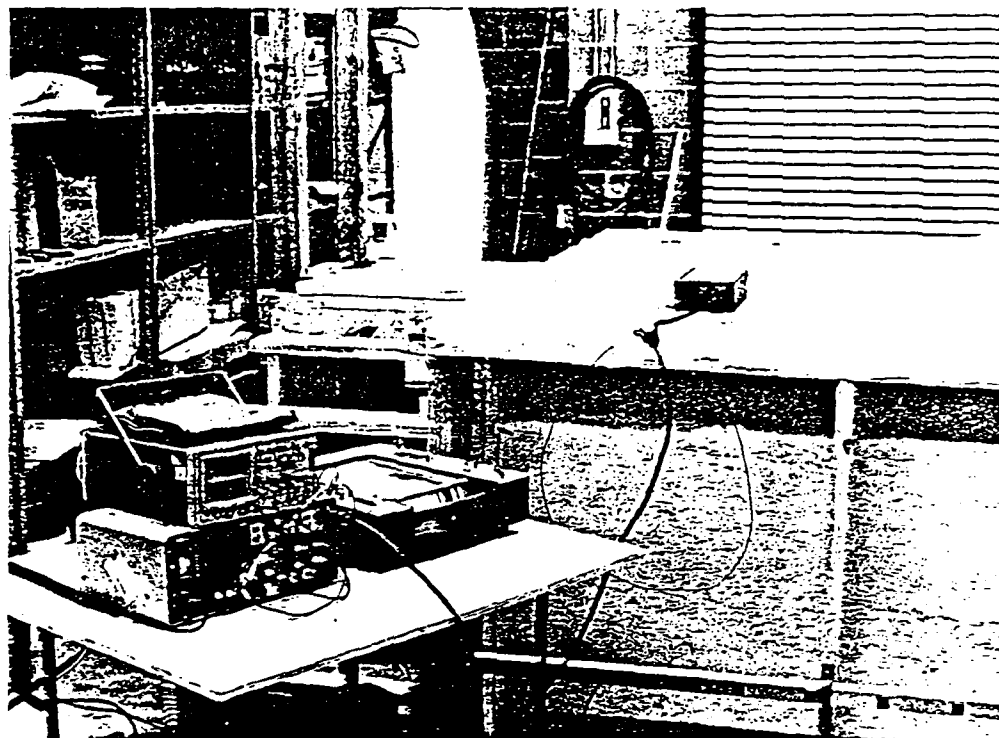


Figure 7 2: GSSI short pulse radar used for soil model tank tests.

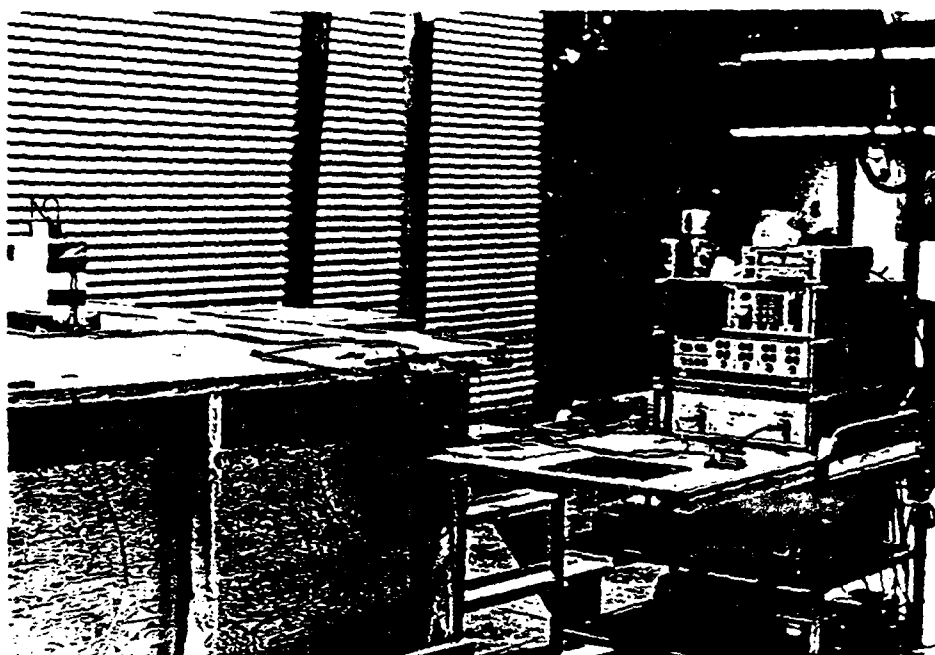


Figure 7.3: HP8510 frequency domain radar equipment for soil model tank tests.

domain systems, plots were also made of the time-domain displays for better visual clarity.

Care was taken to avoid any uncalibrated gain adjustments with the GPR systems in order to maintain measurement accuracy and repeatability. The target signals from both of the short-pulse radars were measured at the receiver outputs. No gain adjustments were possible in the receiver signal chain before the measurement points with the short-pulse radars. The network analyzer calibration procedure performed before each measurement removed the possibility of any uncalibrated gain adjustment errors in its display.

The performances of the GPR systems were not compared based on absolute received signal power levels. Instead, the primary performance criteria used for the GPR comparisons were based on target detectability and the signal-to-clutter levels of the target returns.

Strip-chart recordings were produced for the two short-pulse radars as the antenna systems were pulled across the soil tank. The strip-chart recordings were intended primarily as a qualitative indication of the relative performances of the two short-pulse radars. They were most useful when searching for target return signals having signal-to-clutter ratios less than 6 dB.

A strip-chart recording provides additional information to the GPR operator by displaying the radar scans on paper in a sequential fashion. The radar output waveform is digitized and converted to a grey-level format and printed on paper by a stylus. The paper scrolls forward, and as each radar scan is produced, the stylus scans across the scrolling paper in a direction perpendicular to the scrolling direction, thereby producing a line with modulated grey-level intensity. As more and more scans are recorded on the paper, the strip-chart recording presents a display that allows the observer to visually "integrate" many scans to see the changing target returns.

Unfortunately, the HP 8510 receiver waveform data was not readily available for output to a strip-chart recorder. To generate a strip-chart recording of the HP 8510 data, the digitized display output would have to be exported to a

computer, stored, and then output to the strip-chart recorder. Time did not permit implementation of a strip-chart interface for the HP 8510.

Simple signal-to-clutter measurements were performed with each of these candidate GPR systems. The purpose of these measurements was to evaluate the internal clutter level generated in the GPR systems. However, this clutter level is a function of the antennas and their deployment because any impedance mismatches at the antenna cause reflections that appear in the receiver range window. It was desirable to include this form of clutter in the signal-to-clutter measurement.

It was very difficult to structure an accurate test for the signal-to-clutter measurement. The bow-tie antennas are very sensitive to radiation impedance loading. They must be placed on or near the surface of the ground to avoid producing a response with excessive ringing. The excess ringing contributes to the clutter present in the receiver output waveform. Ideally, the antenna must be placed over a dielectric medium that absorbs all of the energy radiated from the antenna; thus, no signals from external targets and signals will appear in the receiver waveform.

GAR engineers were unable to locate such an ideal medium. The closest available approximation to this ideal absorbing medium that could be used for the signal-to-clutter tests was the clay shale in the Phase 1 test tank (the clay schist in the Phase 2 tank did not have high enough attenuation). The shale exhibited a very high attenuation characteristic. Although the shale tank contained pipe targets, the GPR systems were incapable of producing detectable signals from any of the targets deeper than 27 inches. Therefore, the antenna system was placed over the center of the tank, on the surface, where the pipe targets were a maximum distance from the antennas. Additionally, the antenna system was oriented so that it was cross-polarized with respect to the pipe targets, thereby minimizing potential target return signals. With this configuration, we expected that any target signal returns would fall below the GPR receiver internal clutter level.

The signal-to-clutter measurement required the establishment of a reference signal level. The reference

signal chosen was the return from a 19 inch by 24 inch metal plate target located two inches below the antenna system. Air was used as the dielectric between the antenna system and the plate. The plate chosen as the reference target had large enough dimensions that it intercepted almost all of the signal radiated from the antenna. Thus, a larger plate would have produced an insignificant difference in the plate return amplitude.

The amplitude of the signal return from the plate was measured and used as the reference for each of the GPR systems. The signal return from the plate was within the dynamic range of the GAR radar system sampler and the HP 8510 receiver so that there was no risk of signal compression. However, the exact compression point of the GSSI sampler was unknown.

The antenna systems were then placed over the center of the soil tank in the cross-polarized orientation. The receiver waveforms beyond the surface return were assumed to be dominated by internal clutter signals. Therefore, a measurement was made of the signal level at a location approximately 15 nanoseconds from the beginning of the receiver range window. The largest signal present in a four nanosecond region centered at the 15 nanosecond point was used as the representative clutter level for the signal-to-clutter measurement.

A signal-to-clutter ratio was computed for each GPR system and expressed in decibels. This ratio was computed by dividing the measured amplitude of the return from the metal plate by the measured clutter signal level.

The difficulty in making an accurate and objective signal-to-clutter measurement that included the effects of the antenna system was recognized. Therefore, the signal-to-clutter measurement described above was used as a figure of merit and was not intended to be used as a binding measure of the clutter performance of the candidate GPR systems. Future investigation may well reveal a better method of measuring the signal-to-clutter ratio that would include the antenna systems and avoid the use of a lossy dielectric as a matched load for the antennas. Nonetheless, the signal-to-clutter ratios determined under this program (as described above) were felt to be

adequate in comparing the relative merits of the candidate GPR systems.

7.2 FULL-SCALE GPR FIELD MEASUREMENTS

Once the soil-model tank measurements of Phases 1 and 2 were completed, the corresponding performance of each of the GPR systems was evaluated. GAR engineers concluded that the stepped-FM system using the HP 8510 gave the best signal-to-clutter and dynamic range performance. The basis for the selection of the stepped-FM system is explained in more detail in Section 9. The stepped-FM system was tested on a pipe test field that GAR built several years ago near its Marietta facility.

The pipe test field contains two plastic pipes and four metal pipes, of several diameters and buried at various depths. Figure 7.4 is a top view of the pipe test field showing the pipe diameters, their fabrication material, and their relative spacing. Figure 7.5 is a side view of the pipe test field showing the burial depths of the pipes. As the pipe field is several years old, the pipe burial depths are not precisely known due to settling and other environmental effects. It is estimated that the burial depths are known to within ± 4 inches.

The full-scale field measurements were qualitative in nature. They were meant to demonstrate the detection capabilities of a stepped-FM GPR system. It was felt that quantitative measurements would not be accurate due to the unknown soil conditions of the pipe field. The homogeneity of the soil could not be determined, and the exact burial depths of the pipes were not known.

The full-scale field stepped-FM GPR measurements utilized a time-domain synthesized pulse with a bandwidth of 45 MHz to 700 MHz. A "normal" bandwidth weighting function was used, thus a pulse of three nanoseconds in duration (as measured at the 50% voltage amplitude points) was synthesized. The bistatic antenna system used for the tests consisted of two triangular-sheet dipoles with dimensions approximately 2.5 times those of the antennas used for the laboratory scale-model

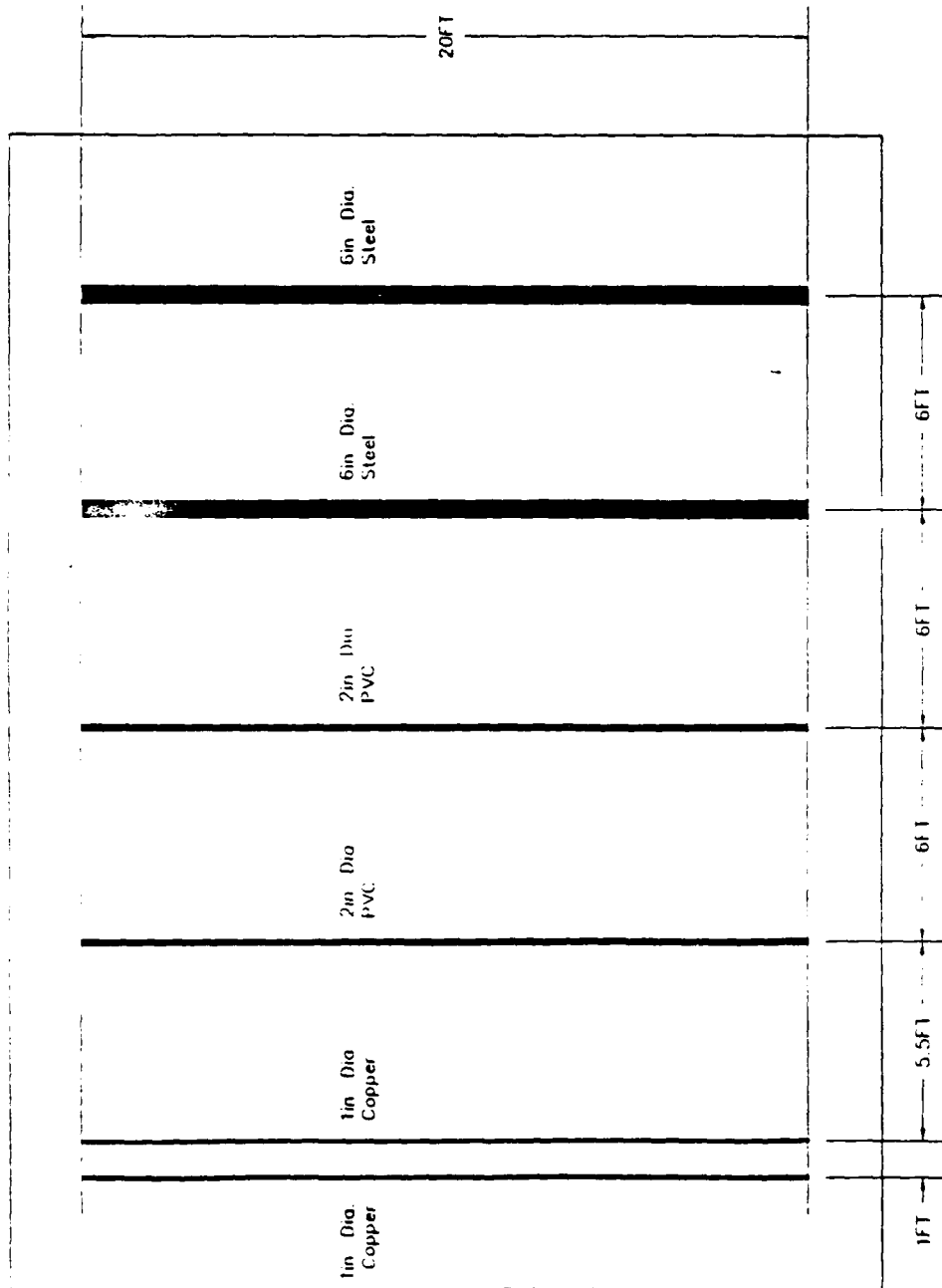


Figure 7.4: Top view drawing of pipe test field showing pipe sizes and locations.

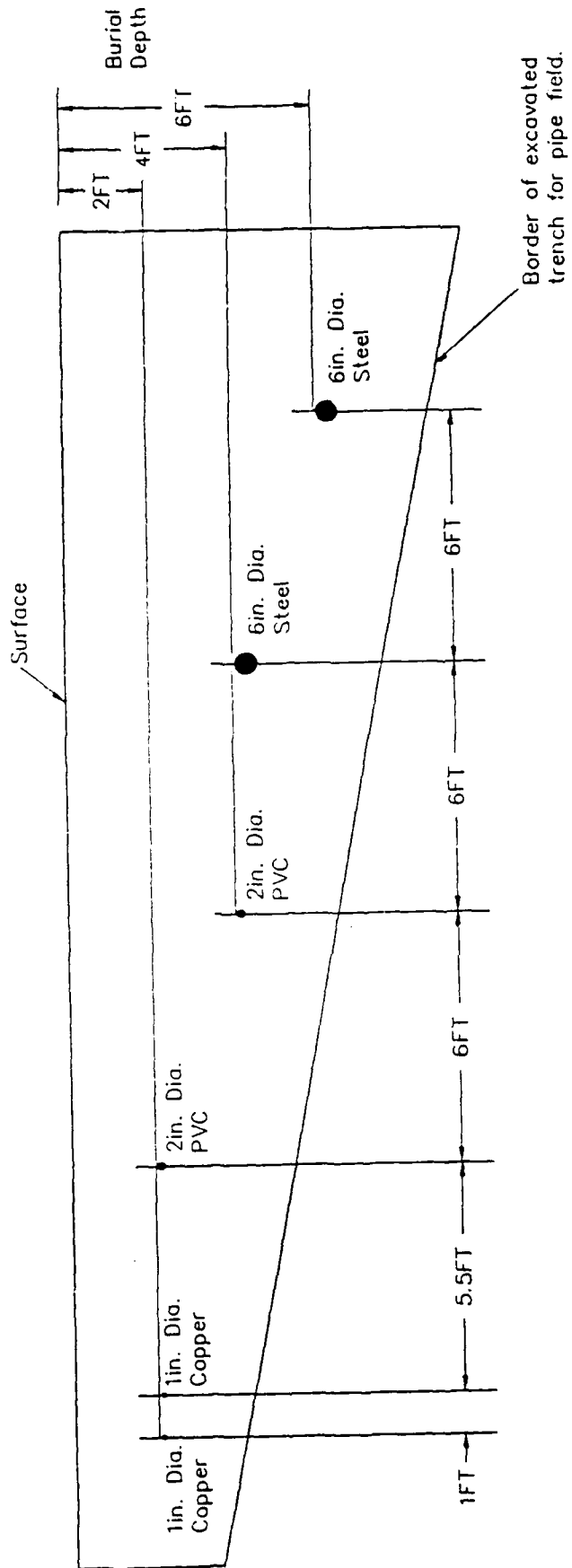


Figure 7.5: Side view drawing of pipe test field showing pipe sizes and locations.

measurements. The antenna system was a unit designed to be used with a GSSI short-pulse radar system having a three to four nanosecond duration transmitter output pulse. The antenna system was adapted for use with the HP 8510. All measurements of the time-domain pipe signal returns were made with the antennas polarized such that the electric field vector was parallel to the pipe axis.

SECTION 8

MEASUREMENT RESULTS

This section summarizes the measurement results obtained while testing the candidate GPR source signal types. The controlled dielectric environment for the scale-model tests provided a basis by which the performances of the GPR systems could be compared. The results from the scale-model tests were evaluated and the scale-model GPR system with the best performance was identified.

A full-scale version of the scale-model GPR with the best performance was then fabricated and tested in a realistic environment. GAR built a test field several years ago containing buried utility pipes to be used for testing GPR systems. The performance of the full-scale GPR was tested on this field.

8.1 PHASE 1 SCALE-MODEL GPR MEASUREMENTS (CLAY SHALE)

The Phase 1 measurements with the scale-model GPR systems used clay shale as the dielectric material in the soil-model tank. The measured dielectric properties of a sample of the clay shale are given in Appendix B. The diameters of the pipe targets, and their burial depths in the soil tank, were consistent with a model scale factor of five. Recall that Figures 5.1 and 5.2 show the target locations within the soil-model tank.

Care must be taken when evaluating results obtained with the scale-model systems. When model-soil dielectric parameters are being extrapolated to a full-scale environment, the conductivity, and hence the attenuation characteristics, of the shale are scaled downward by the scale factor. Target dimensions, burial depths, and the wavelengths of the RF energy are scaled upward.

A summary of the Phase 1 GPR measurements is given in the sections which follow. The summary includes signal-to-clutter evaluations, a relative dielectric constant verification

measurement for the clay shale in the test tank, and target detection measurements.

8.1.1 SIGNAL-TO-CLUTTER MEASUREMENTS

The signal-to-clutter measurement procedure was described in Section 7. The results are given in Table 8.1 below.

TABLE 8.1: RESULTS OF SIGNAL-TO-CLUTTER RATIO MEASUREMENTS FOR THE CANDIDATE GPR SYSTEMS.

<u>GPR System</u>	<u>Signal-to-Clutter Ratio (dB)</u>
GAR Short Pulse	51.5
GSSI Short Pulse	52.8
HP 8510 FM-CW	57.3
HP 8510 Stepped FM	57.5

The measurements for the HP 8510-based systems may have been subject to dynamic range limitations. The reflection from the metal plate used as the reference signal amplitude for the measurements was 34 dB below the calibrated network analyzer reference level for the S_{21} parameter. Thus, signal-to-clutter ratios of 58 dB approach the dynamic range specification of 90 dB for the HP 8510. Consequently, the signal-to-clutter ratios obtainable with the HP 8510-based systems may be larger than those presented in Table 8.1 above.

The sidelobe levels of the signal returns from the surface may have been a key factor, if not the determining factor, in the GPR signal-to-clutter measurements. The surface return signal had sidelobes associated with it that extended into the remainder of the receiver window. The sidelobe levels of the surface return signal had the same relative amplitude relationships as those measured for the transmitted pulses. The sidelobe level of the HP 8510 synthesized pulses was down 60 dB at five nanoseconds from the main lobe peak; the sidelobe level of the GAR monocycle pulse was 50 dB below the pulse. The sidelobe level of the GSSI transmitter pulse could not be measured because the transmitter was contained in a sealed enclosure.

The surface return sidelobe level represents a practical limit for the minimum clutter level to be expected from a GPR. The other sources of clutter, such as connector reflections, antenna reflections, and transmitter noise, increase the clutter level above that caused by the surface return sidelobe alone. The clutter level varies with location in the receiver window and it is difficult to distinguish contributions from various clutter sources.

8.1.2 GPR MEASUREMENT OF THE RELATIVE DIELECTRIC CONSTANT OF THE PHASE 1 SOIL-MODEL TEST TANK

When the soil-model tank was filled, the possibility existed that the dielectric properties of the clay shale in the tank would not match those obtained in the laboratory measurements of an individual sample. These laboratory measurements were always performed on a clay sample that was tightly packed into a test cell. Fortunately, the shale was quite moist and as the soil tank was filled, the clay was tamped periodically to maintain a consistent density. Nevertheless, the attenuation property of the shale tank could not be measured directly as was done with the soil sample. Therefore, an exact value for the attenuation of the shale in the tank was not known.

The dielectric constant and attenuation properties of a given soil vary with density just as they do with moisture. As the density increases, so does the dielectric constant and the attenuation. GPR engineers felt that if the relative dielectric constant of the clay in the tank was the same as that of the laboratory sample, then the attenuation of the clay in the tank would be approximately the same as the attenuation measured for the sample. Therefore, it was necessary to measure the dielectric constant of the soil in the test tank.

The relative dielectric constant of the clay in the tank was computed using the signal returns from the targets. The only measured radar parameter required is the real-time delay between the surface return and a target. If the measurement is performed with a monostatic antenna system, the relative dielectric constant is then given by:

$$\epsilon_r = (ct/2d)^2, \quad (8.1)$$

where t is the real-time separation between the surface return and the target return, d is the known distance from the surface to the target, and c is the speed of light in a vacuum. If Equation (8.1) is modified to include the spacing between the phase centers of bistatic antennas, the relative dielectric constant equation becomes:

$$\epsilon_r = (ct / (2((s/2)^2 + d^2)^{1/2}))^2, \quad (8.2)$$

where s is the spacing between the antenna phase centers. In the case of the bistatic bow-tie antennas, the phase centers of the dipoles were assumed to be the feed points.

The accuracy of this method of determining the dielectric constant of the clay in the tank is affected by several factors: the accuracy and linearity of the GPR equivalent-time receiver range display, the exact spacing between the phase centers of the bistatic antennas, the centering of the antenna system above the target, and the difference between the expected target depth and its actual buried depth. The HP 8510 had the most accurately calibrated range display; therefore, the dielectric constant was calculated using the network analyzer receiver output signals. Furthermore, the effects of errors in determining s and d are minimized by selecting signals from deep targets for computing the dielectric constant of the soil in the tank. However, the shale had high attenuation properties and the deepest targets were not detectable at the receiver, so a relatively shallow target was used for the dielectric constant measurement.

Figure 8.1 is a plot of a received waveform from the HP 8510 using the stepped-FM time-domain mode. Marker 1 is placed on the surface return, Marker 2 is on a 1.25 inch diameter plastic pipe 7.8 inches deep, and Marker 3 is on the return from a metal plate 21.6 inches below the surface. Using the plate return to compute the dielectric constant, the parameters for Equation (8.2) become: $d=0.548$ m, $s=0.165$ m, $t=12.6$ ns, and

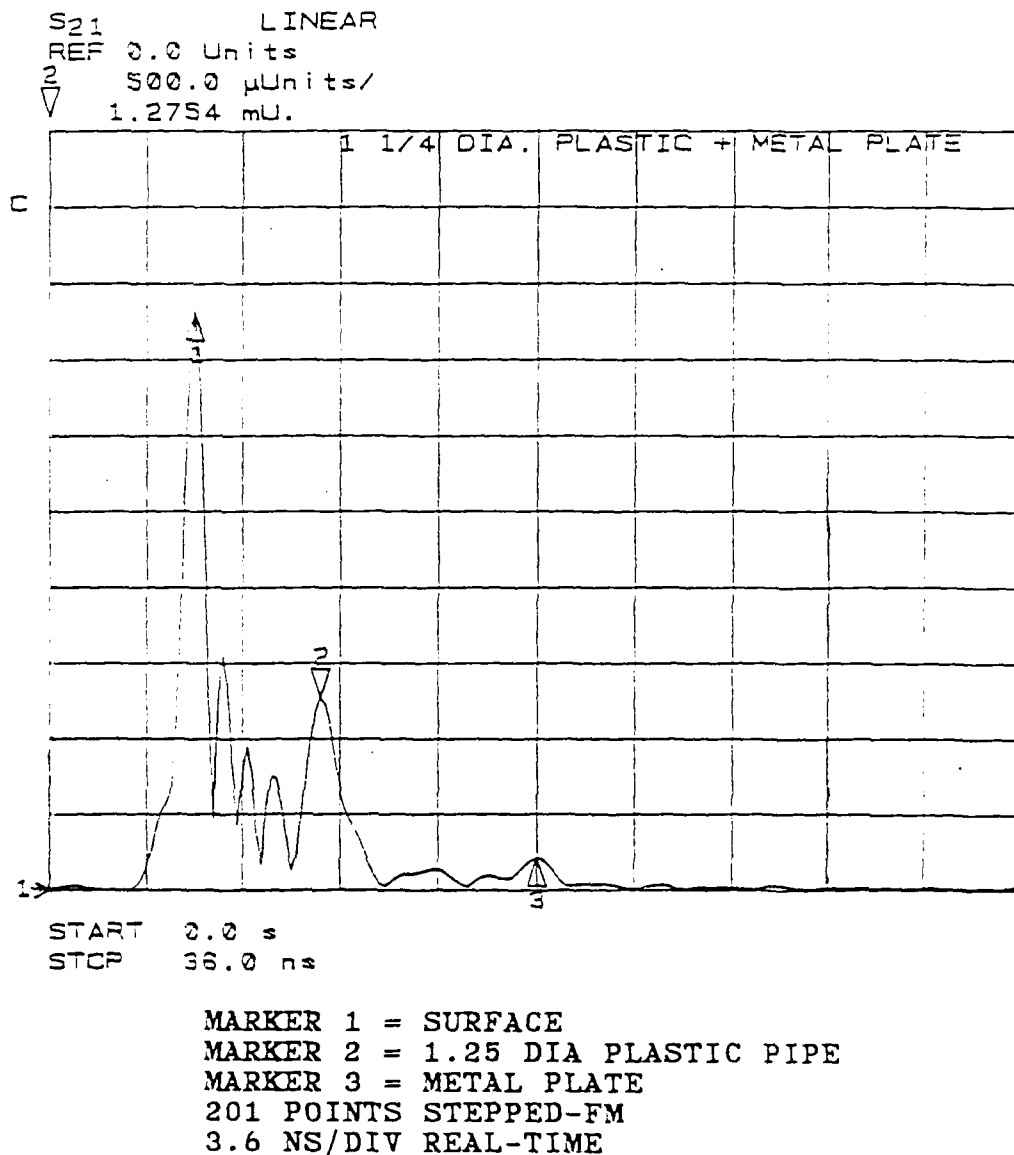


Figure 8.1: Plot of the HP8510 returns of surface (Marker 1 a 1.25 inch dia. plastic pipe (Marker 2), and a metal plate (Marker 3).

$c = 3 \times 10^8$ m/s. The relative dielectric constant is computed to be 11.63.

The laboratory measurement of the dielectric constant of the shale sample is presented in Appendix B. For the frequency band of 200 MHz to 2.0 GHz, the dielectric constant varies between 14 and 16. If the measurement of the relative dielectric constant using the GPR system was accurate, the shale in the tank above the plate target may not have been packed quite as densely as the sample was in the test cell. This means that the attenuation, in dB/m, for the clay in the tank was probably less than that of the sample.

The two measurement techniques yielded similar results for the relative dielectric constant of the shale in the test cell and the shale in the test tank. If the potential sources of error for the test tank measurement are taken into account, the results of the test-cell measurement are an acceptably accurate representation of the electromagnetic properties of the shale in the test tank. Therefore, the test-cell parameters were used for subsequent calculation, involving the electromagnetic parameters of the shale in the test tank.

8.1.3 PHASE 1 SOIL-MODEL TANK TARGET MEASUREMENTS

This section presents the target measurement data for the soil-model tank containing the clay shale. Table 8.2 below summarizes the measured target signal return amplitudes from each of the GPR systems. The table readily allows comparisons of the target-detection performances of the test radars. Also included at the end of this section are photographs and plots of the candidate GPR receiver output waveforms showing some of the target signal returns.

The left-most five columns in Table 8.2 describe the model pipe target environment and an extrapolated full-scale environment based on the model. The model scale factor of five is chosen for the computation of the full-scale environmental parameters, which is consistent with the scale factor used for selection of the model tank parameters. The left-most column is the actual outside diameter, in inches, of the pipe targets buried in the soil-model tank. The second column lists the

TABLE 8.2. SUMMARY OF MEASUREMENT RESULTS FROM GPR TESTS WITH SOIL MODEL TANK FILLED WITH SHALE CLAY.

SCALE-MODEL (scale factor = 5)			FULL-SCALE		GPR Received Target Signal Amplitude			
Pipe Diameter (inches)	Depth From Surface (inches)	Pipe Diameter (inches)	Depth From Surface (feet)	Pipe Material	GAR Short Pulse (millivolts)	GSSI Short Pulse (millivolts)	HP8510 Swept FM (micro-units)	HP8510 Stepped FM (micro-units)
0.88	4.1	4.4	1.71	Metal	1,120	700	8,970	7,760
1.31	7.8	6.6	3.25	Metal	320	120	3,220	3,310
1.31	10.7	6.6	4.46	Metal	120	90	850	900
2.38	15.6	11.9	6.50	Metal	43	20	350	314
3.50	18.0	17.5	7.50	Metal	14	8	55	60
4.50	26.6	22.5	11.08	Metal	**	*	*	*
6.63	36.0	33.2	15.00	Metal	*	*	*	*
0.88	4.1	4.4	1.71	Plastic	320	100	3,320	3,420
1.25	7.8	6.3	3.25	Plastic	145	36	1,190	1,280
1.25	10.7	6.3	4.46	Plastic	40	12	200	200
2.50	15.6	12.5	6.50	Plastic	20	8	117	140
3.50	18.0	17.5	7.50	Plastic	*	*	*	*
4.50	26.6	22.5	11.08	Plastic	*	*	*	*

Shale clay loss at 1 GHz : 50 dB/m

Scaled soil loss at 200 MHz (= 1 GHz/5) : 10dB/m

*Denotes undetectable

**Denotes detectable only with strip chart recording. Target waveform not detectable in receiver output.

depths, in inches, from the surface to the tops of the pipes. The third column lists the equivalent outside diameter of the pipes in a full-scale environment. The fourth column contains the extrapolated depths of the pipes, measured in feet, for a full-scale environment. The fifth column describes the material of the pipe construction: metal or plastic.

The remaining four columns present the measured amplitudes of the signals from the pipe targets for each of the candidate GPR systems. The cases for which the pipes were undetectable are noted in the table. The short-pulse radar amplitudes are expressed in millivolts and the HP 8510 target signal amplitudes are expressed in micro-units. One micro-unit is $1/1,000,000$ th of the amplitude of the normalized signal obtained from the HP 8510 S_{21} at calibration. The S_{21} calibration is performed by removing the antennas from the antenna cables and connecting the cables directly together. Therefore, the S_{21} calibration amplitude is much greater than the signals from the antennas.

Also included near the bottom of Table 8.2 is the shale clay attenuation expressed in dB/m at 1 GHz and an extrapolation of this attenuation to a full-scale environment. The value of the clay attenuation at 1 GHz comes from the graph included in Appendix B.

Care must be taken when comparing the target-detection performances of the GPR systems using the amplitude results in Table 8.2. The absolute amplitudes cannot be compared between radars. This is because each of the radar systems is constructed differently and produces different output levels. Instead, the comparison should be based on the ratios of the amplitudes of the targets as measured with each radar.

For example, the maximum target signal amplitude for each GPR is from the 0.88 inch diameter metal pipe. These measurements (along with the corresponding measurements for the 0.88 inch diameter plastic pipe) can be used as the reference target signal amplitudes for each radar. The other target signal returns can be expressed as a fraction of the amplitude of the corresponding reference level. These ratios are summarized in Table 8.3.

TABLE 8.3. SUMMARY OF NORMALIZED TARGET SIGNAL AMPLITUDES FROM GPR TESTS WITH SOIL MODEL TANK FILLED WITH SHALE CLAY.

Amplitudes are normalized for each pipe material (metal or plastic) for each candidate GPR based on the return from the 0.88 inch diameter pipe (metal or plastic) buried at a depth of 4.1 inches.

SCALE-MODEL (scale factor = 5)			FULL-SCALE		GPR Normalized Target Signal Amplitude			
Pipe Diameter (inches)	Depth From Surface (inches)	Pipe Diameter (inches)	Depth From Surface (feet)	Pipe Material	GAR Short Pulse (millivolts)	GSSI Short Pulse (millivolts)	HP8510 Swept FM (micro-units)	HP8510 Stepped FM (micro-units)
0.88	4.1	4.4	1.71	Metal	1	1	1	1
1.31	7.8	6.6	3.25	Metal	0.286	0.171	0.359	0.427
1.31	10.7	6.6	4.46	Metal	0.107	0.129	0.095	0.116
2.38	15.6	11.9	6.50	Metal	0.038	0.029	0.039	0.040
3.50	18.0	17.5	7.50	Metal	0.012	0.011	0.006	0.008
4.50	26.6	22.5	11.08	Metal	**	*	*	*
6.63	36.0	33.2	15.00	Metal	*	*	*	*
0.88	4.1	4.4	1.71	Plastic	1	1	1	1
1.25	7.8	6.3	3.25	Plastic	0.453	0.360	0.358	0.374
1.25	10.7	6.3	4.46	Plastic	0.125	0.120	0.060	0.058
2.50	15.6	12.5	6.50	Plastic	0.062	0.080	0.035	0.041
3.50	18.0	17.5	7.50	Plastic	*	*	*	*
4.50	26.6	22.5	11.08	Plastic	*	*	*	*

Shale clay loss at 1 GHz : 50 dB/m

Scaled soil loss at 200 MHz (= 1 GHz/5) : 10dB/m

*Denotes undetectable

**Denotes detectable only with strip chart recording. Target waveform not detectable in receiver output.

For the GAR short-pulse radar, the ratio of the 2.38 inch metal pipe return amplitude to the amplitude of the 0.88 inch metal pipe is $43/1120=0.038$. The ratios of the same two target returns for the GSSI system, the HP 8510 swept-FM system, and the HP 8510 stepped-FM system are $20/700=0.029$, $350/8970=0.039$, and $314/7760=0.040$, respectively. These ratios are all within 3 dB of each other, as would be expected. This is because all of the environmental factors affecting the signal returns are the same with each of the radars.

Other target return ratios show greater variation between the GPR systems. The ratio of the 0.88 inch plastic pipe return to the 0.88 metal pipe return shows a 10 dB variation between the radars. The target ratios for the GSSI system, the GAR system, the HP 8510 swept-FM system, and the HP 8510 stepped system are 0.143, 0.277, 0.370, and 0.440, respectively. Several reasons may account for this variation.

First, the pipe target was very close to the surface, causing the target return and the surface return to interfere somewhat. This may have led to an error in measuring the return amplitudes of the 0.88 inch pipes. Second, the GSSI radar used a different antenna than the other three systems, which may have resulted in a different near-range response. Third, the received signal level is sensitive to the antenna coupling to the ground. Optimally, the antennas should be flush with the soil surface. However, the soil surface could not be made perfectly flat, so that some unevenness existed.

Another very important result can be determined from the ratios of the plastic and metal 0.88 inch pipes. On the average, the plastic pipe return is about 9 dB lower in amplitude than the metal pipe return. This implies that the plastic pipe has a radar cross section that is approximately one-third that of the metal pipe in voltage. Similar variations of the signal amplitudes are observed when comparing the returns from the plastic and metal pipes buried at other depths. The implication is that a plastic pipe of a given diameter must be closer to the surface than a metal pipe of the same diameter in order to be detected.

The radar cross section of a plastic pipe filled with a liquid, such as water, will typically be greater than that of a plastic pipe filled with a gas. This is due to the higher

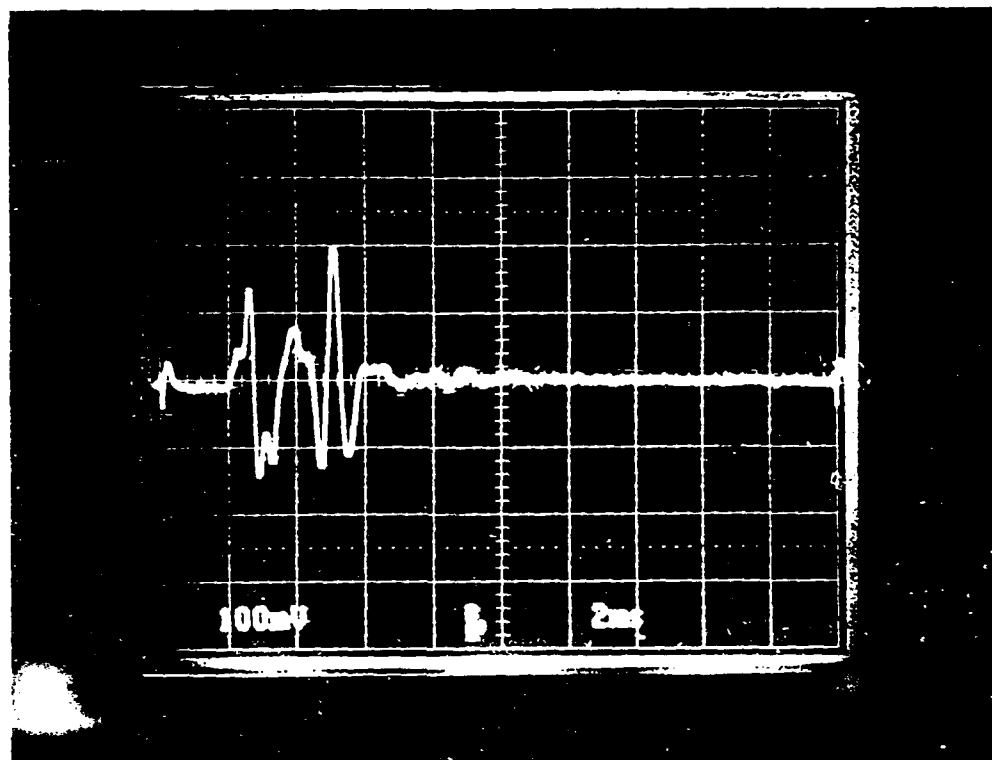
relative dielectric constant of the liquid. The plastic pipes in the soil-model tank were air-filled, and no measurements were made with liquid-filled plastic pipes.

Another phenomenon was noted when generating strip-chart recordings using the two time-domain pulsed radars. The metal pipe signals were detectable at much greater off-center angles than the plastic pipes. (An off-center orientation is obtained by first placing the GPR antenna directly over the pipe and then moving the antenna in a direction perpendicular to the longitudinal axis of the pipe.) This difference in off-center responses was greater than that which could be explained simply based on the larger return obtained in general from the metal pipe than from the plastic pipe. This means that the radar cross section of an air-filled plastic pipe varies differently with respect to the off-center angle than does that of a metal pipe. Thus, algorithms to extract pipe returns from radar receiver waveforms should account for these differences in the radar cross section patterns of the two classes of pipes.

A thorough measurement of the radar cross section patterns of metal and plastic pipes of similar diameter with respect to depth would be quite interesting. Results from such an investigation would be valuable to the GPR designer and to the designer of pipe-detection signal processing algorithms. Such measurements, however, were beyond the scope of this program.

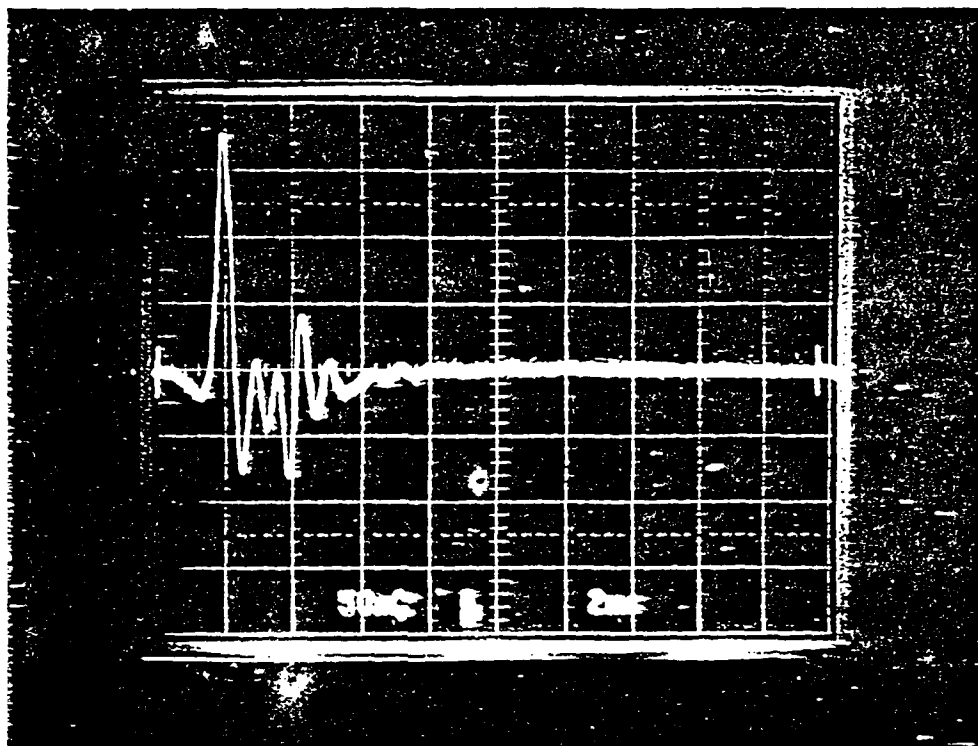
Figures 8.2 through 8.17 are photographs and plots of the received waveforms from each of the GPR systems. The antenna systems were placed in four different locations on the surface of the soil-model tank. The antenna systems were always centered directly above the pipe and polarized in parallel with the pipe axis to ensure maximum return signal. The surface and target return signals are identified in each figure. The location of the antenna systems in each figure is described below.

In Figures 8.2 through 8.5, the antenna system was placed above the 1.31 inch metal pipe buried at a depth of 7.8 inches. Figures 8.6 through 8.9 show the returns from the 1.25 inch diameter plastic pipe at a depth of 7.8 inches with the metal plate located beneath the pipe at a depth of 21.6 inches. In this case, the antenna was placed directly above the pipe, and the plate was slightly off-center. Figures 8.10 through 8.13



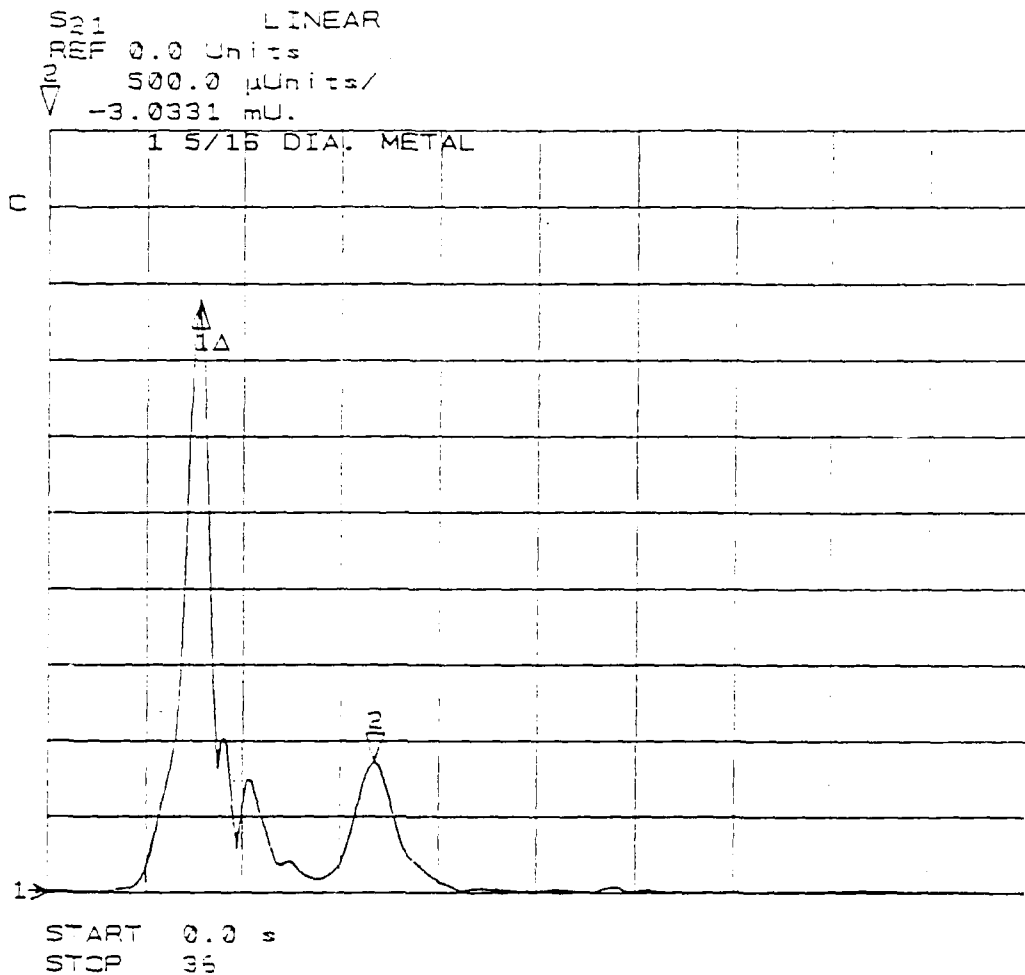
SURFACE AT 1.5 DIV FROM LEFT
1.31 DIA METAL PIPE AT 2.5 DIV FROM LEFT
4 NS/DIV REAL-TIME

Figure 8.2: Phase 1 measurement. GAR short-pulse radar received waveform showing the 1.31 inch diameter metal pipe return at a depth of 7.8 inches.



SURFACE AT 1.2 DIV FROM LEFT
 1.31 DIA METAL PIPE AT 2.2 DIV FROM LEFT
 4 NS/DIV REAL-TIME

Figure 8.3: Phase 1 measurement. GSSI short-pulse radar received waveform showing the 1.31 inch diameter metal pipe return at a depth of 7.8 inches.



MARKER 1 = SURFACE
 MARKER 2 = 1.31 DIA METAL PIPE
 201 POINTS SWEPT-FM
 .3.6 NS/DIV REAL-TIME

Figure 8.4: Phase 1 measurement. HP8510 swept-FM received waveform showing the 1.31 inch diameter metal pipe return at a depth of 7.8 inches.

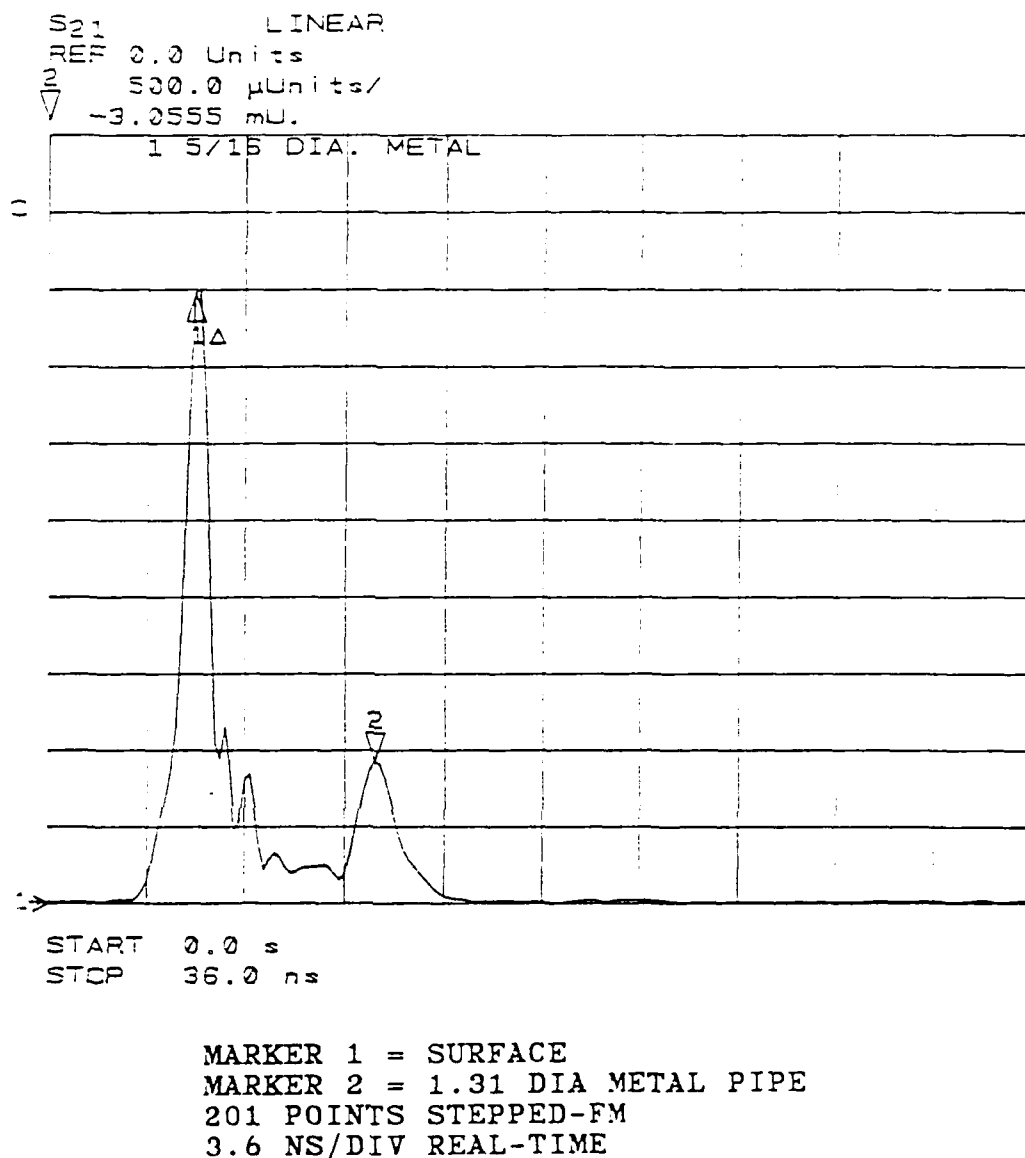
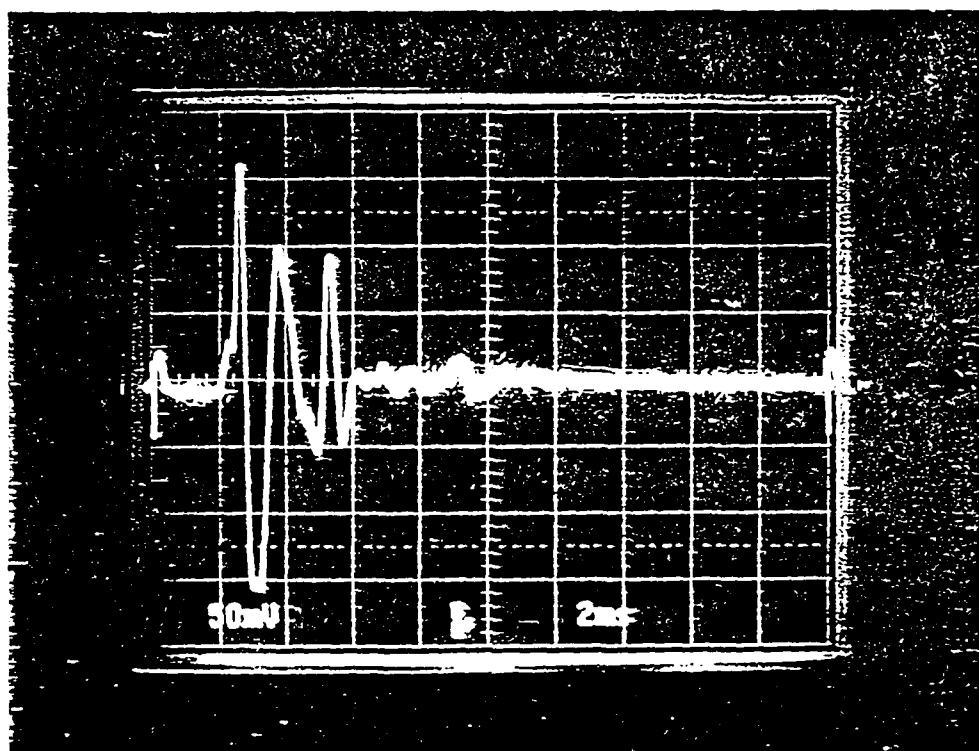
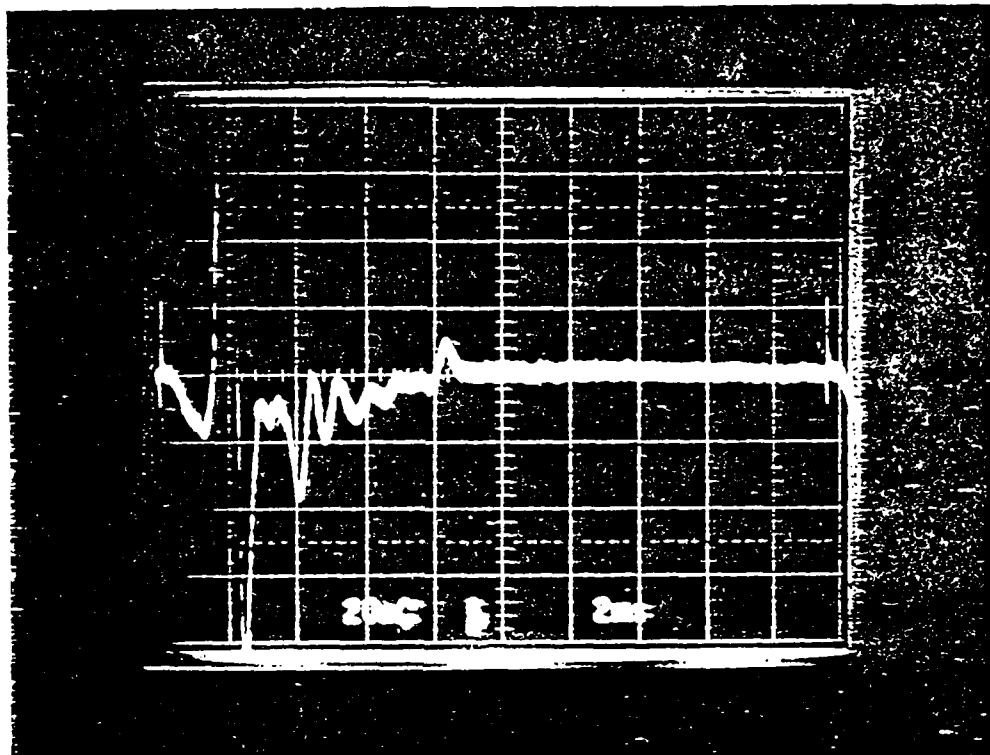


Figure 8.5: Phase 1 measurement. HP8510 stepped-FM received waveform showing the 1.31 inch diameter metal pipe return at a depth of 7.8 inches.



SURFACE AT 1.5 DIV FROM LEFT
 1.25 DIA PLASTIC PIPE AT 2.6 DIV FROM LEFT
 METAL PLATE AT 4.6 DIV FROM LEFT
 4 NS/DIV REAL-TIME

Figure 8.6: Phase 1 measurement. GAR short-pulse radar received waveform showing the returns from the 1.25 inch plastic pipe at 7.8 inches and the metal plate at 21.6 inches.



SURFACE AT 1.2 DIV FROM LEFT
1.25 DIA PLASTIC PIPE AT 2.2 DIV FROM LEFT
METAL PLATE AT 4.2 DIV FROM LEFT
4 NS/DIV REAL-TIME

Figure 8.7: Phase 1 measurement. GSSI short-pulse radar received waveform showing the return from the 1.25 inch diameter plastic pipe at 7.8 inches and the metal plate at 21.6 inches.

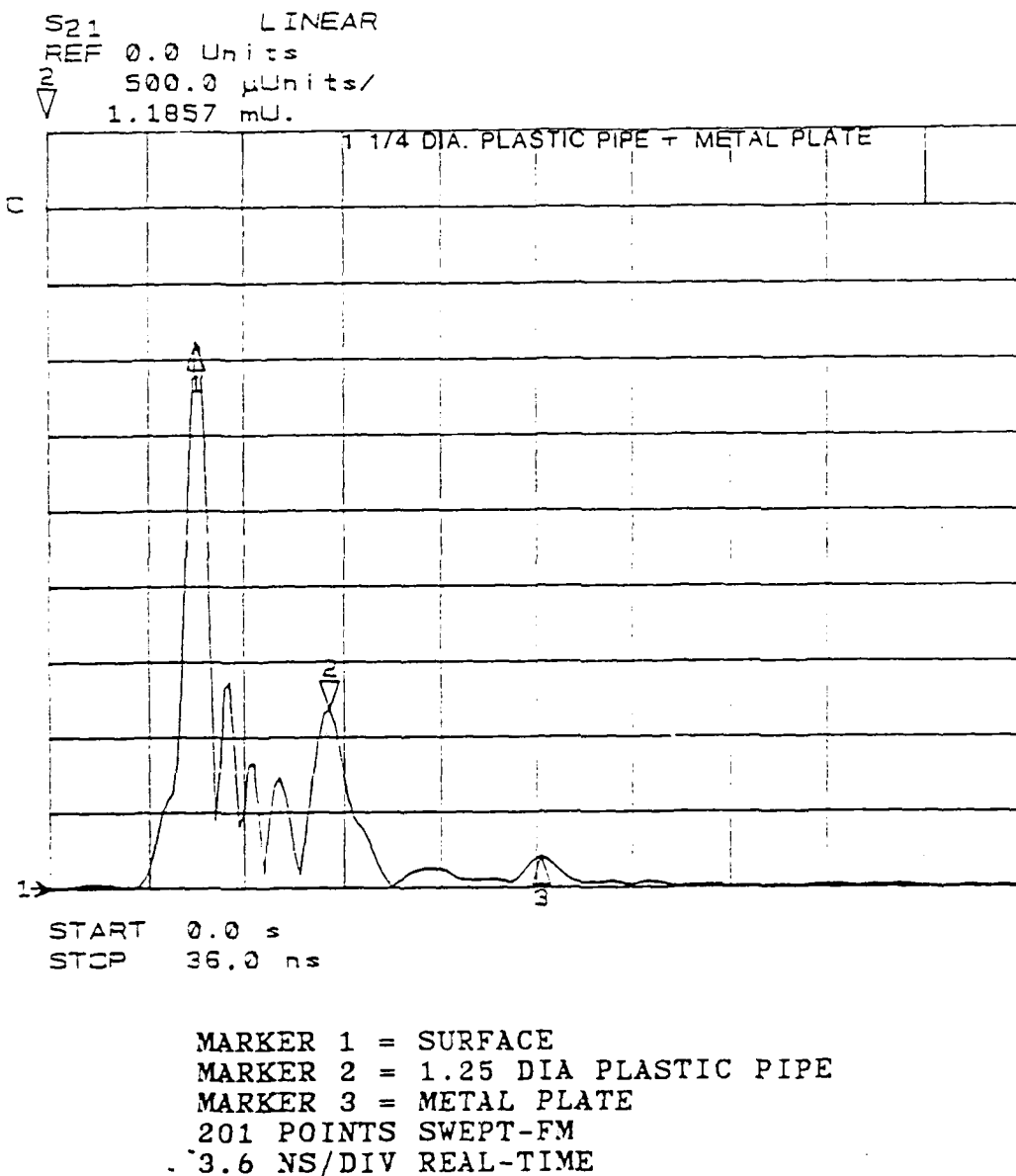
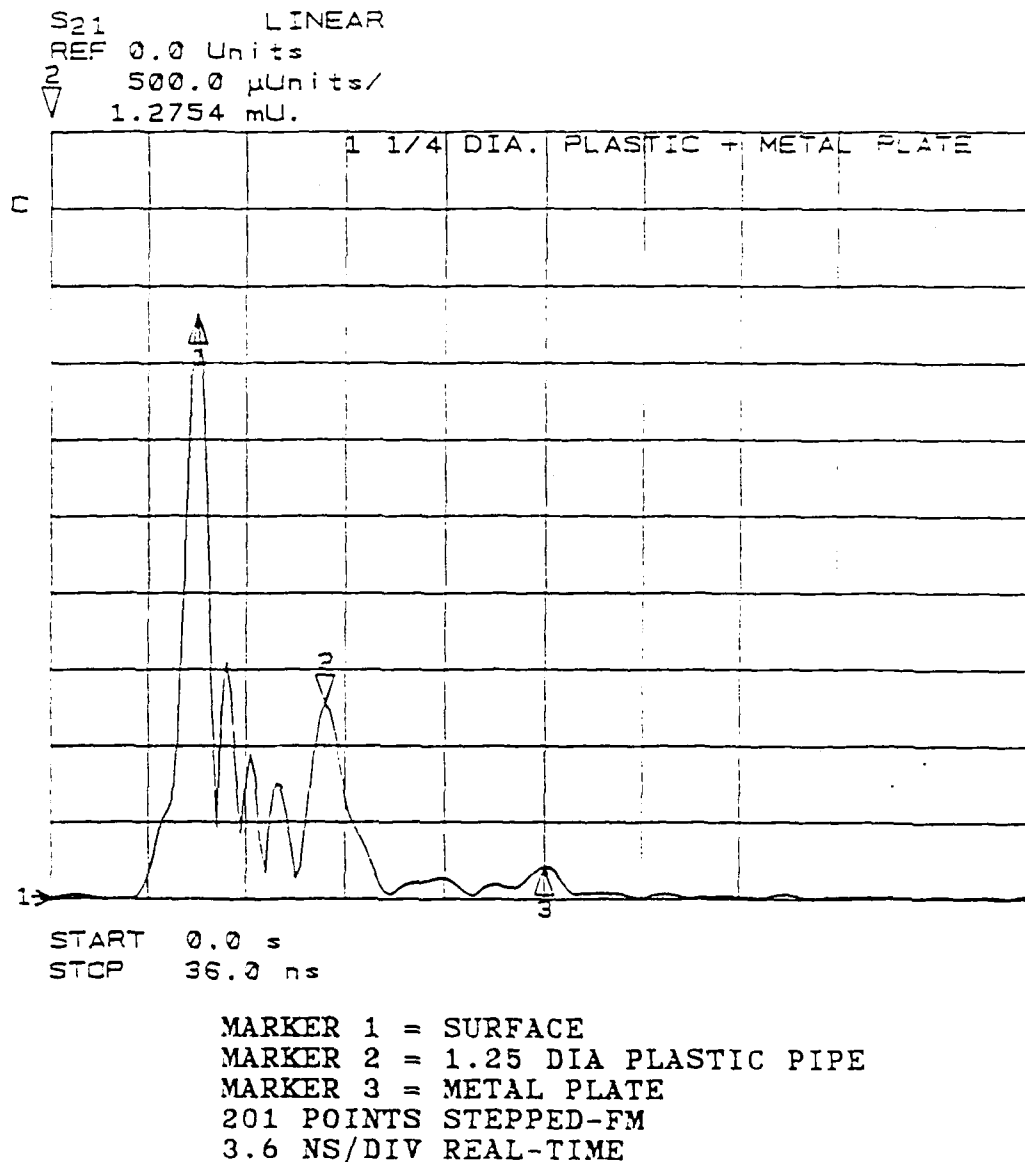
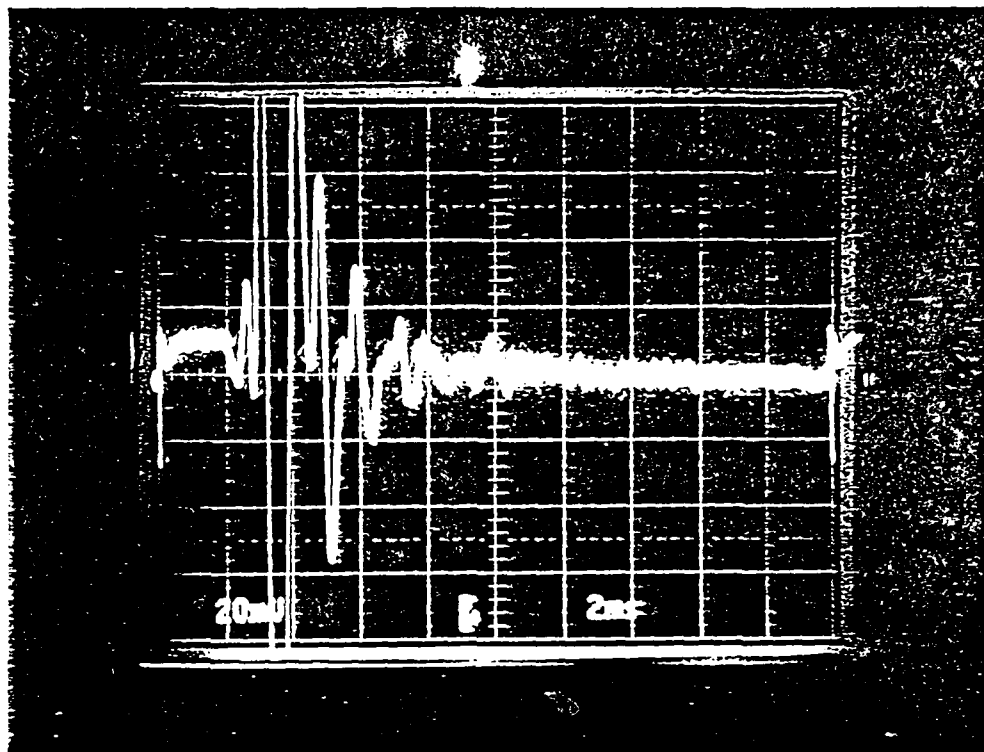


Figure 8.8: Phase 1 measurement. HP8510 swept-FM received waveform showing the return from the 1.25 inch diameter plastic pipe at 7.8 inches and the metal plate at 21.6 inches.



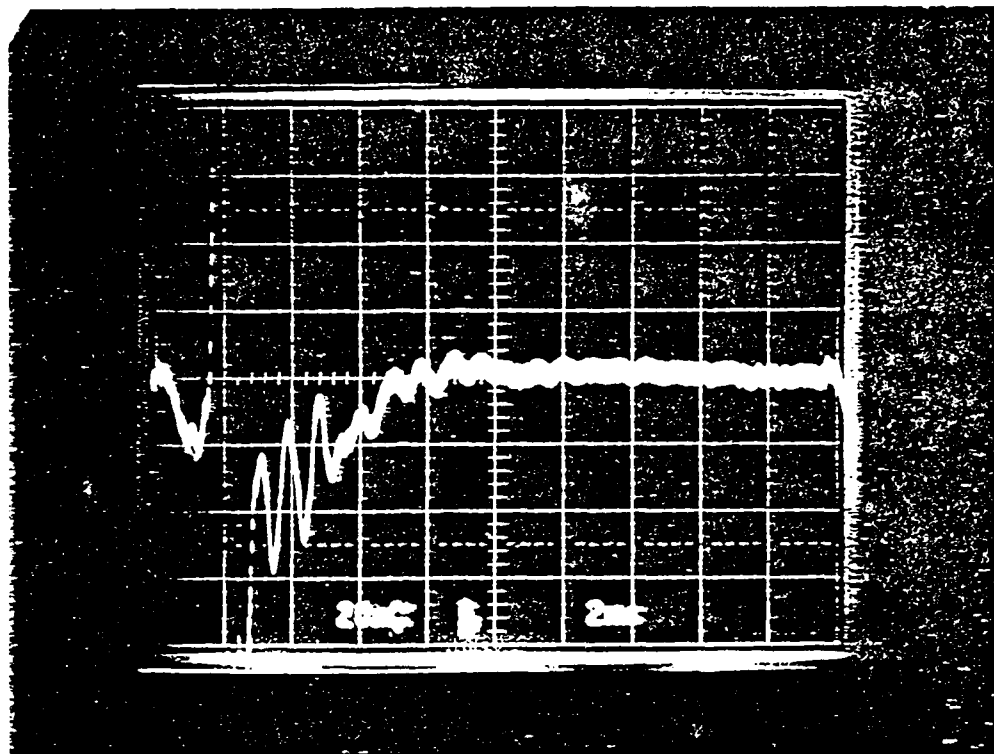
MARKER 1 = SURFACE
 MARKER 2 = 1.25 DIA PLASTIC PIPE
 MARKER 3 = METAL PLATE
 201 POINTS STEPPED-FM
 3.6 NS/DIV REAL-TIME

Figure 8.9: Phase 1 measurement. HP8510 stepped-FM received waveform showing the return from the 1.25 inch diameter plastic pipe at 7.8 inches and the metal plate at 21.6 inches.



SURFACE AT 1.8 DIV FROM LEFT
3.5 DIA METAL PIPE AT 5 DIV FROM LEFT
4 NS/DIV REAL-TIME

Figure 8.10: Phase 1 measurement. GAR short-pulse radar received waveform showing the return from the 3.5 inch metal pipe at 18 inches.



SURFACE AT 1.3 DIV FROM LEFT
3.5 DIA METAL PIPE AT 4.4 DIV FROM LEFT
4 NS/DIV REAL-TIME

Figure 8.11: Phase 1 measurement. GSSI short-pulse radar received waveform showing the return from the 3.5 inch metal pipe at 18 inches.

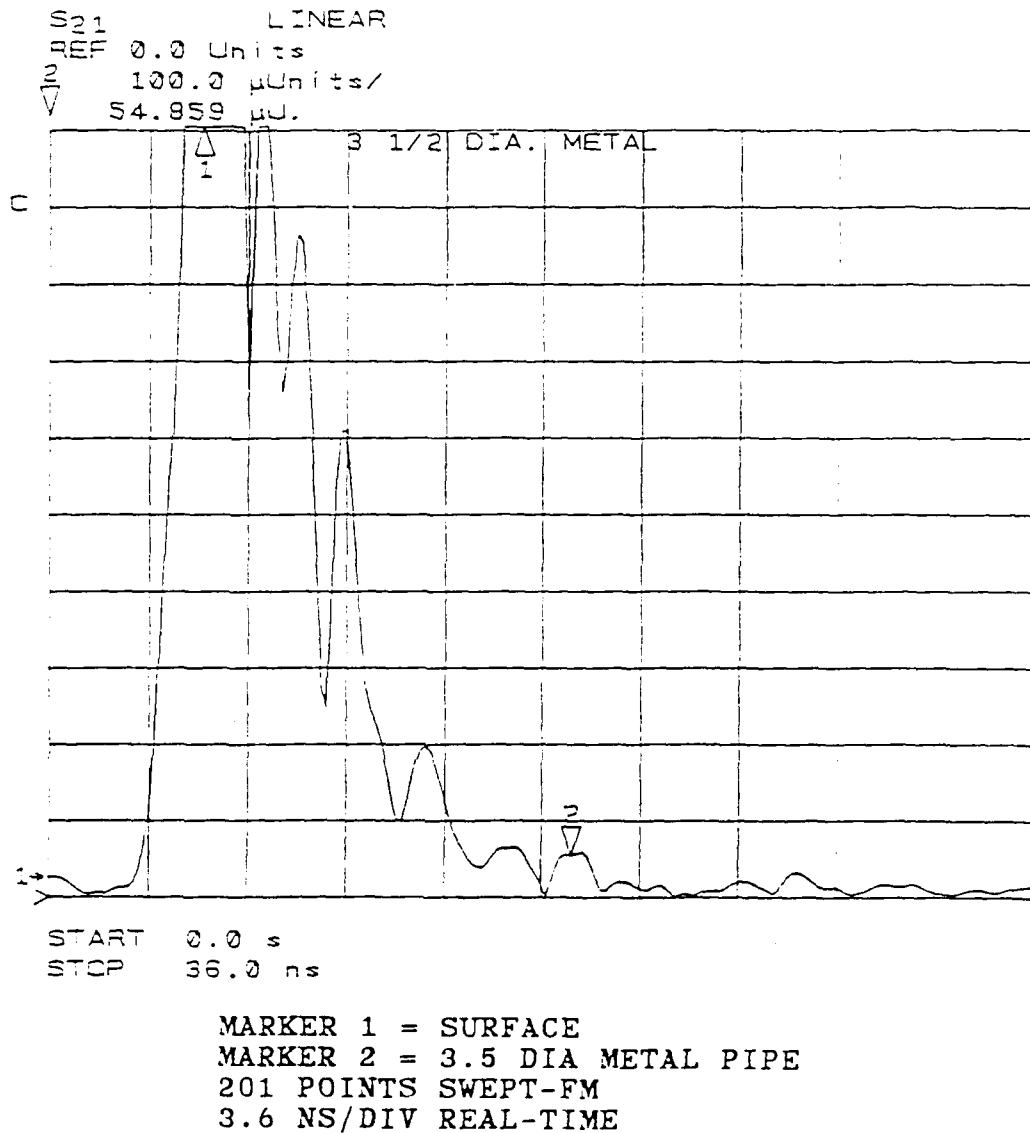
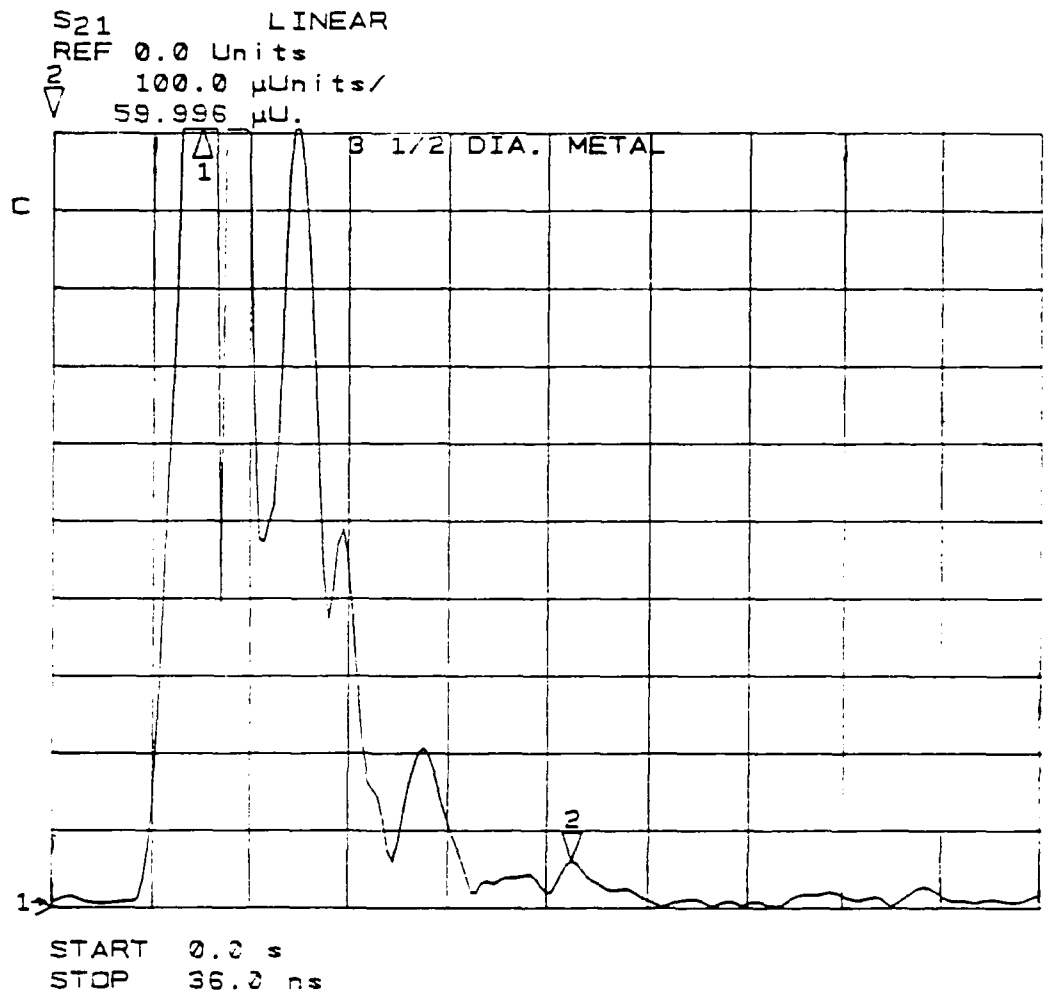
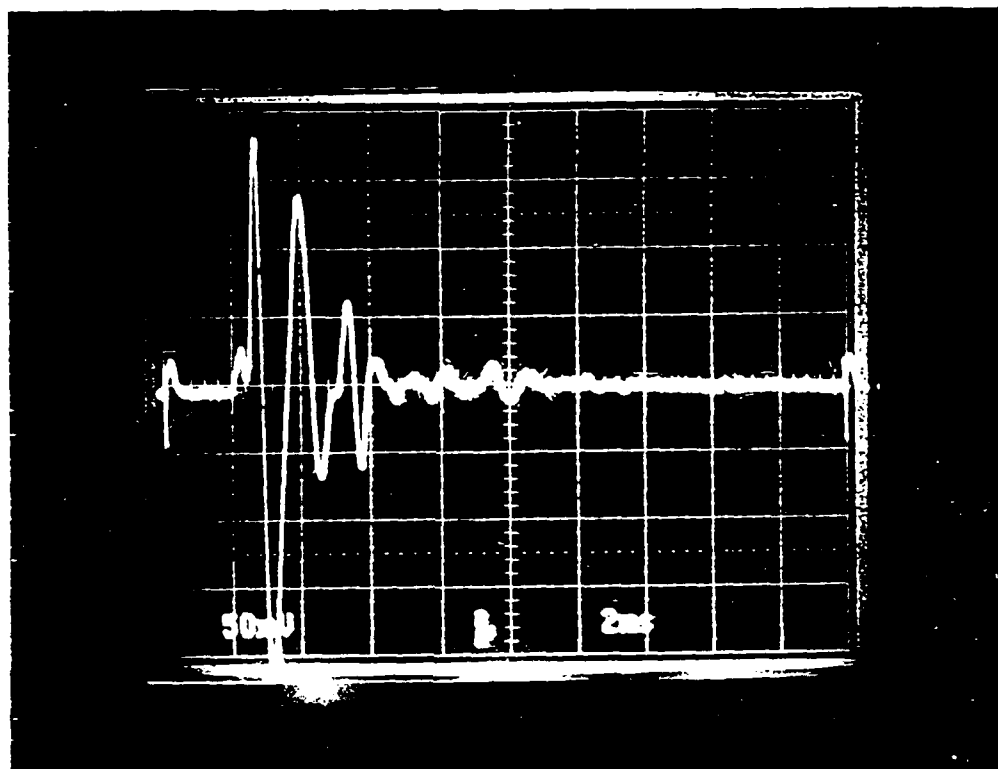


Figure 8.12: Phase 1 measurement. HP8510 swept-FM received waveform showing the return from the 3.5 inch metal pipe at 18 inches.



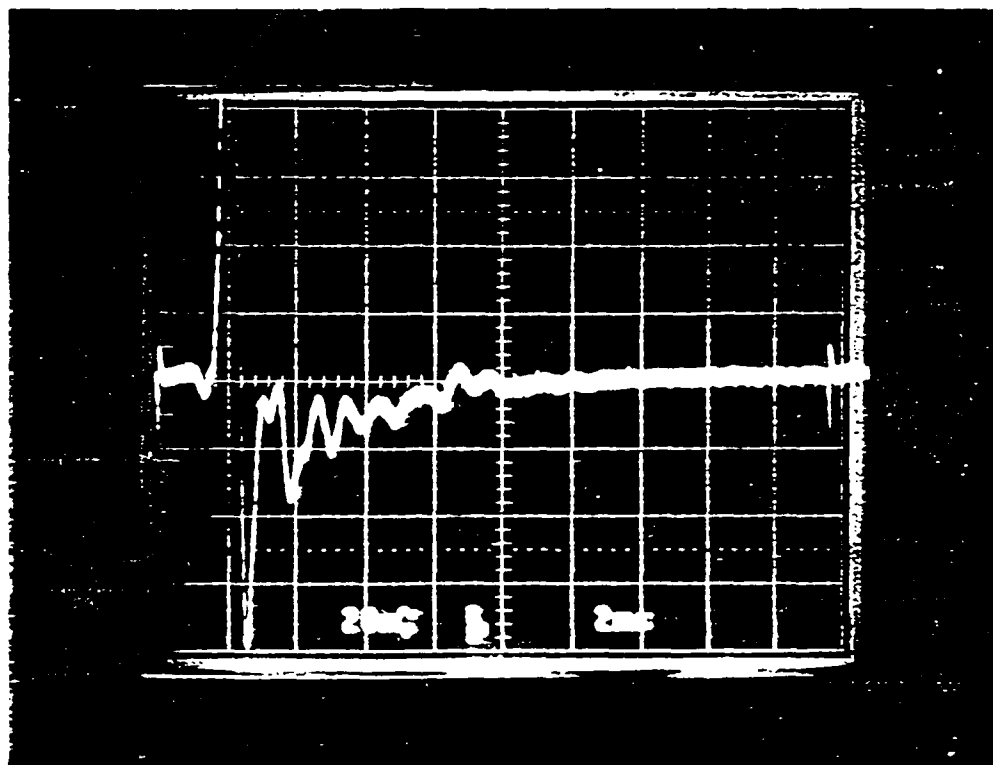
MARKER 1 = SURFACE
MARKER 2 = 3.5 DIA METAL PIPE
201 POINTS STEPPED-FM
3.6 NS/DIV REAL-TIME

Figure 8.13: Phase 1 measurement. HP8510 stepped-FM received waveform showing the return from the 3.5 inch metal pipe at 18 inches.



SURFACE AT 1.6 DIV FROM LEFT
 2.5 DIA PLASTIC PIPE AT 3.9 DIV FROM LEFT
 4 NS/DIV REAL-TIME

Figure 8.14: Phase 1 measurement. GAR short-pulse radar received waveform showing the return from the 2.5 inch diameter plastic pipe at 15.6 inches.



SURFACE AT 1.3 DIV FROM LEFT
2.5 DIA PLASTIC PIPE AT 3.4 DIV FROM LEFT
4 NS/DIV REAL-TIME

Figure 8.15: Phase 1 measurement. GSSI short-pulse radar received waveform showing the return from the 2.5 inch diameter plastic pipe at 15.6 inches.

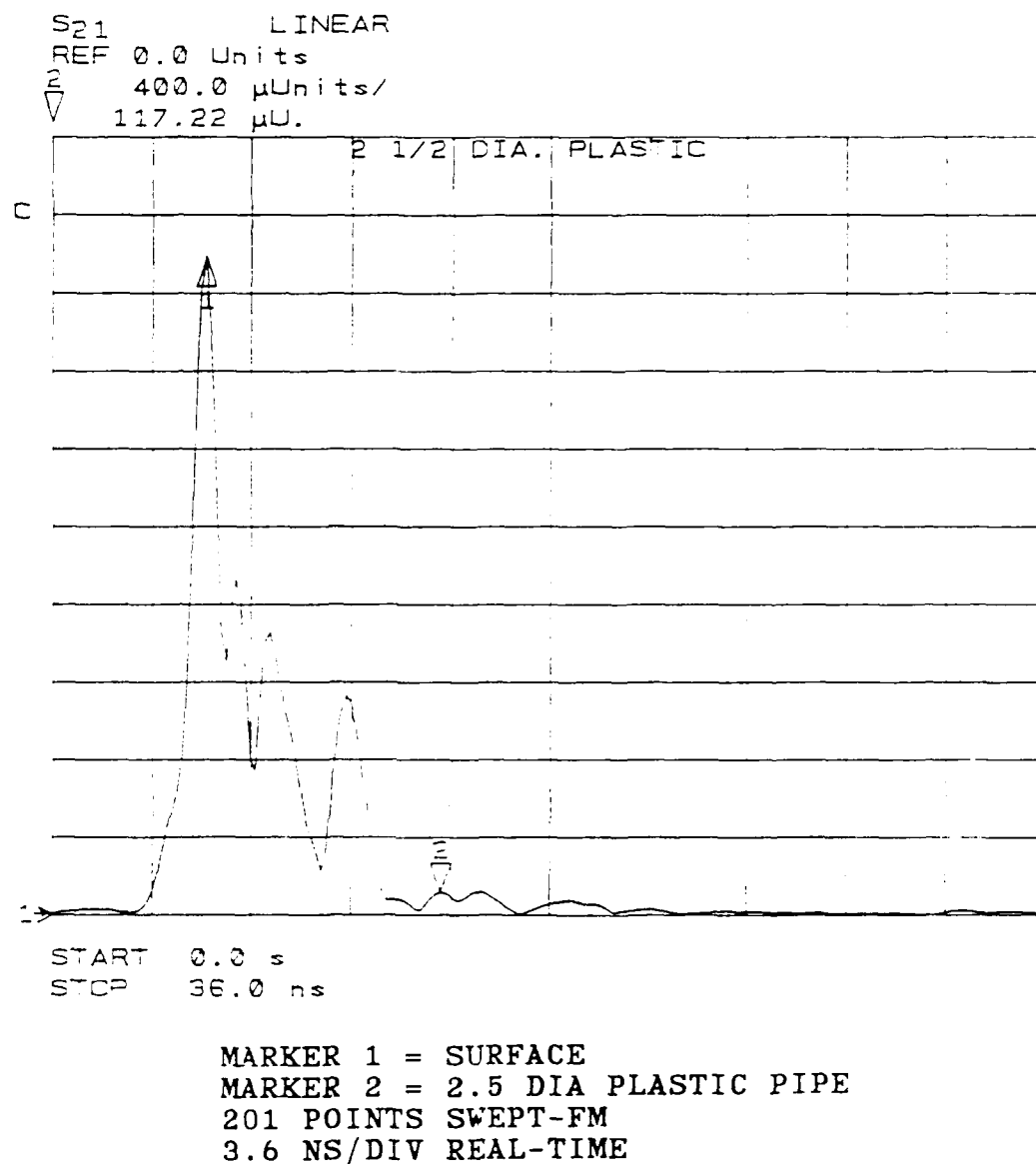


Figure 8.16: Phase 1 measurement. HP8510 swept-FM received waveform showing the return from the 2.5 inch diameter plastic pipe at 15.6 inches.

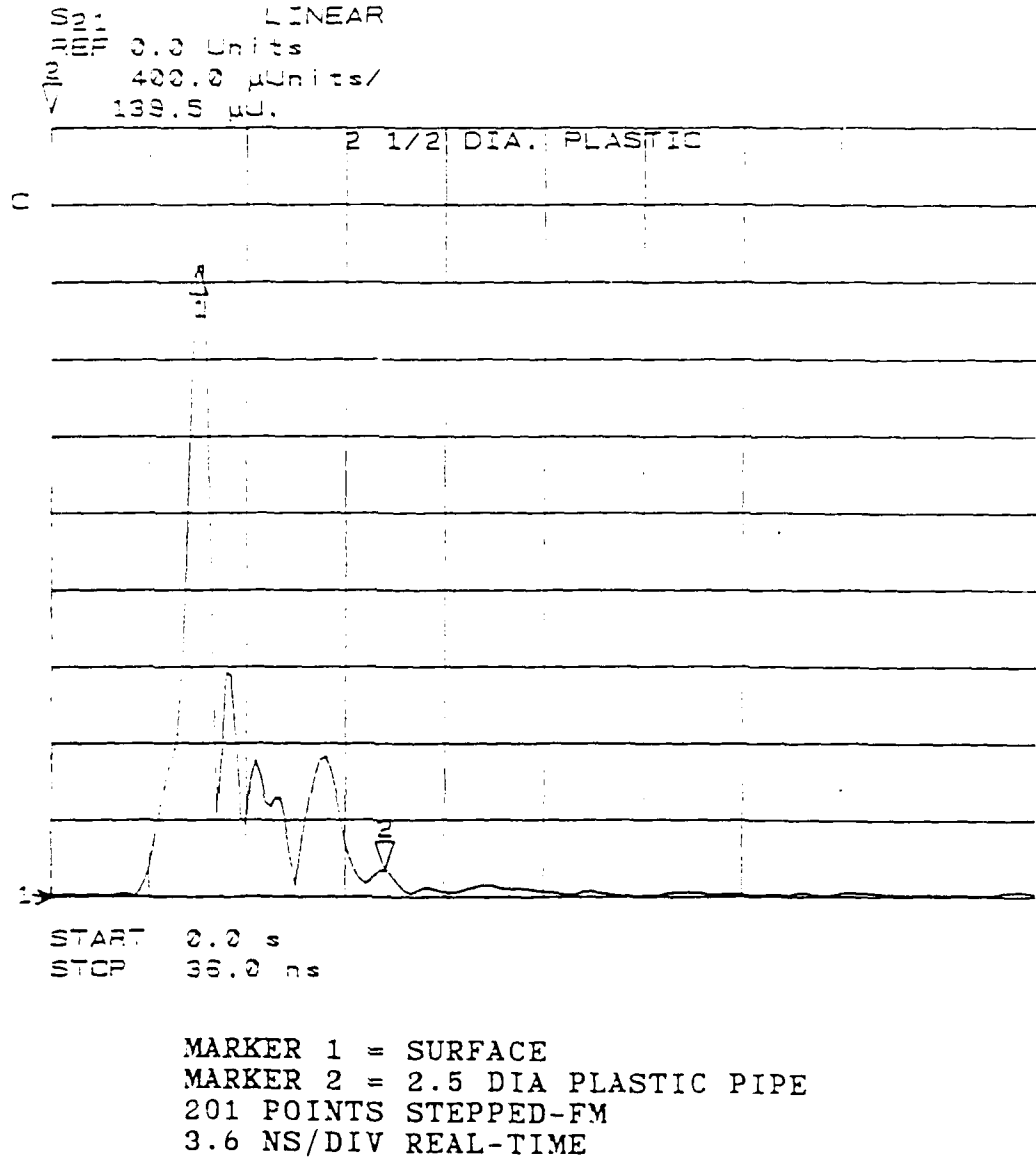


Figure 8.17: Phase 1 measurement. HP8510 stepped-FM receiver waveform showing the return from the 2.5 inch diameter plastic pipe at 15.6 inches.

show the received signals from the 3.5 inch diameter metal pipe at a depth of 18 inches. Finally, Figures 8.14 through 8.17 show the received waveform from the 2.5 inch plastic pipe buried at a depth of 15.6 inches.

8.2 PHASE 2 SCALE-MODEL GPR MEASUREMENTS (CLAY SCHIST)

The Phase 2 measurements were performed with clay schist in the soil-model tank. The measured dielectric properties of a sample of the clay schist are given in Appendix B. The tank was filled using the same procedure as was used with the clay shale of the Phase 1 measurements. The targets and their placements were exactly the same as for the Phase 1 measurements.

The Phase 2 measurements consisted of the verification of the soil dielectric constant and the actual target measurements. A signal-to-clutter measurement was not performed because the schist did not have a high enough attenuation to make it suitable as a matched load for the antenna. A summary of the Phase 2 measurements is given in the sections which follow.

8.2.1 GPR MEASUREMENT OF THE RELATIVE DIELECTRIC CONSTANT OF THE PHASE 2 SOIL-MODEL TEST TANK

The measurement procedure to determine the relative dielectric constant of the clay schist was the same as that used for the Phase 1 measurement. In this case, however, the return from the metal pipe 36 inches below the surface was used as a reference. Figure 8.18 shows the pipe return signal from the HP 8510 operating in the stepped mode. Marker 1 is located on the surface return and Marker 2 is on the pipe return. The pipe return is located 22 nanoseconds from the surface. Using Equation (8.2) and $s = 0.082\text{m}$, one computes the relative dielectric constant to be 12.94.

Two samples of the schist were tested using the open circuit sample cell in order to determine the dielectric properties of the soil in the tank. The first sample was taken from soil at the brick manufacturer's location and the second

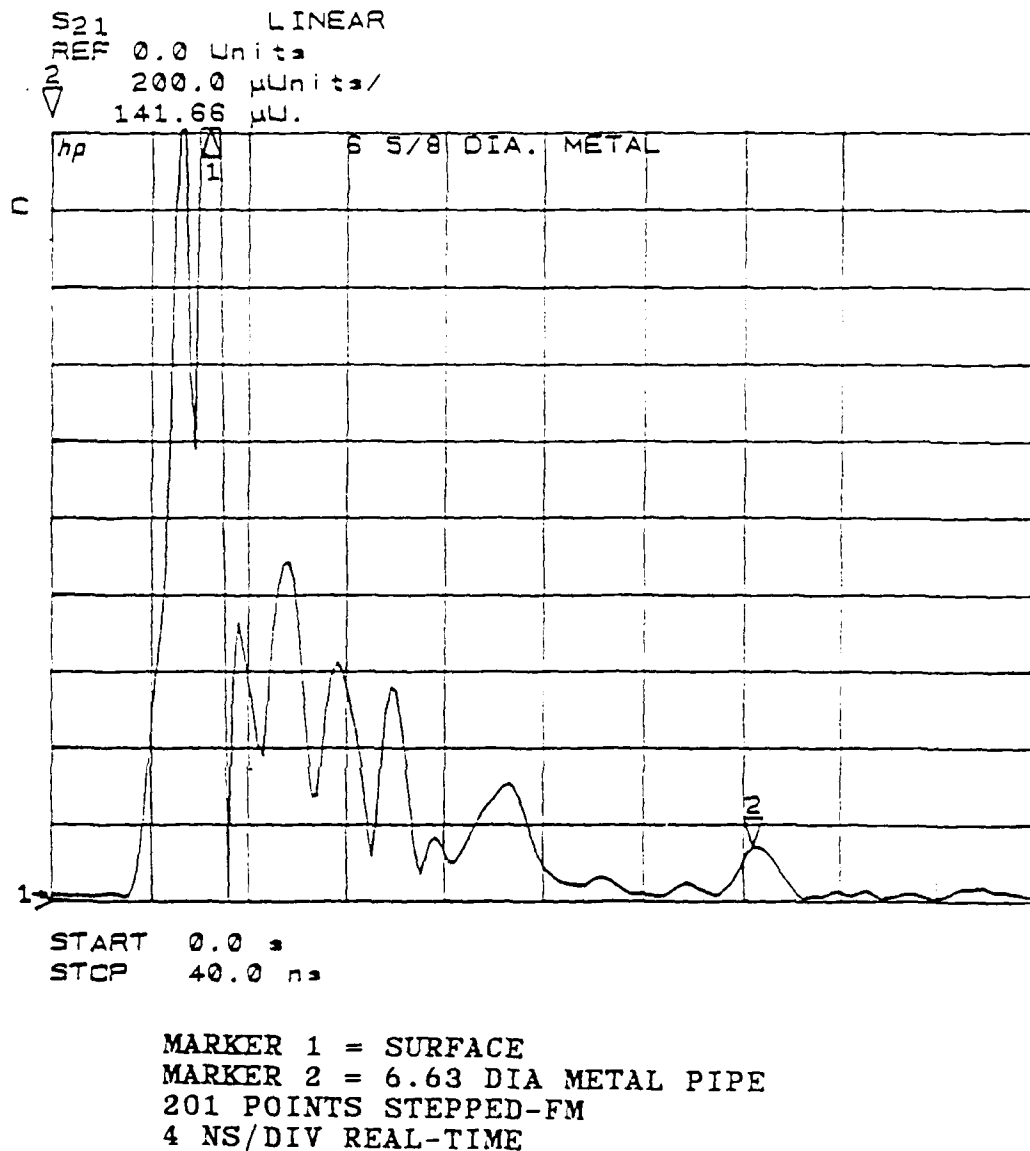


Figure 8.18: Phase 2 measurement. Plot of the HP8510 returns of the surface (Marker 1), and the 6.63 inch diameter metal pipe (Marker 2).

was taken from soil that was used in the test tank. The first sample produced a relative dielectric constant of approximately 22, which is considerably higher than the value obtained using the GPR system. Consequently, the second soil sample was measured using two packing densities, firm and dense, in an effort to produce a relative dielectric constant measurement that was closer to the GPR system measurement. All three sets of measurements are presented in Appendix B.

The third set of measurements (dense packing) revealed a relative dielectric constant varying between 11 and 14.5 over the frequency range of 200 MHz to 2.0 GHz. However, the curve does exhibit an undulation that is not typical of such a measurement. It was felt that this undulation could be attributed to the difficulty in producing a uniformly dense packing of the soil sample in the test cell. Nevertheless, the similarity between the GPR dielectric constant measurement and the densely packed test cell measurement of the second sample implied that the test cell measurement of the attenuation could characterize the soil in the test tank with a reasonable degree of accuracy. Therefore, the matching test cell measurements could be used to extrapolate the scale-model system to a full-scale environment.

8.2.2 PHASE 2 SOIL-MODEL TANK TARGET MEASUREMENTS

The Phase 2 target measurements were performed in a similar manner as the Phase 1 target measurements. Table 8.4 summarizes the results of these target measurements. This table is structured in exactly the same way as Table 8.2. Table 8.5 is similar to Table 8.3 from Section 8.1.3 in that it lists the normalized received signals for each GPR, where normalization is done relative to the return from the corresponding 0.88 inch pipe (metal or plastic) for the GPR of interest. In addition, photographs and plots of the GPR output waveforms are included at the end of this section.

When examining Table 8.4, one should note that all of the targets were detected with all of the GPR systems. This is due, of course, to the lower attenuation of the schist in the tank. For the same reason, target signal return amplitudes from the Phase 2 measurements were in general significantly

TABLE 8.4. SUMMARY OF MEASUREMENT RESULTS FROM GPR TESTS WITH SOIL MODEL TANK FILLED WITH SCHIST CLAY.

SCALE-MODEL (scale factor = 5)			FULL-SCALE		GPR Received Target Signal Amplitude			
Pipe Diameter (inches)	Depth From Surface (inches)	Pipe Diameter (inches)	Depth From Surface (feet)	Pipe Material	GAR Short Pulse (millivolts)	GSSI Short Pulse (millivolts)	HP8510 Swept FM (micro-units)	HP8510 Stepped FM (micro-units)
0.88	4.1	4.4	1.71	Metal	980	800	14,140	14,688
1.31	7.8	6.6	3.25	Metal	480	340	7,280	7,120
1.31	10.7	6.6	4.46	Metal	340	240	3,910	4,026
2.38	15.6	11.9	6.50	Metal	230	145	2,147	2,256
3.50	18.0	17.5	7.50	Metal	160	125	2,124	2,322
4.50	26.6	22.5	11.08	Metal	90	55	688	766
6.63	36.0	33.2	15.00	Metal	30	18	136	142
0.88	4.1	4.4	1.71	Plastic	360	260	5,800	5,108
1.25	7.8	6.3	3.25	Plastic	200	180	2,590	2,685
1.25	10.7	6.3	4.46	Plastic	215	140	2,430	2,966
2.50	15.6	12.5	6.50	Plastic	100	85	1,170	1,153
3.50	18.0	17.5	7.50	Plastic	80	66	886	869
4.50	26.6	22.5	11.08	Plastic	40	30	365	143

Schist clay loss at 1 GHz : 33 dB/m

Scaled soil loss at 200 MHz (= 1 GHz/5) : 6.6 dB/m

TABLE 8.5. SUMMARY OF NORMALIZED TARGET SIGNAL AMPLITUDES FROM GPR TESTS WITH SOIL MODEL TANK FILLED WITH SCHIST CLAY.

Amplitudes are normalized for each pipe material (metal or plastic) for each candidate GPR based on the return from the 0.88 inch diameter pipe (metal or plastic) buried at a depth of 4.1 inches.

SCALE-MODEL (scale factor = 5)			FULL-SCALE		GPR Normalized Target Signal Amplitude			
Pipe Diameter (inches)	Depth From Surface (inches)	Pipe Diameter (inches)	Depth From Surface (feet)	Pipe Material	GAR Short Pulse (millivolts)	GSSI Short Pulse (millivolts)	HP8510 Swept FM (micro-units)	HP8510 Stepped FM (micro-units)
0.88	4.1	4.4	1.71	Metal	1	1	1	1
1.31	7.8	6.6	3.25	Metal	0.490	0.425	0.515	0.485
1.31	10.7	6.6	4.46	Metal	0.347	0.300	0.277	0.274
2.38	15.6	11.9	6.50	Metal	0.235	0.181	0.152	0.154
3.50	18.0	17.5	7.50	Metal	0.163	0.156	0.150	0.158
4.50	26.6	22.5	11.08	Metal	0.092	0.069	0.049	0.052
6.63	36.0	33.2	15.00	Metal	0.031	0.022	0.010	0.010
0.88	4.1	4.4	1.71	Plastic	1	1	1	1
1.25	7.8	6.3	3.25	Plastic	0.556	0.692	0.447	0.526
1.25	10.7	6.3	4.46	Plastic	0.597	0.538	0.419	0.581
2.50	15.6	12.5	6.50	Plastic	0.278	0.327	0.202	0.226
3.50	18.0	17.5	7.50	Plastic	0.222	0.254	0.153	0.170
4.50	26.6	22.5	11.08	Plastic	0.111	0.115	0.063	0.030

Schist clay loss at 1 GHz : 33 dB/m

Scaled soil loss at 200 MHz (= 1 GHz/5) : 6.6dB/m

greater than comparable signal returns from the Phase 1 measurements. Table 8.6 presents the ratios of target signal amplitudes measured for the schist clay case divided by the corresponding amplitudes measured for the shale clay case.

An exception to the trend of larger signal returns with the schist clay was observed with the GAR short-pulse radar returns from the 0.88 inch diameter metal pipe buried at 4.1 inches. The metal pipe return was actually lower in this case by 13 percent. Contrast this with the results from the frequency-domain systems. The increase in return amplitude from the 0.88 inch diameter pipes in schist clay using the frequency domain systems was at least 49 percent, and ranged as high as 89 percent. The GSSI short-pulse radar showed an increase in the metal pipe return of 14 percent, and an increase in the plastic pipe return of 160 percent.

In general, the percentage increases in Phase 2 target return amplitudes relative to Phase 1 measurements for the two frequency-domain systems and the GSSI short-pulse radar were much higher than the comparable increases observed with the GAR short-pulse radar. These differences can only be attributed to the differences in the frequency content of the RF energy in the pulses generated by the GAR short-pulse radar as compared to those generated by the GSSI and the HP 8510 systems.

The ratios of deep-target returns (the pipes with diameters of 2.5 inches or more) to returns from the 0.88 inch pipes for the GAR short-pulse radar were higher than the same ratios for the frequency-domain systems (see Table 8.5). The ratios of the deep-target returns to the 0.88 inch pipe returns for the GSSI radar were similar to those of the GAR radar. However, the pipe returns measured with the GAR short pulse radar did not exhibit increases in going from Phase 1 to Phase 2 measurements as large as those exhibited by the frequency-domain systems.

Figures 8.19 through 8.38 are photographs and plots of the received waveforms from each GPR systems with the antennas in five different locations on the surface of the soil-model tank. The antennas were centered above each pipe of interest and polarized in parallel with the pipe axis to maximize the signal returns. The surface and target signal returns are identified. The photographs are described briefly in the paragraph below.

TABLE 8.6. SUMMARY OF RELATIVE TARGET SIGNAL AMPLITUDES (REFERENCED TO SHALE CLAY CASE) FOR GPR TESTS WITH SCHIST CLAY.

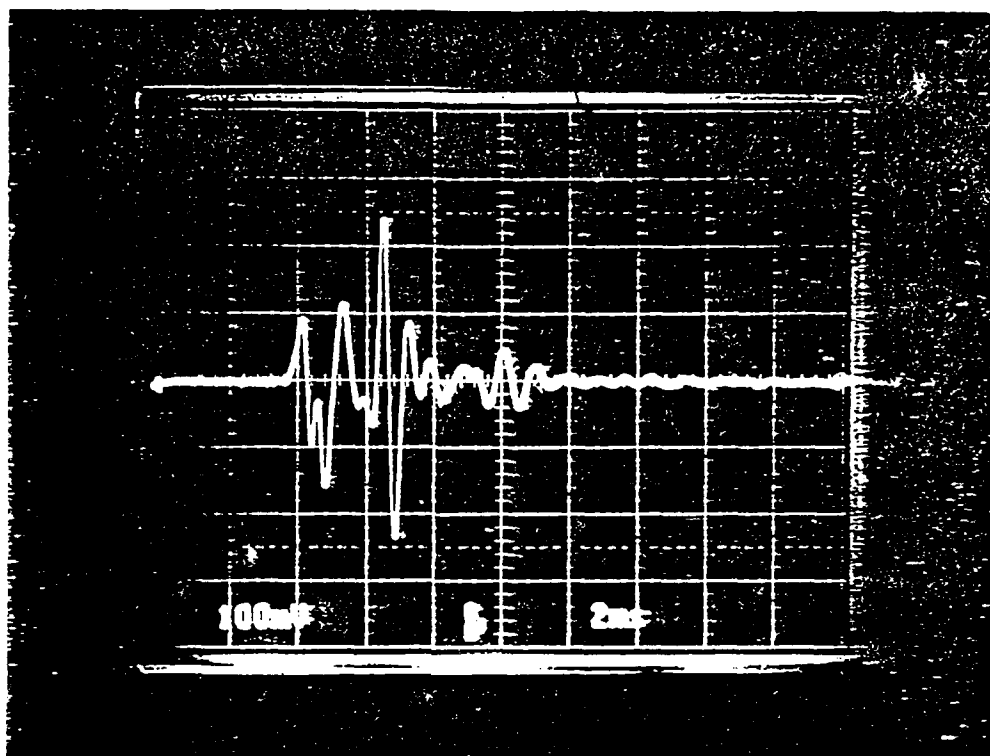
Individual table entries are generated by dividing the target return measured in the schist clay test by that measured in the shale clay test.

SCALE-MODEL (scale factor = 5)			FULL-SCALE		Relative Normalized Target Signal Amplitude Referenced to Shale Clay case				
Pipe Diameter (inches)	Depth From Surface (inches)	Pipe Diameter (inches)	Depth From Surface (feet)	Pipe Material	GAR Short Pulse (millivolts)	GSSI Short Pulse (millivolts)	HP8510 Swept FM (micro-units)	HP8510 Stepped FM (micro-units)	
0.88	4.1	4.4	1.71	Metal	0.875	1.14	1.58	1.89	
1.31	7.8	6.6	3.25	Metal	1.50	2.83	2.26	2.15	
1.31	10.7	6.6	4.46	Metal	2.83	2.67	4.60	4.47	
2.38	15.6	11.9	6.50	Metal	5.35	7.25	6.13	7.18	
3.50	18.0	17.5	7.50	Metal	11.4	15.6	38.6	38.7	
4.50	26.6	22.5	11.08	Metal	*	*	*	*	
6.63	36.0	33.2	15.00	Metal	*	*	*	*	
0.88	4.1	4.4	1.71	Plastic	1.12	2.60	1.75	1.49	
1.25	7.8	6.3	3.25	Plastic	1.38	5.00	2.18	2.10	
1.25	10.7	6.3	4.46	Plastic	5.38	11.7	12.2	14.83	
2.50	15.6	12.5	6.50	Plastic	5.00	10.6	10.0	8.24	
3.50	18.0	17.5	7.50	Plastic	*	*	*	*	
4.50	26.6	22.5	11.08	Plastic	*	*	*	*	

Schist clay loss at 1 GHz : 33 dB/m

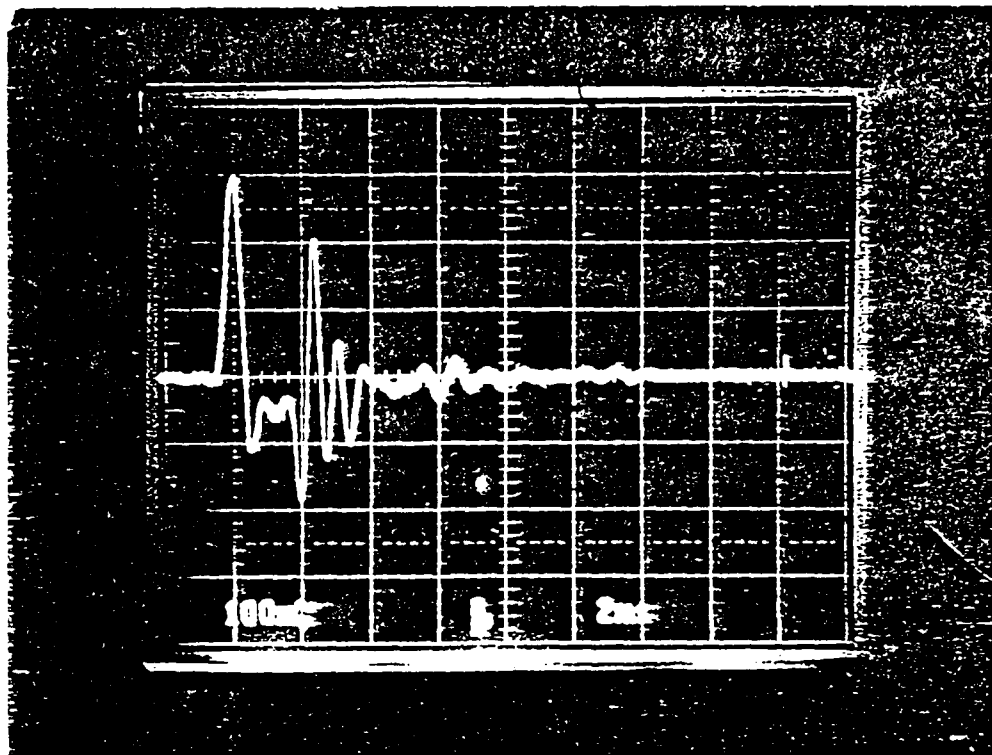
Scaled soil loss at 200 MHz (= 1 GHz/5) : 6.6dB/m

*Denotes cases in which pipe was undetectable in shale clay.



SURFACE AT 2.4 DIV FROM LEFT
1.31 DIA METAL PIPE AT 3.2 DIV FROM LEFT
4 NS/DIV REAL-TIME

Figure 8.19: Phase 2 measurement. GAR short-pulse radar received waveform showing the return from the 1.31 inch metal pipe at 7.8 inches.



SURFACE AT 1.0 DIV FROM LEFT
1.31 DIA METAL PIPE AT 2.2 DIV FROM LEFT
4 NS/DIV REAL-TIME

Figure 8.20: Phase 2 measurement. GSSI short-pulse radar received waveform showing the return from the 1.31 inch metal pipe at 7.8 inches. (4ns/Div, real time)

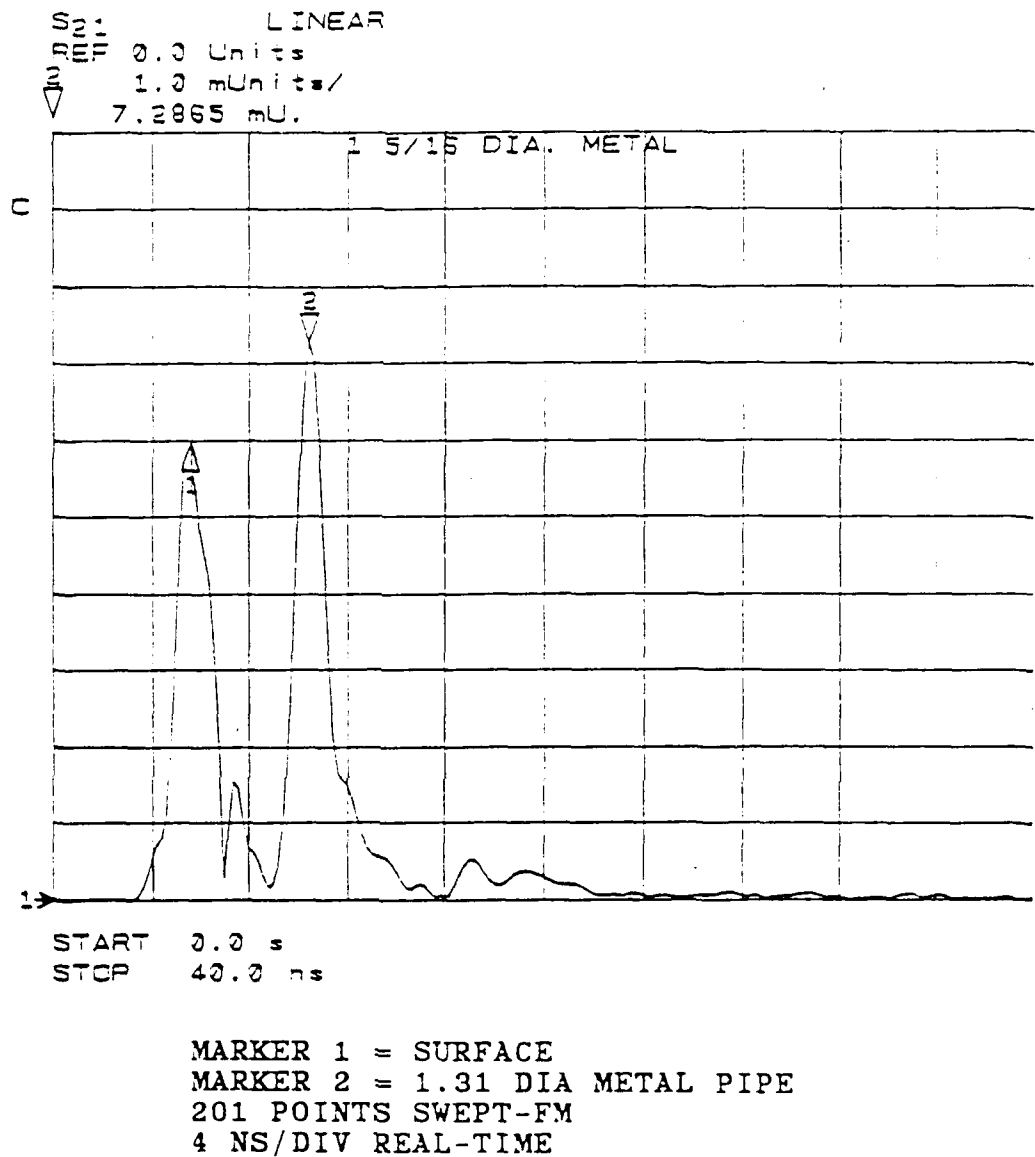


Figure 8.21: Phase 2 measurement. HP8510 swept-FM received waveform showing the return from the 1.31 inch metal pipe at 7.8 inches.

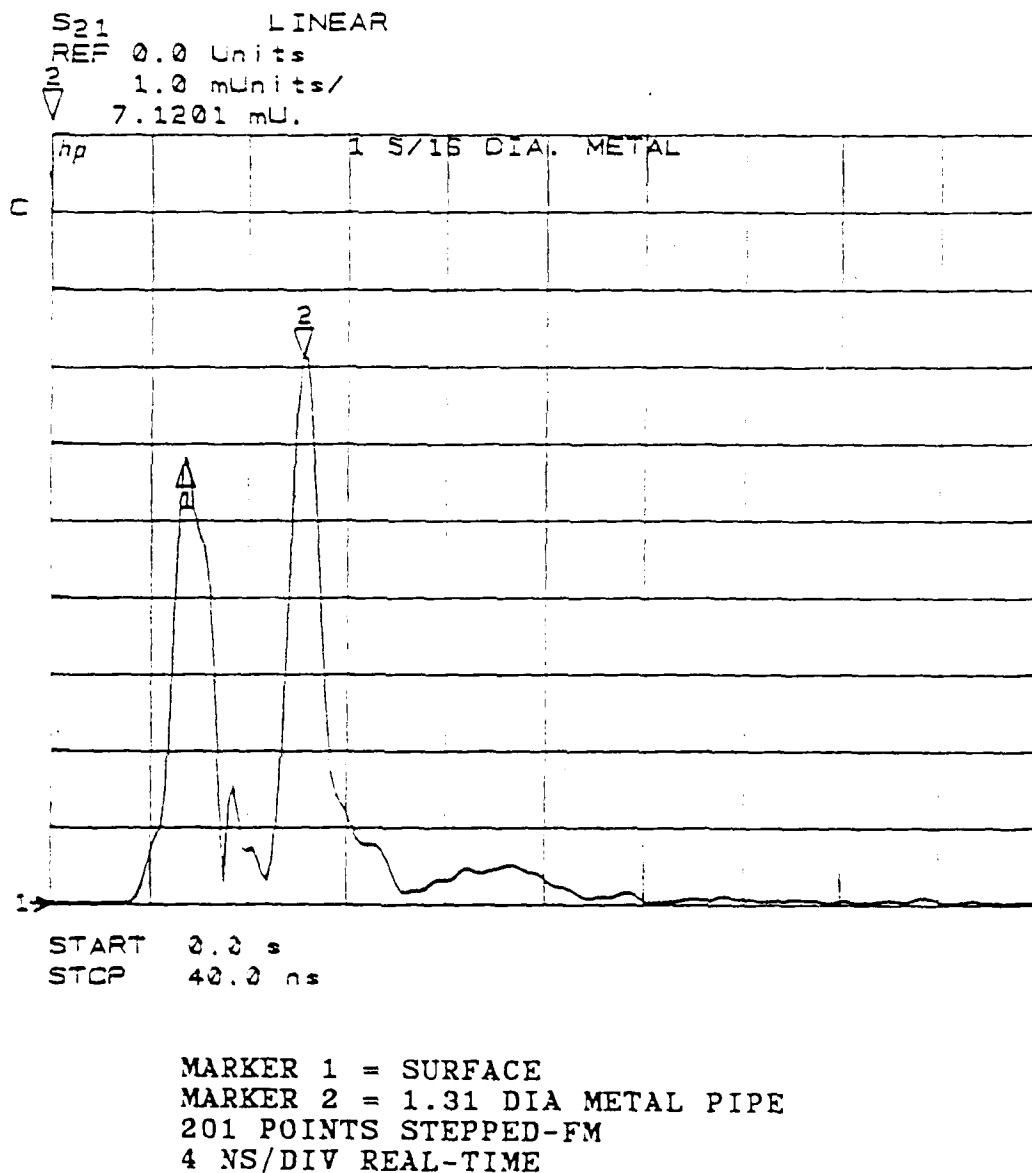
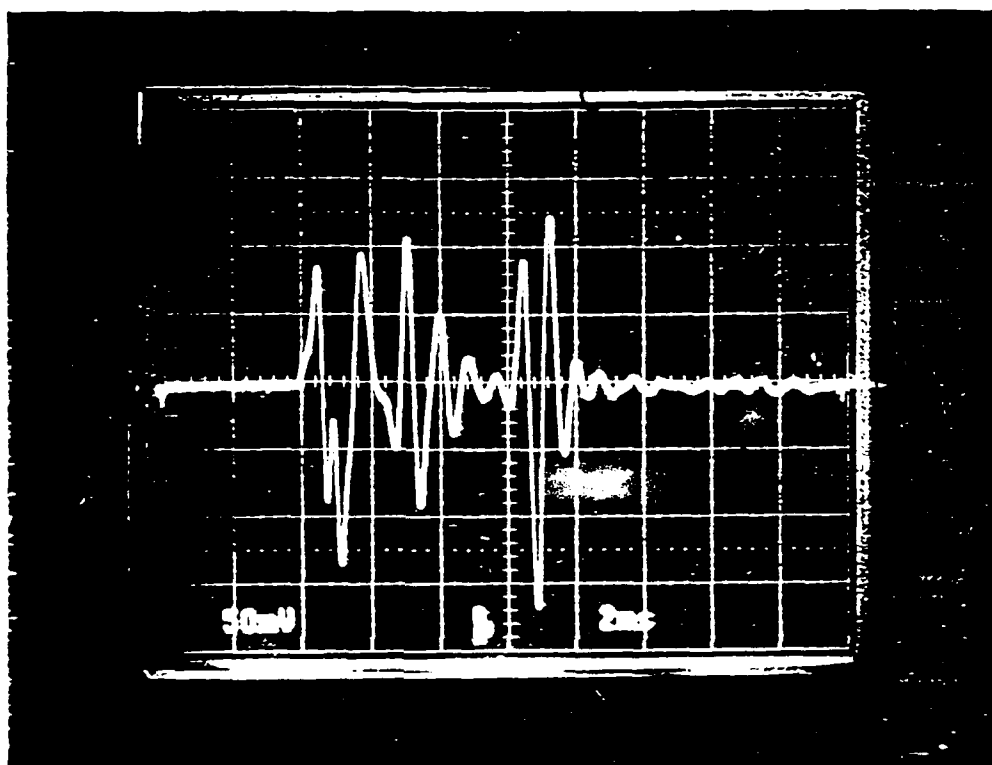
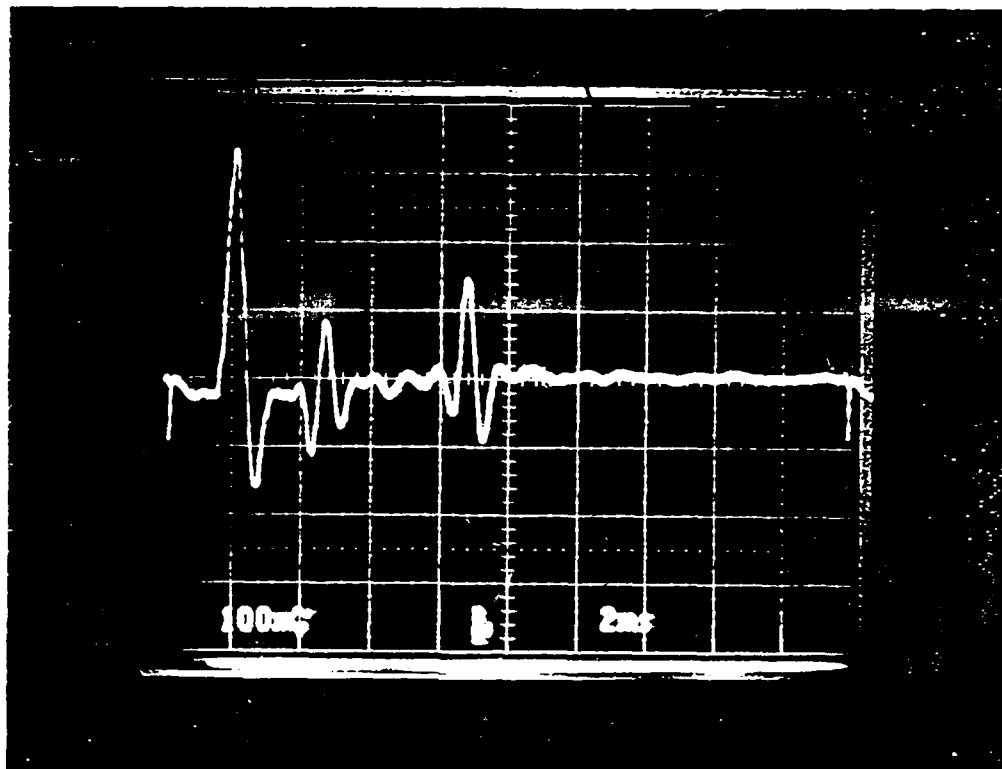


Figure 8.22: Phase 2 measurement. HP8510 stepped-FM receive waveform showing the return from the 1.31 inch metal pipe at 7.8 inches.



SURFACE AT 2.5 DIV FROM LEFT
 1.25 DIA PLASTIC PIPE AT 3.5 DIV FROM LEFT
 METAL PLATE AT 5.3 DIV FROM LEFT
 4 NS/DIV REAL-TIME

Figure 8.23: Phase 2 measurement. GAR short-pulse radar received waveform showing the returns from the 1.25 inch diameter plastic pipe at 7.8 inches and the metal plate at 21.6 inches.



SURFACE AT 1.0 DIV FROM LEFT
1.25 DIA PLASTIC PIPE AT 2.3 DIV FROM LEFT
METAL PLATE AT 4.4 DIV FROM LEFT
4 NS/DIV REAL-TIME

Figure 8.24: Phase 2 measurement. GSSI short-pulse radar received waveform showing the returns from the 1.25 inch diameter plastic pipe at 7.8 inches and the metal plate at 21.6 inches.

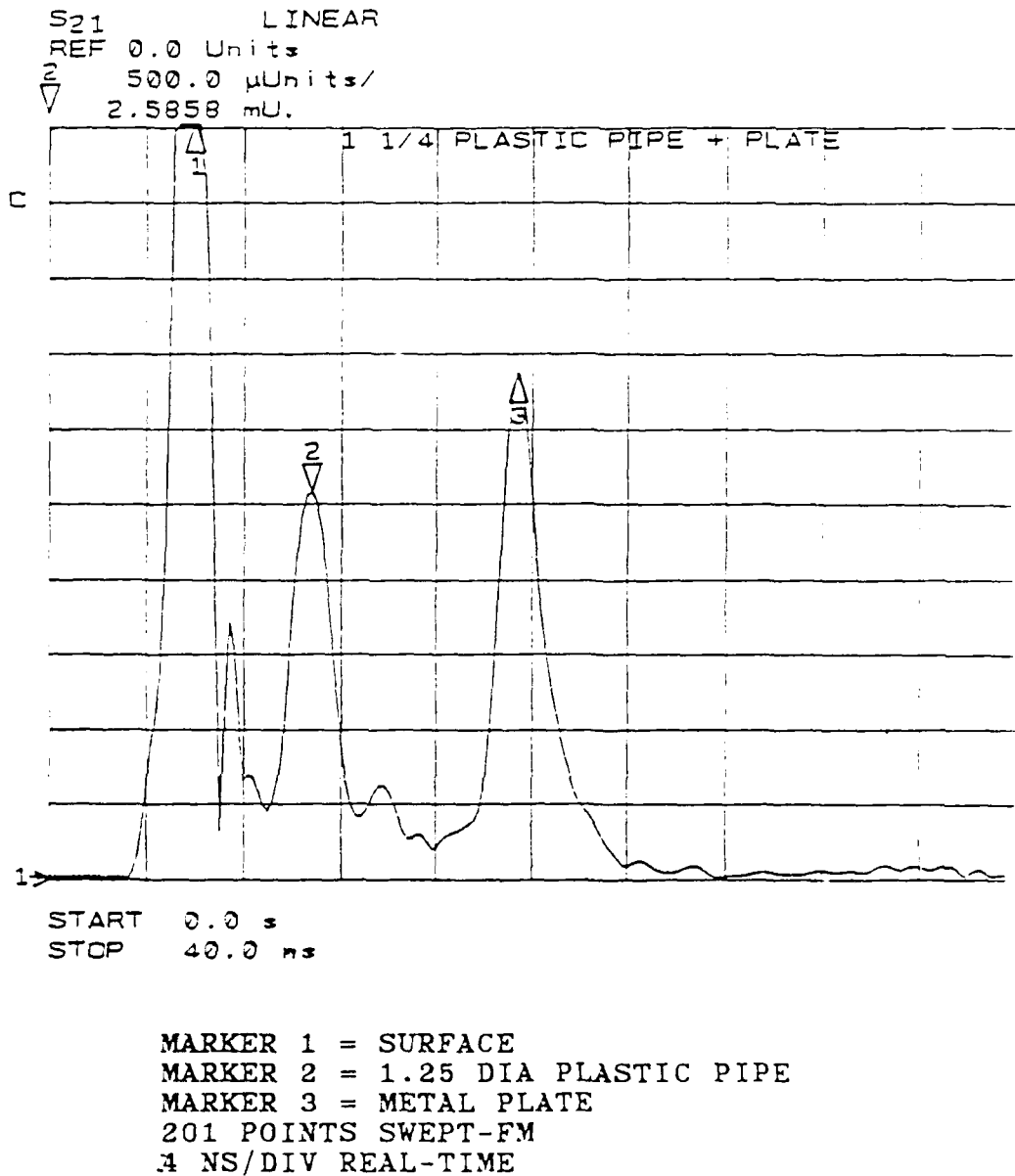


Figure 8.25: Phase 2 measurement. HP8510 swept-FM received waveform showing the returns from the 1.25 inch diameter plastic pipe at 7.8 inches and the metal plate at 21.6 inches.

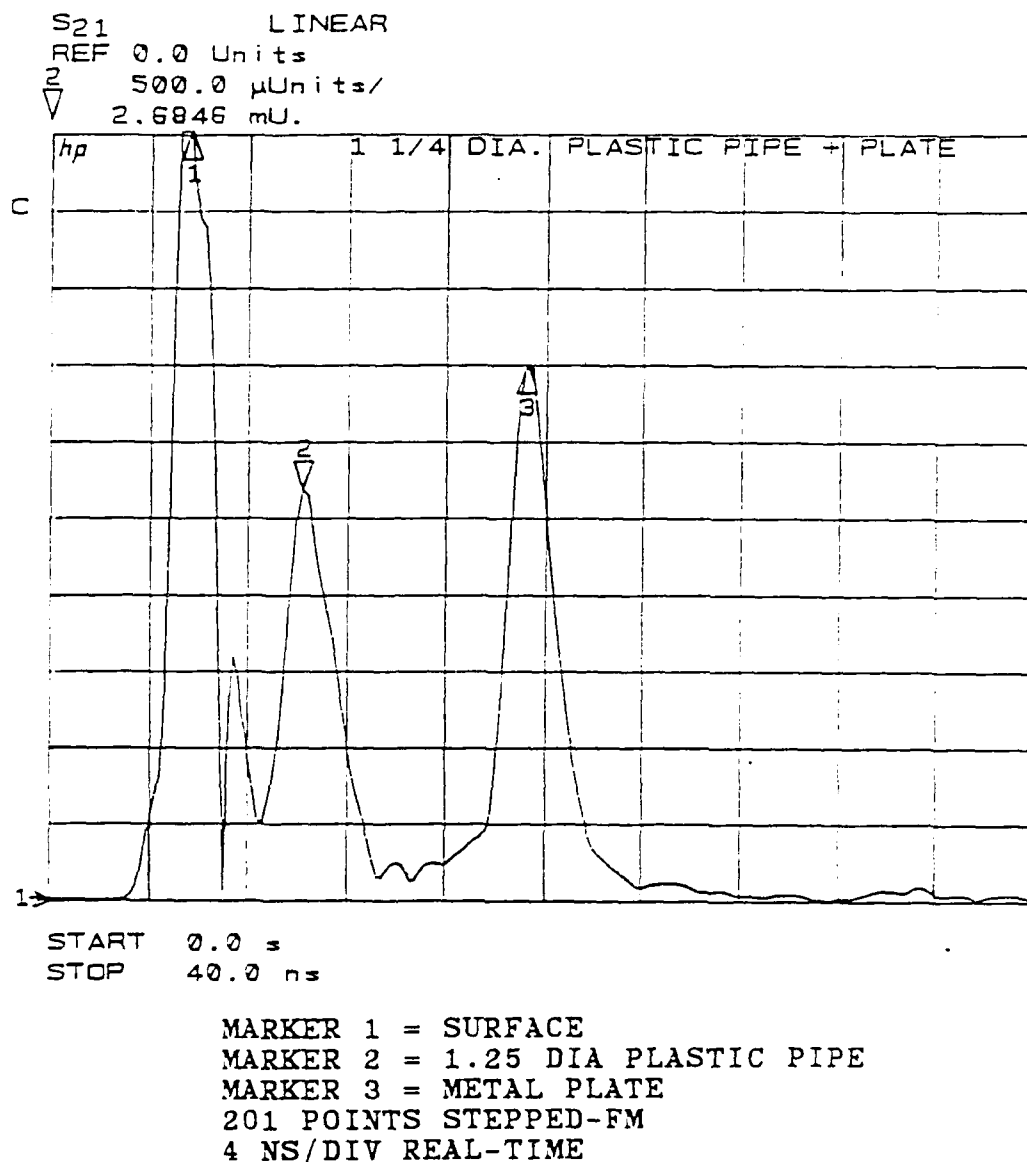
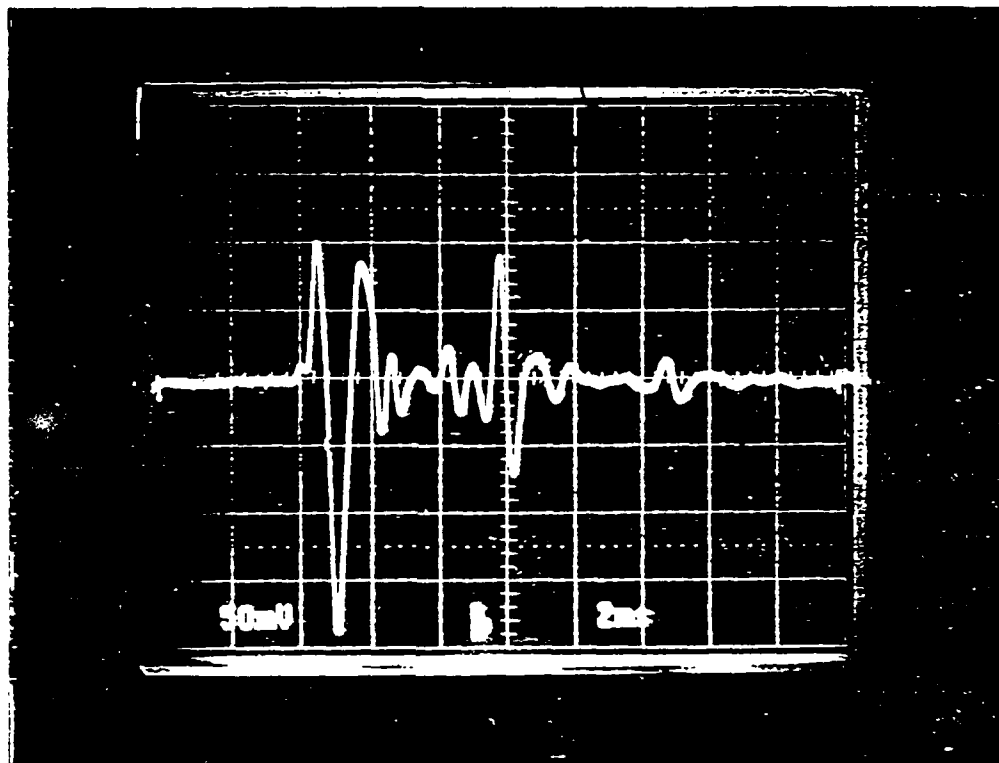
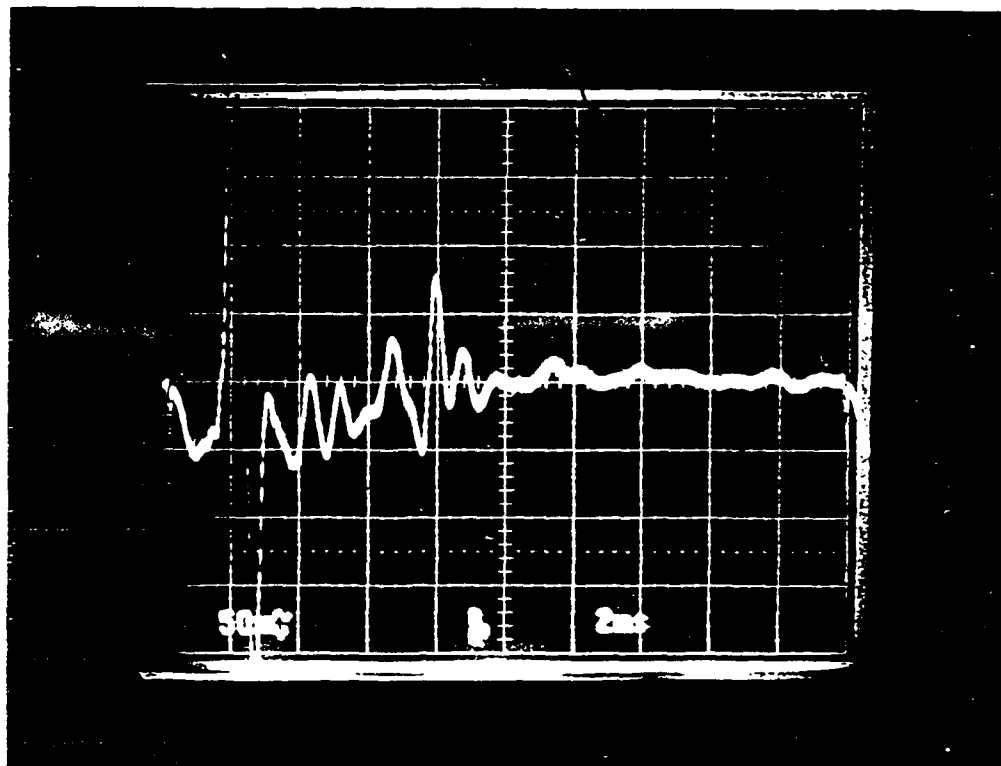


Figure 8.26: Phase 2 measurement. HP8510 stepped-FM received waveform showing the returns from the 1.25 inch diameter plastic pipe at 7.8 inches and the metal plate at 21.6 inches.



SURFACE AT 2.5 DIV FROM LEFT
3.5 DIA METAL PIPE AT 4.9 DIV FROM LEFT
6.63 DIA METAL PIPE AT 7.4 DIV FROM LEFT
4 NS/DIV REAL-TIME

Figure 8.27: Phase 2 measurement. GAR short-pulse radar received waveform showing the return from the 3.5 inch diameter metal pipe at 18 inches.



SURFACE AT 1.3 DIV FROM LEFT
3.5 DIA METAL PIPE AT 4 DIV FROM LEFT
4 NS/DIV REAL-TIME

Figure 8.28: Phase 2 measurement. GSSI short-pulse radar received waveform showing the return from the 3.5 inch diameter metal pipe at 18 inches.

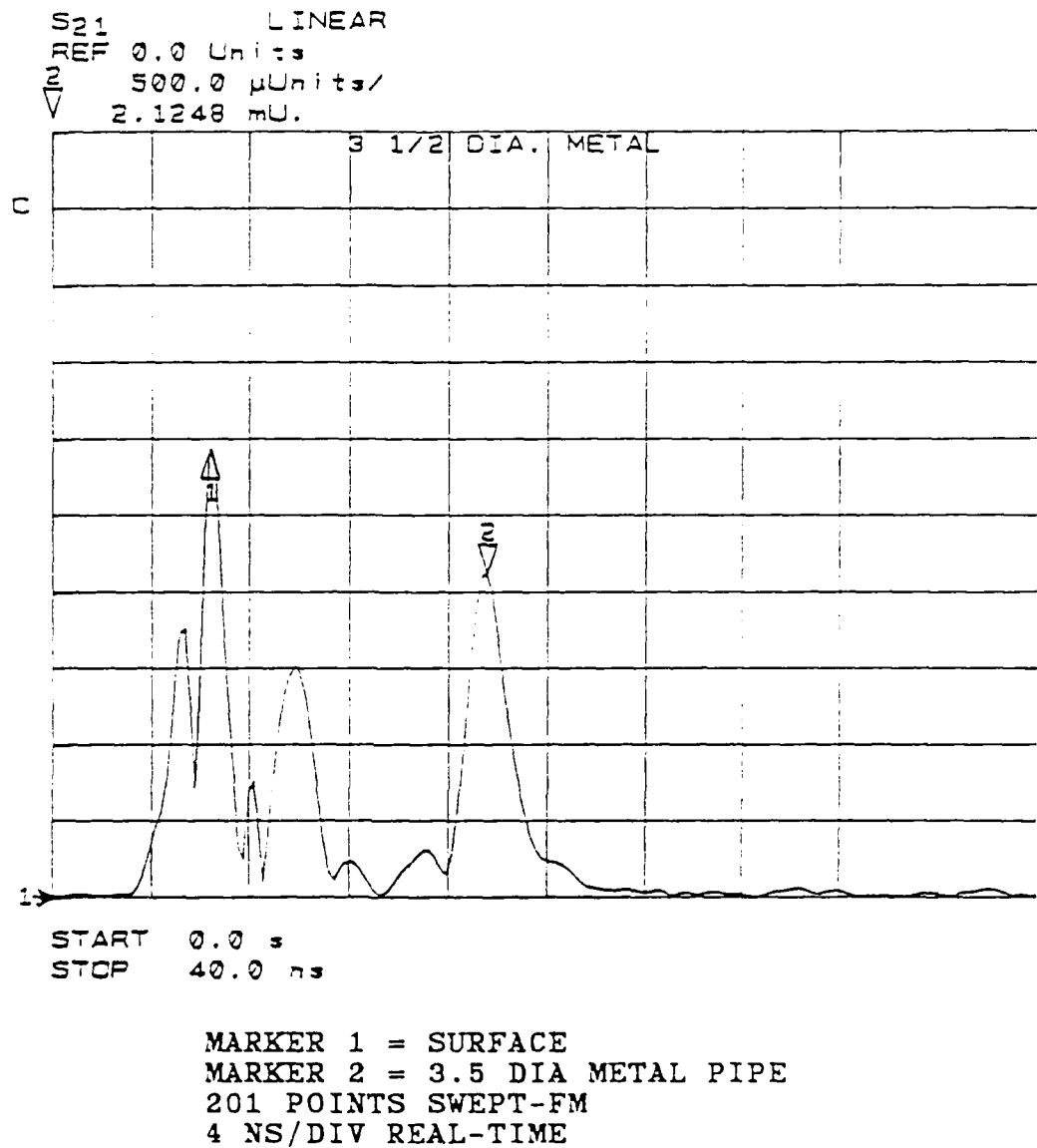


Figure 8.29: Phase 2 measurement. HP8510 swept-FM received waveform showing the return from the 3.5 inch diameter metal pipe at 18 inches.

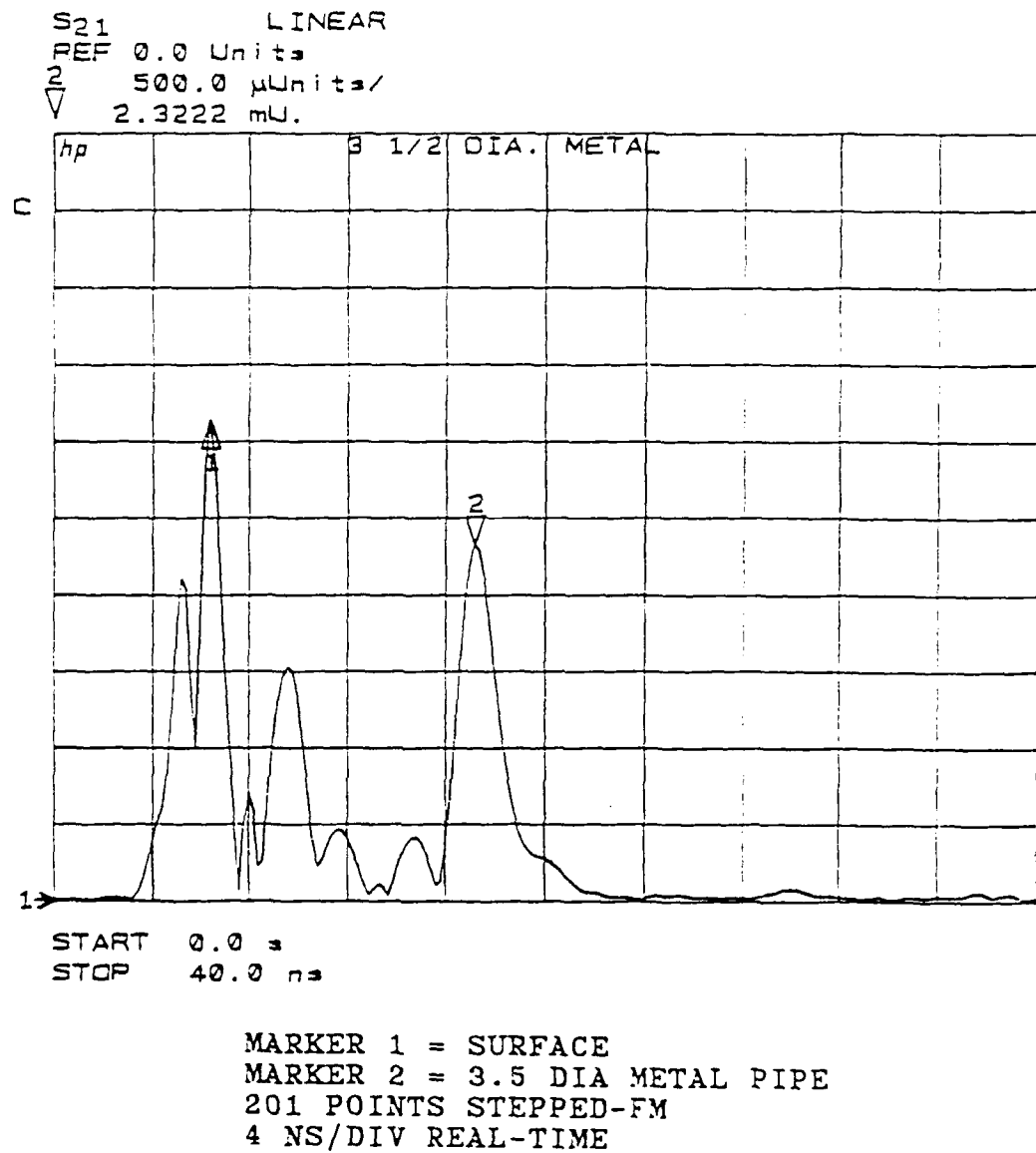
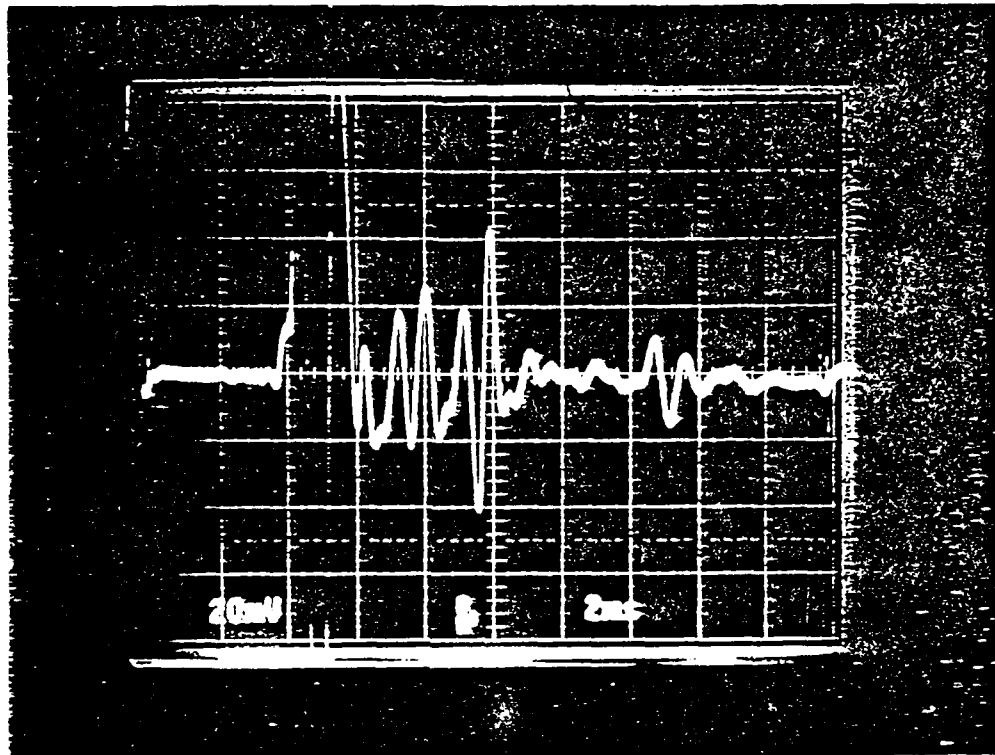
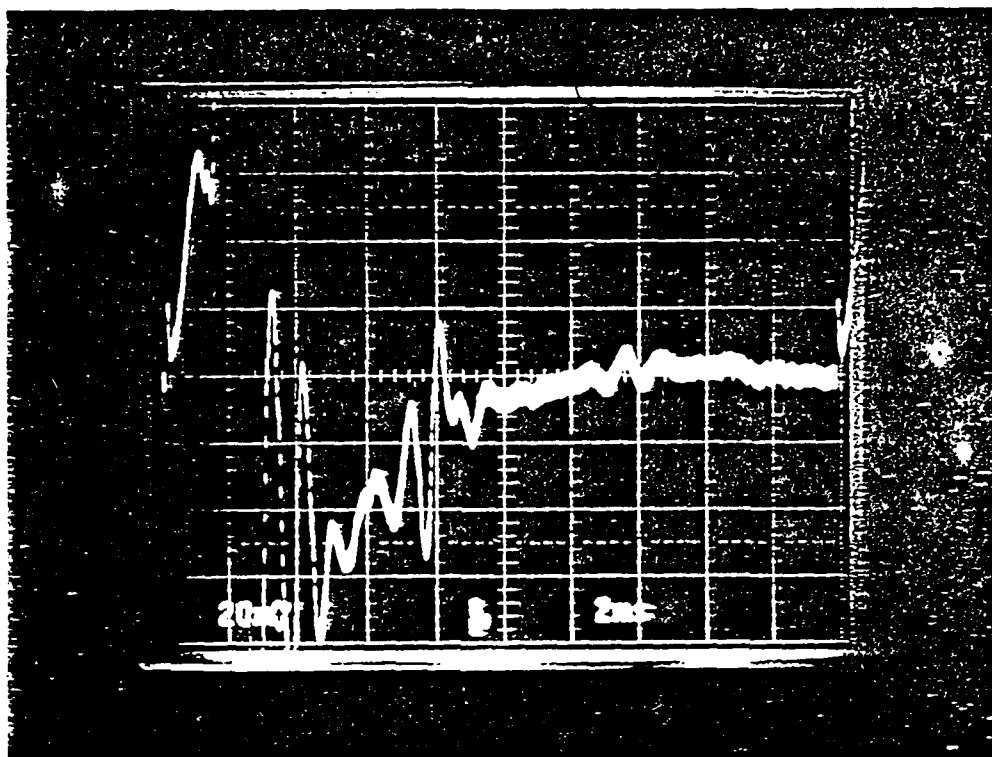


Figure 8.30: Phase 2 measurement. HP8510 stepped-FM received waveform showing the return from the 3.5 inch diameter metal pipe at 18 inches.



SURFACE AT 2.5 DIV FROM LEFT
3.5 DIA PLASTIC PIPE AT 4.9 DIV FROM LEFT
4 NS/DIV REAL-TIME

Figure 8.31: Phase 2 measurement. GAR short-pulse radar received waveform showing the return from the 3.5 inch diameter plastic pipe at 18 inches.



SURFACE AT 1 DIV FROM LEFT
 3.5 DIA PLASTIC PIPE AT 4 DIV FROM LEFT
 4 NS/DIV REAL-TIME

Figure 8.32: Phase 2 measurement. GSSI short-pulse radar received waveform showing the return from the 3.5 inch diameter plastic pipe at 18 inches.

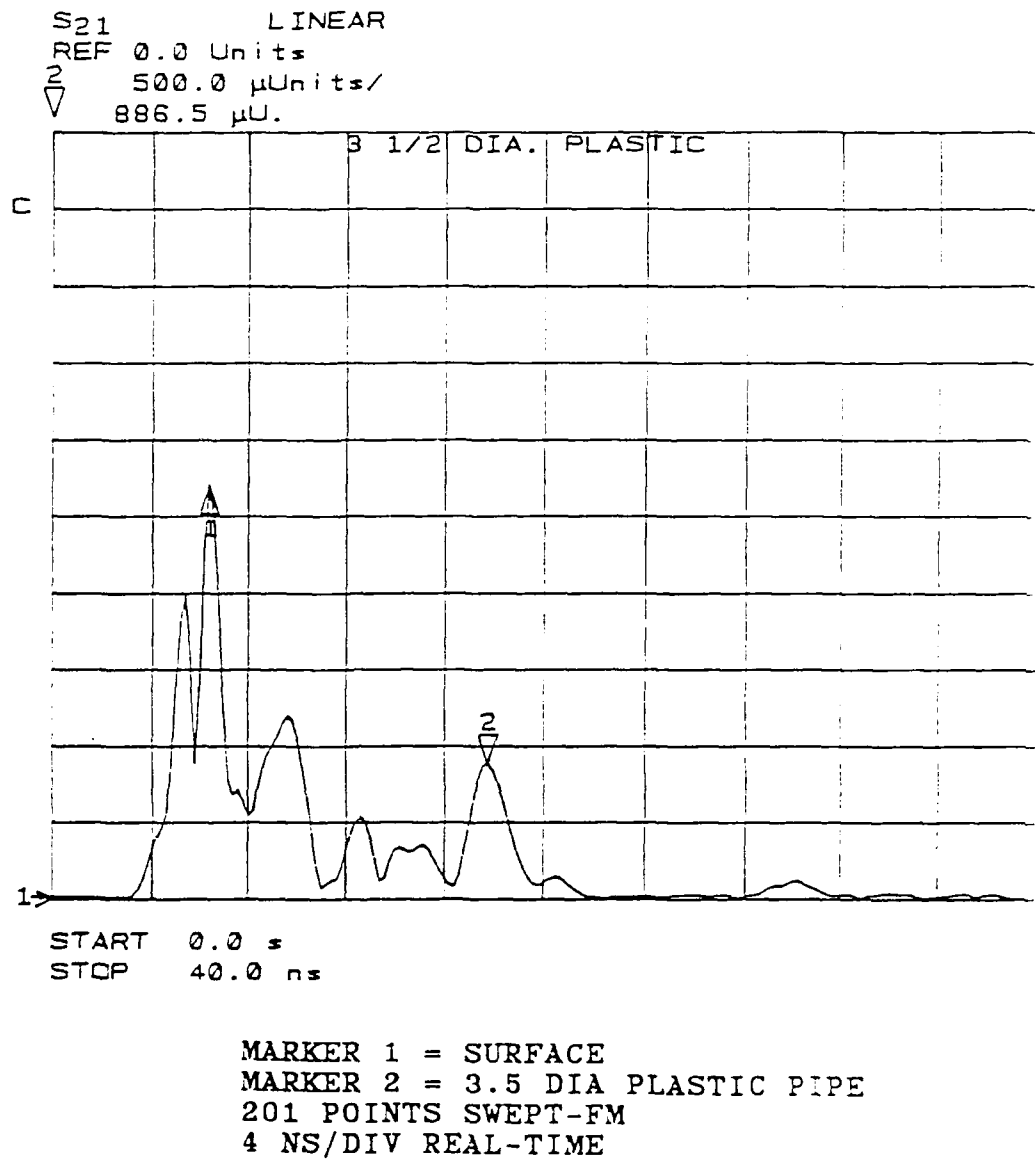


Figure 8.33: Phase 2 measurement. HP8510 swept-FM received waveform showing the return from the 3.5 inch diameter plastic pipe at 18 inches.

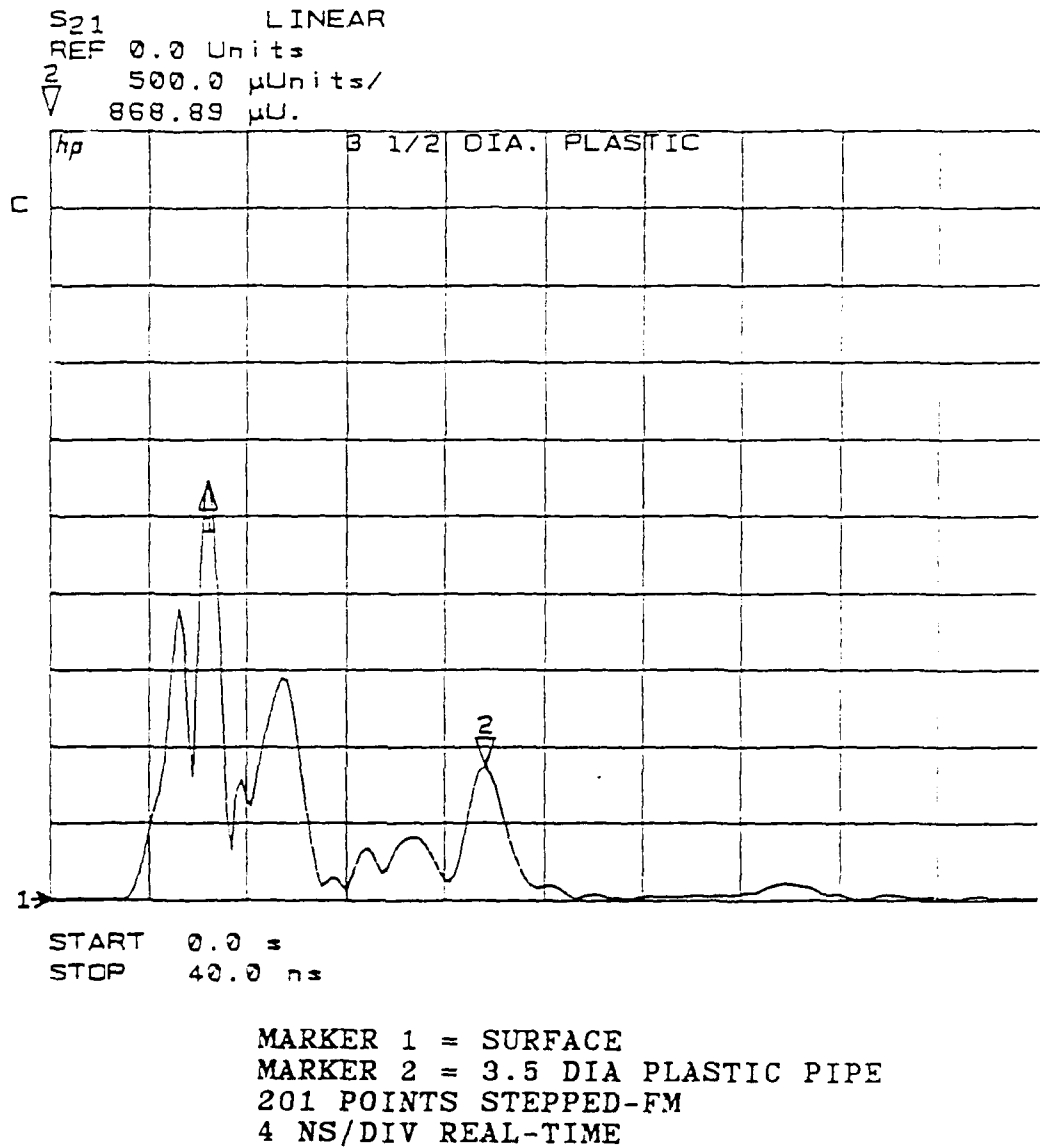
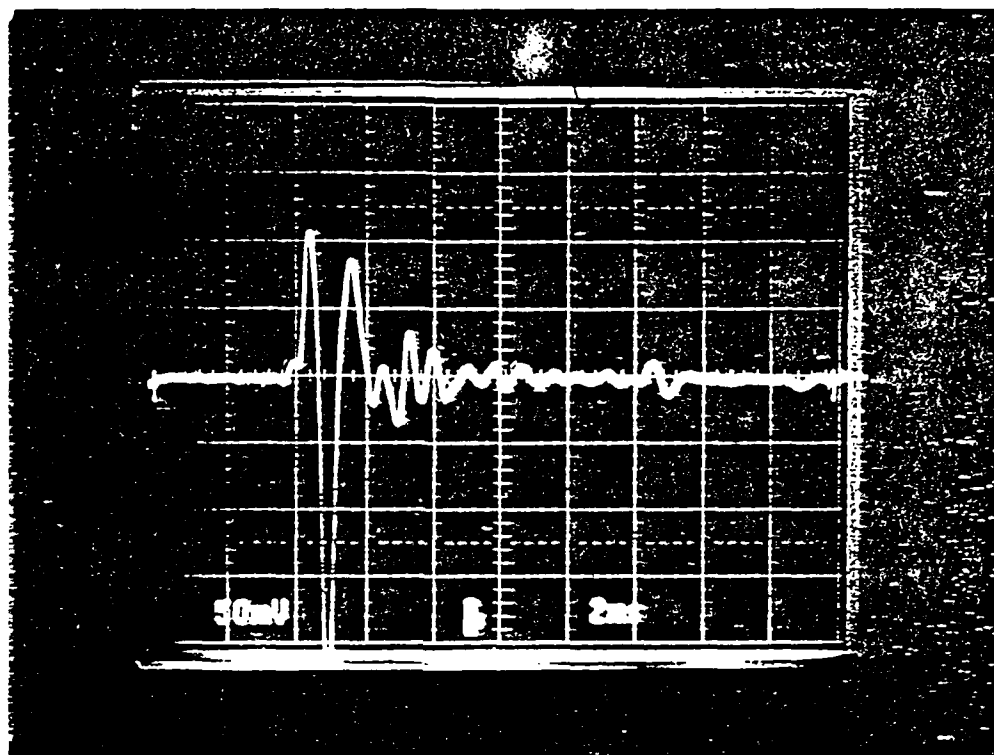
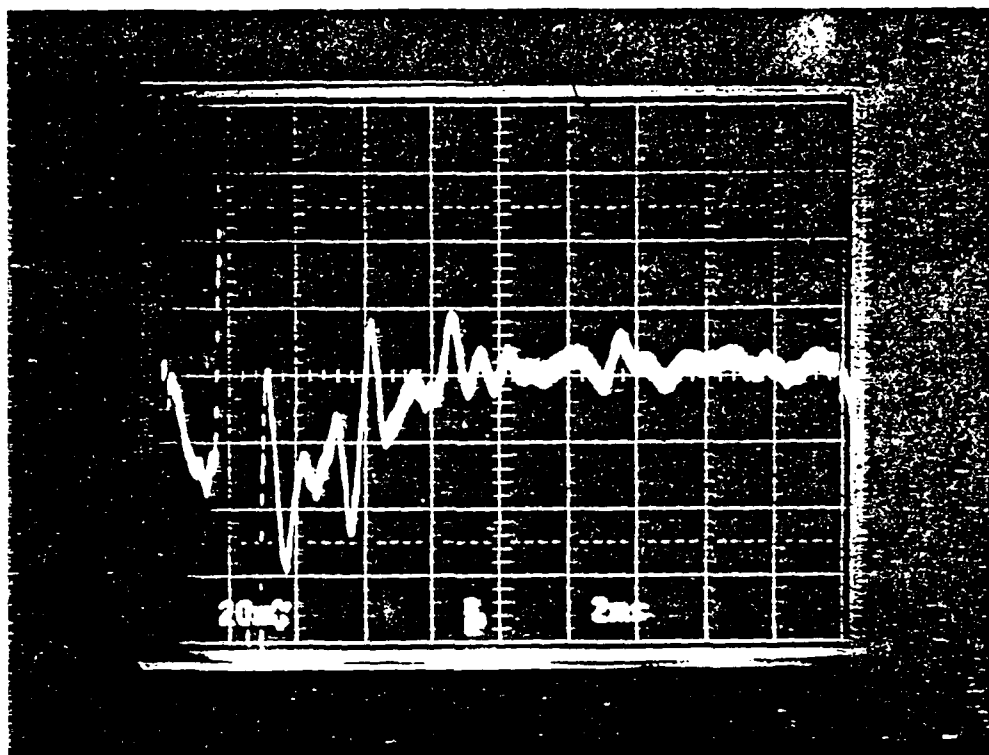


Figure 8.34: Phase 2 measurement. HP8510 stepped-FM receive waveform showing the return from the 3.5 inch diameter plastic pipe at 18 inches.



SURFACE AT 2.5 DIV FROM LEFT
6.63 DIA METAL PIPE AT 7.3 DIV FROM LEFT
4 NS/DIV REAL-TIME

Figure 8.35: Phase 2 measurement. GAR short-pulse radar received waveform showing the return from the 6.63 inch diameter metal pipe at 36 inches.



SURFACE AT 1.4 DIV FROM LEFT
6.63 DIA METAL PIPE AT 6.8 DIV FROM LEFT
4 NS/DIV REAL-TIME

Figure 8.36: Phase 2 measurement. GSSI short-pulse radar received waveform showing the return from the 6.63 inch diameter metal pipe at 36 inches.

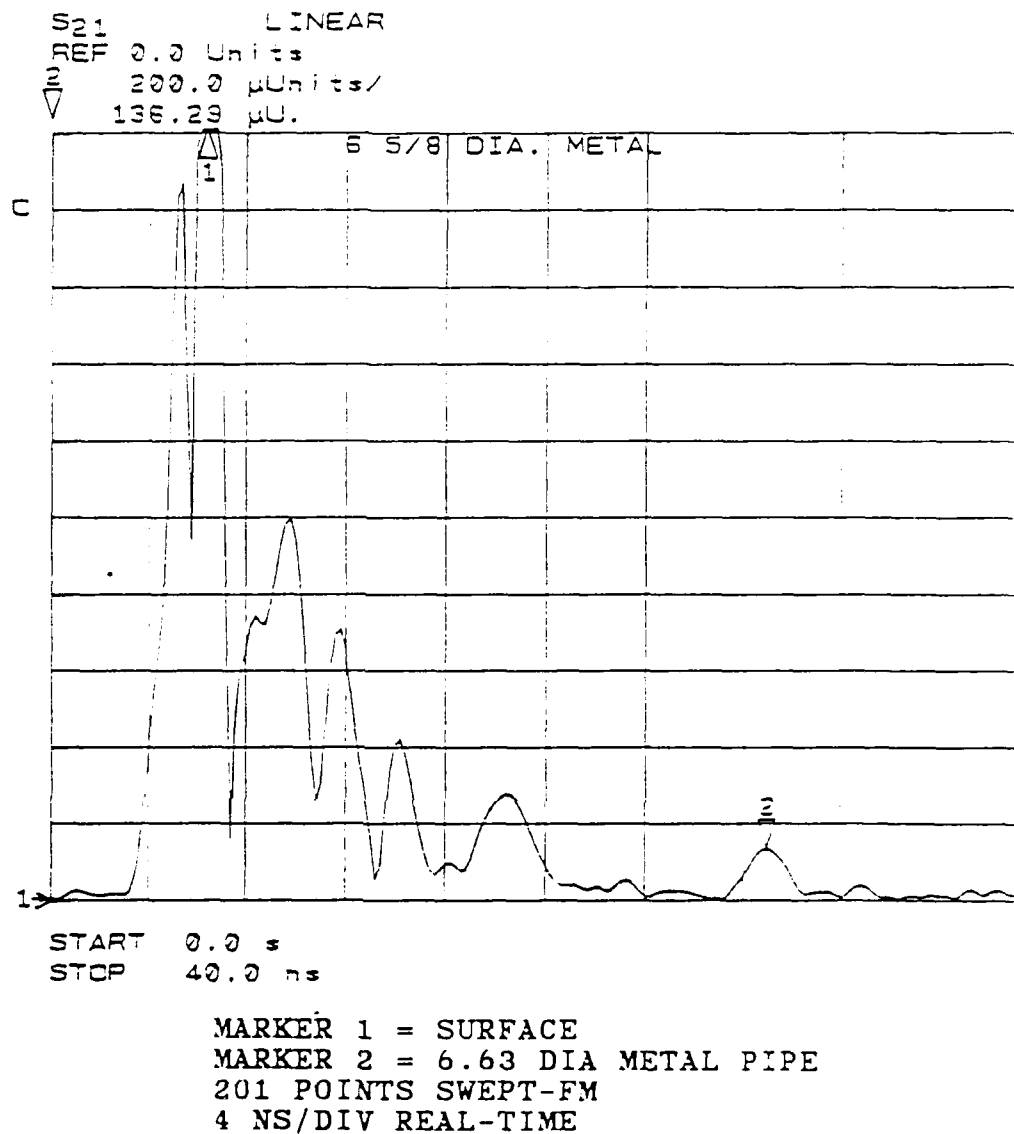


Figure 8.37: Phase 2 measurement. HP8510 swept-FM received waveform showing the return from the 6.63 inch diameter metal pipe at 36 inches.

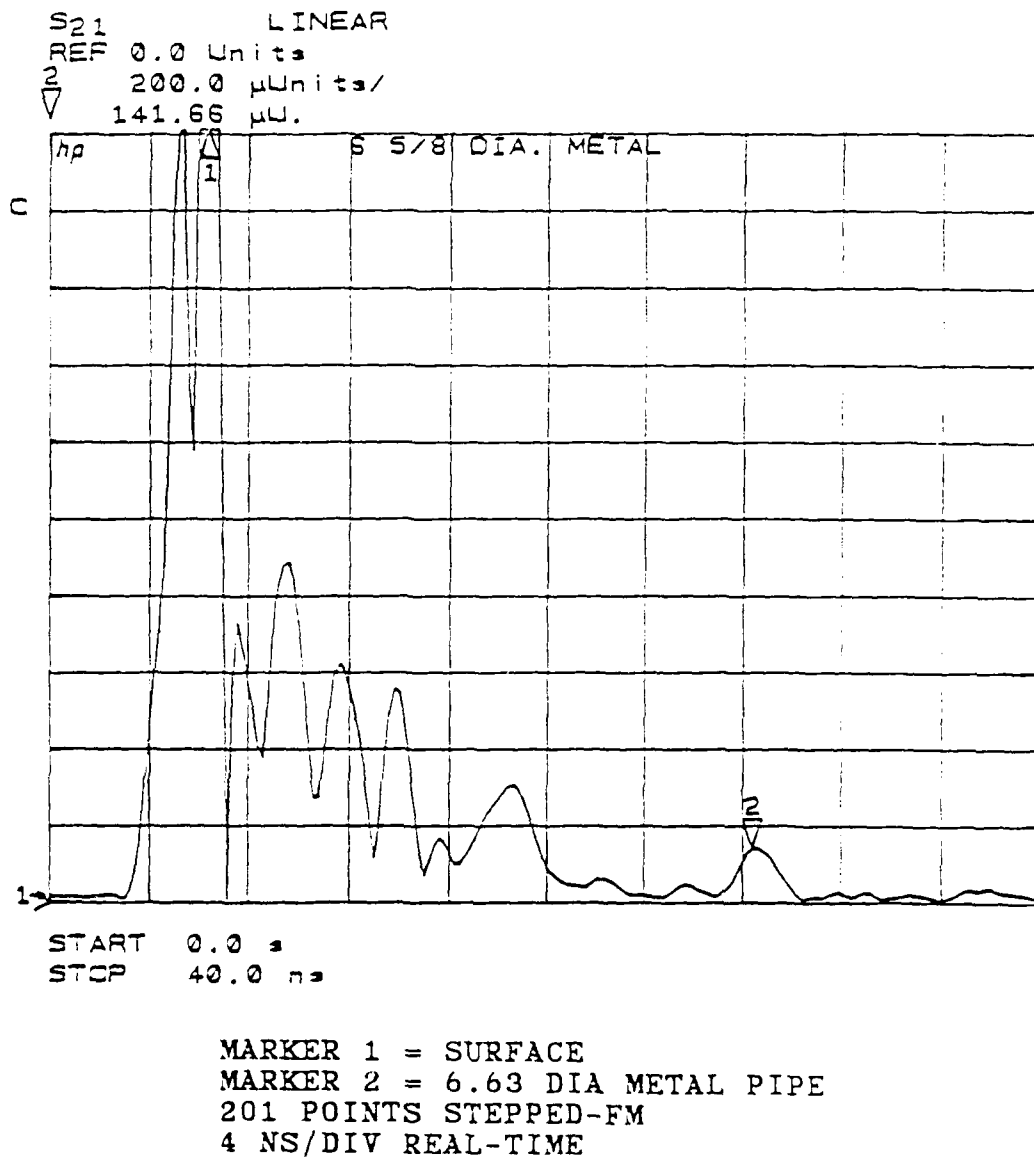


Figure 8.38: Phase 2 measurement. HP8510 stepped-FM received waveform showing the return from the 6.63 inch diameter metal pipe at 36 inches.

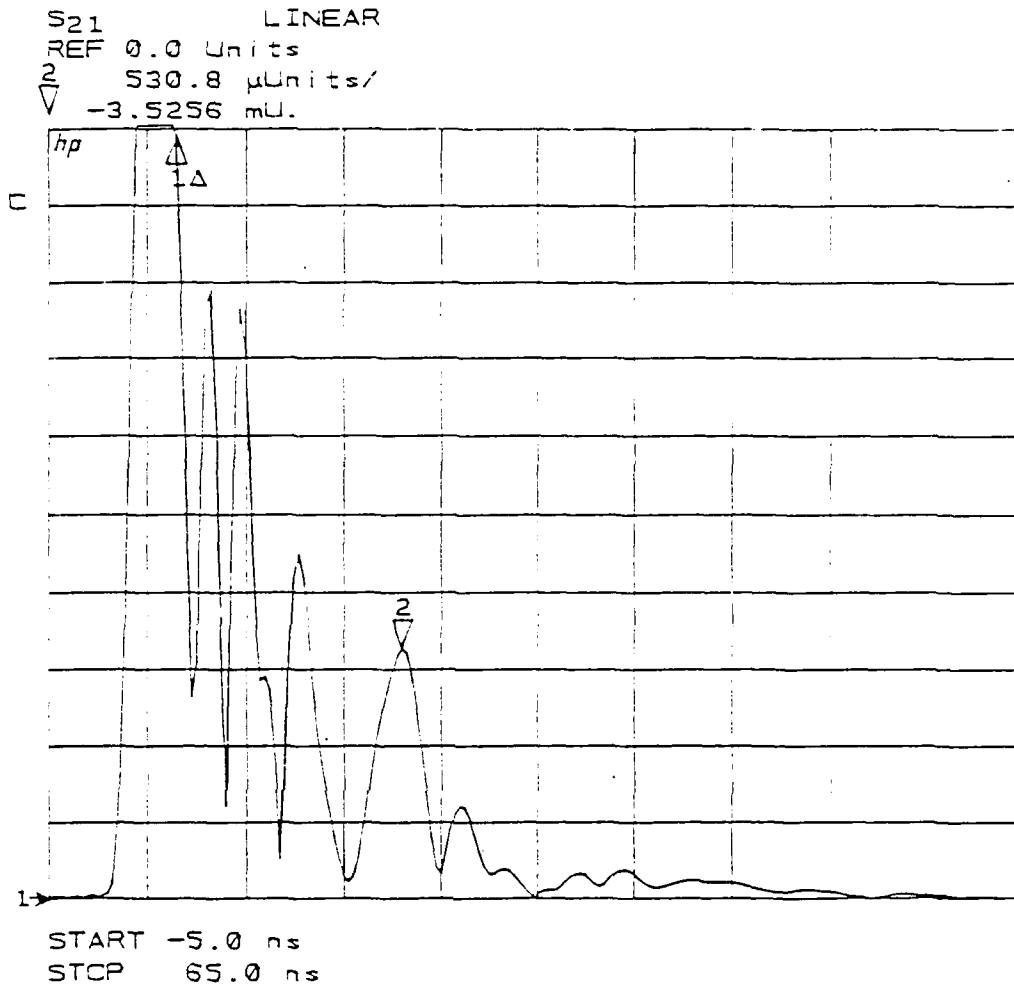
In Figures 8.19 through 8.22, the antennas were placed above the 1.31 inch metal pipe buried at a depth of 7.3 inches. Figures 8.23 through 8.26 are the returns from the 1.25 inch diameter plastic pipe at a depth of 7.8 inches. The return from the metal plate below the pipe at a depth of 21.6 inches is also visible in these figures. Figures 8.27 through 8.30 show the received signals from the 3.5 inch diameter metal pipe buried at a depth of 18 inches. Figures 8.31 through 8.34 show the received waveforms from the 3.5 inch plastic pipe buried at 18 inches. Finally, Figures 8.35 through 8.38 show the received waveforms from the GPR systems with the antennas directly above the 6.63 inch metal pipe buried at a depth of 36 inches.

8.3 FULL-SCALE GPR MEASUREMENTS WITH HP 8510

The full-scale GPR measurements were conducted with a stepped-FM frequency-domain system as described in Section 7.2 above. During a measurement the bistatic antenna system was placed directly above each pipe target and a plot of the resultant received waveform was generated. For the case of the two closely spaced copper pipes, the antenna system was centered between them.

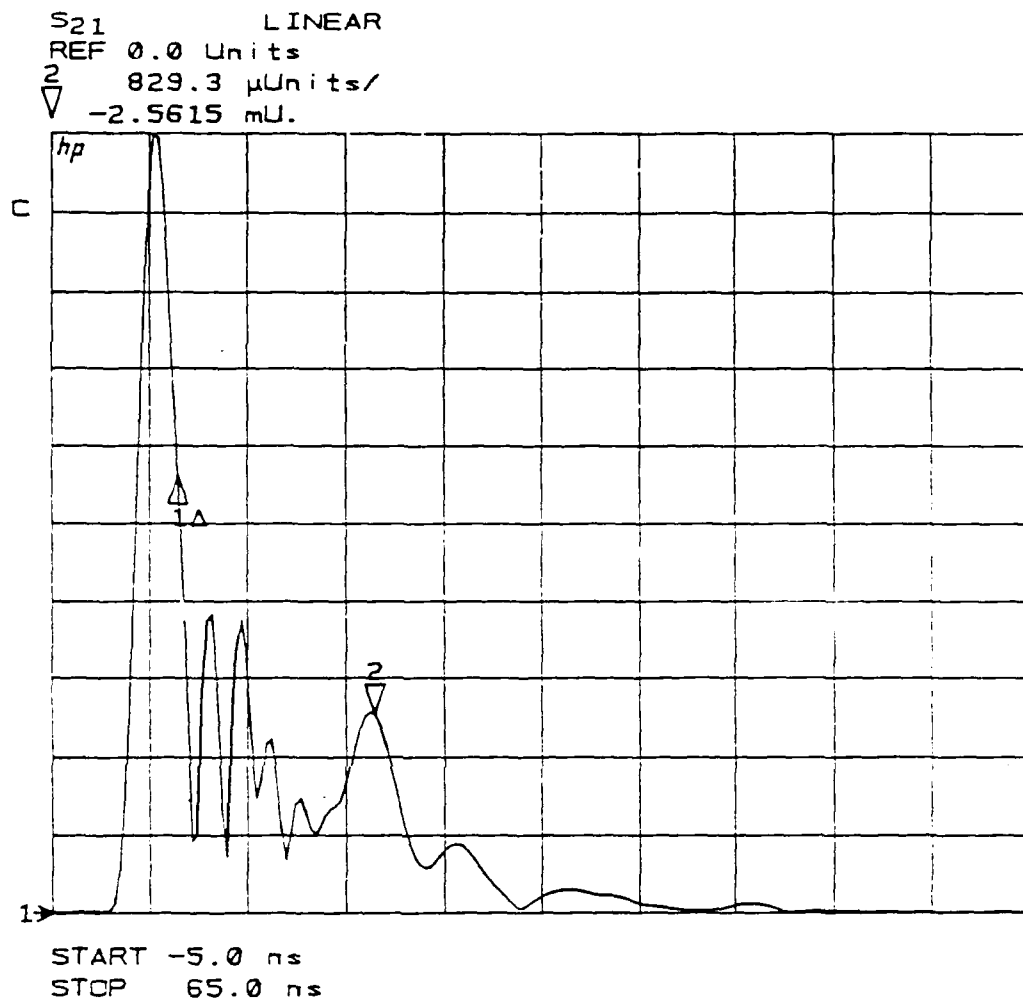
Figures 8.39 through 8.43 are the plots of the received waveforms from the various pipe targets. Figure 8.39 is the received waveform when the antenna was centered between the two copper pipes, Figures 8.40 and 8.41 are the waveforms from the two-foot deep and four-foot deep plastic pipes respectively, and Figures 8.42 and 8.43 are plots of the received waveforms from the four-foot deep and six-foot deep metal pipes respectively. In each of the plots, marker number two is placed on the signal return from the target.

In Figure 8.39, marker number two is placed on the combined signal return from the two copper pipes. The two pipes were at an equal distance from the antenna, and therefore the returns are combined. Moving the antenna away from the center point between the pipes revealed separate returns from each, because the ranges to the two pipes was different. Thus, the one-foot spacing between the copper pipes was greater than the resolution cell of the three-nanosecond pulse, enabling the



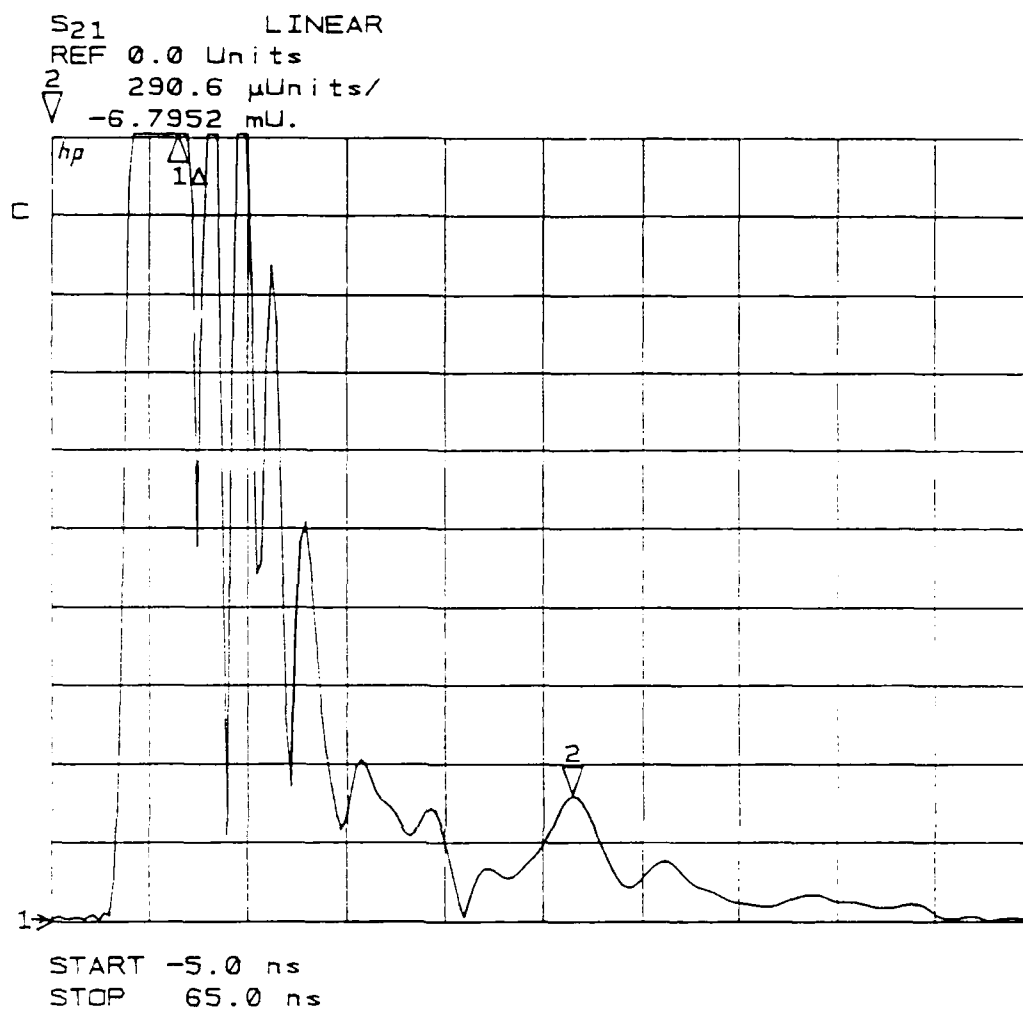
MARKER 1 = SURFACE
 MARKER 2 = COMBINED RETURN FROM TWO
 1 INCH DIA METAL PIPES
 201 POINTS STEPPED-FM
 7 NS/DIV REAL-TIME

Figure 8.39: Full-scale field measurement. HP8510 stepped-received waveform showing the combined return from two copper pipes spaced 1 foot apart and buried 2 feet deep. The antenna is placed between the pipes.



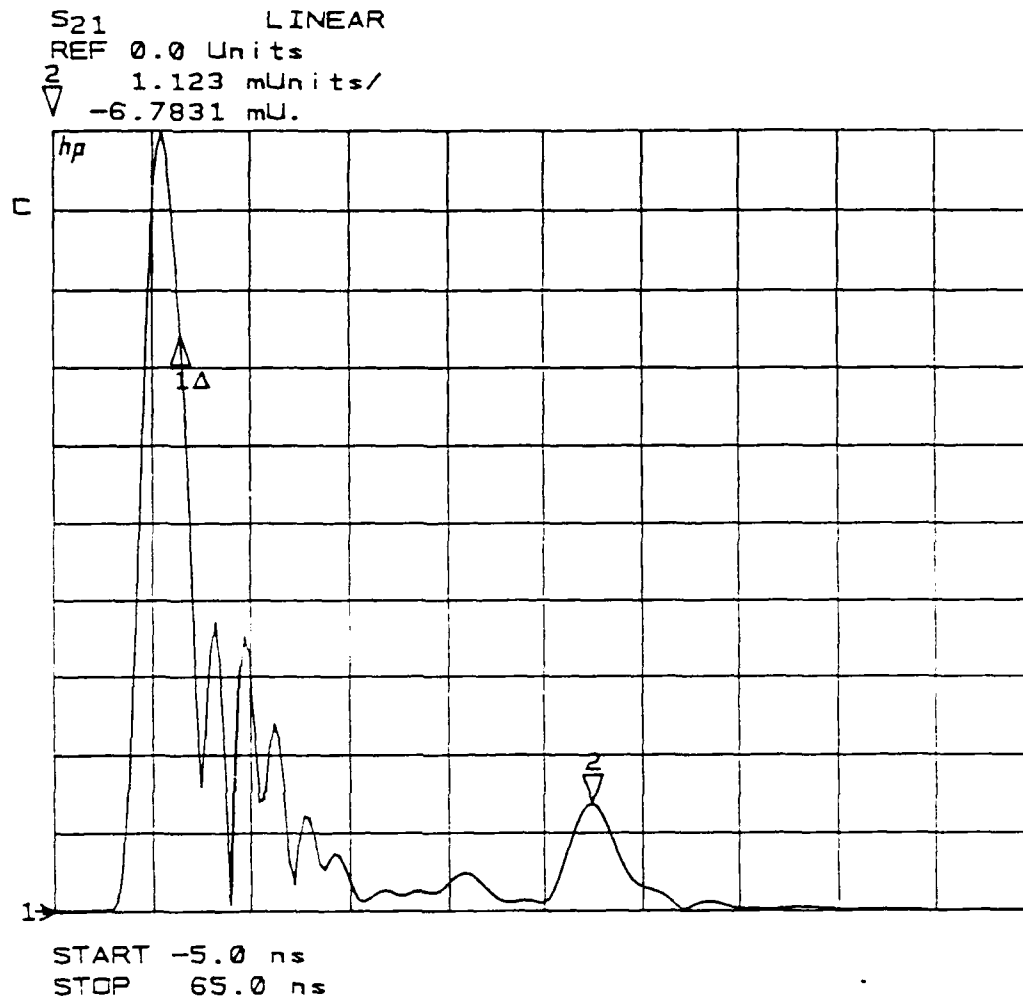
MARKER 1 = SURFACE
 MARKER 2 = 2 INCH DIA PLASTIC PIPE
 201 POINTS STEPPED-FM
 7 NS/DIV REAL-TIME

Figure 8.40: Full-scale field measurement. HP8510 stepped-FM received waveform showing the return from a 2 inch diameter plastic pipe buried 2 feet deep.



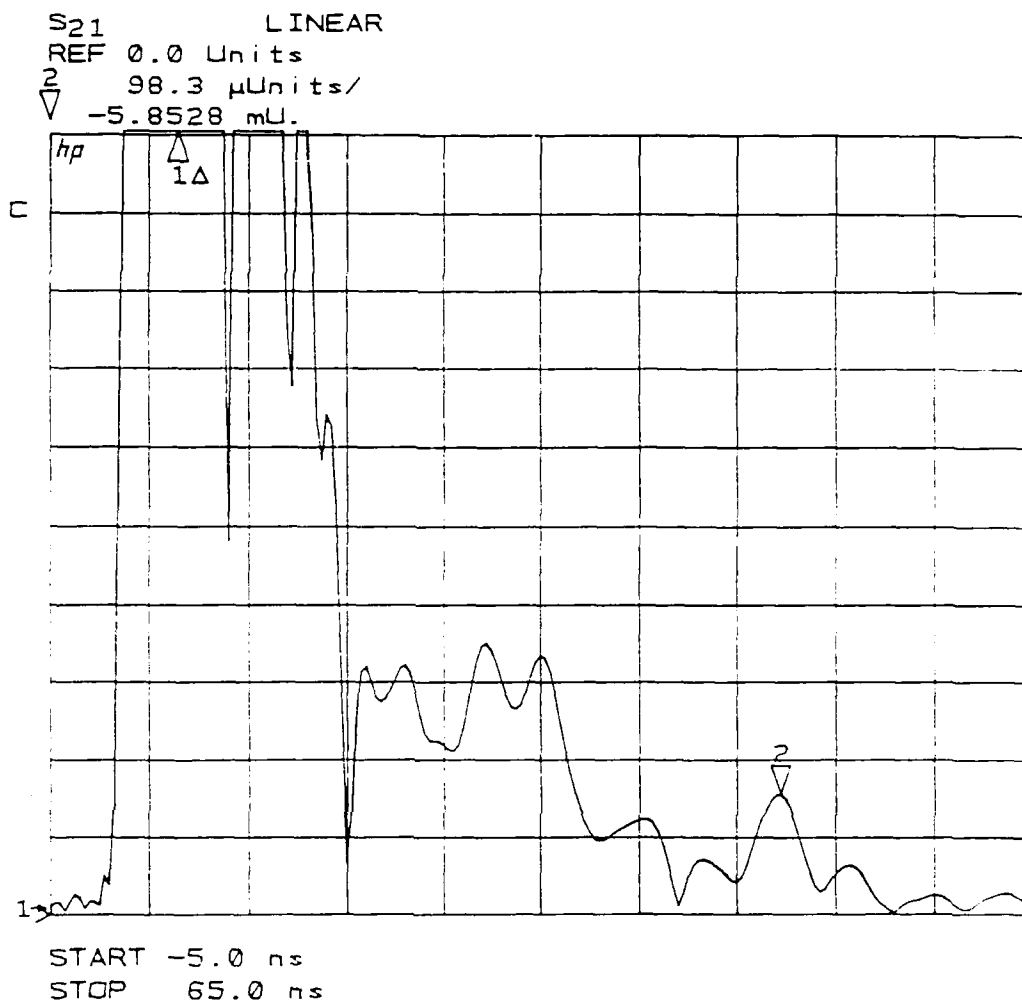
MARKER 1 = SURFACE
MARKER 2 = 2 INCH DIA PLASTIC PIPE
201 POINTS STEPPED-FM
7 NS/DIV REAL-TIME

Figure 8.41: Full-scale field measurement. HP8510 stepped-FM received waveform showing the return from a 2 inch diameter plastic pipe buried 4 feet deep.



MARKER 1 = SURFACE
MARKER 2 = 6 INCH DIA METAL PIPE
201 POINTS STEPPED-FM
7 NS/DIV REAL-TIME

Figure 8.42: Full-scale field measurement. HP8510 stepped-FM received waveform showing the return from a 6 inch diameter metal pipe buried 4 feet deep.



MARKER 1 = SURFACE
MARKER 2 = 6 INCH DIA METAL PIPE
201 POINTS STEPPED-FM
7 NS/DIV REAL-TIME

Figure 8.43: Full-scale field measurement. HP8510 stepped-FM received waveform showing the return from a 6 inch diameter metal pipe buried 6 feet deep.

returns from the individual pipes to be distinguished when the antenna was moved on the surface across the pipes.

Other qualitative observations demonstrated the dependence of target signal strength on target radar cross section. The amplitude of the return from the two-inch diameter plastic pipe buried at four feet was approximately one-third of the amplitude of the return from the six-inch diameter metal pipe buried at the same depth.

The frequency-domain GPR used in the full-scale measurements was able to detect the six-inch diameter metal pipe at a six-foot depth. However, it is doubtful that the same pipe in a similar soil buried at ten feet could be reliably detected. This is because the equations modelling the metallic cylinder radar cross section (either Equation 4.2 or 4.4) combined with the Radar Range Equation, Equation 4.1, predicts that the target return signal power has a $1/R^3$ dependence as well as a loss term that is also exponentially dependent on R. The $1/R^3$ term alone predicts a received signal power from a target at ten feet to be 21.6% of the power from the same target at six feet. Since the attenuation characteristics of the soil in the pipe test field were not known and could not be measured for the entire field, the exact effects of the attenuation term could not be predicted. However, the combination of the two terms mentioned above would reduce the amplitude of the return from a six-inch diameter pipe buried at ten feet to below the level of the clutter present in the received signal.

The full-scale measurements using the stepped-FM frequency-domain GPR system demonstrated its capability to detect buried pipe targets. As expected, the qualitative results illustrated the dependence of the target detectability on its radar cross section and burial depth. The unknown attenuation characteristics of the soil in the pipe test field and the exact burial depths of the targets prevented a correlation between the scale-model results of the Phase 1 and Phase 2 measurements and the full-scale measurements.

SECTION 9

SELECTION OF THE OPTIMUM GPR SOURCE SIGNAL BASED ON THE PHASE 1 AND PHASE 2 SOIL-MODEL TANK MEASUREMENTS

This section contains an evaluation of the results obtained from the Phase 1 and Phase 2 measurements conducted with the scale-model GPR systems. The effectiveness of the scale-modeling procedure is examined as well. Finally, a selection of the optimum GPR source signal type is made, based on the results from the scale-model tests.

9.1 EVALUATION OF THE EFFECTIVENESS OF THE SCALE-MODEL TESTS

The scale-modeling technique used for this program to evaluate the GPR systems had advantages and disadvantages. However, GAR engineers feel that it provided good results overall. It was effective enough to allow a confident choice of the best of the four candidate GPR source signal types to be made, based on an assumed set of design criteria.

The shale soil-model tank of the Phase 1 measurements provided the most useful scale-model results. The loss characteristic of the shale was high enough so that it scaled to a more realistic full-scale environment than did the loss characteristic of the schist clay. The loss characteristic of the shale in the soil-model tank was probably close to that of the clay shale sample measured with the test cell. This can be reasonably inferred since the experimental dielectric constant measurements using the GPR systems produced a similar value to that obtained from the test-cell measurements. Thus, a realistic conversion of the Phase 1 model measurement results to a full scale scenario could be done.

Several laboratory test-cell measurements were performed on samples of the clay schist soil in order to correlate the attenuation properties of the soil-model tank to those of the laboratory measurements. One set of laboratory sample measurements did produce results that corresponded well with the GPR dielectric constant measurement of the soil in the test tank. Therefore, it was felt that the attenuation

characteristic of the soil sample could be extrapolated to a full-scale environment.

When comparing the attenuation properties of the schist and the shale, it was felt that the shale provided a more useful soil to be used as a scale model. Its higher attenuation properties allow the modelling of full-scaled systems with more realistic attenuation characteristics that does the schist.

GAR engineers were not able to exactly determine the loss characteristics of either of the soil-model tanks. This was because the packing density of the soil throughout the model tank could not be determined. Furthermore, we did not know how homogeneous the soil was in the tank, even though considerable efforts were made to maintain homogeneity. The procedure of testing a soil sample in a test cell with the network analyzer could not replicate the exact packing density of the soil tank.

In one respect, the investigators were fortunate that the relative dielectric constant of the schist was not as high as the value measured in the test cell. The GPR measurements of the relative dielectric constants of the schist soil-model tank and of the shale soil-model tank indicated that the dielectric constants were very similar (12.94 for the schist and 11.63 for the shale). This meant that the effective aperture and gain of the triangular-sheet dipole antenna were essentially the same for both soil-model tanks. Thus, the radiation bandwidth of the antenna was about the same for both tanks.

This observation is important because it allows a direct evaluation of which GPR system uses the optimum bandwidth shape, or equivalently, the optimum pulse shape. If the antenna effective aperture and gain were very different from the shale tank to the schist tank, the antenna would radiate over a different bandwidth in one tank than in the other. This would bias one pulse shape over the other, because the different GPR pulse shapes concentrate RF energy in different frequency bands.

Viewed from another perspective, this similarity between the schist and shale dielectric constants allowed program investigators to better isolate a single soil variable of interest. This variable of interest is the soil attenuation

which must be scaled by the scale factor in the scale-model environment. The reader should recall that in contrast, the dielectric constant is not scaled, but remains the same in the full-scale scenario as in the scale-model environment. Since the two soils differed in attenuation much more than in dielectric constant, one can safely assume that many of the differences between the Phase I and Phase II results are due virtually exclusively to this attenuation difference.

Even though there was some uncertainty associated with the soil parameters in the schist soil-model tank, the Phase 2 measurements were quite valuable in determining an optimum GPR source signal type. Those measurements revealed that the effects on the response of the frequency-domain systems when moving from a high-loss to a lower-loss environment were much more dramatic than the same effects on the GAR short-pulse radar. This was true, to a lesser degree, of the GSSI short-pulse radar with respect to the GAR radar. The implication is that the pulse shape of the GAR short-pulse radar had an RF bandwidth that is less sensitive to the specific soil environment and thus is perhaps better suited for deep ground penetration in varying environments than the pulse shape synthesized by the HP 8510-based systems or the pulse of the GSSI radar.

The ability to make this comparison is precisely why the pulse widths of the GAR radar and the two frequency-domain systems were chosen to be the same. Recall that an absolute evaluation and comparison of the GSSI measurement results with those of the other radars is not possible because the GSSI unit had a different antenna system and a pulse width that was not exactly known.

The RF bandwidth of the monocycle pulse of the GAR radar provided a better match to the attenuation characteristics of the soil than did the bandwidth of the network analyzer pulse or that of the GSSI short-pulse. The RF bandwidth of the other pulses had more high-frequency content than the GAR monocycle. Thus, a greater percentage of the energy in the bandwidth of the HP 8510 pulse was attenuated in the soil than with the GAR monocycle.

9.2 DETERMINATION OF THE OPTIMUM GPR SOURCE SIGNAL

The selection of an optimum GPR system is not a simple task. Some of the considerations involved in the choice were discussed earlier in this report. However, different RF bandwidths will be required for different applications. A GPR designed for deep-penetration must radiate low RF frequencies to avoid the drastic attenuation characteristics of the soil at higher frequencies. Conversely, a high-resolution GPR must use a wider bandwidth than the deep-penetrating GPR system. Therefore, the optimum GPR must have selectable RF bandwidths to provide the best performance in varying soil environments. Based on the preceding analysis and the results from this measurement program, a selection of an optimum GPR system can be made as follows.

9.2.1 EVALUATION OF THE GPR SYSTEMS TESTED

When deep penetration is the goal, the best RF bandwidth shape for a GPR will concentrate most of the RF energy into the passband of the antenna and the soil. Of the GPR systems tested, the monocycle pulse shape, and its associated RF bandwidth, appeared to offer significant advantages in this case. On the other hand, if high resolution is the goal, then a bandwidth shape with relatively higher frequency content will be preferable.

Ideally, one would want a GPR system with a selectable bandwidth shape, a shape that accentuates the lower-frequency components for deeper penetration applications, and the higher frequency components for higher resolution applications. Each selectable bandwidth shape could be different altogether, or the overall bandwidth shape (amplitudes and phases of the frequency components) could be the same for all of the different selectable bandwidths, with only the center frequency adjusted from case to case.

This selectable bandwidth capability is effectively provided by the HP 8510 in terms of its selectable frequency-domain weighting functions (see Section 6.3.1.2.1). In contrast, incorporation of such a feature in time-domain systems such as the GAR and GSSI GPRs would be difficult. The

ease with which this feature can be incorporated into a frequency-domain GPR is certainly a major factor favoring selection of such a unit as the best GPR system for location of underground utilities.

The clutter performance of the GPR system is also an extremely important factor. As illustrated in Table 8.1, the frequency-domain GPR systems, based on the HP 8510, were found to have better clutter performance than the pulsed GPR systems. This was partially due to the additional clutter associated with the coupling of high-frequency noise from the short-pulse transmitters into the receiver through the power supplies and ground planes. The CW transmitter of the HP 8510 does not generate these transients that produce that type of clutter problem. Also, one has difficulty in building short-pulse transmitters that have 50 ohm output impedances. Such output impedances are required to terminate any undesired reflections that travel back toward the transmitter from discontinuities or mismatches in the RF transmission system.

Higher average power levels can be generated more easily with the FM-CW GPR systems than with the short-pulse systems. This is due to the fundamental problems associated with generating narrow, high amplitude pulses. Also, low-PRF pulsed radars must generate a higher amplitude transmitter pulse than a high-PRF pulsed radar in order to achieve the same average power level. As an example, a 20-watt peak pulse with a five percent duty cycle produces one watt of average power. One-watt RF amplifiers are easier to obtain and less costly than 20-watt RF amplifiers.

The GPR dynamic range is another important consideration. The frequency-domain GPR systems tested had better dynamic range characteristics than the short-pulse radars. Baseband short-pulse radars inevitably use broadband samplers on the receiver front end. The samplers are noisy and have high noise figures. The frequency-domain GPR systems can avoid the use of broadband samplers on the receiver front end, usually resulting in a lower receiver noise figure.

The complexity of the frequency-domain GPR system based on the network analyzer is much greater than that of the short-pulse radar systems. This is true of almost any frequency-domain radar, even if it is not based on the HP 8510. A truly

high-performance frequency-domain radar must use a synthesized frequency source and a means of frequency control. Furthermore, the RF circuitry of the frequency-domain GPR is more complex. Also, significant signal processing is usually required with the frequency-domain GPR in order to obtain easily interpreted output information. In contrast, the short-pulse radars produce easily recorded time-domain output data that can be immediately interpreted to some degree without requiring further processing. However, to achieve optimum performance, signal processing must also be applied to the short-pulse radar output.

The time-domain GPR electronic equipment is smaller and lighter than its frequency-domain counterpart. Even though high-power pulsers for short-pulse radar systems require large power supplies than the lower-powered frequency-domain-based radars, the frequency-domain systems are still larger and heavier.

The short-pulse radar systems are usually built to be quite rugged. The HP 8510, however, could not be exposed to the same treatment that some GPR systems receive in field use. Of course, a rugged high-performance frequency domain GPR can be built. However, a large, complex, frequency-domain radar may still exhibit less field reliability than comparable short-pulse radar systems.

Reliability is often a function of the system complexity. Large numbers of components within a system usually implies a lower mean time before failure than for a system containing fewer components. To minimize reliability problems with a frequency-domain GPR system, the more complex subsystems, such as digital signal processing components and vibration-sensitive components, may be permanently located in a vehicle in order to minimize handling by field technicians performing the GPR measurements. Additional reliability considerations would include the specification of environmentally rugged components. For a more complex GPR such as a frequency-domain radar system, selection of rugged components may be difficult and expensive.

Another factor affecting the choice of a GPR technology is system cost. The frequency-domain systems are usually far more expensive than the short-pulse radars. If FFT and frequency-domain signal processing capabilities are added to short-pulse

radars such as those tested, their costs will increase, but they will probably still be significantly less expensive than a high-performance frequency-domain GPR system.

9.2.2 SELECTION OF THE OPTIMUM GPR SYSTEM

The following general specifications are requirements for a high performance GPR system designed to meet the goals of deep penetration and high resolution. The specifications can be applied to any GPR technology: frequency-domain, or time-domain.

The GPR system for utility location must be designed to operate with several RF bandwidths. Three nominal RF bandwidth ranges are recommended: one for deep penetration and lower resolution, one for medium penetration and medium resolution, and one for shallow penetration and high resolution. The suggested bandwidths given below are meant as guidelines.

We recommend that for deep-penetrating, lower-resolution applications, the RF bandwidth should be confined to a range of 50 MHz to 200 MHz. For medium-resolution, medium-penetration applications, a bandwidth of 200 MHz to 600 MHz should be used. For high resolution, a bandwidth of 500 MHz to 1500 MHz is suggested. These RF bandwidths correspond to approximate pulse widths of 6.7 ns, 2.5 ns, and 1 ns, respectively.

A multiple-bandwidth GPR system will probably require a separate antenna system for each bandwidth. Nevertheless, for maximum performance, the GPR system should use a bistatic antenna configuration. This may present a problem at low RF frequencies because each of the antennas might be quite large. In such a case, a monostatic GPR design can be used, but performance will probably not be as good as with a bistatic configuration.

9.3 THE MAXIMUM PERFORMANCE GPR

Based on this program, GAR engineers concluded that a frequency-domain GPR based on a stepped-frequency design

provides the highest performance capabilities. Such a system can be built to meet the dynamic range, sensitivity, average transmitter power, and RF bandwidth shape and flexibility requirements for high-performance GPR applications more readily than its pulsed, time-domain counterpart. Furthermore, a stepped-FM GPR utilizing a synthesized frequency source potentially offers superior performance over the swept-FM system due to reduced phase noise effects and frequency inaccuracies (see Section 6.3.1.3). However, a swept-FM GPR can offer significant improvements in measurement speed over the stepped-FM GPR.

The RF bandwidth shape of the GPR should be consistent with that of a monocycle pulse, or a similar shape, in order to match the antenna radiation capabilities and the soil attenuation characteristics. Such a bandwidth shape can be achieved by modulating the individual transmitted RF frequencies, or it can be achieved by weighting the received RF frequency components. In general, weighting the received signals is the simplest technique.

One method of implementing a stepped-FM GPR would be to radiate each individual RF frequency, while keeping the receiver tuned to that frequency for a time equal to at least the duration of the transmitted RF pulse plus the maximum range time. Then the transmitter and receiver are stepped to the next frequency, repeating the procedure until all of the frequencies have been radiated and received. After processing the received data from these individual frequencies, the measurement is complete. The cycle is repeated again for the next measurement.

An important performance goal in a stepped-FM system is to radiate the individual RF frequency components with very pure spectral contents. A pure spectral content is impossible to achieve, however, because the individual transmitted RF frequencies must be turned on and off, or modulated, for some fixed time duration. The shape of the pulse used to modulate the RF frequency is typically rectangular. Thus, each of the RF frequencies acts as a "carrier" frequency for the modulation pulse. To approximate the spectrum of a CW RF frequency, the modulation pulse must be infinitely long in duration, which is clearly impossible in a realizable system. Progressively

shorter modulation pulses broaden the spectrum of the individual RF frequency components.

On the other hand, the design engineer wishes to make the modulation pulse narrow because this decreases the time that the GPR must dwell on each frequency. Conversely, increased modulated pulse widths decrease the harmonic content of the individually transmitted RF components. A compromise must be reached between the modulating pulse width, the processing techniques to be applied to the received waveforms, and the desired measurement speed.

Recall that the unambiguous range specification of the stepped-FM GPR determines the frequency difference between the individual RF frequencies that must be used to reconstruct a simulated pulse. The specification of the overall RF bandwidth and the frequency component spacing determines the number of frequency components required to span the bandwidth. Thus, operating at the minimum possible unambiguous range permits the use of fewer frequency components, which reduces the GPR system complexity. An added benefit of the reduced number of radiated frequency components is a potential increase in measurement, or scan, speed. On the other hand, a reduction in the minimum unambiguous range of the GPR reduces the maximum depth which can be "seen" by the radar. Thus, a trade-off exists here as well.

Some level of signal processing capability is clearly required for the stepped-FM radar system. A minimum requirement is to provide frequency bandwidth control, both for weighting functions to reduce the synthesized pulse sidelobe levels, and for RF bandwidth selection for different penetration or resolution applications. Additional signal processing algorithms should include FFT and inverse-FFT software to allow advanced processing techniques to be applied to the received GPR waveforms. The GPR should have the capability of waveform averaging to reduce noise effects. The averaging, of course, would impact the GPR measurement speed. Also, it may be desirable to provide a means of calibration to remove undesired effects of cables and connectors, similar to the calibration capabilities of the HP 8510.

The GPR will require measurement data rates, or "scan" rates of at least 10 Hz, and should probably include the

capability of a 50 Hz scan rate. These data scan rates will be a challenge for a synthesized, stepped-FM design to accomplish, due to the synthesizer switching speed limitations. However a swept-FM, or a stepped-FM system that does not phase lock to the individual frequency components as it switches, can operate at even higher measurement speeds.

The design and construction of the GPR receiver and transmitter circuits must be done with great care to maximize the signal-to-clutter and signal-to-noise performance. The number of RF connectors in critical transmission lines should be minimized to avoid parasitic reflections. All RF components should provide good impedance matches to the transmission lines, or they will also produce reflections at their input and output ports that will contribute to the internal system clutter.

The selection of the transmitter power level is dependent on safety requirements, electromagnetic interference regulations, the depth penetration specification, and the RF bandwidth of the GPR. Safety regulations and EMI requirements provide the upper limit on transmitter power. Given this constraint, the GPR transmitter should operate with a power level that is high enough to produce a recognizable target signal level at the receiver from a specified target geometry, at a specified burial depth, with a specified soil attenuation. Higher transmitter powers will act to increase the target signal dynamic range above the receiver noise floor, assuming that the receiver does not compress the high level returns. However, recall that a GPR system is often clutter-limited, therefore increasing the transmitter power may be ineffective in helping to detect low-amplitude targets.

The RF receiver should be designed to have a low noise figure. This will probably require a low-noise amplifier on the receiver front end. Such an amplifier will reduce the effects of a noisy mixer or sampler following it in the RF signal path. It may also help to increase the receiver sensitivity. Although it is simple, and can provide high performance in some respects, using a sampler on the receiver front end should be avoided due to its noise performance and limited dynamic range capability.

The receiver must utilize I and Q (in-phase and quadrature-phase) detection to provide a vector representation of the received waveform so that proper phase relationships between the RF frequency components can be maintained. This is a stringent requirement, because phase and amplitude distortions, especially if only a few RF frequency components are used, will result in errors when reconstructing the pulse.

SECTION 10

REFERENCES

1. Stewart, C., "Summary of Mine Detection Research, Volume 2," Technical Report 1636-TR, Project 8-07-011-420, U. S. Army Engineer Research and Development Laboratories, Corps of Engineers, Fort Belvoir, Virginia, May 1960.
2. Davis, T. J. and R. Liem, "Assessment of Ground Probing Radar Data Processing/Conditioning Methods," Final Report on Contract no. N62583/84 MT210, Sigma Research, Inc., Seattle, Washington, December 1984.
3. Geophysical Survey Systems, Inc. "Operation Manual, Subsurface Interface Radar SIR System 8," Hudson, New Hampshire.
4. Bechtel, M. E. and A. V. Alongi, "Research on a Vehicular-Mounted Mine-Detector Radar," Final Technical Report on Contract no. DAAK02-72-C-0444, Calspan Corporation, Buffalo, New York, November 1973.
5. Belsher, D. R., R. H. McLaughlin, A. G. Repjar, and H. E. Bussey, "Microwave Detection of Lost Wells and Unknown Water-Filled Voids in Coal Mines," NBSIR 84-3017, National Bureau of Standards, Boulder, Colorado, September 1984.
6. Wohlers, R. J., "The GW1A, an Extremely Wide Bandwidth Low-Dispersion Antenna," Contract no. DAAK02-69-C-0149, Cornell Aeronautical Laboratory, Inc., Buffalo, New York.
7. King, W. P. and G. S. Smith, Antennas in Matter: Fundamentals, Theory, and Applications, MIT Press, Cambridge, Massachusetts, 1981.
8. Carson, R. S., High - Frequency Amplifiers, Wiley and Sons, New York, 1975.

9. Brown, G. H. and O. M. Woodward, "Experimentally Determined Radiation Characteristics of Conical and Triangular Antennas," RCA Review, December 1952.

APPENDIX A

Measured Electromagnetic Properties of Various Soil Types

GEORGIA RED CLAY

A large sample of Georgia red clay (Cobb County, GA) was baked to remove the natural water. Six smaller samples were prepared from the dry clay and deionized distilled water with approximately the following water contents (percent water by dry weight) 0, 2, 5, 10, 20 and 30%. The measured values of percent water by weight, percent water by dry weight, and density are in Table 2.

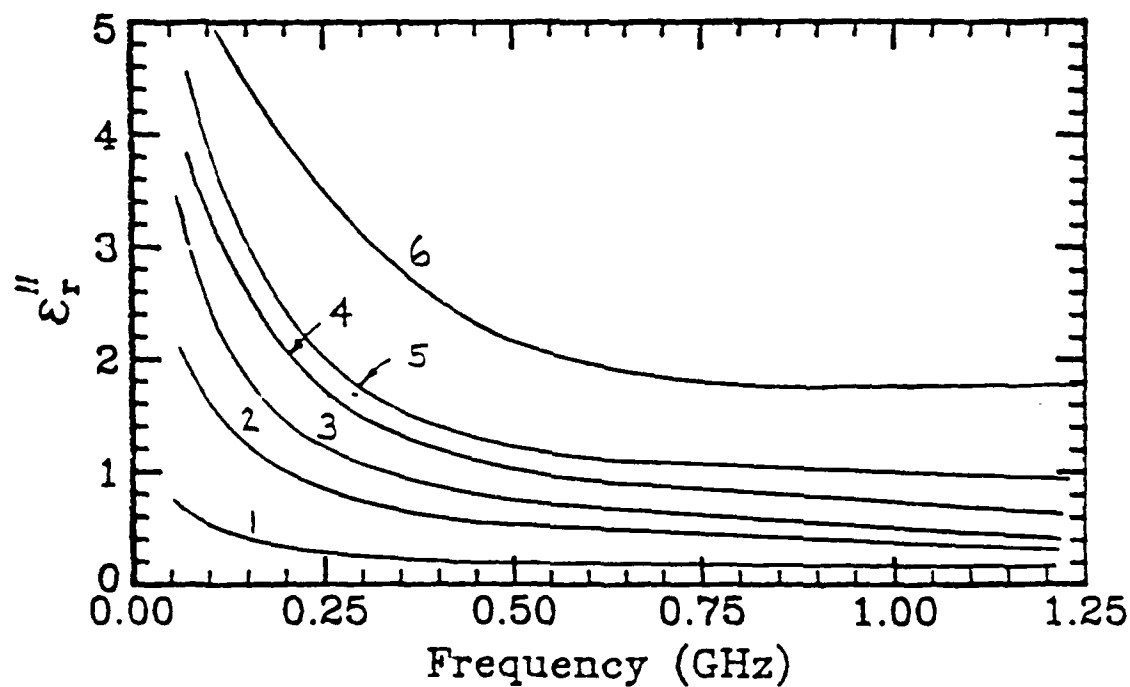
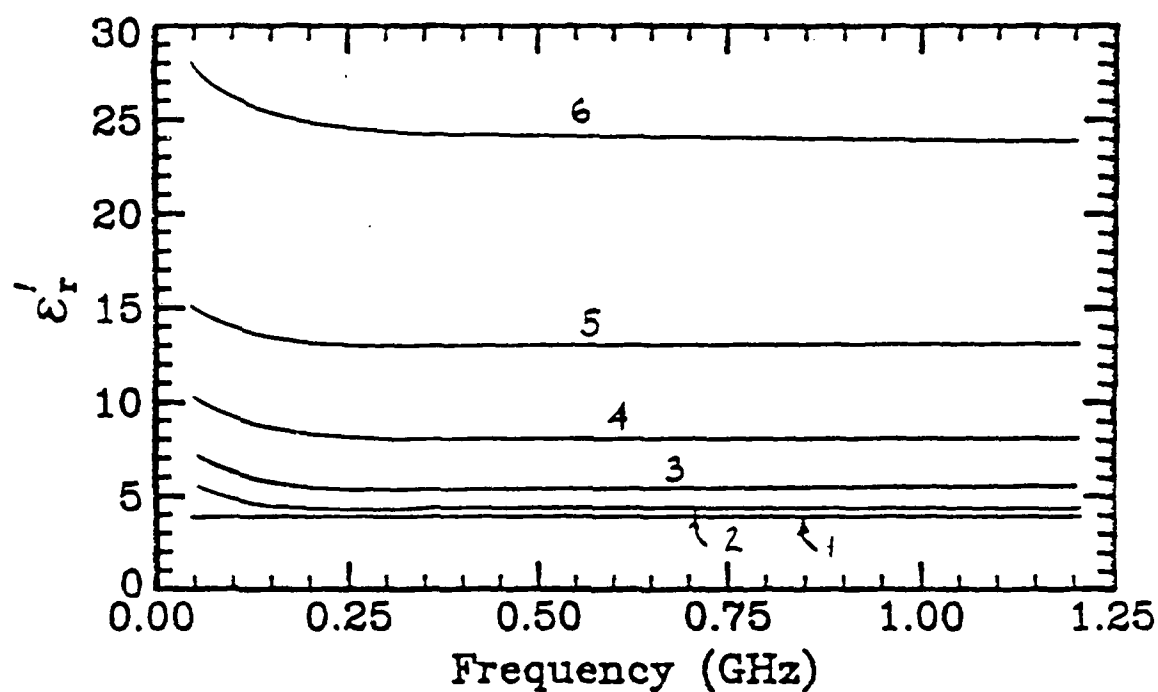
The measured electrical parameters ϵ_r' , ϵ_r'' , σ_e and α are presented as a function of frequency, $50 \text{ MHz} \leq f \leq 1.25 \text{ GHz}$, in the two attached figures. The data for the six samples are plotted on the same graphs to show the effects of the water content. These graphs clearly demonstrate the increases in the dielectric constant ϵ_r' and effective conductivity σ_e that occur with increasing water content. The attenuations for these samples are in most cases much smaller than those for the Japanese soils.

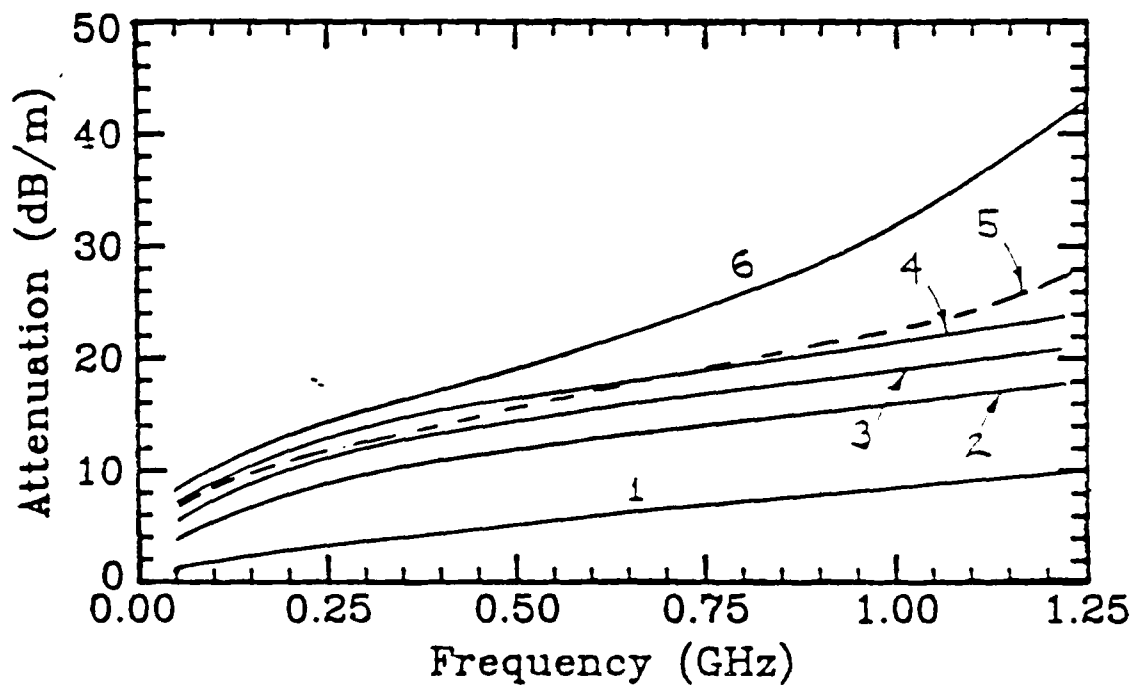
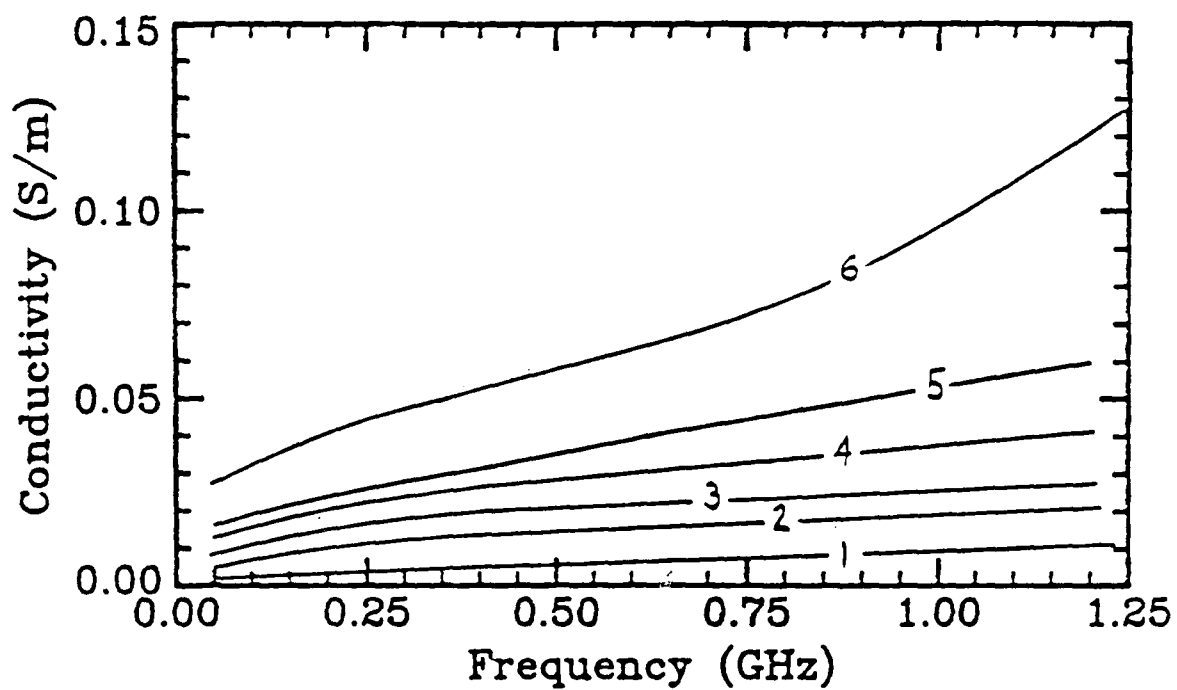
RED CLAY

(Cobb County, GA)

NUMBER	PERCENT WATER BY WEIGHT	PERCENT WATER BY DRY WATER	DENSITY gm/cm ³
1	≈ 0	≈ 0	1.46
2	2.0	2.0	1.49
3	4.6	4.8	1.55
4	8.7	9.6	1.66
5	15.9	18.9	1.72
6	22.3	28.7	1.88

RED CLAY - COBB CO., GA.





SAND/WATER MEASUREMENTS

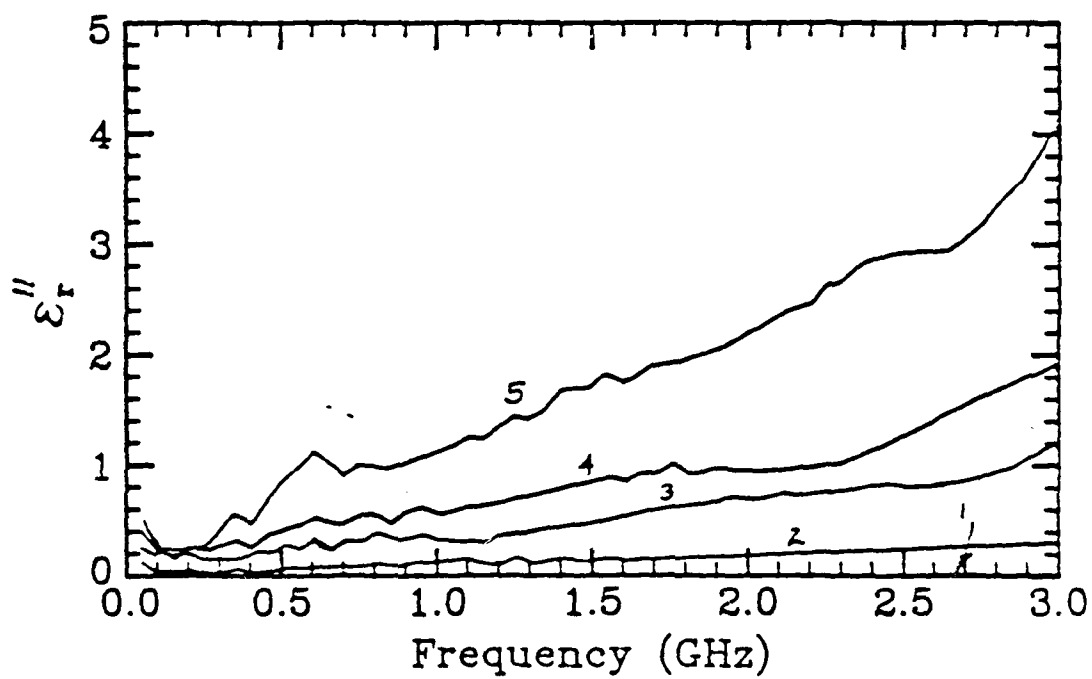
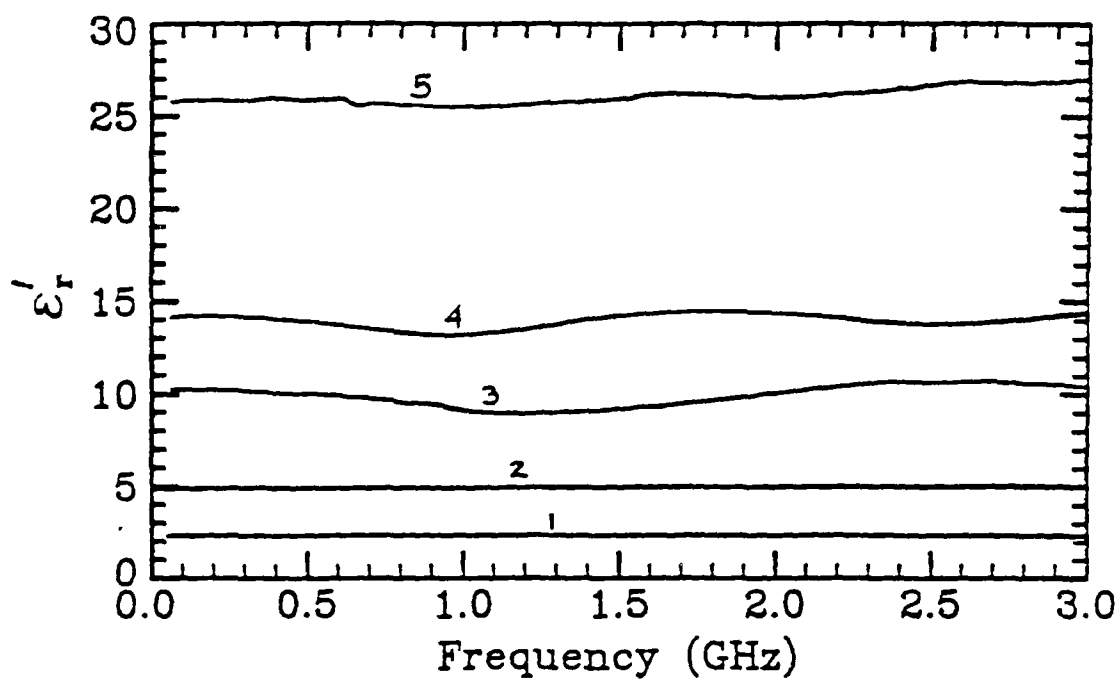
The electrical parameters of five sand/water mixtures were measured, and the results are recorded in the accompanying graphs. The parameters were measured over the frequency range $50 \text{ MHz} \leq f \leq 3 \text{ GHz}$.

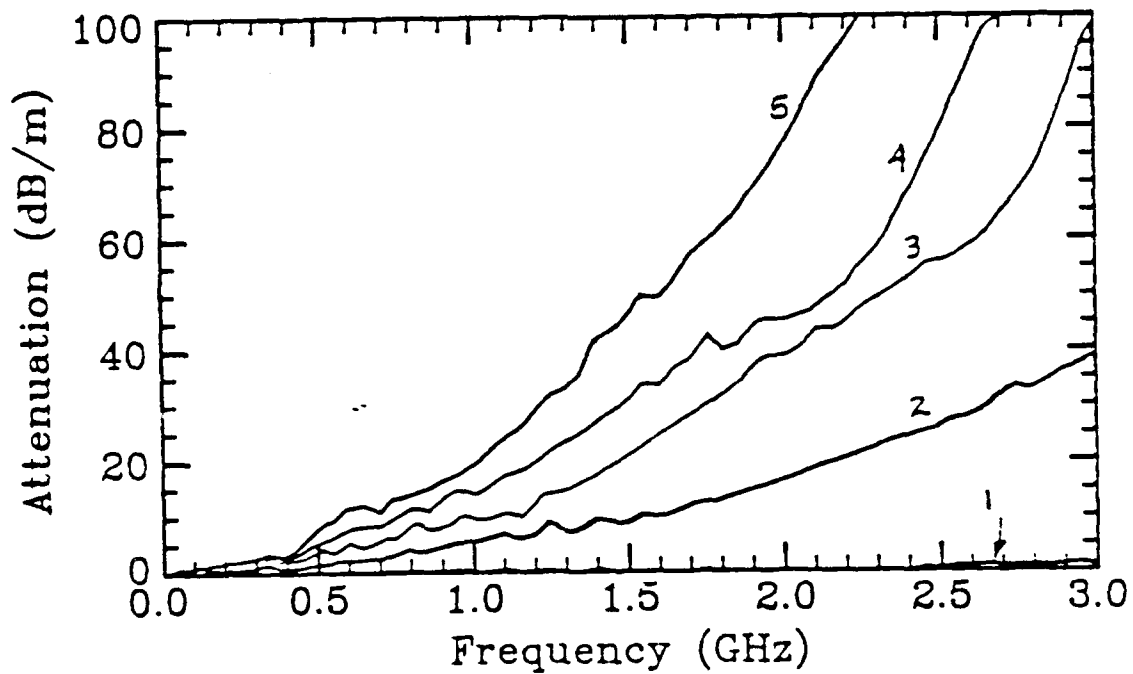
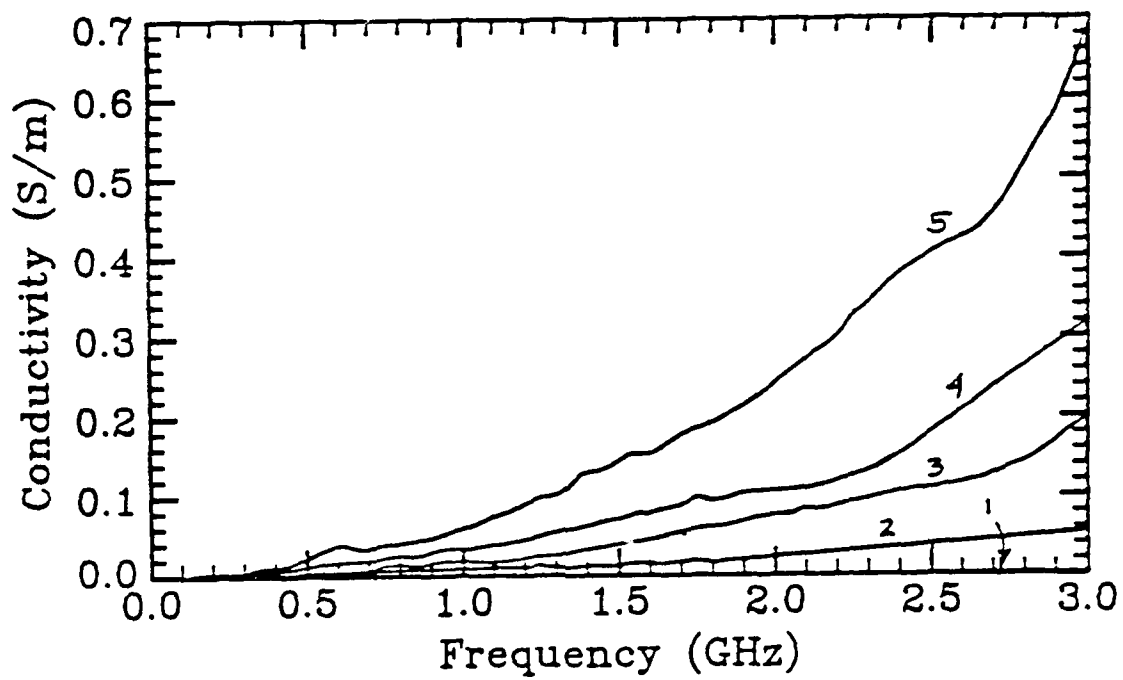
The "dry" sand was mixed with distilled water to obtain various percentages of water by weight. The highest water content was obtained by completely saturating the sand. The parameters for the mixtures are given in the accompanying table.

Note that there are ripples on the data for the higher water content mixtures. The ripples are the result of nonuniform packing of the sand in the measurement cell.

SAND-WATER MIXTURES

<u>Sample No.</u>	<u>Percent Water by Weight</u>	<u>Percent Water by dry Weight</u>	<u>Density gm/cm³</u>	<u>Nominal ϵ_r</u>
1	-	-	1.37	2.3
(Dry)				
2	9.1	10.0	1.38	5
3	11.7	13.2	1.52	10
4	16.7	20.0	1.57	14
5	21.3	27.1	1.92	26
(Saturated)				





JAPANESE SOILS

Samples from each of the seven Japanese soils were oven dried and used to determine the water content. The results of these measurements (percent water by weight, percent water by dry weight, and density) are summarized in Table 1.

A brief physical description of each sample follows:

- Sample 1: redish brown, soil plus clay, fine particles.
- Sample 2: dark brown to black, sandy soil.
- Sample 3: dark tan to gray, dry soil, several small rocks in sample.
- Sample 4: mostly large soft rocks, some dark tan soil.
- Sample 5: dark tan to black, coarse sandy soil.
- Sample 6: dark gray clay, very cohesive, very fine particles, very homogenous.
- Sample 7: black clay with some sand and rocks, very cohesive.

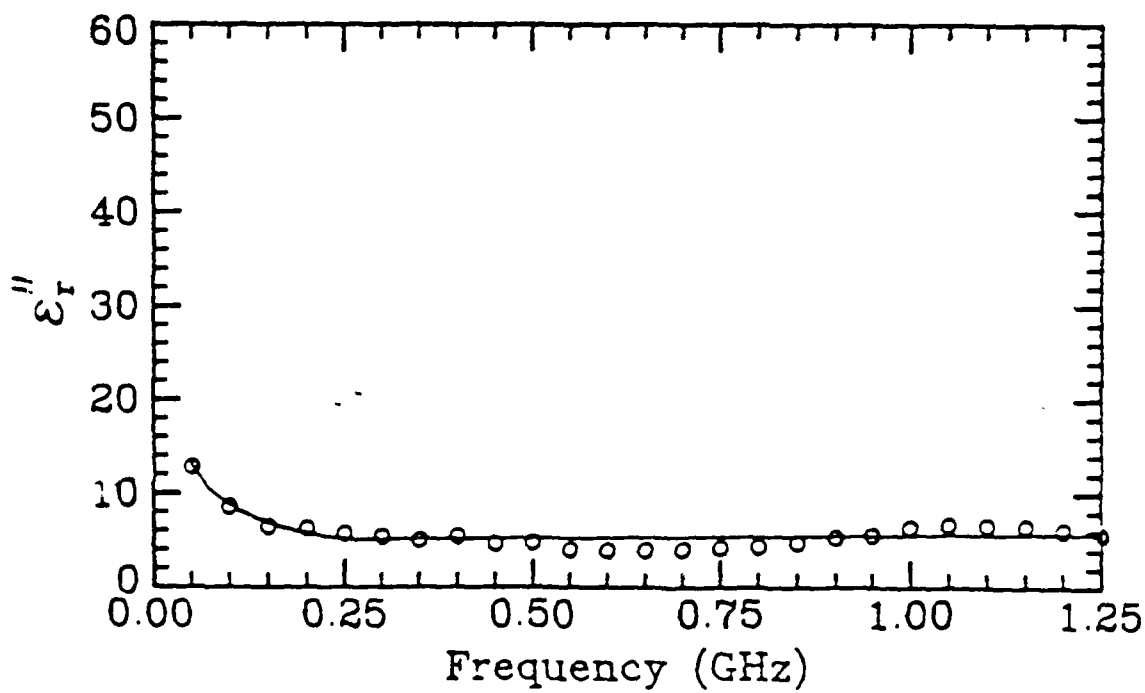
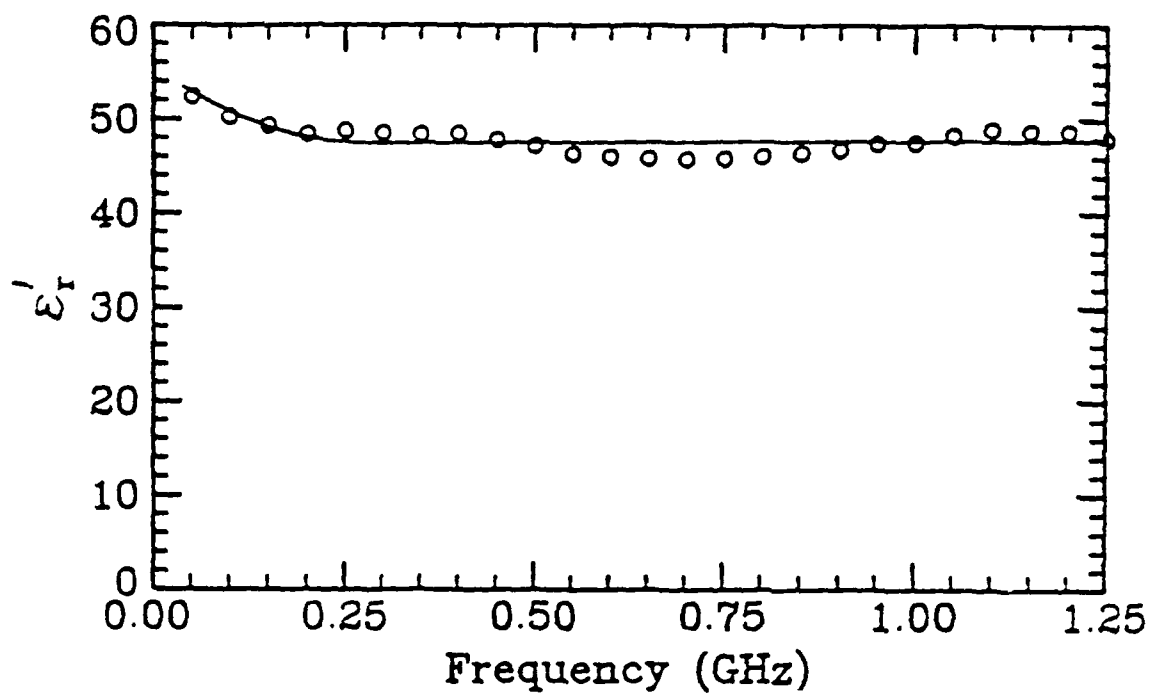
The complex relative permittivity $\epsilon_r = \epsilon_r' - j\epsilon_r''$ was measured for each sample, and the effective conductivity σ_e and attenuation constant α (dB/m) were computed from ϵ_r . The results are presented as a function of frequency, $50 \text{ MHz} \leq f \leq 1.25 \text{ GHz}$, in the attached graphs.

The average dielectric constants (real part of the relative permittivity, ϵ_r') are graphed as a function of the water content of the samples below.

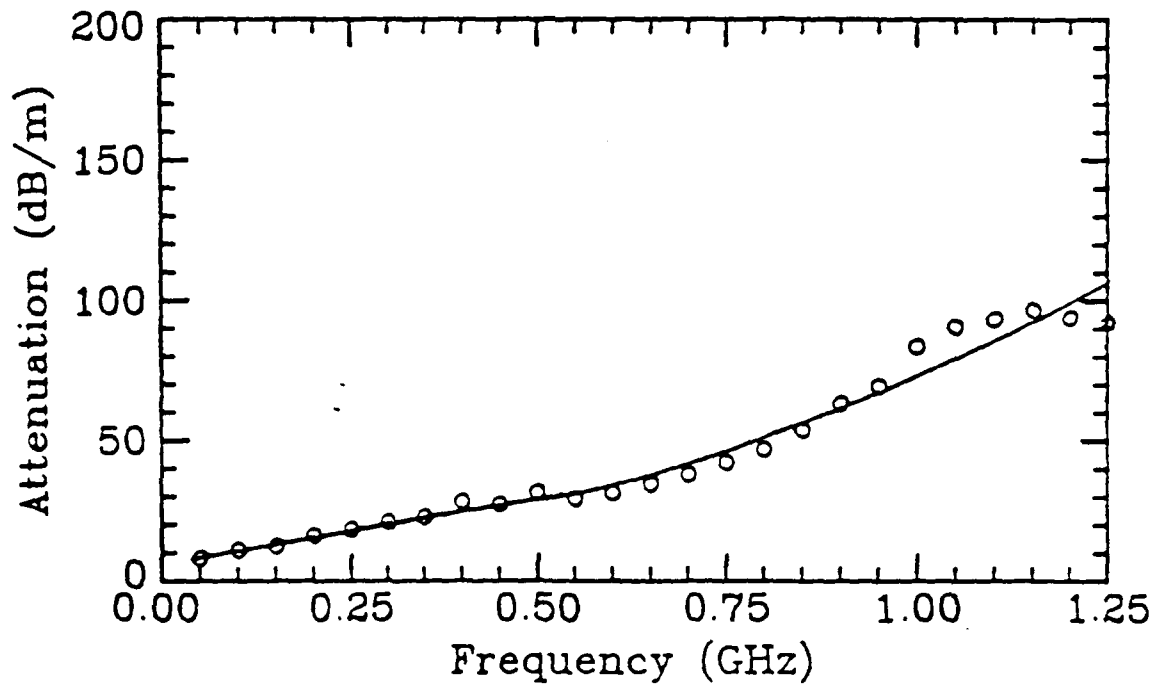
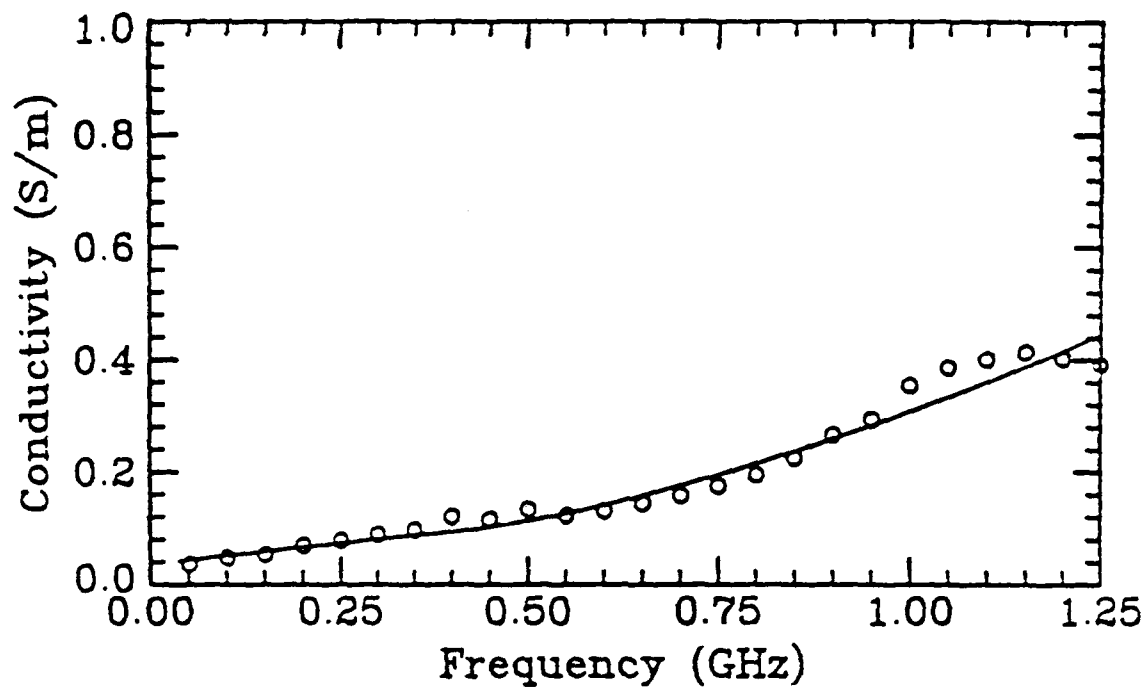
JAPANESE SOILS

NUMBER	PERCENT WATER BY WEIGHT	PERCENT WATER BY DRY WEIGHT	DENSITY gm/cm ³
1	48	91	1.32
2	16	19	1.83
3	19	23	1.69
4	26	35	1.68
5	11	13	1.86
6	40	66	1.53
7	20	25	1.86

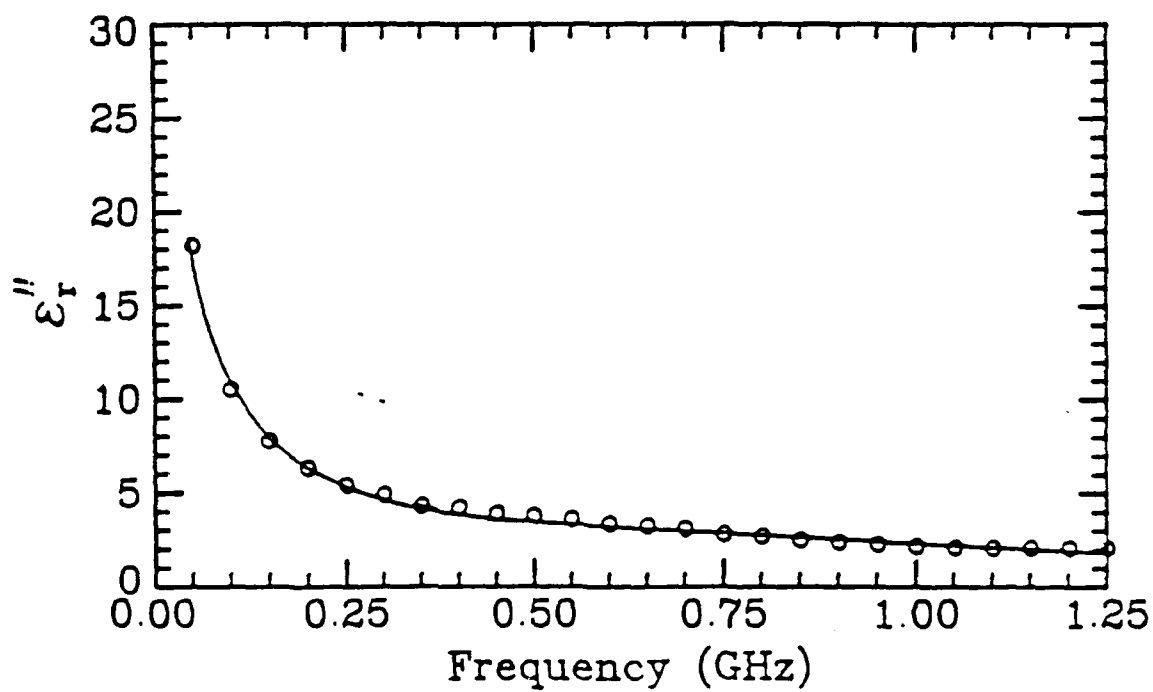
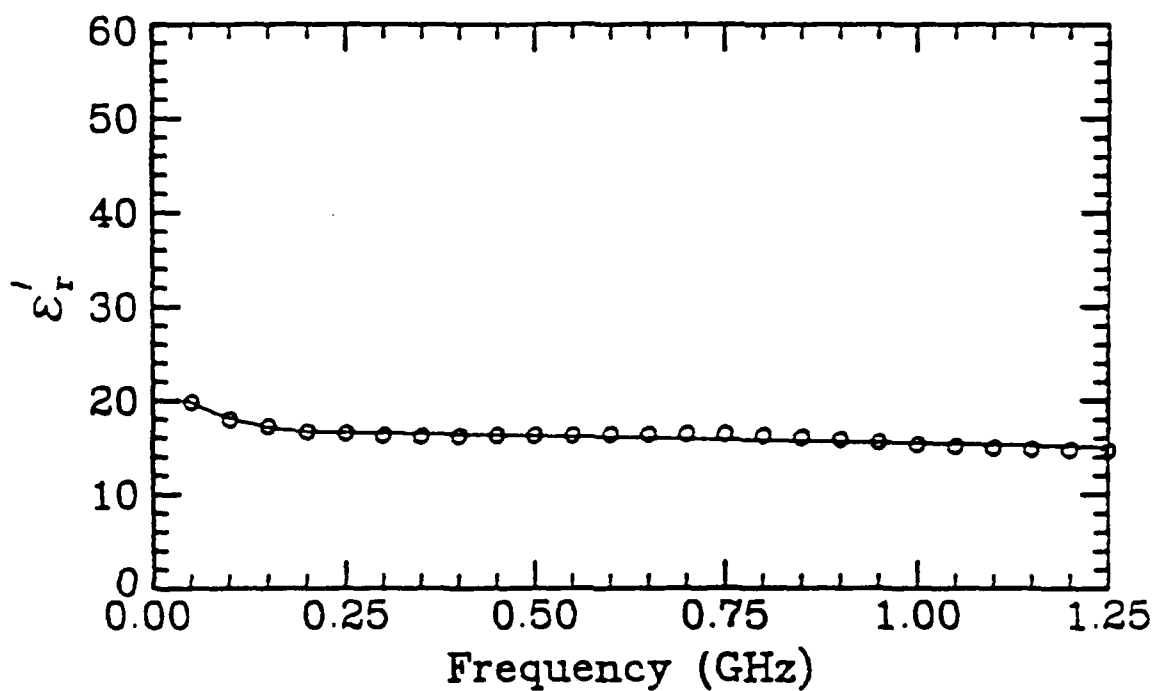
Sample 1



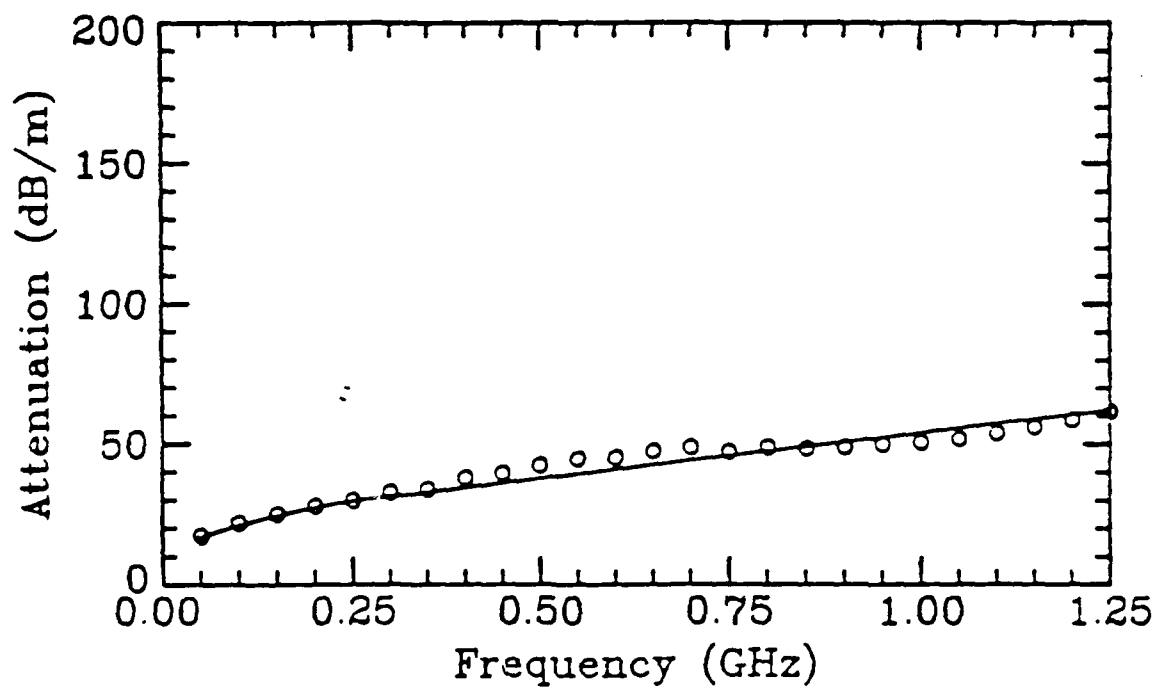
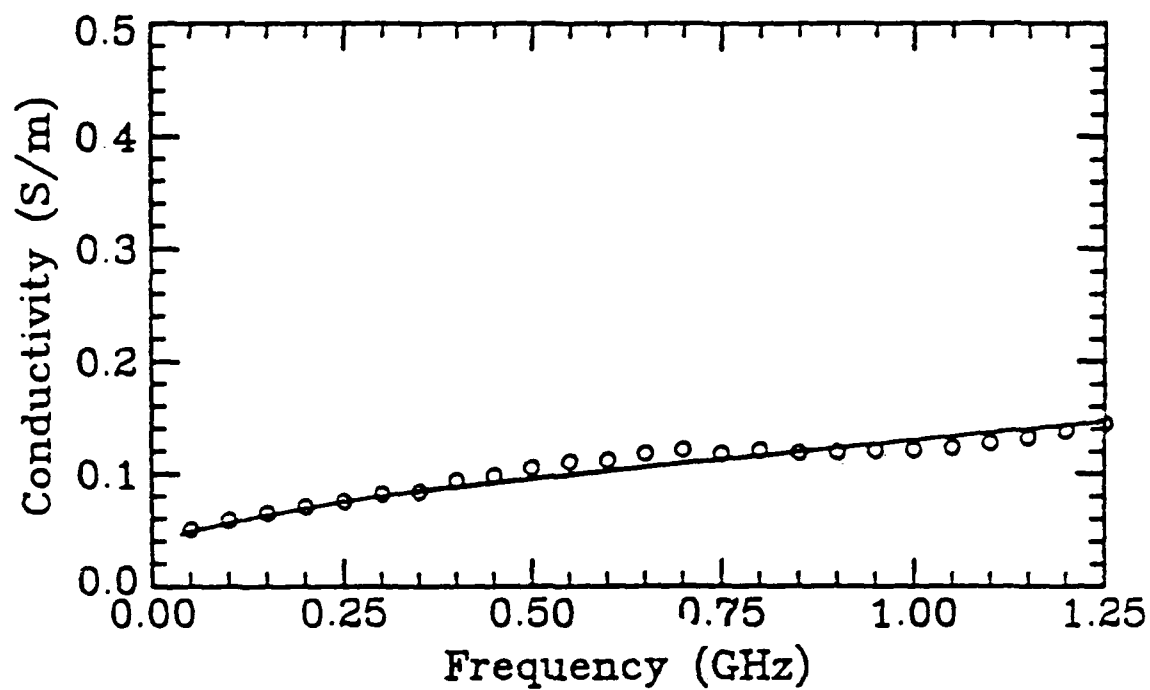
Sample 1



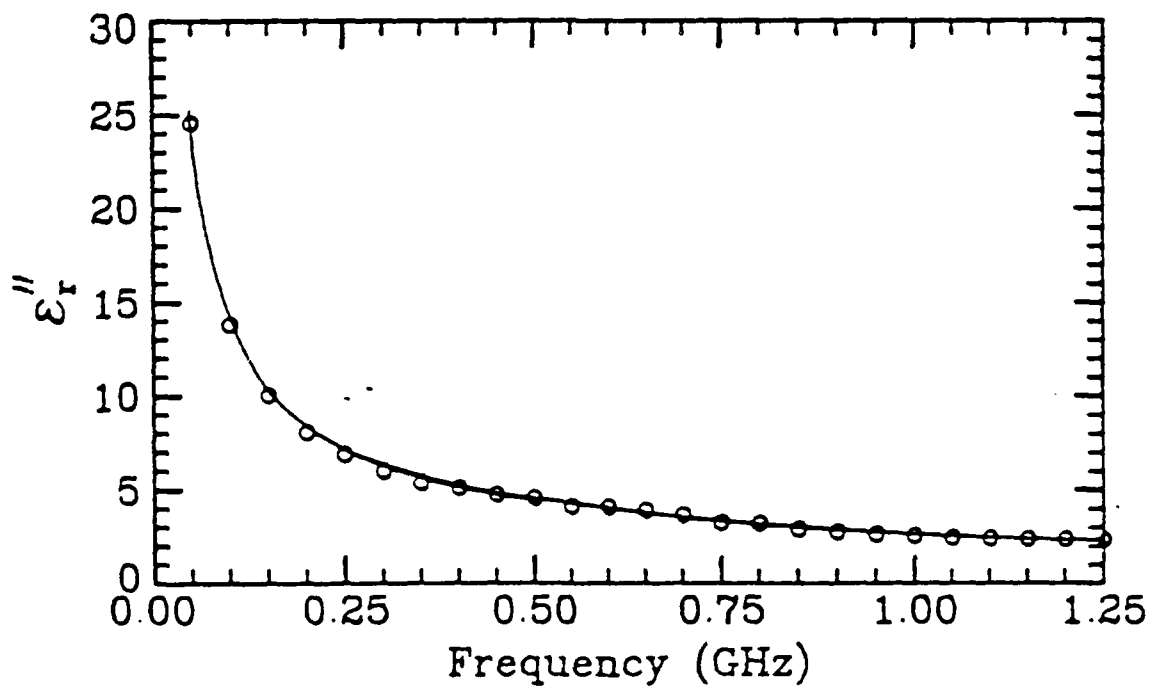
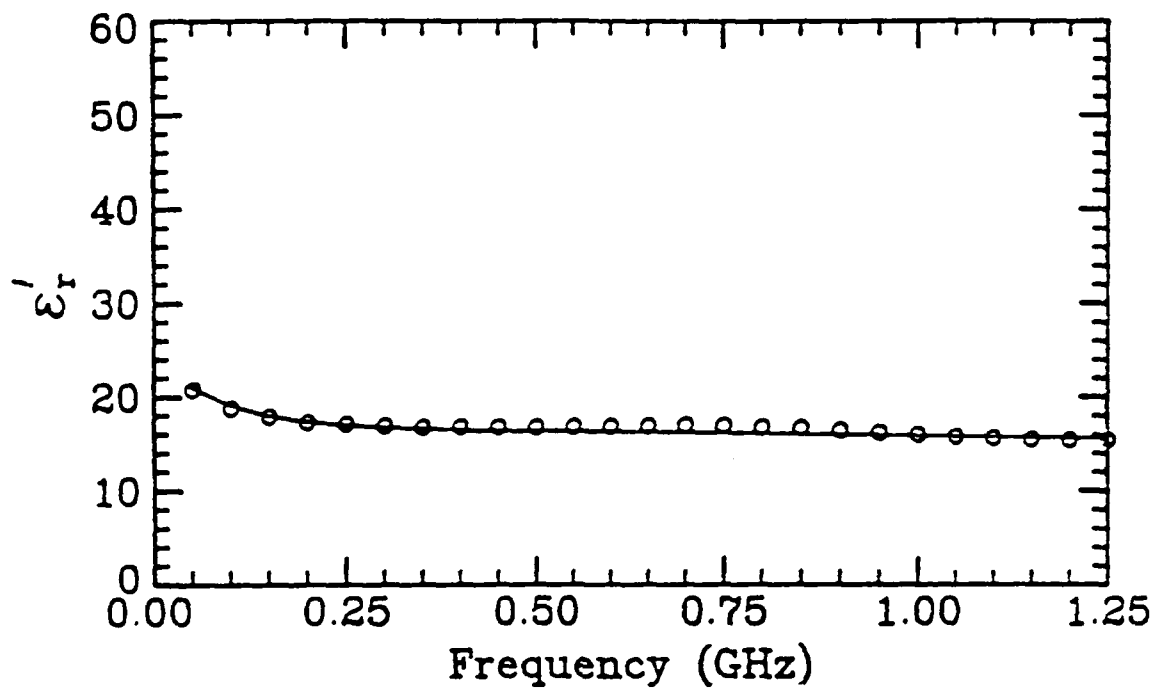
Sample 2



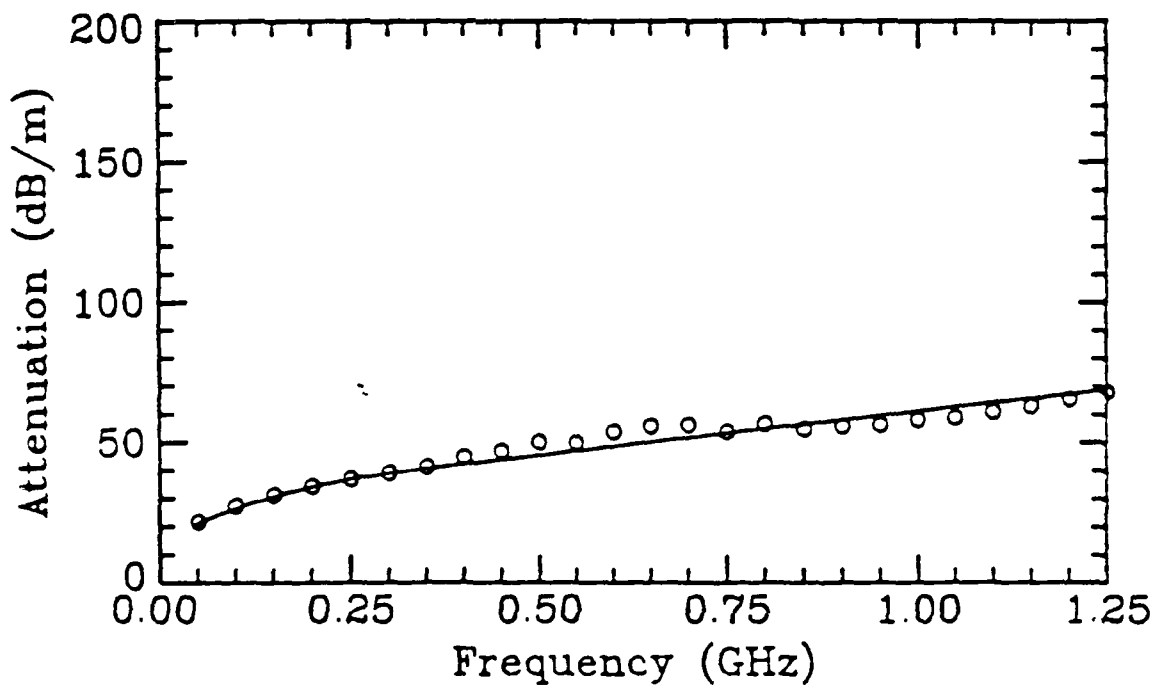
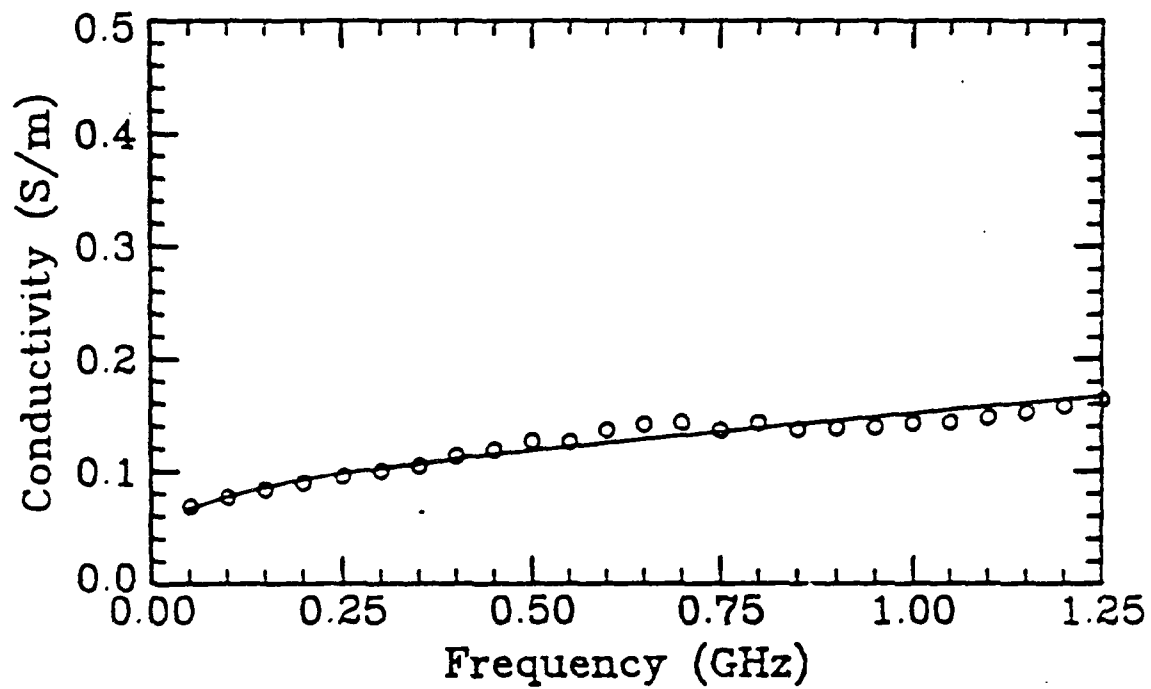
Sample 2



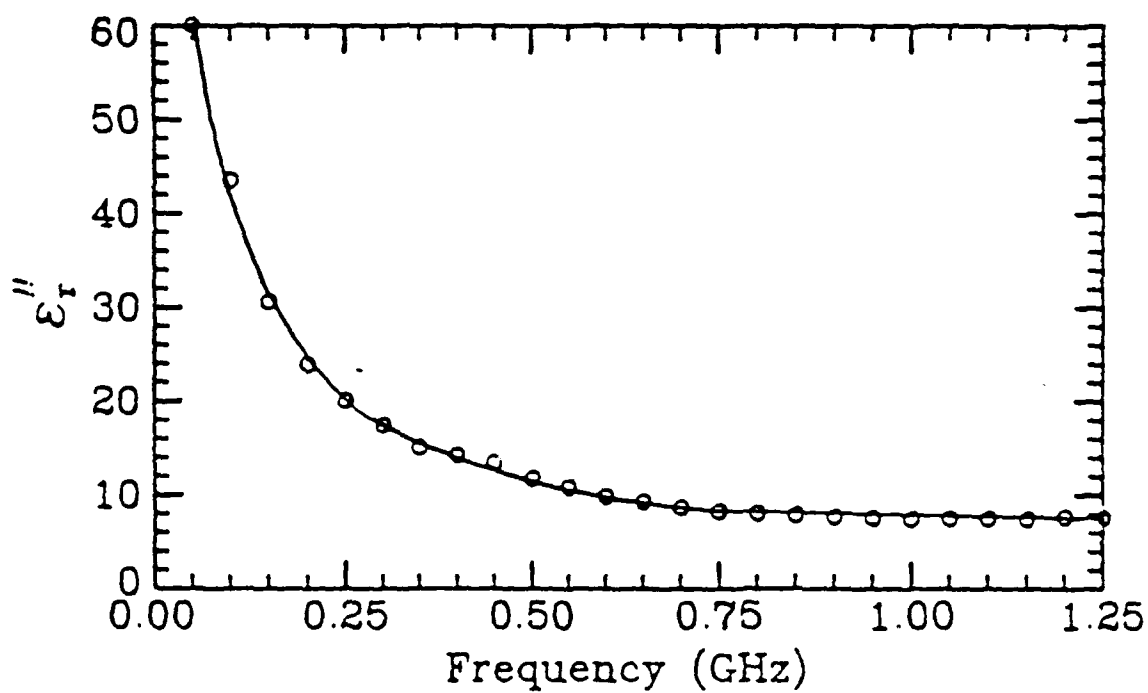
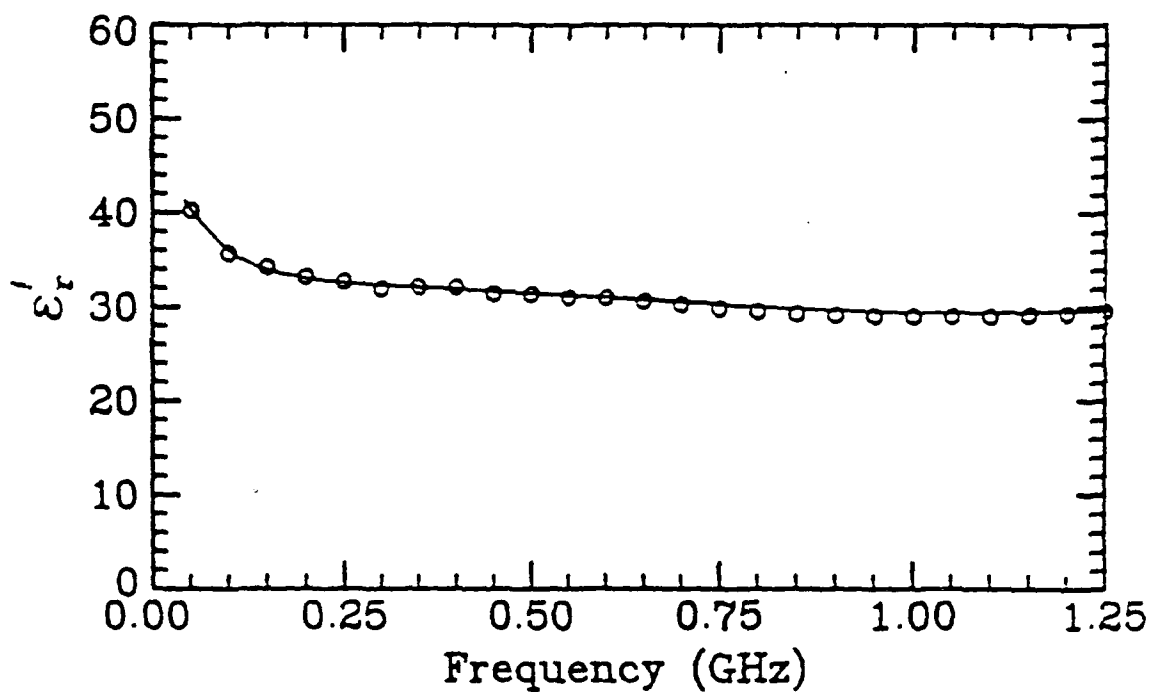
Sample 3



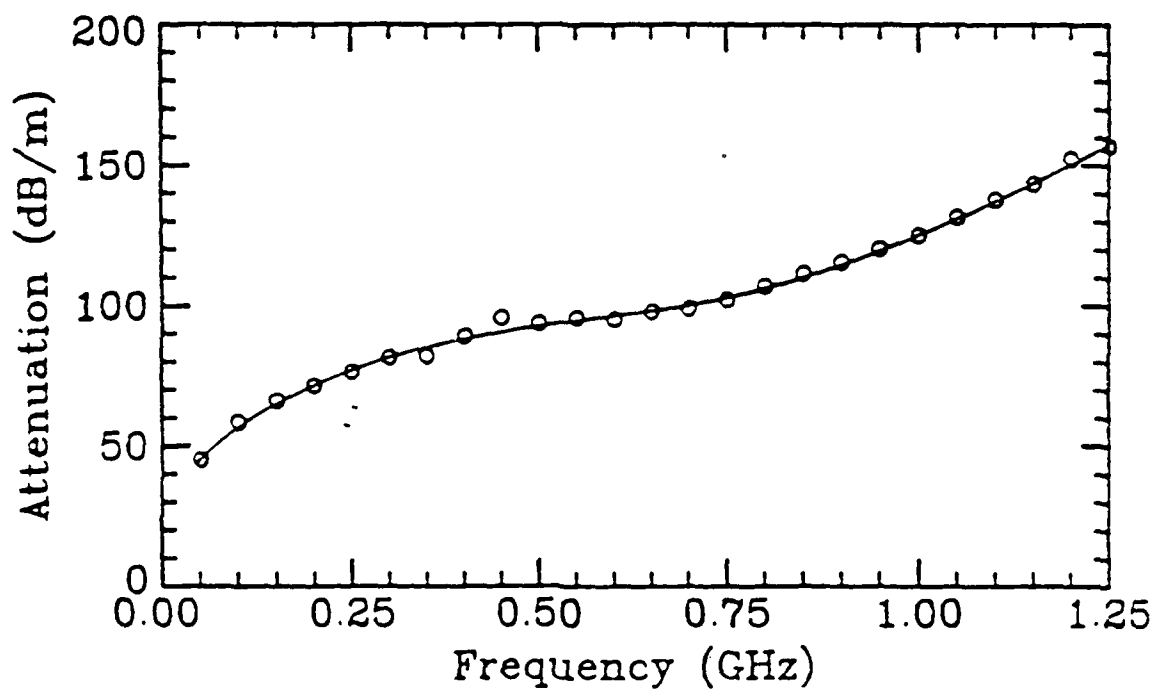
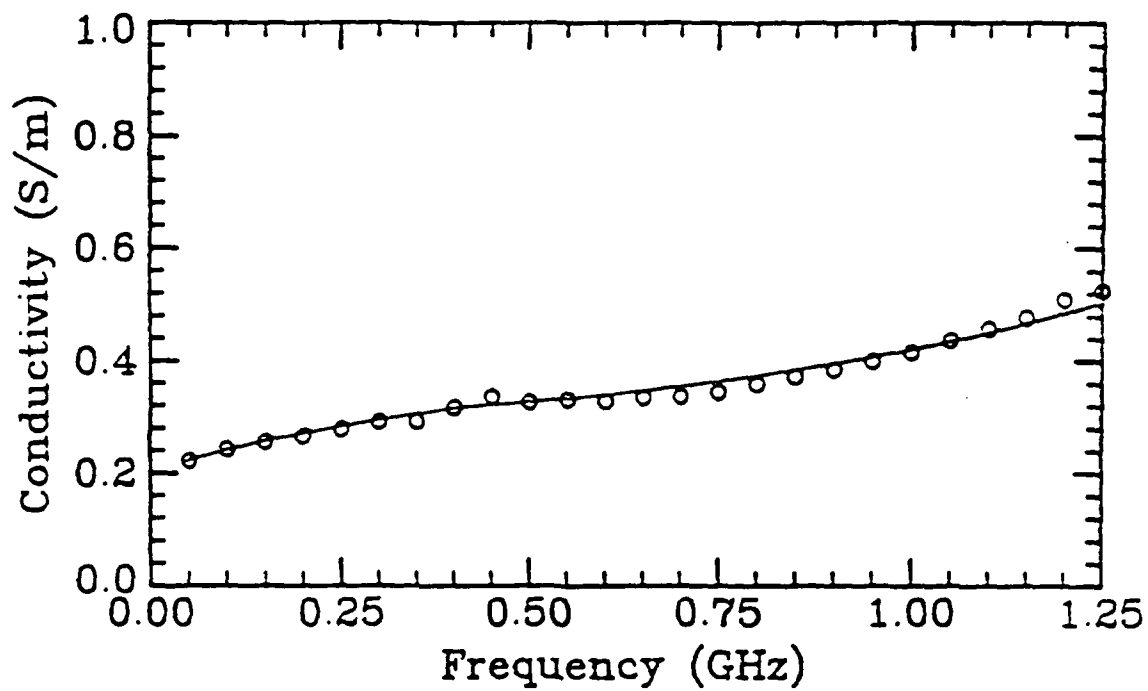
Sample 3



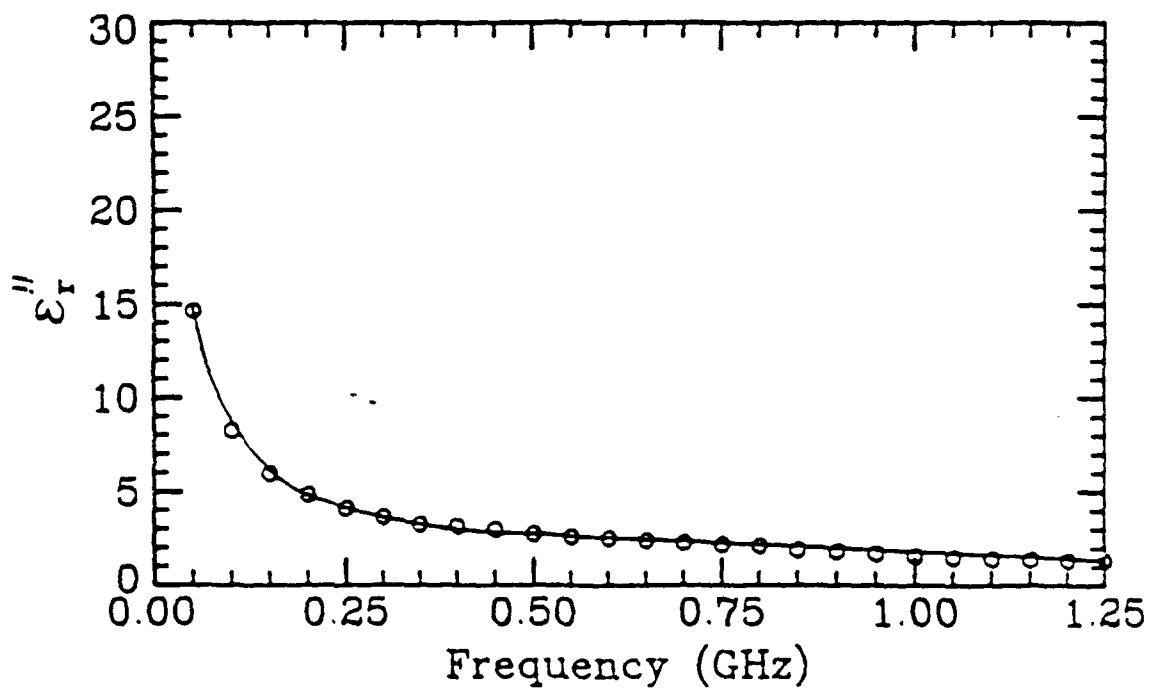
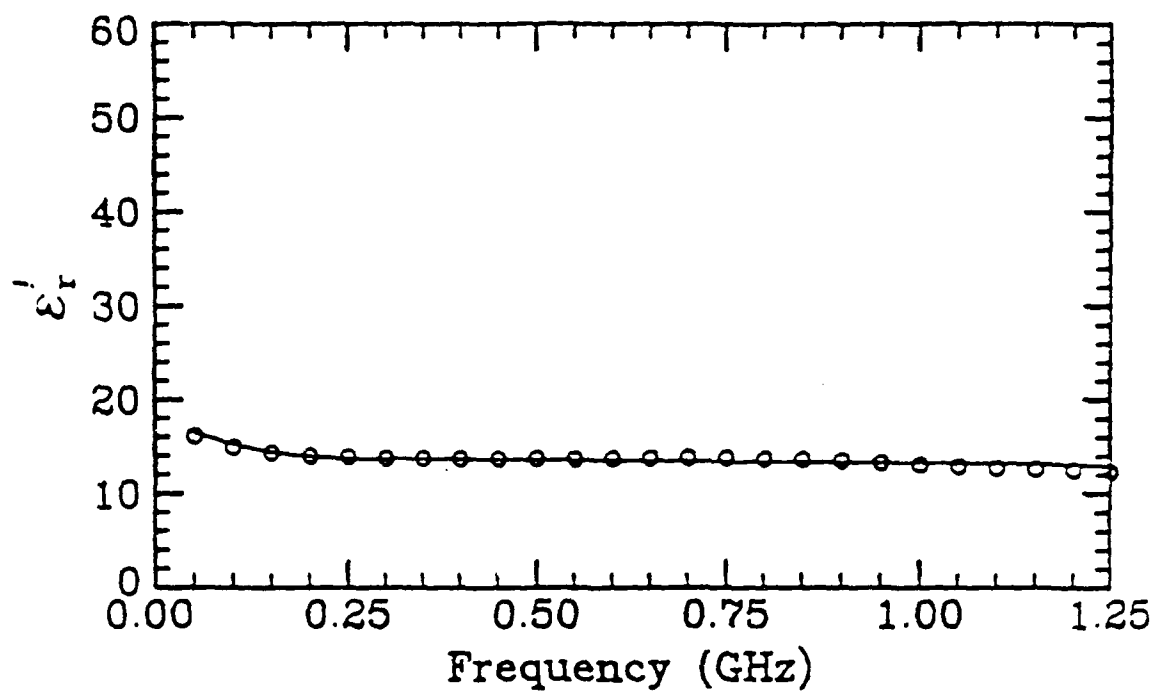
Sample 4



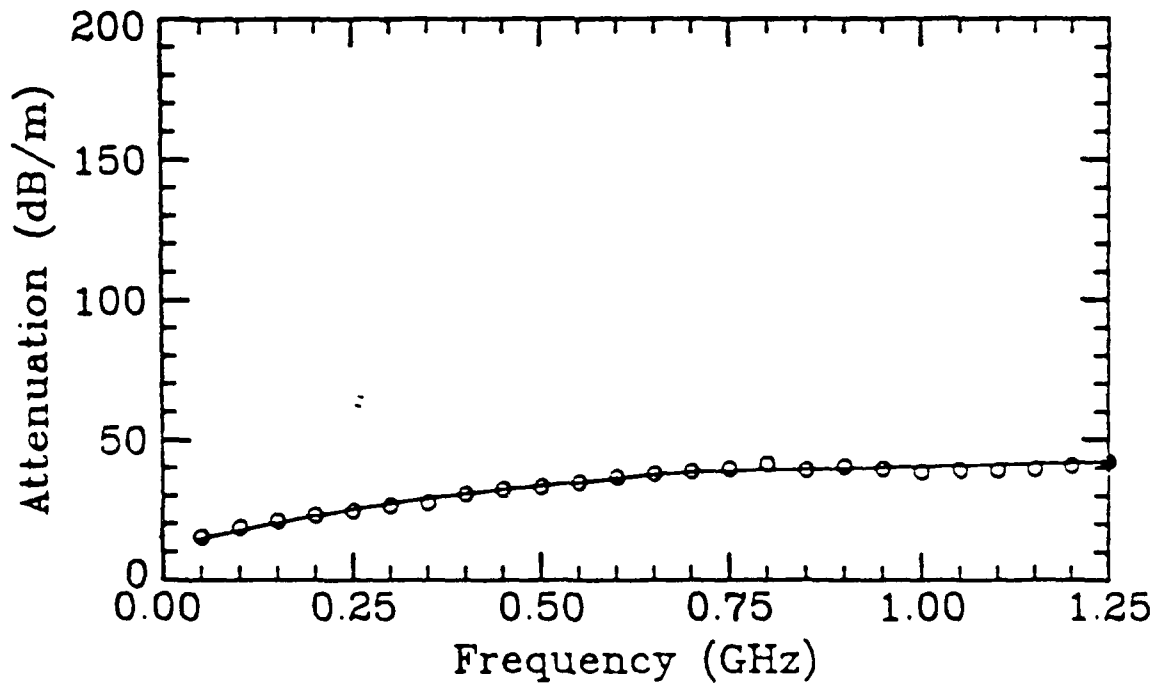
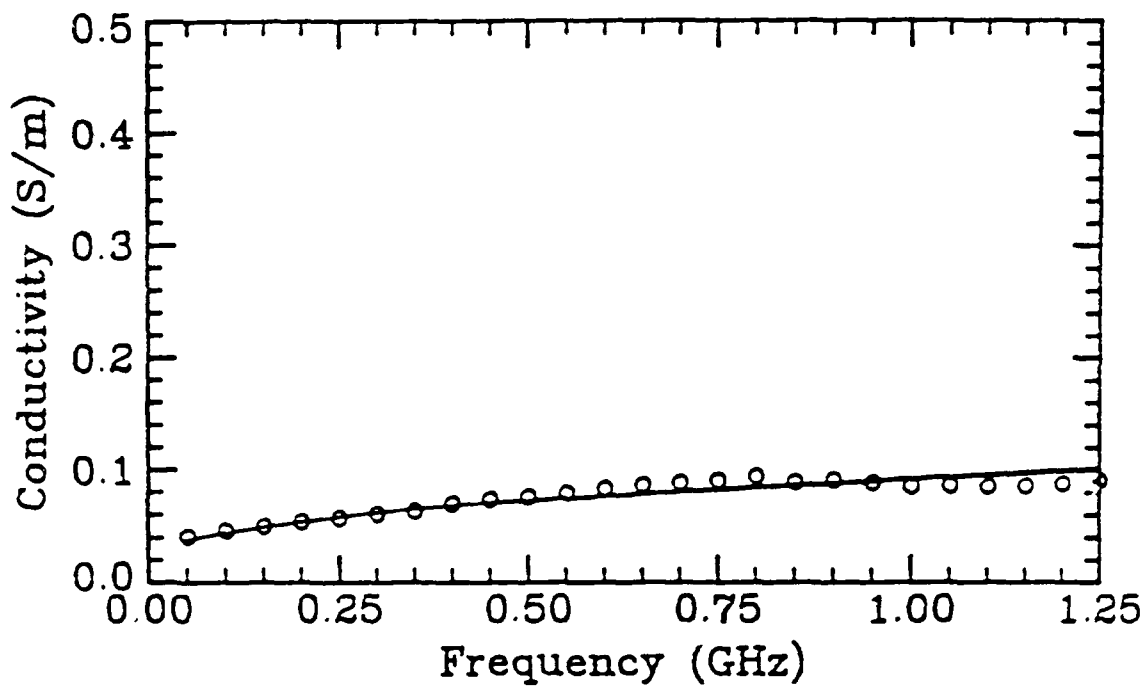
Sample 4



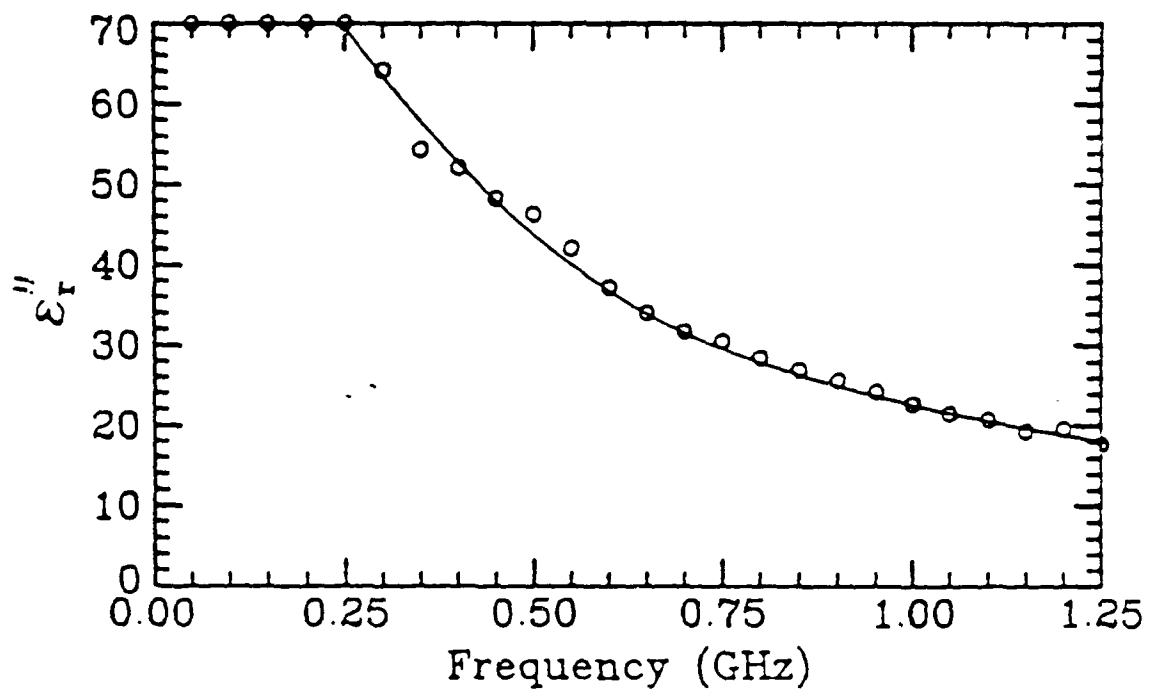
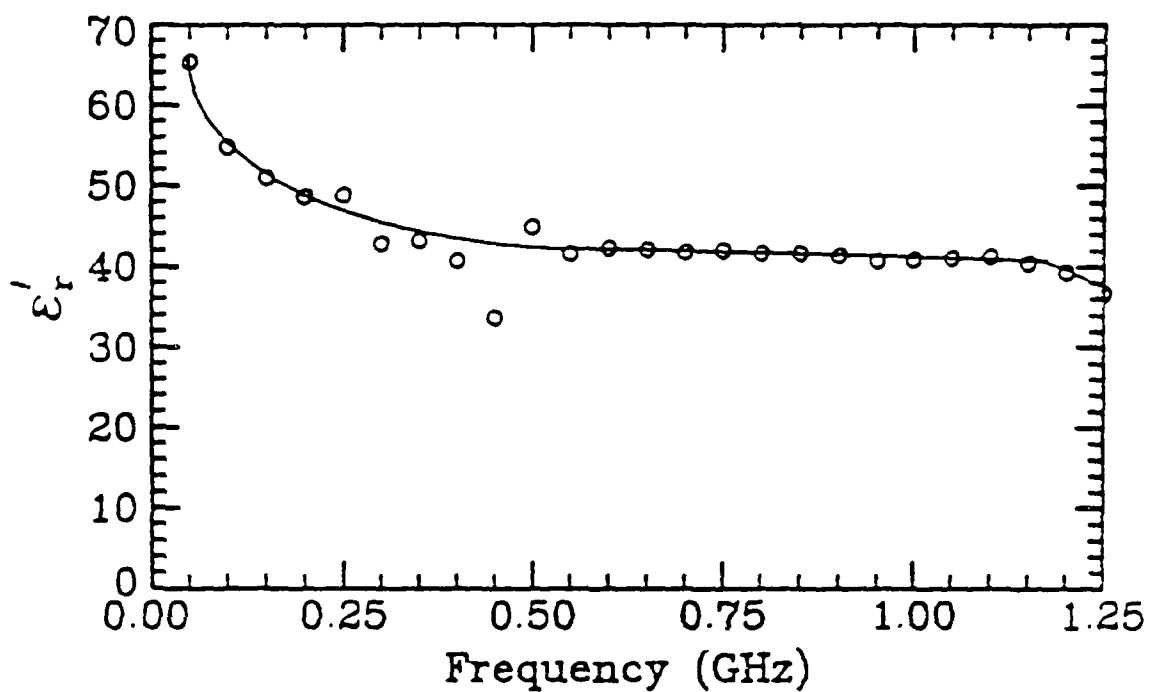
Sample 5



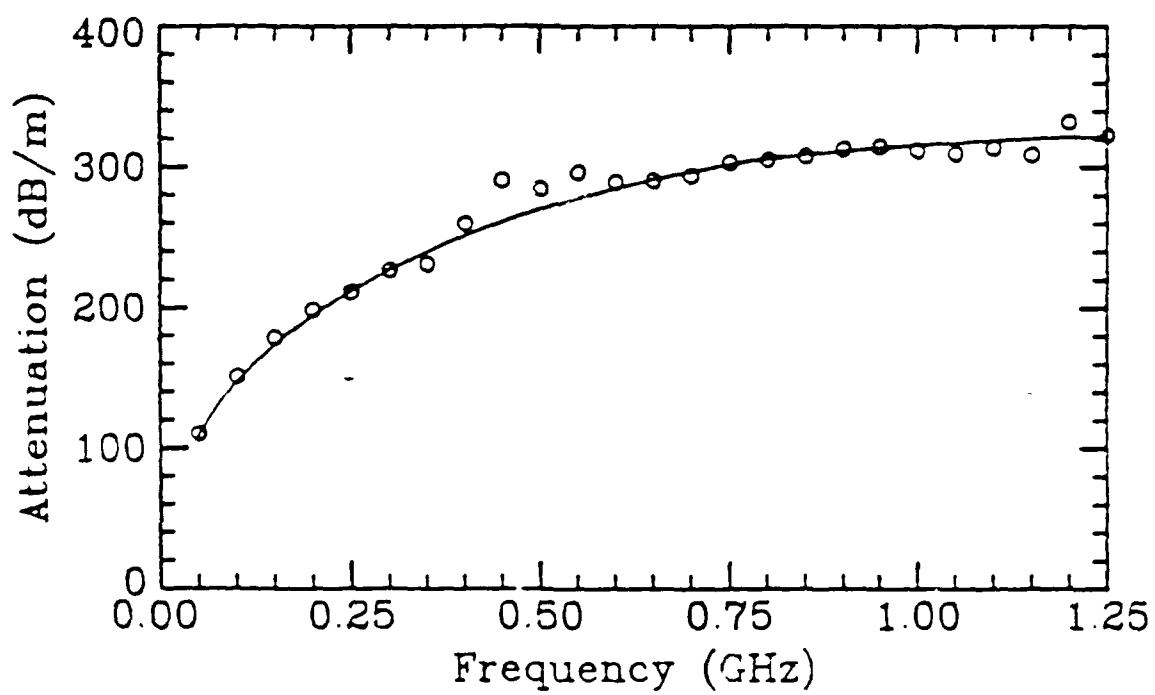
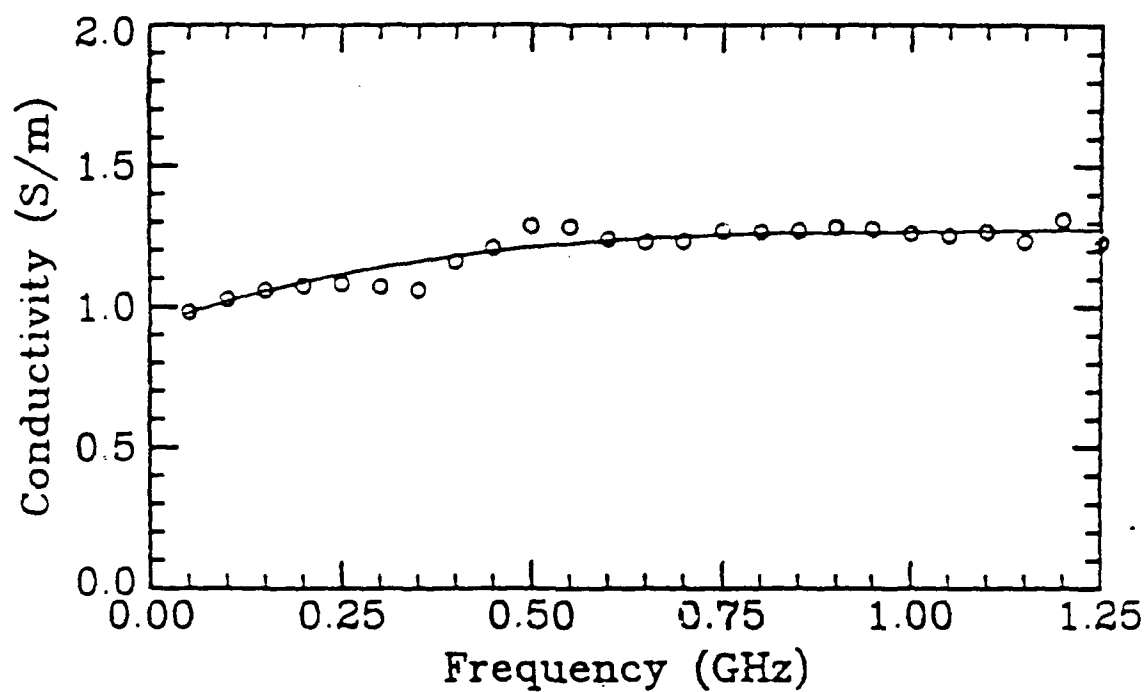
Sample 5



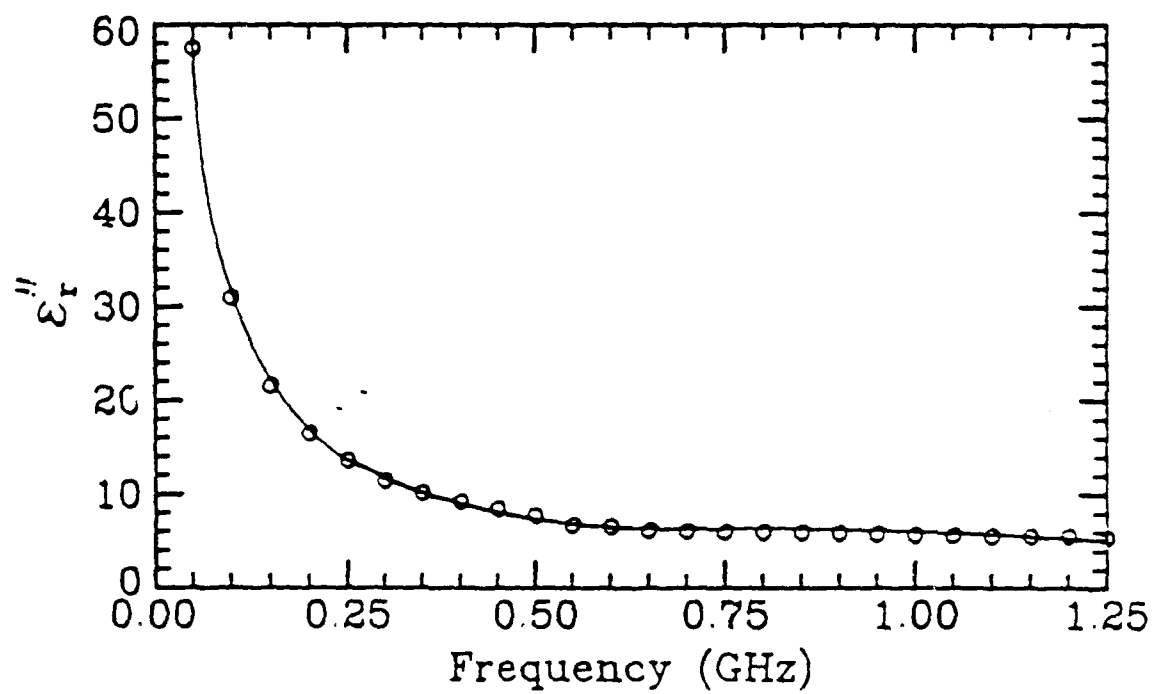
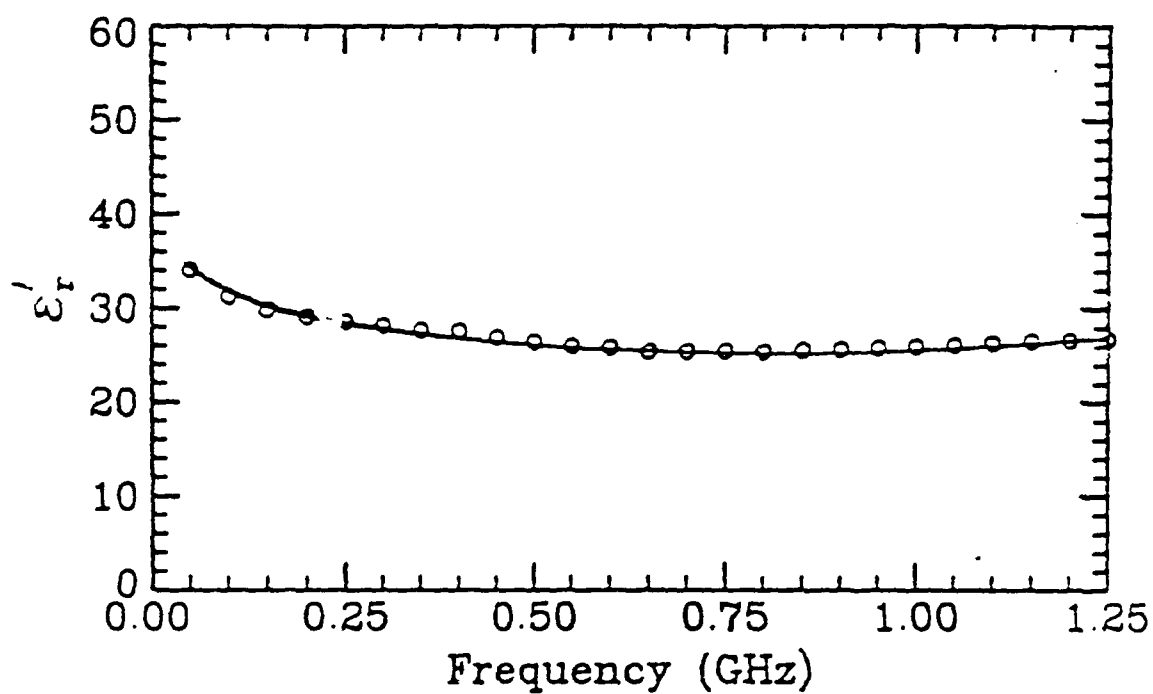
Sample 6



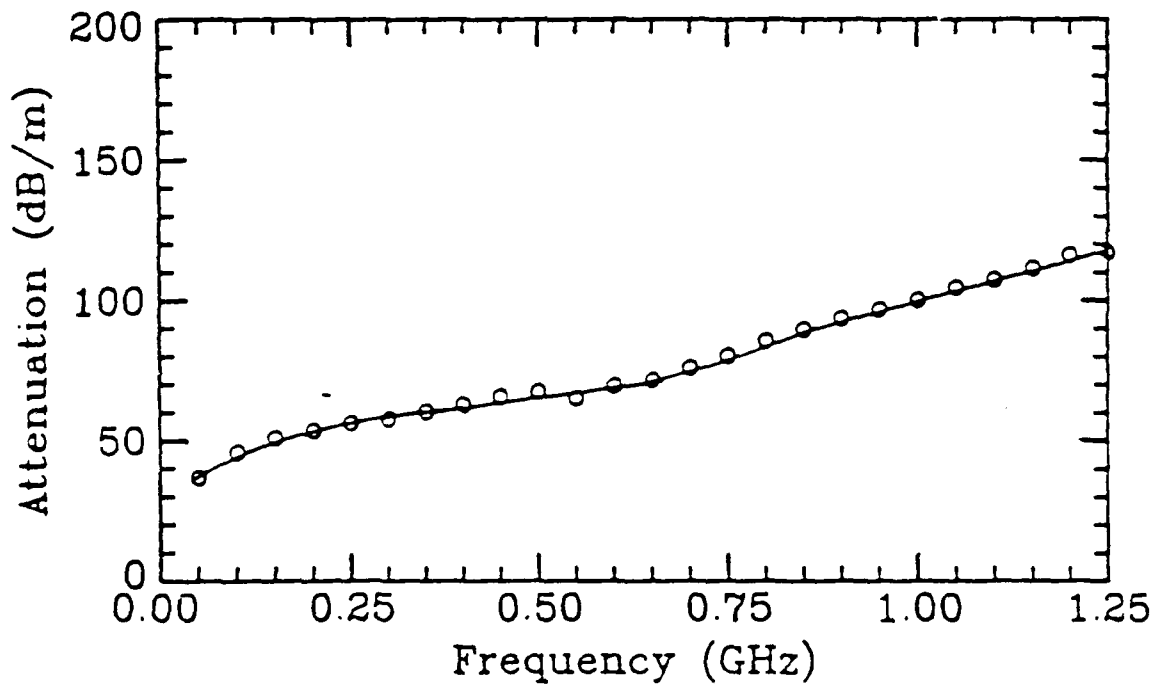
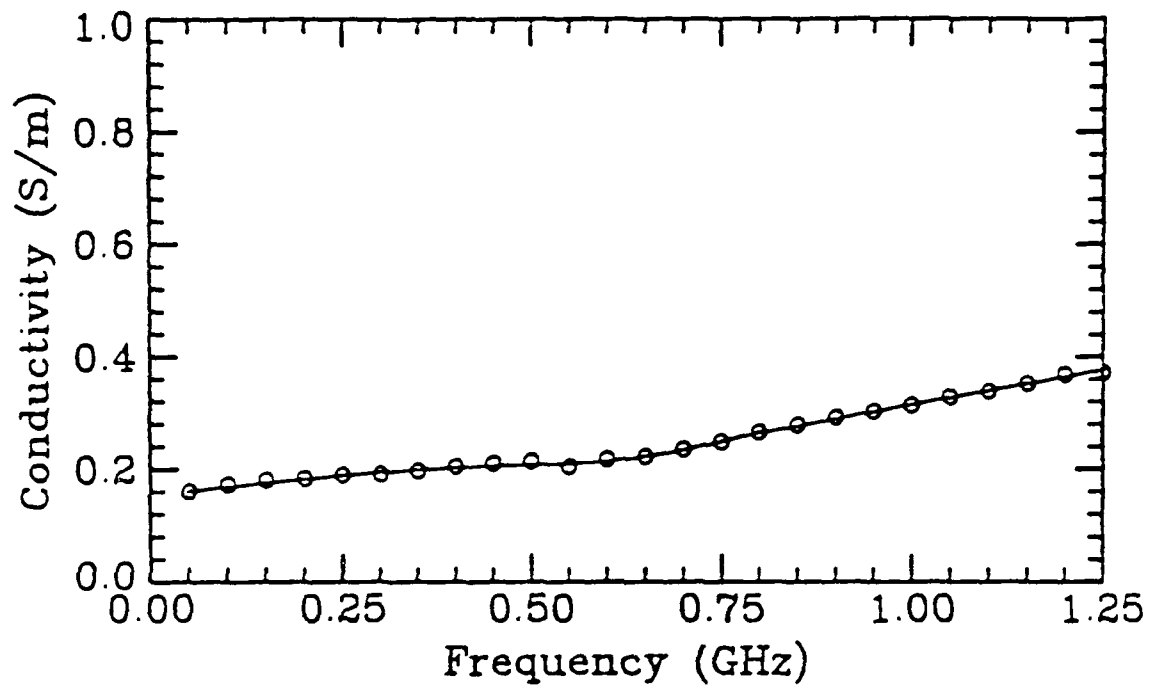
Sample 6



Sample 7



Sample 7



APPENDIX B

Measured Electromagnetic Properties of the Clay Shale and
Clay Schist Used in the Soil Model Pit

BICKERSTAFF CLAY MEASUREMENTS

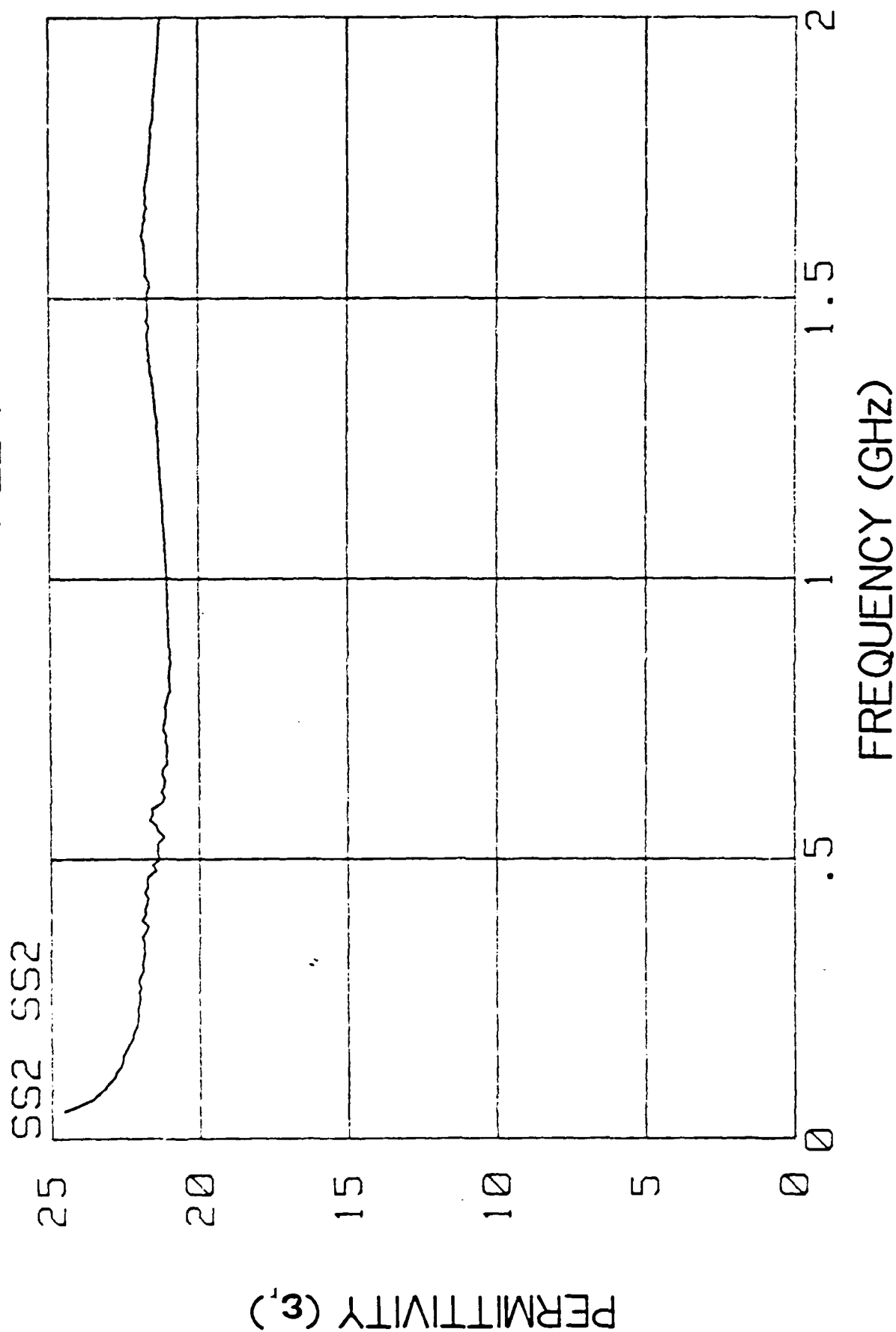
The electrical parameters of two types of clay obtained from the Bickerstaff Brick Co. were measured, and the results are recorded in the accompanying graphs. The parameters were measured over the frequency range of 0 - 2.0 GHz. The first two sets of clay samples were taken at Bickerstaff and included a sample of clay schist and a sample of clay shale.

The first two sets of samples had the following properties:

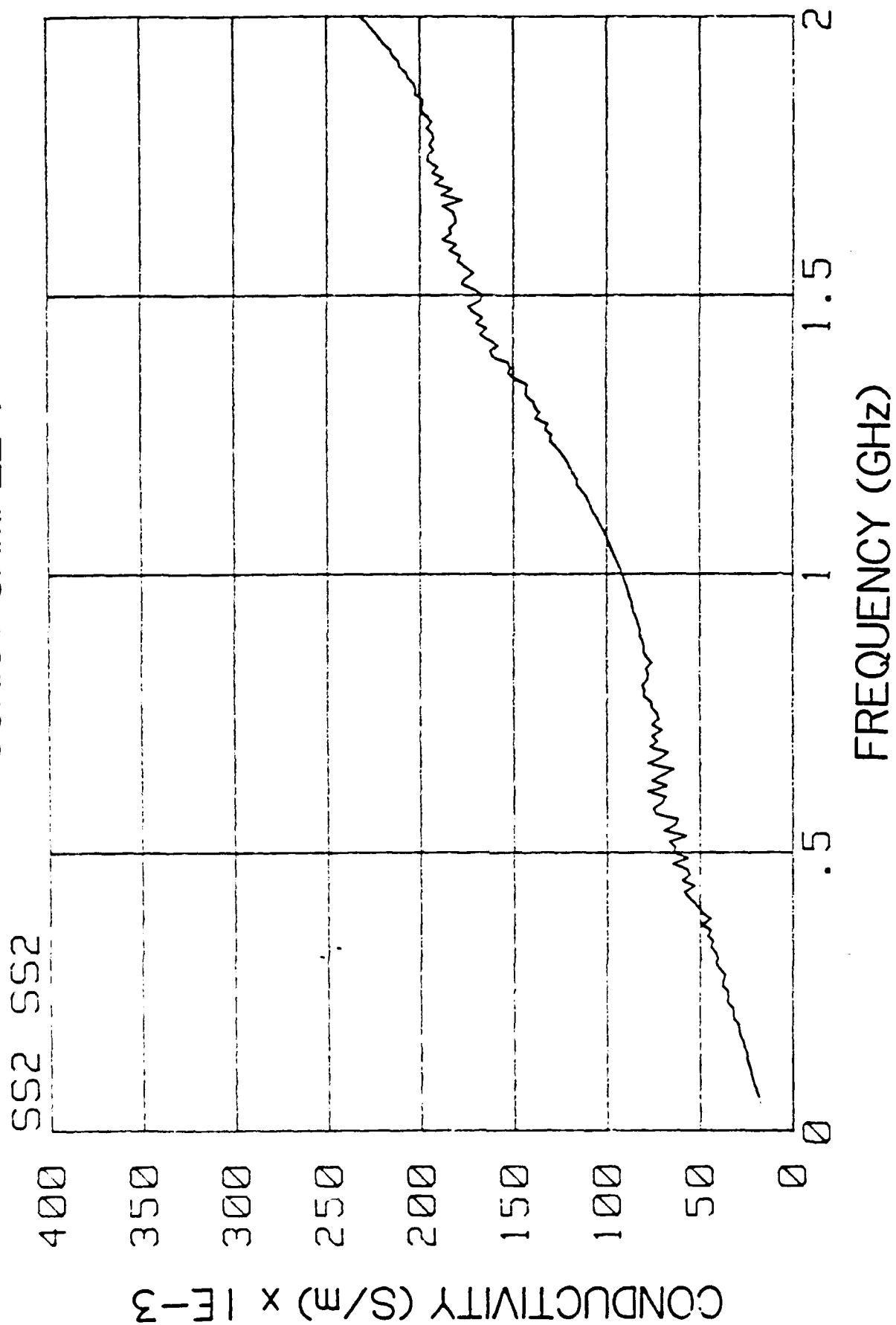
	<u>Density</u>	<u>Percent Water to Dry Weight</u>
Schist	1.88 gm/ml	21
Shale	1.92 gm/ml	14

Two additional sets of solid electric property measurements were made using a sample of schist from the test tank. The two sets of measurements were performed with different packing densities of the samples in the test cell. These measurement results appear beginning on pages B-9.

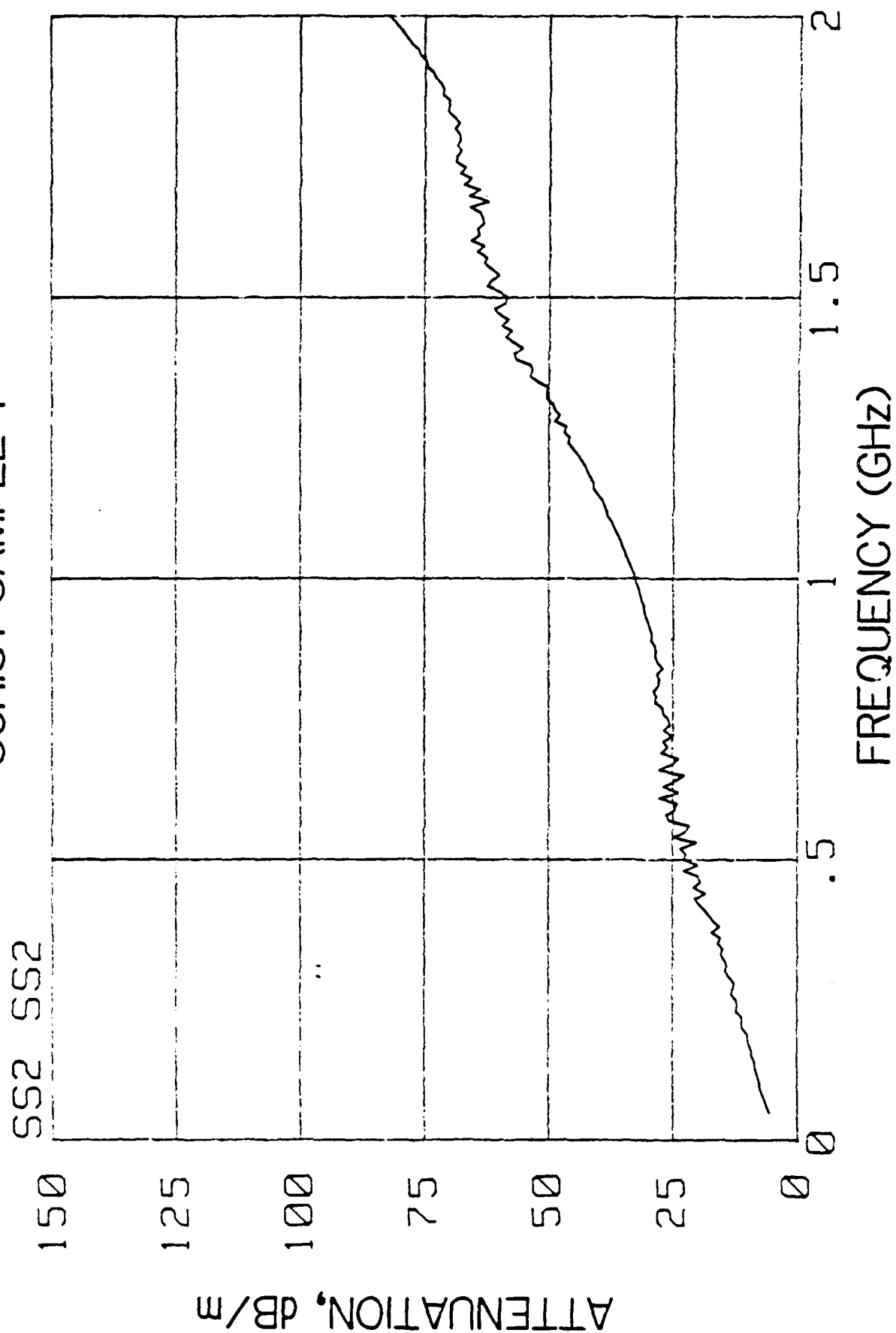
SCHIST SAMPLE I

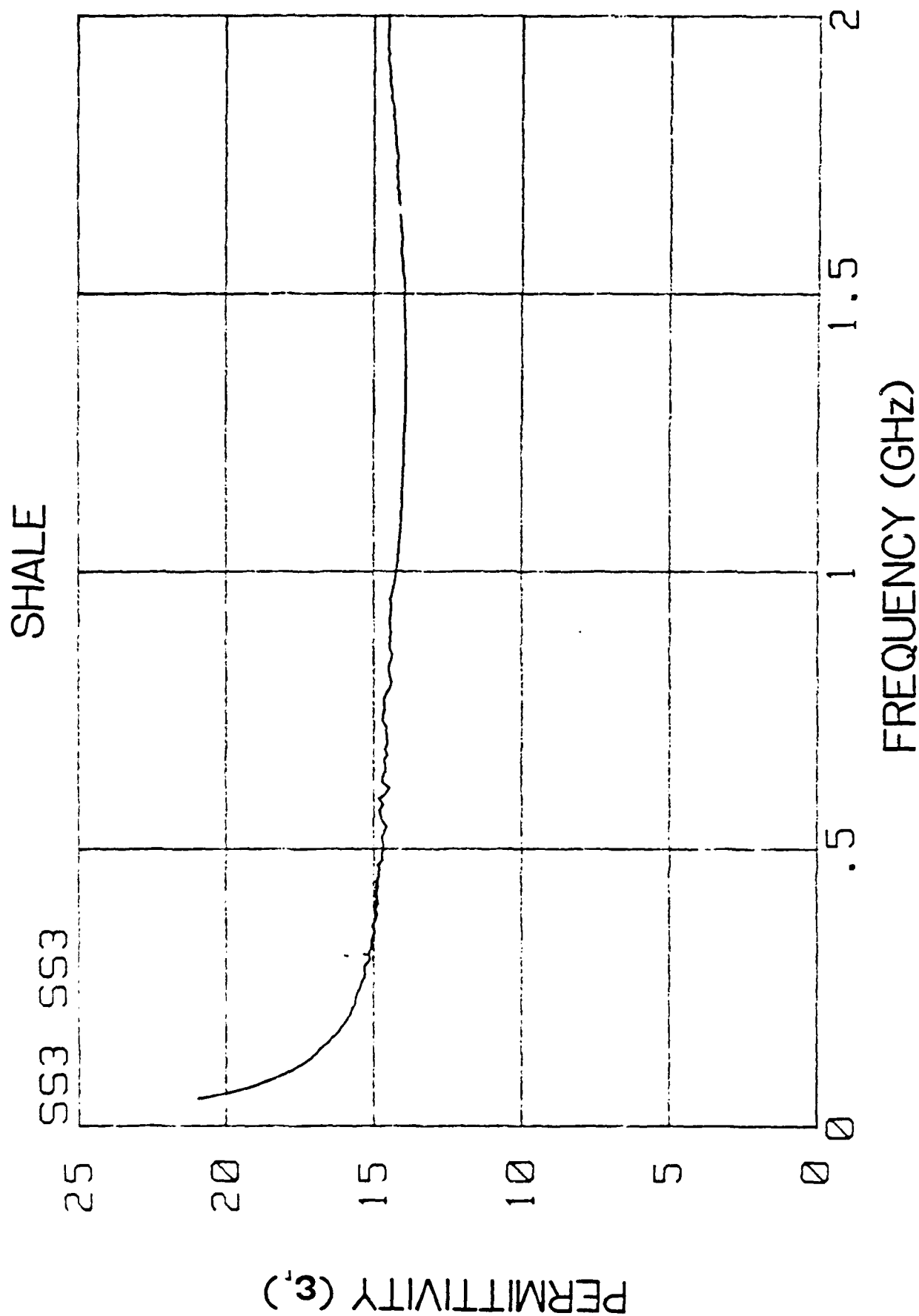


SCHIST SAMPLE I



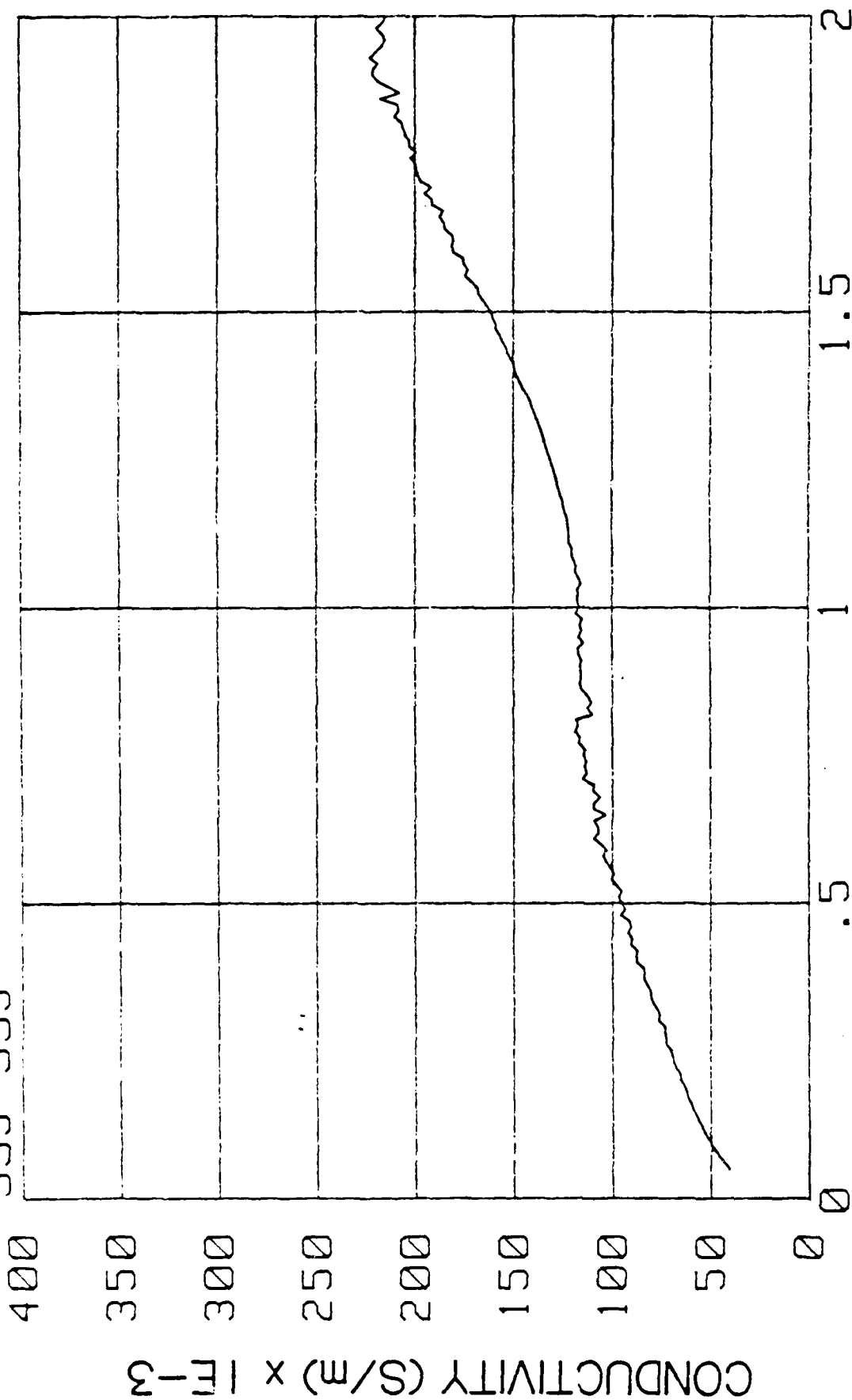
SCHIST SAMPLE 1





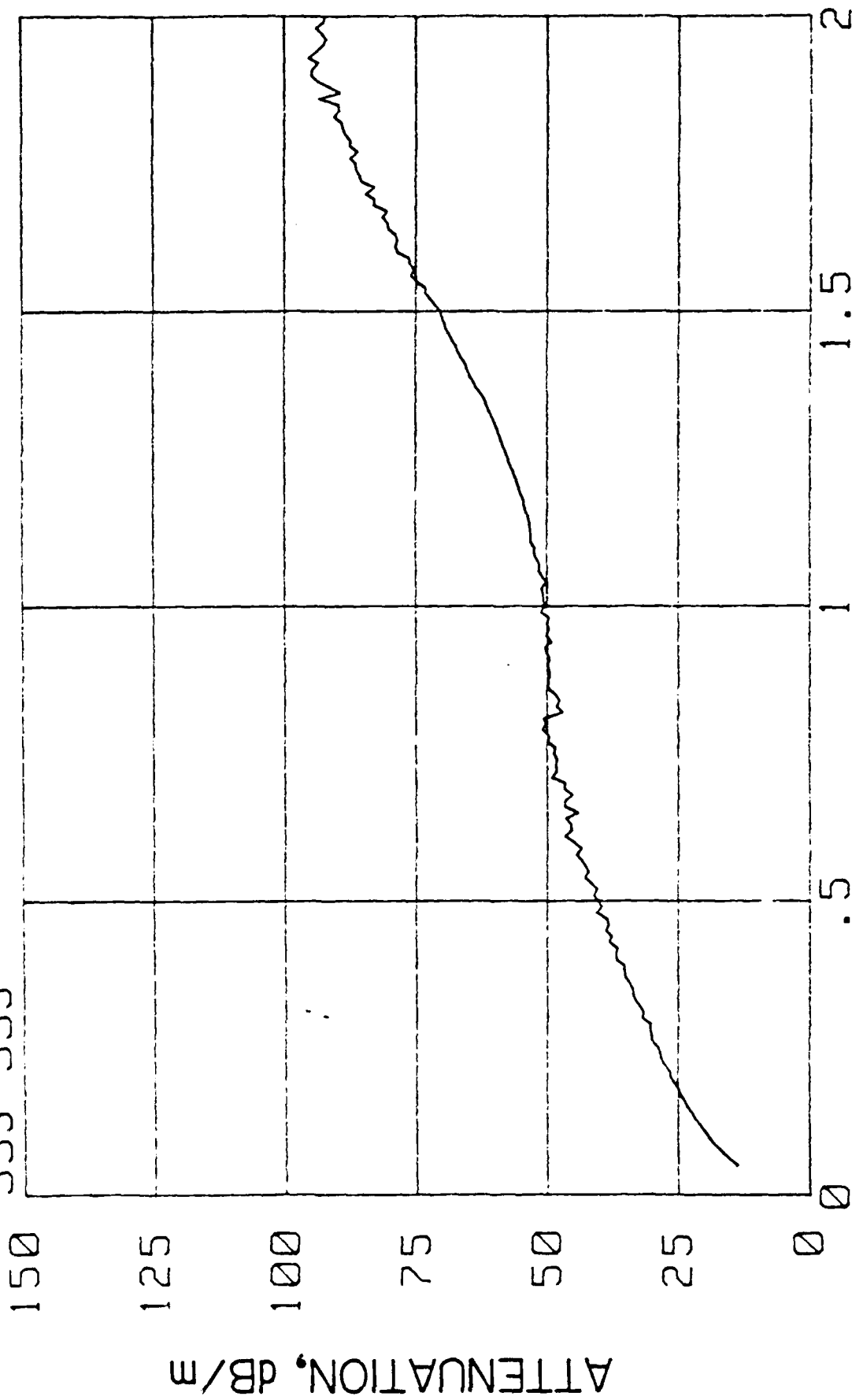
SHALE

SS3 SS3

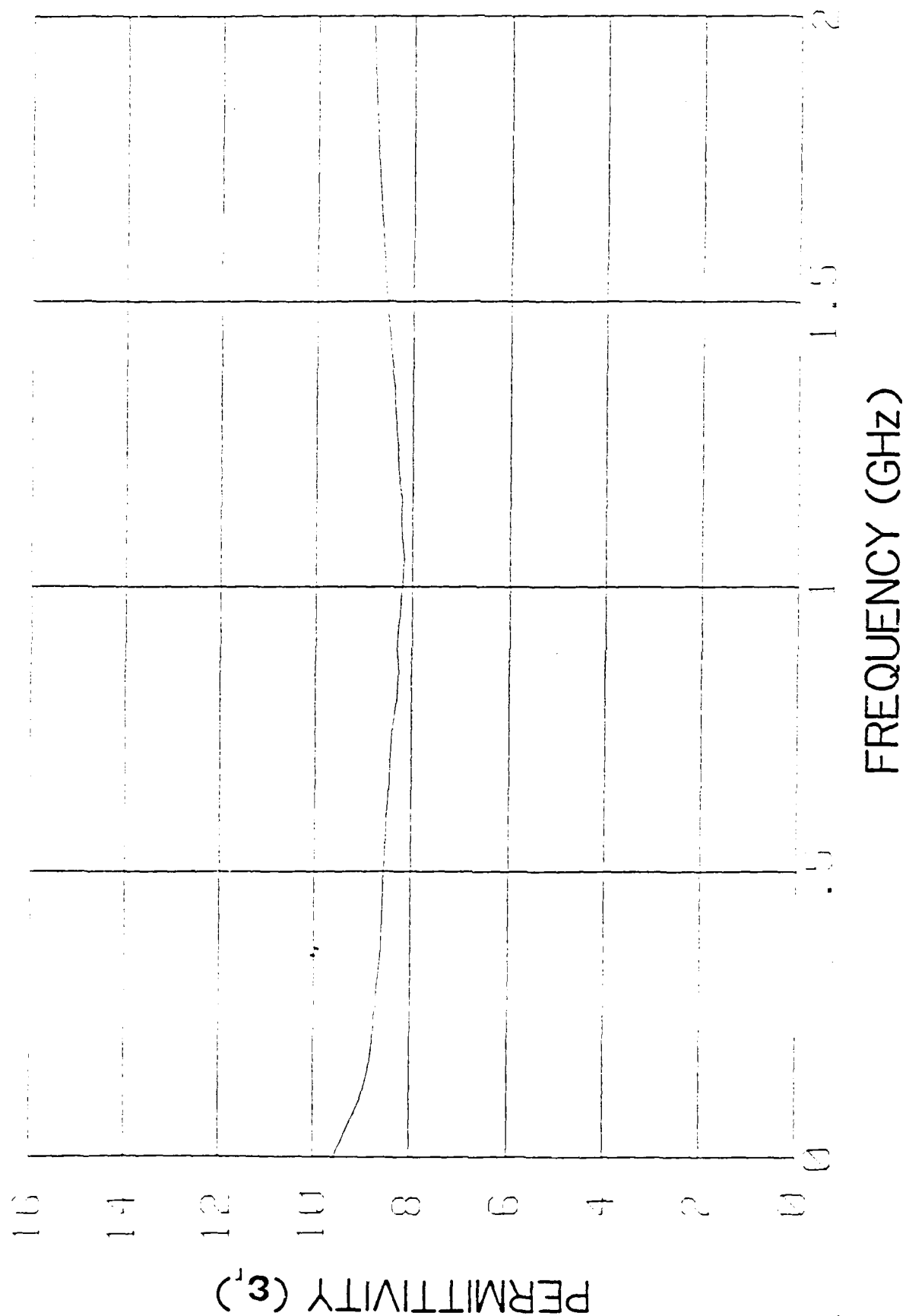


SHALE

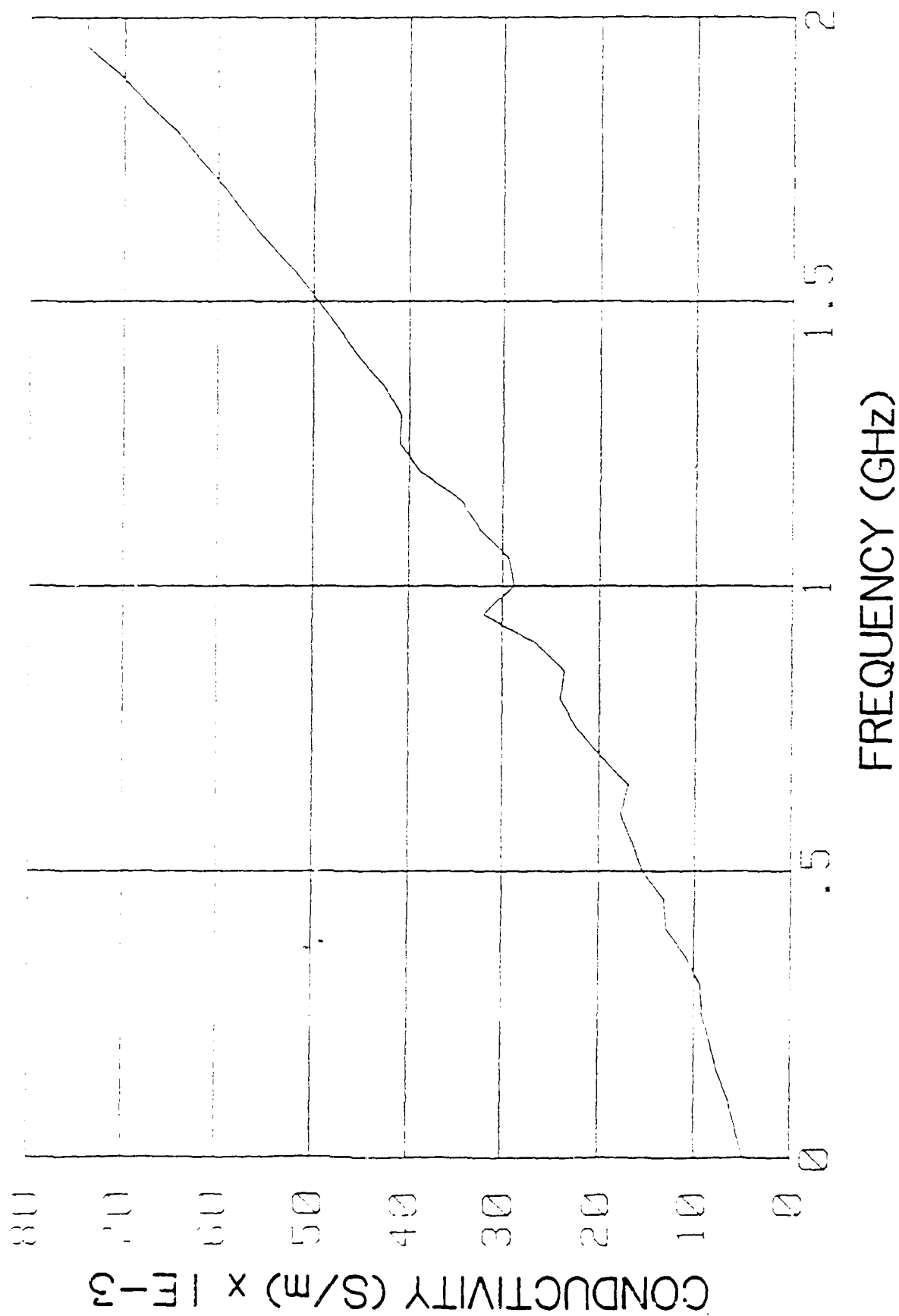
SS3 SS3



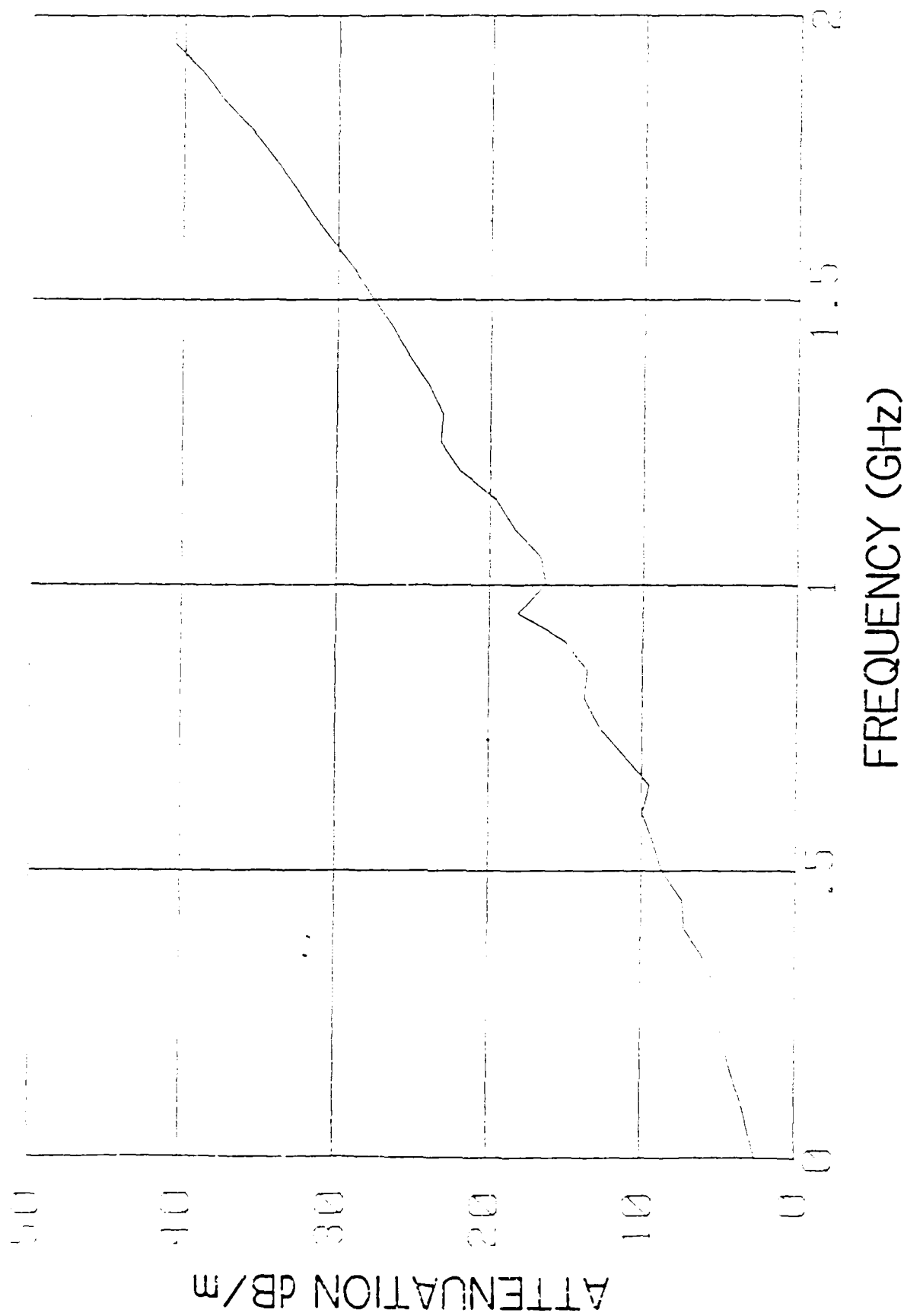
SCHIST SAMPLE 2 FIRM PACK



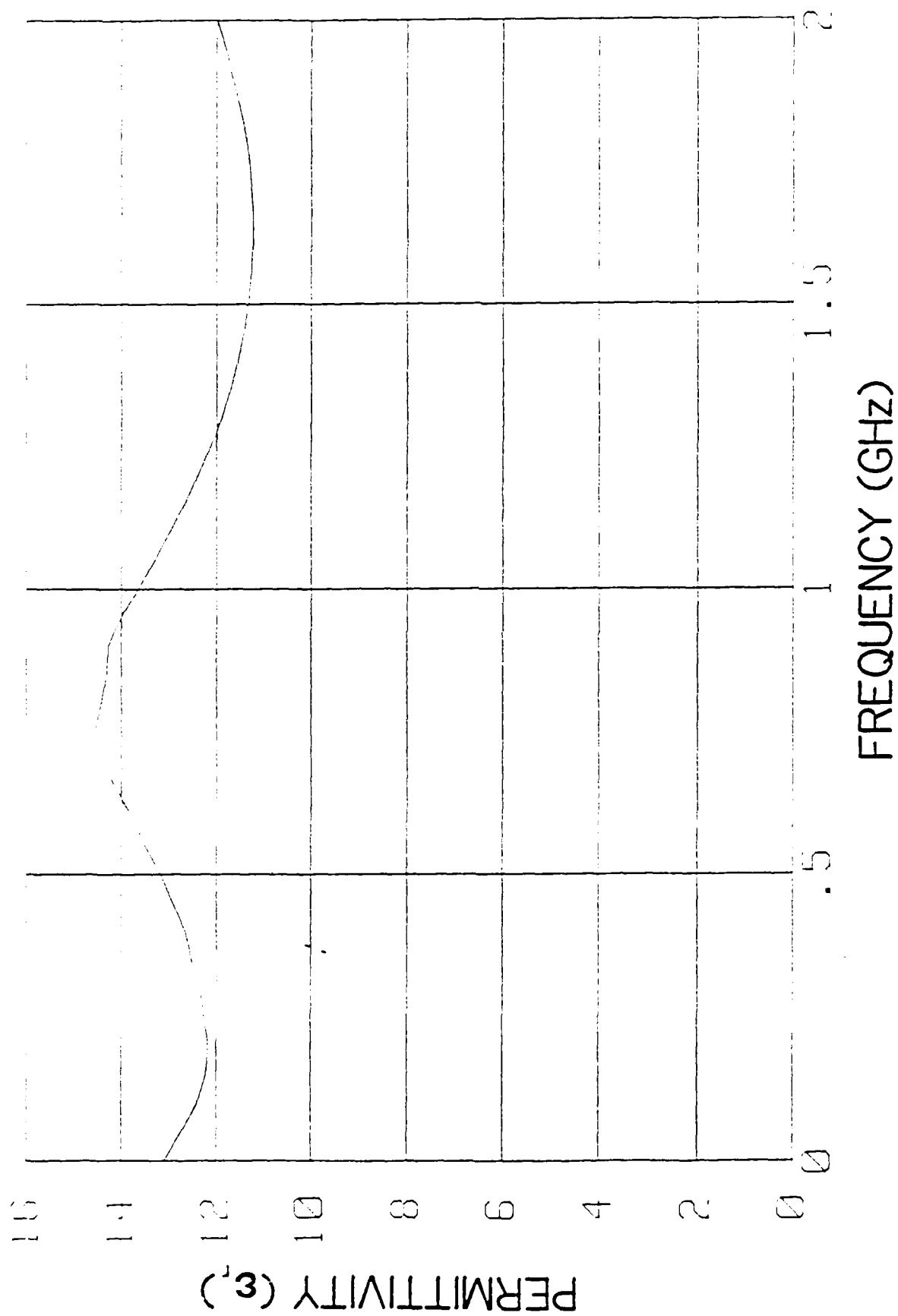
SCHIST SAMPLE 2 FIRM PACK



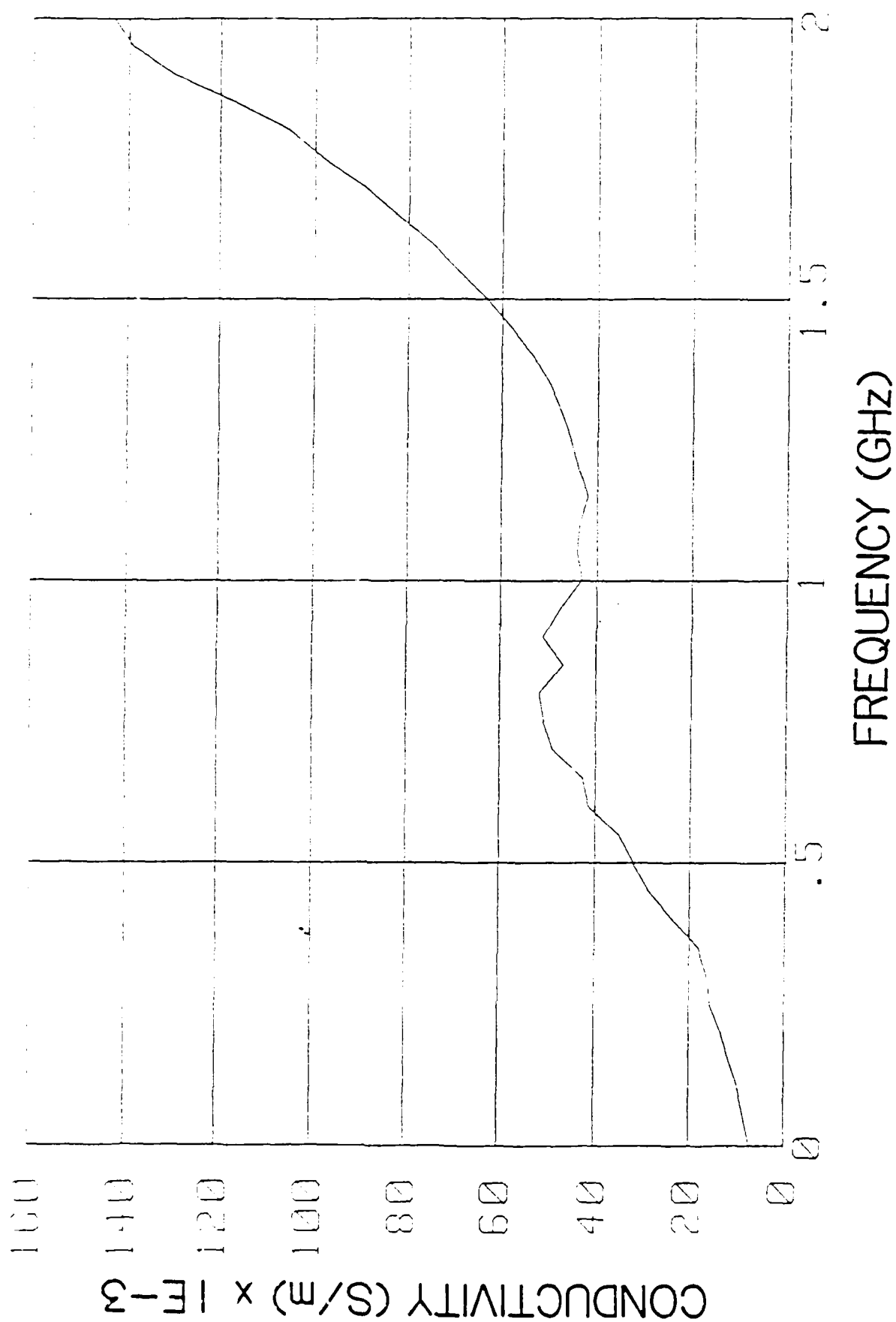
SCHIST SAMPLE 2 FIRM PACK



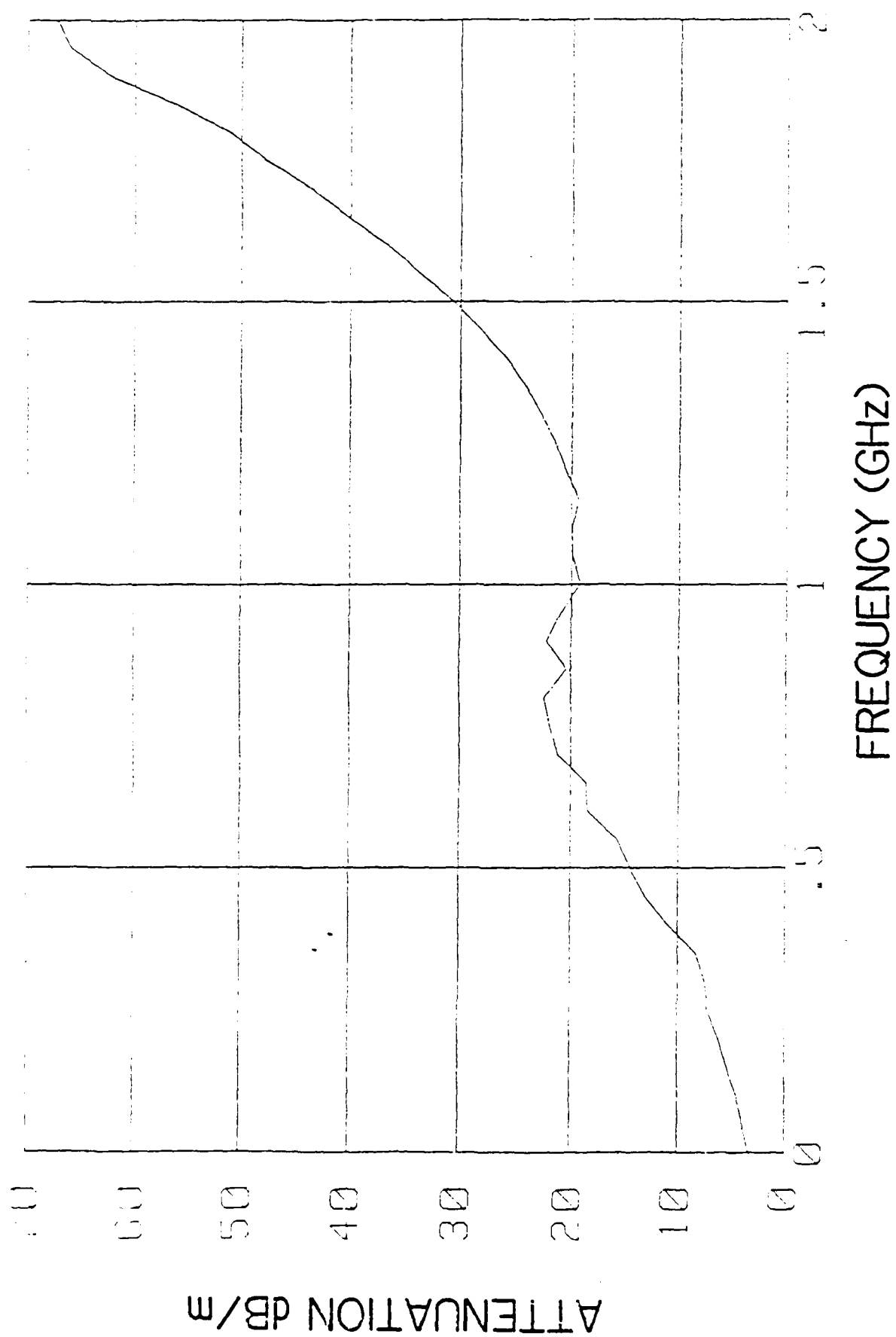
SCHIST SAMPLE 2 DENSE PACK



SCHIST SAMPLE 2 DENSE PACK



SCHIST SAMPLE 2 DENSE PACK



Copy available to DTIC does not
permit fully legible reproduction

Copy available to DTIC does not
permit fully legible reproduction

APPENDIX C

HP8510 Network Analyzer System Overview - Excerpt from the
HP8510 Manual

Copy available to DTIC does not
permit fully legible reproduction

INTRODUCTION

The HP 8510 network analyzer system is an advanced and sophisticated measuring instrument designed to make microwave measurements of many kinds. But the basic principles of its operation are fairly simple. The information in this part of the HP 8510 system manual is designed to help you get the most from your HP 8510 system by explaining some of the basic principles of its operation and the equipment that should be used with it. Actual measurements are described in the next section of this manual, as an Introductory Measurement Sequence.

In the present section, the HP 8510 network analyzer system is described and a typical measurement is explained in terms of a system block diagram. Digital microprocessing of the data, sources compatible with the HP 8510 system, and the HP 8510 system test sets are also described using block diagrams.

Extremely accurate and complex measurements are possible with the HP 8510 system, and for this reason accessories such as cables, attenuators, extension lines, adapters, and calibration and verification kits are unusually important. Accessories which should be used with the HP 8510 system are listed and discussed after the system, its sources, and its test sets, have been described.

Copy or use of this document does not
permit fully legible reproduction

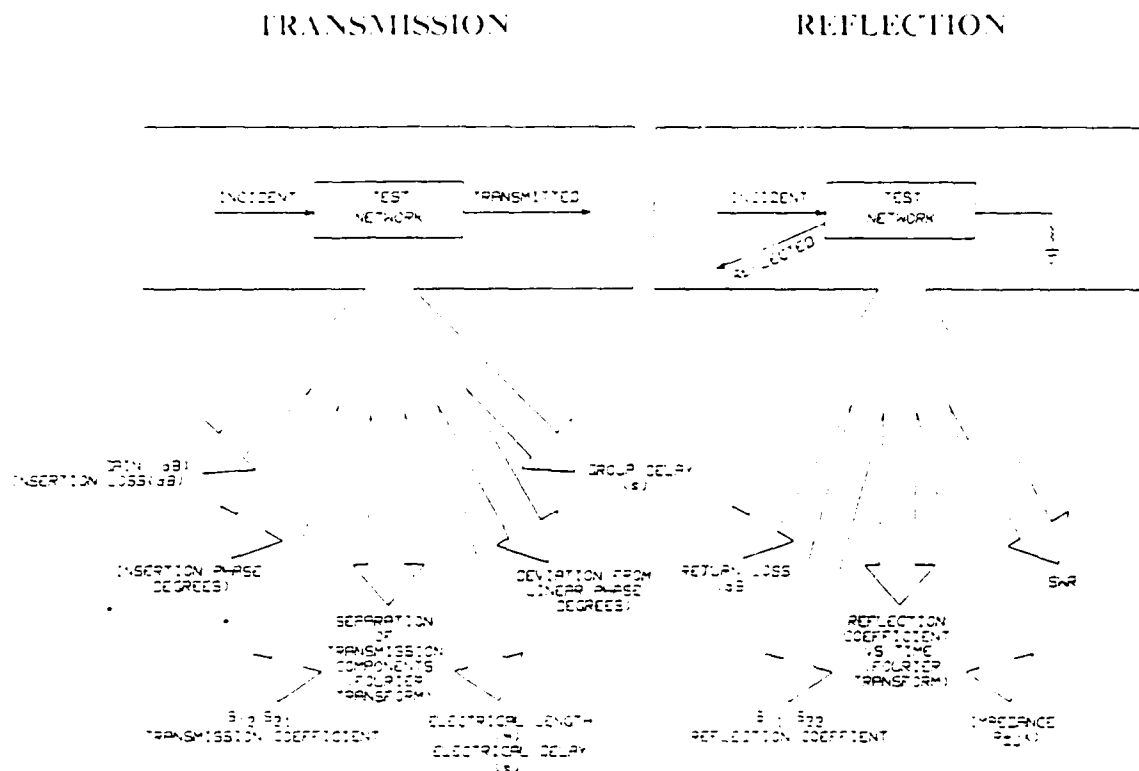


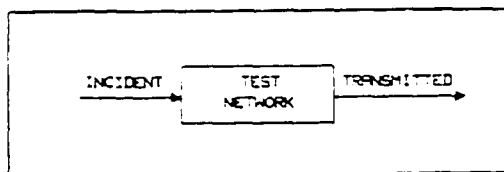
Figure 1. Transmission and Reflection Measurements

Copy available to DTIC does not permit fully legible reproduction

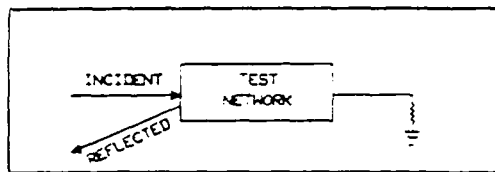
BASIC PRINCIPLES

Vector network analyzers such as the HP 8510 network analyzer system measure the magnitude and phase characteristics of linear networks such as filters, amplifiers, attenuators, and antennas. As with all network analyzers, two kinds of measurements are made: reflection measurements and transmission measurements. An incident signal generated by an RF source is compared with the signal transmitted through the device or reflected from its input.

TRANSMISSION



REFLECTION



Transmission measurements are made by comparing the transmitted signal to the incident signal. This results in measurement data on transmission characteristics of the network such as:

- Insertion Loss or Gain.
- Transmission Coefficient.
- Electrical Delay.
- from which Electrical Length can be obtained.
- Deviation from Linear Phase.
- Group Delay.

Reflection measurements are made by comparing the reflected signal to the incident signal. This results in measurement data on reflection characteristics of the device such as:

- Return Loss.
- Standing Wave Ratio (SWR).
- Reflection Coefficient.
- Impedance.

Mathematical analysis of transmission and reflection data on the swept response of the network also makes it possible to determine the position and magnitude of impedance changes with respect to a reference plane. This analysis, called time domain analysis, is done using Fourier Transform principles and is possible on HP 8510 network analyzer systems equipped with time domain Option 010.

HP 8510 NETWORK ANALYZER SYSTEM

The HP 8510 network analyzer system has four essential parts:

- a source,
- a test set,
- a signal detector and analog-to-digital converter, and
- a digital microprocessor and display.

The source provides the RF signal. The test set separates this signal into an incident signal sent to the device-under-test and a reference signal against which the transmitted and reflected signals are later compared. It also receives transmitted and reflected signals from the device-under-test. The signal detector and analog-to-digital converter takes all of these signals and converts them to digital information for high-speed processing. The digital microprocessor controls the system, analyzes the digitized signals, corrects errors, and displays the results in a variety of formats.

In the HP 8510 network analyzer system, these essential parts are individual HP instruments configured together make up the HP 8510 system:

- HP 834x-series synthesized sweeper,
- or
- HP 835x-series sweep oscillator with an appropriate
HP 835xx-series plug-in,
- HP 851x-series test set;
- HP 85102A IF detector;
- HP 85101A display processor.

Additional system components can include hardcopy output devices such as a printer and/or a plotter, and an HP series 200 computer serving as an external controller for programmed operation.

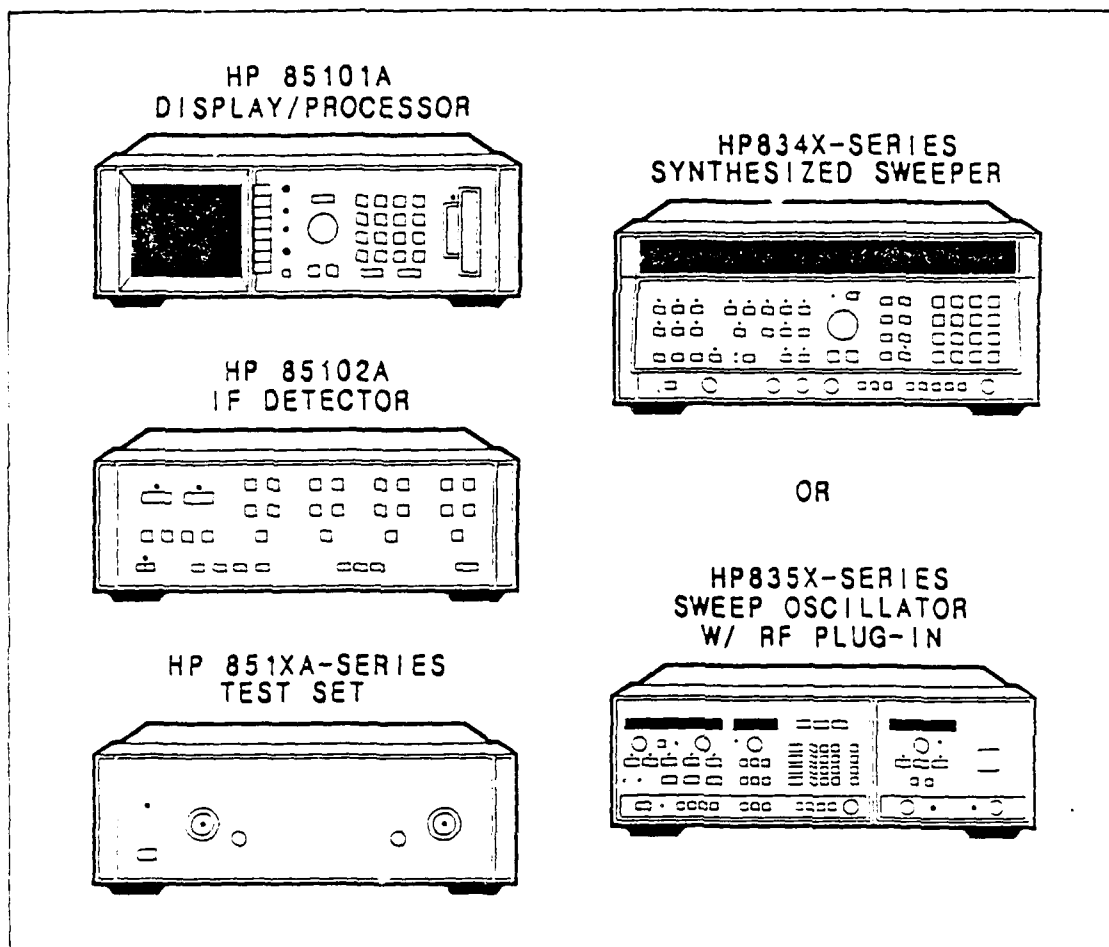


Figure 2 HP 8510 Network Analyzer System

SYSTEM BLOCK DIAGRAM

A simplified block diagram of the HP 8510 network analyzer system is shown in Figure 3.

As Figure 3 shows, the HP 8510 network analyzer is a high performance vector receiver with four inputs, two independent measurement channels, and an internal microcomputer to automate measurement and data processing operations. A special System Bus provides fast digital communication between the instruments that make up the system, allowing the network analyzer to make full use of the source and test set capabilities. This interface also provides direct data transfer to the hardcopy device for neat, permanent records of the measurement display.

During a typical measurement with the source operating in the ramp sweep mode, the source is swept from the lower to the higher measurement frequency in a linear ramp. Signal separation components in the test set apply a portion of the incident signal and the responses from the device under test to the first frequency conversion stage.

Digital communication between the receiver and the test set pretunes the 65 to 300 MHz voltage-tuned local oscillator (VTO) so that one of its harmonics mixes with the stimulus to produce a first IF frequency close to 20 MHz. Fine tuning is accomplished by comparing the IF frequency with the internal 20 MHz crystal reference and sweeping the local oscillator to track the stimulus frequency.

When the local oscillator reaches its upper frequency limit, the sweep is stopped, the local oscillator is retuned, phase lock is reestablished, and the sweep is continued. Since the first local oscillator frequency is selected algorithmically from the known stimulus frequency, the measurement is free from harmonic skip.

The second frequency conversion produces an IF frequency of 100 kHz for application to the detection and data processing elements of the receiver. Because the frequency conversions are phase coherent and the IF signal paths are carefully matched, magnitude and phase relationships between the input signals are maintained throughout the frequency conversion and detection steps. Automatic, fully calibrated autoranging IF gain steps maintain the IF signal at optimum levels for detection over a wide dynamic range.

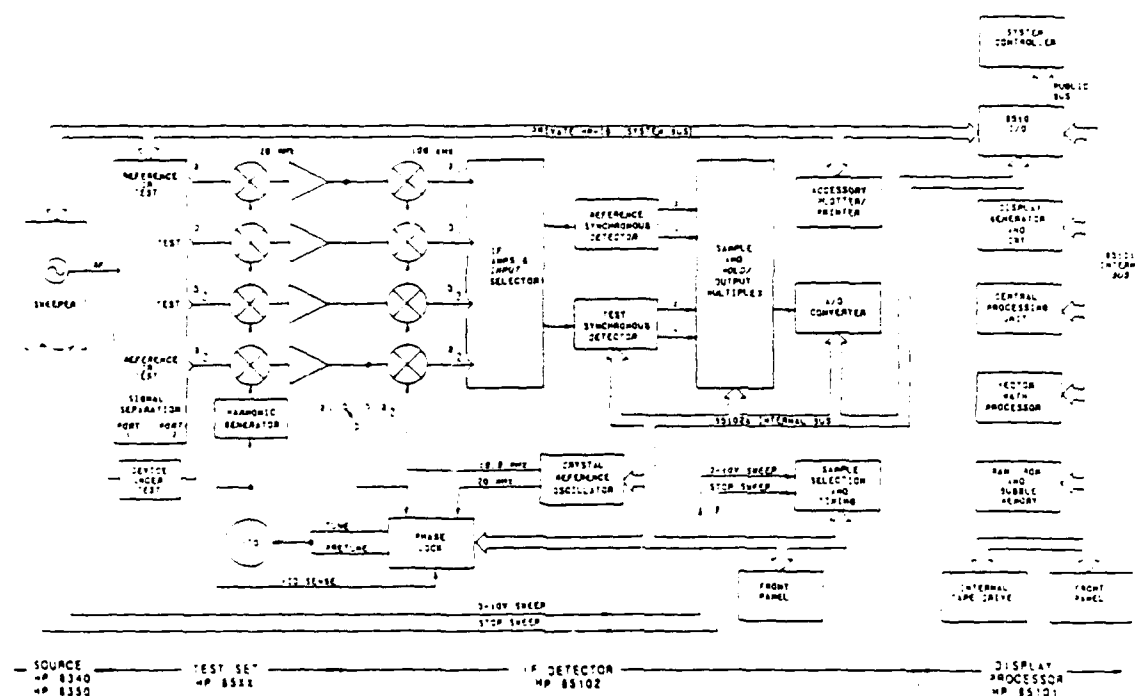


Figure 3. Simplified Block Diagram

The reference detector channel can use either input a_1 or a_2 as the reference signal. The test detector can use any of the inputs as the test signal. During the sweep, the selected inputs are sampled up to 401 times, with sample timing accomplished by sensing the 0 to 10 volt sweep output from the source. With 401 points selected, at each positive 0.025 volt change in the sweep voltage all selected inputs are sampled and applied to the reference and test synchronous detectors.

The synchronous detectors develop the real (X) and imaginary (Y) parts of the signal. The X,Y pairs are sequentially converted to digital values and read by the Central Processing Unit (CPU). Then digital techniques are used that practically eliminate drift, offsets, and circularity errors as sources of measurement uncertainty.

POST-DETECTION DIGITAL SIGNAL PROCESSING

Post-detection digital signal processing (Figure 4) proceeds under control of the CPU, a microprocessor equipped with 256 kBytes of RAM, 256 kBytes of magnetic bubble memory, and 26 kBytes of ROM.

The CPU takes advantage of multi-tasking software architecture and several distributed processors to provide a very fast display update rate. It accepts the digitized real and imaginary data and corrects gain and quadrature errors before the reference and test pairs are ratioed and stored in the raw data array. If averaging is on, the incoming data is averaged with the existing data as it is stored.

While the data acquisition software is continually filling the raw data array, the data processing software is processing the data for the two independent display channels.

If error correction is turned on, the raw data and error coefficients from the selected calibration coefficient set are used in appropriate computations by a dedicated vector math processor. Next, phase offsets commanded by the electrical delay and reference plane extension are added to the data. If a time domain presentation is selected, the corrected data is converted from the frequency domain to the time domain using the inverse Fourier Chirp Z transform technique and stored into the corrected data arrays.

The memory arrays are filled from the corrected data array under control of the user with trace data for use in vector computations with the current corrected data. If trace math is selected, vector multiplication, division, addition, or subtraction is performed. The resulting data are formatted according to the FORMAT selection, point-to-point smoothing is applied, if selected, and stored into the formatted data arrays. The traces are now scaled, and output to the display memory where the trace data is combined with various CRT annotation data. A dedicated display processor asynchronously converts the formatted data and annotations for display at a flicker-free rate on the vector-writing CRT.

When the operating system detects a front panel button push, it executes the command immediately (as when a parameter change is made), or it makes the selected function the active function and awaits input from the knob, numeric pad, or STEP keys (as when there is a scale/division change), or it presents a softkey menu. Selecting some functions aborts the data processing operation. For example, MEASUREMENT RESTART restarts all measurement related functions to the beginning of the data acquisition group (a group is that number of sweeps needed to make the measurement completely; how many sweeps are taken thus depends on the measurement); PRESET initializes the system to a pre-defined state.

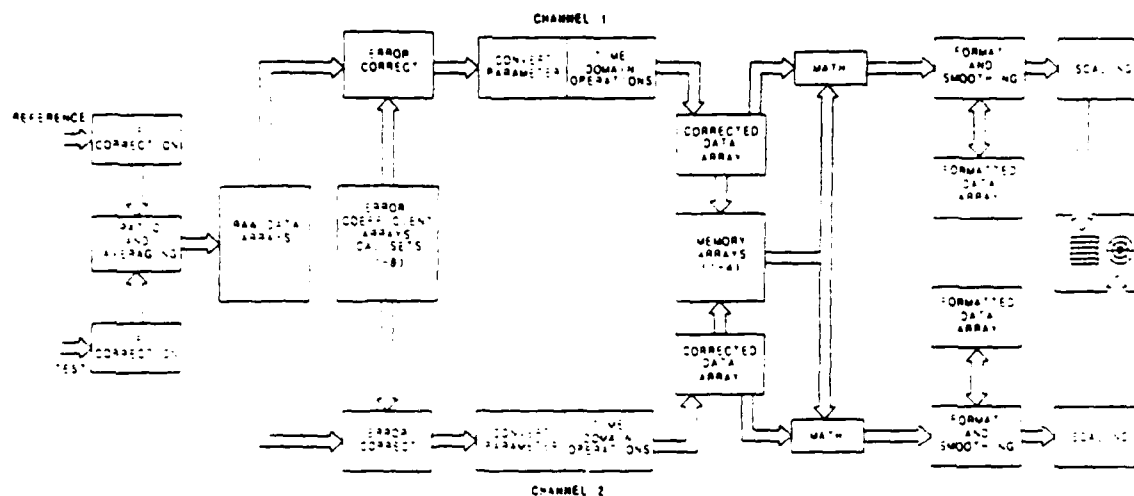


Figure 4. Post-Detection Digital Signal Processing

SOURCES

The RF source in an HP 8510 network analyzer system can be either an HP 834x-series synthesized sweeper or HP 835x-series sweep oscillator with an HP 835xx-series plug-in (Figures 5 and 6). These sources have the correct analog interface signals and full compatibility with the digital 8510 System Bus. If an HP 835x-series sweep oscillator is used, both the sweep oscillator and the plug-in may need to be retrofitted with certain later revisions of the firmware to be compatible with the HP 8510 system. Consult your Hewlett-Packard representative if you need more information on compatibility questions.

The 8510 system bus allows the network analyzer to act as the system controller by managing the source using standard HP-IB protocol. Capabilities added by the system bus include alternate sweep, in which a different frequency range may be selected for each measurement channel, and control of necessary source functions using the HP 8510 front panel controls.

Both types of sources can operate in the Ramp Sweep mode, in which the network analyzer directs the source to sweep in a linear ramp over the selected frequency range. HP 834x-series instruments provide better performance in this Ramp Sweep mode than do HP 835x-series instruments, because of the "Lock-and-Roll" tuning technique used in the HP 834x series. In this "Lock and Roll" technique, the first frequency of the sweep is set with synthesizer accuracy and a linear analog sweep proceeds to the stop frequency. For sweep widths less than 5 MHz, fully locked synthesizer performance is obtained over the complete sweep. Instruments in the HP 835x series are open-loop YIG-tuned sources.

The HP 8340-A can also operate in the Step Sweep mode. In this mode, synthesizer-class frequency accuracy and repeatability is obtained by phase-locking the source at each of the up to 401 frequency steps over the selected frequency range. This mode provides the highest accuracy although at a reduced measurement speed.

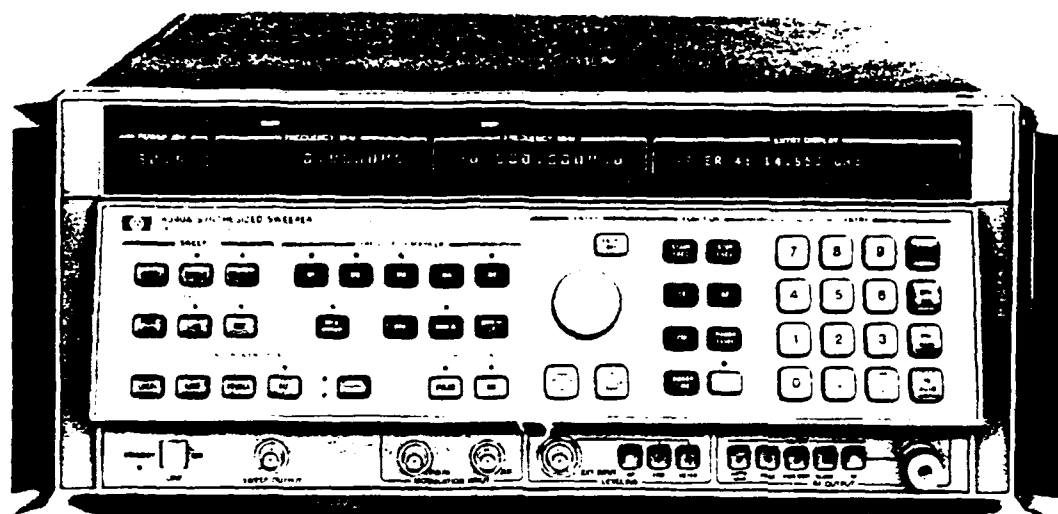


Figure 5. HP 834x-Series Synthesized Sweeper

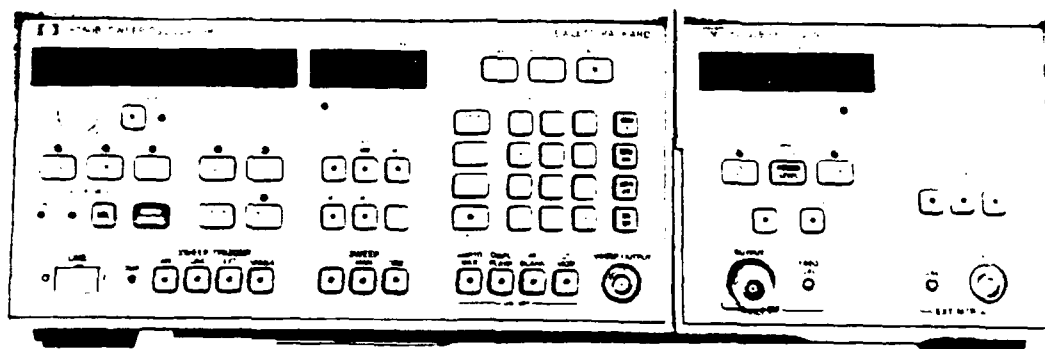


Figure 6. HP 835x-Series Sweep Oscillator with
HP 835xx Plug-In

TEST SETS

The HP 851x-series test sets in the HP 8510 network analyzer system have three main functions. They provide:

- the input output ports to connect the device-under-test;
- signal separation to separate the reference and test signals;
- and RF to 20 MHz conversion.

(The HP 8511A frequency converter differs slightly in that it does not have signal separation devices, thus allowing custom configurations.) The frequency converter is fully integrated into the signal separation path to provide optimum performance. Taking the test-to-reference-signal ratio in S-parameter test sets after electronic switching eliminates signal path selection repeatability errors. Parameter selection is controlled from the network analyzer front panel.

Table 1. HP 851x-Series Test Sets

Test Set Model Number, Type	Test/ Input Port Connector	Frequency Range
HP 8511A Frequency Converter	3.5mm (f)	0.045 - 26.5 GHz
HP 8512A Reflection/ Transmission	7mm	0.500 - 18.0 GHz
HP 8513A Reflection/ Transmission	3.5mm (m)	0.045 - 26.5 GHz
HP 8514A S-Parameter	7mm	0.500 - 18.0 GHz
HP 8515A S-Parameter	3.5mm (m)	0.045 - 26.5 GHz

NOTE - HP 8512 and HP 8514 test sets are usable to 0.045 GHz, although with degraded performance specifications.

Reflection/Transmission Test Sets. The HP 8512A and HP 8513A reflection/transmission test sets (Figure 7) provide automatic selection of S_{11} or S_{21} . Fully error-corrected measurements for one-port devices can be made using the 1-Port calibration procedure. The comprehensive One-Path 2-Port calibration procedure provides full error correction for two-port devices if the device-under-test is manually reversed. The HP 8512A test set must use a 20 dB attenuator at the device end of the transmission return cable; the HP 8513A test set must use a 10 dB attenuator at the device end of the transmission return cable.

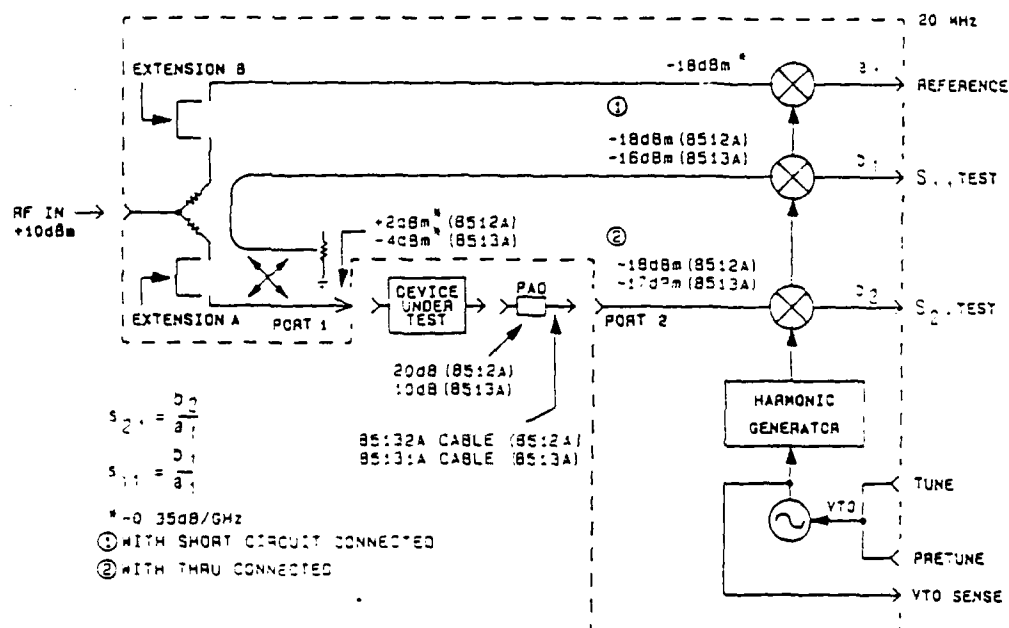


Figure 7. Reflection/Transmission Test Sets Signal Flow

S-Parameter Test Sets. The HP 8514A and HP 8515A S-parameter test sets (Figure 8) provide automatic selection of S_{11} , S_{21} , S_{12} , and S_{22} . The stimulus is automatically switched for forward and reverse measurements, allowing fully error corrected measurements for one-port devices and for two-port devices without the need manually to reverse the device-under-test. Bias input and sense connections are provided to allow testing active devices. Internal 0 to 90 dB, 10 dB step attenuators are provided to control the incident stimulus level at the device-under-test input, without causing a change in the reference signal level.

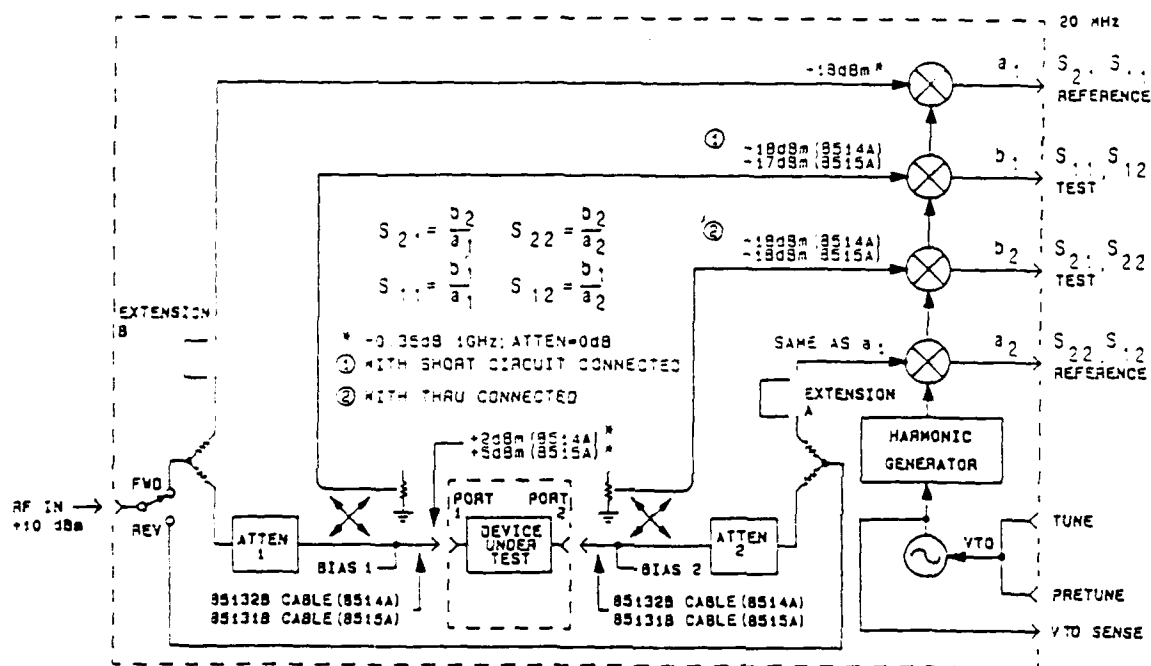


Figure 8. S-Parameter Test Sets Signal Flow

Custom Test Sets. To configure signal separation of your own design, use the HP 8511A Frequency converter (Figure 9). If your test setup does not follow the conventions of the reflection transmission or S-parameter test set, use the REDEFINE PARAMETER sequence of the HP 8510 system to select appropriate reference and test inputs to be used for the measurement.

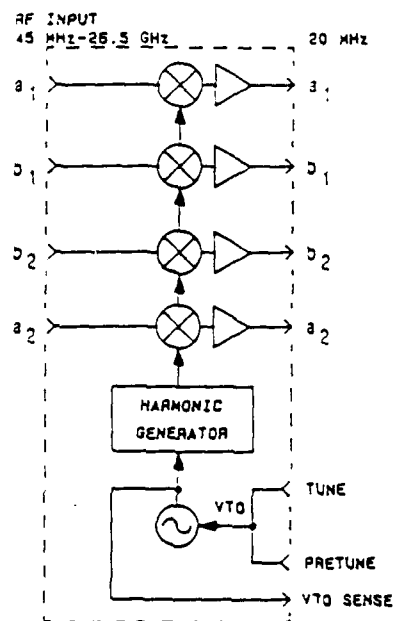


Figure 9 HP 8511A Frequency Converter

TEST PORT RETURN CABLES, ATTENUATORS

High quality cables, attenuators, adapters, and other accessories are essential if one is to achieve accurate, repeatable measurements. Worn or unstable cables and connectors will increase measurement errors due to directivity, mismatch, and frequency response effects. Check cables and connectors regularly and replace them whenever necessary.

Test port return cables used with an HP 8510 network analyzer system must be durable and stable, and care is required to avoid damaging them. Cables can be destroyed by excessive (less than 5-inch radius) bends. Even with careful use, cables do wear out eventually, and for this reason all cables should be treated as consumable items to be replaced as often as necessary. The most important characteristic of all cables is minimum magnitude and phase change between movements (flexures) of the cable. Replace a cable when large magnitude and/or phase changes occur when the cable is moved.

The cables recommended below, in good condition, must be used for detailed performance verification of the HP 8510 system. These cable sets have low insertion loss, good electrical match, and high return loss, and they are stable in use. For other applications, any high quality cable set can be used.

Recommended cables and (when required) 20 or 10 dB attenuators for the test set configurations that can be used in an HP 8510 network analyzer system are:

Table 2. Recommended Cables and Attenuators

Test Set Model Number	Test Port Connector	Return Cables, Attenuators
HP 8512A	7 mm	HP 85132A, 8492A-020
HP 8513A	3.5 mm (m)	HP 85131A, 8493C-010
HP 8514A	7 mm	HP 85132B (2 in set)
HP 8515A	3.5 mm (m)	HP 85131B (2 in set)

EXTENSION LINES

External reference-signal-path extension lines on the test set rear panels are used to balance the reference and test signal path lengths according to the port 1 and port 2 connections to the test device. These extension lines (and the signal paths they apply to) depend on the test set and are as follows. The standard lengths described in the next several paragraphs balance the cable configurations already listed in Table 2.

TEST SET	LABEL	SIGNAL PATH
Reflection-Transmission Test Sets		
HP 8512A	EXTENSION A	b_1, b_2
	EXTENSION B	a_1
HP 8513A	EXTENSION A	a_1
	EXTENSION B	b_1, b_2
S-Parameter Test Sets		
HP 8514A	EXTENSION A	a_1
	EXTENSION B	a_2
HP 8515A	EXTENSION A	a_1
	EXTENSION B	a_2

Reflection/Transmission Test Sets: HP 8512A, HP 8513A. When using a standard test setup (HP 85132A or HP 85131A cable and attenuator) with a device-under-test connected directly to Port 1, use the short extensions, HP part number 08512-20019. On these test sets, one of the lines is in the test signal path, and this fact makes it possible to add bias tees, step or fixed attenuators, amplifiers, isolators, or other devices.

S-Parameter Test Sets: HP 8514A, HP 8515A. When using a standard test setup with the device-under-test connected at the ends of the HP 85131B or HP 85132B test port return cables, use the long extensions, HP part number 08414-20013. When connecting the device-under-test directly at Port 1 and using a single HP 85131A or HP 85132A cable, use the short extension lines, HP part number 08512-20019. - -

Extension Lines may be changed to other lengths of high quality cable (low insertion loss, high return loss, stable in use) in order to balance electrical lengths in other configurations. Signal path balance is less important when using the HP 8340 synthesized sweeper, particularly in the Step sweep mode.

ADAPTERS

If adapters must be used to connect the devices under test, use only high-quality adapters such as those supplied in the HP 85052A (3.5mm) and the HP 85054A (Type-N) calibration kits. Keep the mating surfaces clean, inspect all connectors visually before every use, and use connector gages to verify that the mating tolerances are within specifications. Always use a torque wrench, set to the correct torque, when tightening or removing connections.

Test sets which have 3.5mm connectors on the test ports (e.g. HP 8513A, HP 8515A) can be used with test port return cables which have 7mm connectors by using the adapters in the HP 85130A special 3.5mm-to-7mm adapter set. These adapters provide a rugged interface for attaching the 7mm test port return cables.

For best results, these HP 85130A adapters (not the adapters in the HP 85052A 3.5mm calibration kit) should be used if 7mm calibration or verification devices are used for calibration or performance verification of a 3.5mm test set (e.g. HP 8513A or HP 8515A). The adapters in the calibration kit are suitable only in the opposite case, when 3.5mm devices are used with a 7mm test set.

**Copy available to DTIC does not
permit fully legible reproduction**

CALIBRATION KITS

Use only the highest quality calibration standards: devices which have a known response and are stable in use. Only if the calibration devices used have an accuracy equal to or greater than those in the HP 85050A (7mm) and HP 85052A (3.5mm) calibration kits will they provide the calibration and error correction accuracy needed to achieve full, specified measurement accuracy with the HP 8510 network analyzer system.

Also be aware that calibration standards, like all devices, can become worn and unstable with use. When a calibration device is no longer stable and repeatable, or shows signs of connector damage or wear, it must be replaced. Detailed handling and storage instructions appear in the calibration kit operating and service manuals.

Characteristics for the standards in the HP 85050A (7mm), HP 85052A (3.5mm) and HP 85054A (Type-N) calibration kits are loaded from the tape cartridge supplied with the calibration kits. Characteristics can also be defined by the user. Each calibration kit is supplied with a data cartridge on which is stored the nominal characteristics for each of the calibration devices in the kit.

The HP 85050A 7mm calibration kit consists of open and short circuit terminations, fixed and sliding loads, a 7mm connector gage, gage calibration block and aligning pin, extra precision 6-slot center collets, a center collet extractor, a 7mm connector torque wrench, and the device data cartridge. Option 010 adds a 30 cm beadless airline, which is used for time domain applications.

The HP 85052A 3.5mm calibration kit consists of male and female open and short circuit terminations, fixed and sliding loads, 7mm-to-3.5mm adapters, matched 3.5mm-to-3.5mm adapters, a 3.5mm connector torque wrench, 3.5mm connector gages and gage calibration block, and the device data cartridge. Option 010 adds a 15cm beadless airline, which is used for time domain applications.

The HP 85054A Type-N Calibration Kit consists of male and female Type-N open and short circuit terminations, fixed and sliding loads, 7mm-to-Type-N adapters, and the device data cartridge.

When other calibration kits are used, nominal characteristics of the standards can be defined by the user from the front panel of the HP 8510, using the MODIFY CAL KIT sequence described in Measurement Calibration part of this manual. After the calibration kit standards are defined, the data can be recorded on tape then loaded from tape whenever required.

VERIFICATION KITS

Performance verification standards are used to determine that the system can be calibrated and produce good measurement results. Devices in the verification kits are precision devices which should be treated with care and used only in specific situations, not on a day-to-day basis. These devices have been characterized on a standards-class network analyzer by experienced factory personnel. If you use proper calibration and measurement techniques, your measurement results should be comparable to the data supplied with the devices, within the system specifications.

Only verification devices which have an accuracy equal to or greater than those in the HP 85051A (7mm) and HP 85053A (3.5mm) verification kits can be used to verify HP 8510 network analyzer system specifications.

The HP 85051A (7mm) and HP 85053A (3.5mm) verification kits both include fixed attenuators (20 dB and 50 dB for 7mm, 20 dB and 40 dB for 3.5mm) and beadless and stepped two-port airline mismatch standards. Data for the devices includes a device data sheet which lists fully error-corrected data and measurement uncertainty data on all devices in the kit at various specified frequencies. This measurement uncertainty includes both the uncertainty of the HP factory measurement system and the specified uncertainty of the user's system.

The device data sheet with the HP 85051A 7mm verification kit lists data at 20 frequencies, 19 of them within the specified range of the HP 8512A and HP 8514A test sets. The device data sheet with the HP 85053A 3.5mm verification kit lists data at 18 frequencies. The data cartridge contains formatted trace data on the devices before they were shipped from the factory, as measured on a standards-class HP 8510 network analyzer system. The formatted trace data contains information for 201 frequencies.

To verify system performance using these standards, perform standard 7mm or 3.5mm two-port calibration and measurement procedures, present corrected response of standard device, then read the marker at the specified frequency points and compare your measured data with the standard data supplied with the devices. Refer to the Performance Tests section of the HP 8510 system manual for detailed system performance verification instructions.

~~Copy~~ available to DTIC does not
~~permit~~ fully legible reproduction

APPENDIX D

HP8510 Network Analyzer Time Domain Measurements - Excerpts
from the HP8510 Manual

~~Copy~~ available to DTIC does not
~~permit~~ fully legible reproduction

INTRODUCTION

This part of the HP 8510 network analyzer system manual explains how to make reflection and transmission measurements in the *time domain*. Measurements actually made in the frequency domain are transformed mathematically into the time domain using the internal high-speed computer in the HP 8510, and this requires that the system be equipped with Time Domain Option 010, either at the time of original shipment or by means of the HP 85012A Time Domain Software Package.

The time domain band pass mode is especially useful for measuring band-limited devices and in making fault location measurements. The time domain low pass mode simulates the traditional TDR measurement and makes it possible to determine the type of discontinuity present in a device. Both modes are explained here, as are special time domain features such as masking, windowing, and gating.

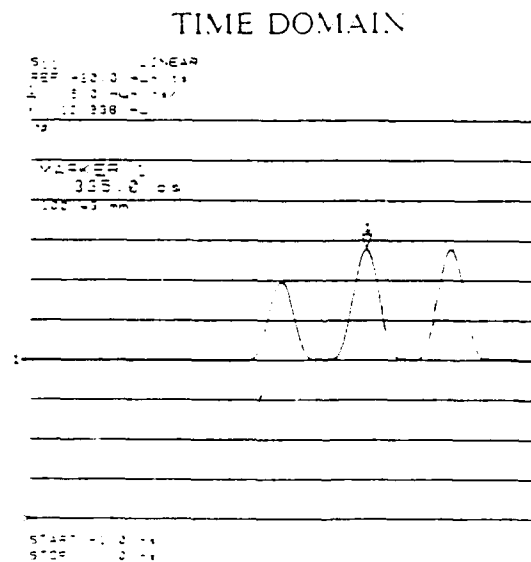
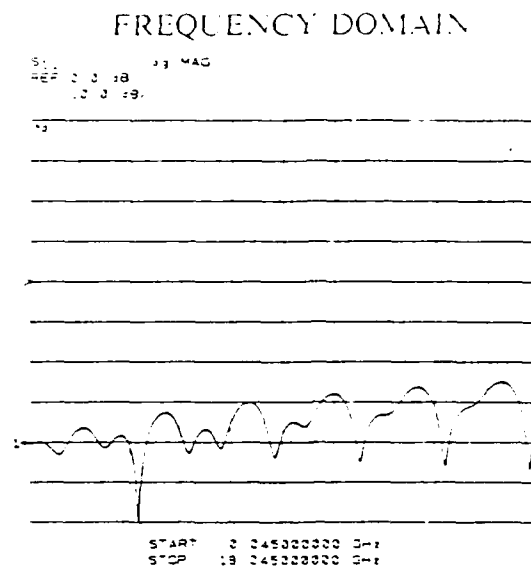


Figure 76. Frequency Domain and Time Domain Measurement

Stop: 19.045000000 GHz
Start: 0.045000000 GHz

250 Time Domain Measurements

GENERAL THEORY

The relationship between the Frequency Domain response and the Time Domain response of a network is described by the Fourier Transform:

FREQUENCY DOMAIN

TIME DOMAIN

$$H(f) \xrightarrow{\text{Fourier Transform}} h(t)$$

It is therefore possible to measure the response of a device under test (DUT) in the Frequency Domain and then mathematically calculate the inverse Fourier Transform of the data to give the Time Domain response. The internal high-speed computer in the HP 8510 does this calculation using Chirp-Z Fast Fourier Transform computation techniques. The resulting measurement is the fully error-corrected Time Domain reflection or transmission response of the device displayed in near real time.

In Figure 76, the Frequency and Time Domain responses of the same device are displayed. The Frequency Domain reflection measurement is a composite response of all of the discontinuities present in the device under test.

The Time Domain measurement shows the effect of each individual discontinuity as a function of time (or distance). The time domain response shows that the device response consists of three separate impedance changes, with the second discontinuity having a reflection coefficient magnitude of 0.013. This discontinuity is located 167.5 picoseconds from the reference plane relative to the speed of light in a vacuum. (In the time domain trace shown in Figure 76, the display and the marker show the round-trip time to the reflection and back: 335 ps.)

TIME DOMAIN MODES

The HP 8510 network analyzer system has two different modes of operation for Time Domain measurements, Band Pass and Low Pass.

The Band Pass mode, the most general purpose mode of operation, gives the impulse response of the device. Band Pass will work with any device and over any frequency range and is the least complicated mode to use.

The Low Pass mode is used to simulate the traditional Time Domain Reflectometer (TDR) measurement. The response gives the user information to determine the type of discontinuity present (R, L, or C). The Low Pass mode will also provide either the impulse or step response of the device.

TIME DOMAIN BAND PASS

The Band Pass mode is so named because it will work with band-limited devices. This is a distinct advantage over traditional TDR, which requires that the DUT be able to operate down to dc. With Band Pass there are no restrictions on the frequency range of the measurement.

Reflection Measurements Using Band Pass

Before making Time Domain reflection measurements, it is necessary to perform the appropriate measurement calibration.

- Press **PRESET**.
- Perform an **S₁₁ 1-PORT** calibration.
Leave the sliding load connected and observe the Frequency Domain response as the sliding element is moved.
- Press **DOMAIN, TIME BAND PASS**.
- Press **AUTO** to display the trace and observe the Time Domain response as the sliding element is moved.

The typical Frequency Domain and Time Domain responses of a sliding load are shown in Figure 77.

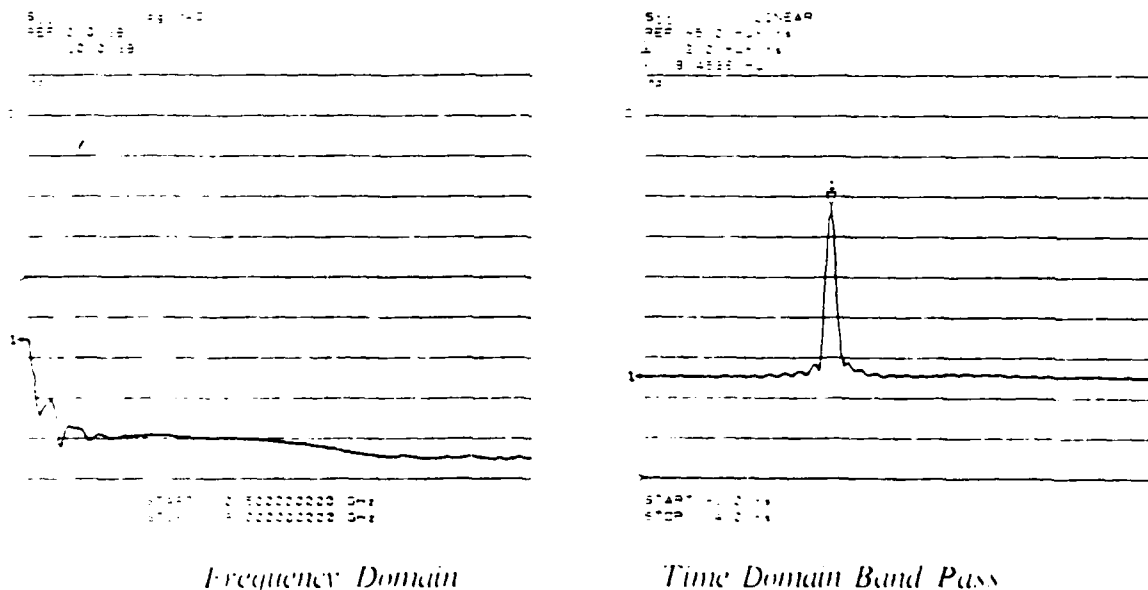


Figure 77. Measurement of a Sliding Load

Move the sliding element and observe the response in both the Frequency Domain and the Band Pass Time Domain. The Frequency Domain measurement of the sliding load should change very little when the slide is moved (unless the calibration is bad). However, the Time Domain measurement shows the individual response of the load element, and it moves along the horizontal axis as the slide is moved.

Interpreting the Band Pass Response Horizontal Axis. In Band Pass reflection measurements, the horizontal axis represents the amount of time that it takes for an impulse, launched at the test port, to reach the discontinuity and return. Thus, this is the two-way travel time to the discontinuity, which in Figure 77 is the load element of the sliding load.

The Marker reads out both the time (x2) and the electrical length (x2) to the discontinuity. The electrical length is obtained by multiplying the time by the velocity of light in a vacuum (2.997925E8 m/sec). To get the physical length, multiply the electrical length by the relative velocity of light in the transmission medium.

In the Time Domain, the **STIMULUS** keys (**START**, **STOP**, **CENTER**, and **SPAN**) refer to time, and they can be used to change the horizontal (time) axis of the display independent of the frequency range chosen. This can be done using the knob, step keys, or the keypad. The keypad terminators also refer to time in seconds (with the lowercase prefixes).

Interpreting the Band Pass Response Vertical Axis. The quantity displayed on the vertical axis depends on the format selected. Band Pass is **PRESET** to the Linear Magnitude format which displays the response in reflection coefficient (ρ) units. This can be thought of as an average reflection coefficient of the discontinuity over the frequency range of the measurement.

Other useful formats are listed in Table 13. The Band Pass response gives the magnitude of the reflection only and has no impedance information (R, L, or C). This information is available, however, in the Low Pass response.

Table 13. Useful Time Domain Band Pass Formats

FORMAT	PARAMETER
LINEAR MAG LOG MAG SWR	REFLECTION COEFFICIENT UNITS RETURN LOSS (dB) SWR UNITS

Fault Location Measurements Using Band Pass

The Band Pass mode is very useful in making fault location measurements. Figure 78 shows the Band Pass Time Domain measurement of a length of coaxial cable having multiple discontinuities and terminated in 50 ohms. Note the responses of each discontinuity and of the terminating element.

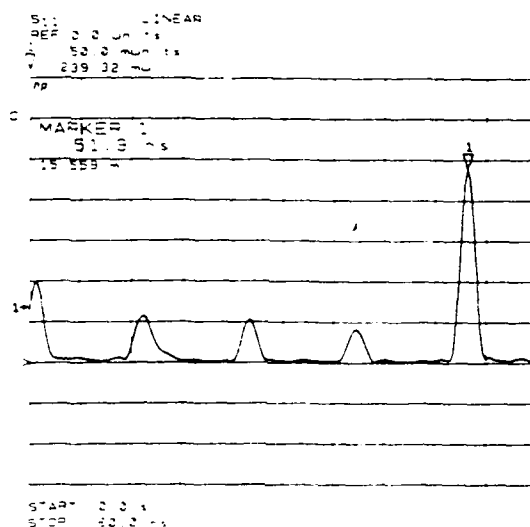


Figure 78. Cable Fault Location Measurement Using Band Pass

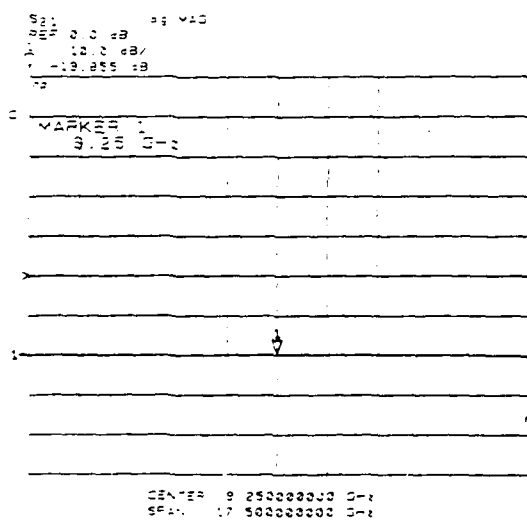
Also, because the Band Pass mode will work over any frequency range, it can be used to do fault location in band-limited transmission media, such as waveguide.

Transmission Measurements in Band Pass

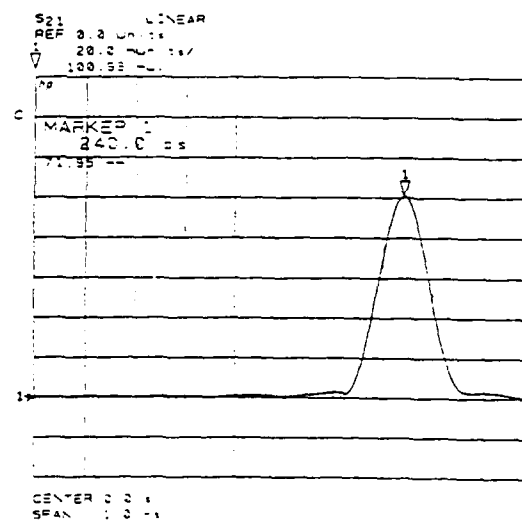
The Band Pass mode is also useful in making transmission measurements. Before making Time Domain transmission measurements, it is necessary to perform the appropriate measurement calibration.

- Press **PRESET**.
- Perform an **S₂₁ RESPONSE, FULL 2-PORT**, or **ONE PATH 2-PORT** calibration.
- Connect a 20 dB coaxial attenuator and observe the Frequency Domain response.
- Press **DOMAIN, TIME BAND PASS**.
- Press **AUTO** to display the trace.

The Frequency Domain and Time Domain responses of a 20 dB attenuator are shown in Figure 79.



Frequency Domain Response



Time Domain Response

Figure 79 Transmission Measurement in Time Domain Band Pass

Interpreting the Band Pass Transmission Response Horizontal Axis. In Time Domain transmission measurements, the horizontal axis is displayed in units of time. The response of the thru connection used in the calibration is an impulse at $t = 0$ and with unit height, indicating that the impulse made it through in zero time and with no loss. When a device is inserted, the time axis indicates the propagation delay or electrical length of the device. Note that in Time Domain transmission measurements, the value displayed is the actual electrical length (not $\times 2$). The Marker reads out the electrical length in both time and distance. You must multiply the distance number by the relative velocity of the transmission medium to get the actual physical length.

Interpreting the Band Pass Transmission Response Vertical Axis. The vertical axis displays the transmission response in transmission coefficient units (τ) in the Linear Magnitude format and the transmission loss or gain in dB in the Log Magnitude format. This can be thought of as an average of the transmission response over the frequency range of the measurement. For the 20 dB attenuator example, the Band Pass response has a magnitude of 0.10 transmission coefficient units (-20 dB insertion loss).

TIME DOMAIN LOW PASS

The Low Pass mode of Time Domain is used to simulate the traditional TDR measurement. This mode gives the user information to determine the type of discontinuity (R, L, or C) that is present. Low Pass provides the best resolution (fastest rise time), and it may be used to give either the Step or Impulse response of a device.

The Low Pass mode is less general purpose than Band Pass in that it places strict limitations on the frequency range of the measurement. It requires that the frequency Domain data points be harmonically related from dc to STOP frequency ($STOP = N \times START$, where $N = \text{NUMBER of POINTS}$). The dc frequency response is extrapolated from the low frequency data. The requirement to pass dc is the same limitation that exists for traditional TDR measurements.

Setting Frequency Range for Time Domain Low Pass

Before making measurements in the Low Pass mode, the frequency range of the measurement must be set so that $STOP = n \times START$, where n is the number of points. This can be done directly by the user, or else it will be done automatically when the SET FREQ. (LOW PASS) softkey is pressed. This key is included in the CAL Menu and also after the TIME LOW PASS softkey. Because the HP 8510 will not convert to the Low Pass mode until the SET FREQ. (LOW PASS) key is pressed at least once, it is very important that this be done before calibrating. Otherwise, going to Low Pass will change the measurement frequencies which will turn off error correction.

Pressing SET FREQ. (LOW PASS) will set the STOP frequency as close as possible to the value entered by the user, and it will set the START frequency equal to $STOP / N$. As an example, if the user selects 101 points, with $START = 100$ MHz, and $STOP = 505$ GHz, then pressing SET FREQ. (LOW PASS) will change START to 50.0 MHz ($= STOP / 101$).

Because the lowest measurement frequency for the HP 8510 is 45 MHz, for each value of N there is a minimum allowable STOP frequency that can be used, and this is given by $N \times 45$ MHz. Table 14 describes the minimum frequency range that can be used for each value of N when making Low Pass Time Domain measurements.

**Copy available to DTIC does not
permit fully legible reproduction**

Table 14. Minimum Frequency Ranges For Time Domain Low Pass

NUMBER of POINTS (N)	MINIMUM FREQUENCY RANGE
51	45 MHz to 2.295 GHz
101	45 MHz to 4.545 GHz
201	45 MHz to 9.045 GHz
401	45 MHz to 18.045 GHz
NOTE: If the source cannot operate over the required frequency range, the HP 8510 will nevertheless attempt the operation.	

If the STOP frequency entered is lower than the minimum that is available for the value of N selected, then pressing the SET FREQ. (LOW PASS) softkey will change the STOP frequency to that minimum value. For example, if Number of Points = 201, START = 100 MHz, and STOP = 6.00 GHz, then pressing SET FREQ. (LOW PASS) will change START to 45 MHz and STOP to 9.045 GHz (= START \times 201). Because of these restrictions on the frequency range of the measurement, the Low Pass mode is most useful for measuring lowpass broad band devices.

Analyzing Low Pass Reflections

As mentioned, the Low Pass mode gives the TDR response of the device under test. This response contains information that is useful in determining the type of discontinuity present. Before making actual measurements in the Low Pass mode, it is helpful to review the Low Pass responses of known discontinuities. Each circuit element of Figure 80 was simulated to show the corresponding Low Pass Time Domain S_{11} response waveform. The Low Pass mode will give the response of the device to either a Step or an Impulse stimulus. (Mathematically, the Low Pass Impulse stimulus is the derivative of the Step stimulus.)

These Time Domain responses were generated using the Circuit Modeling Program which is supplied with the Time Domain option (described at the end of the Time Domain section).

LOW PASS REFLECTIONS (REAL FORMAT)

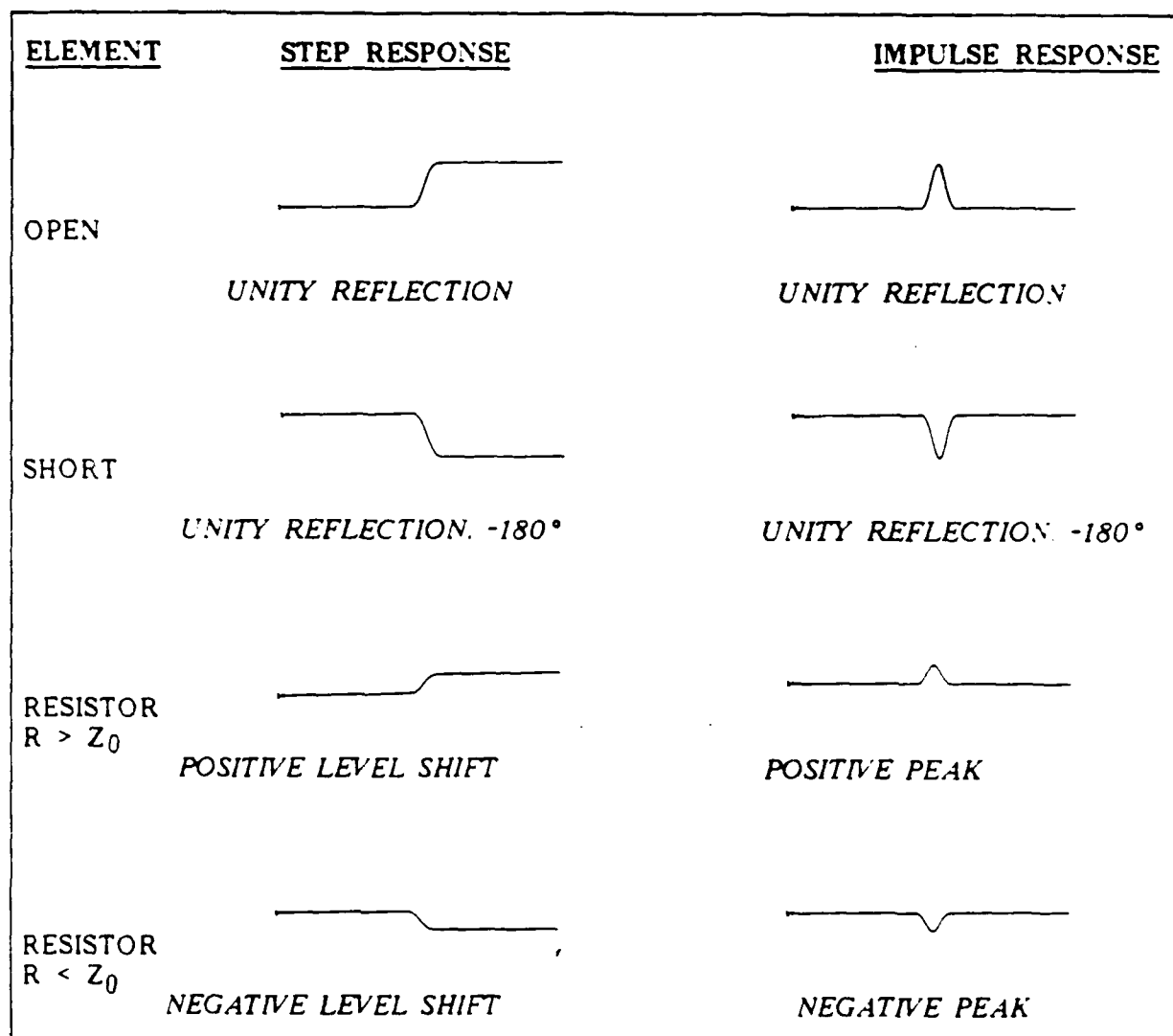


Figure 80. Low Pass Step and Impulse Response Waveforms (1 of 2)

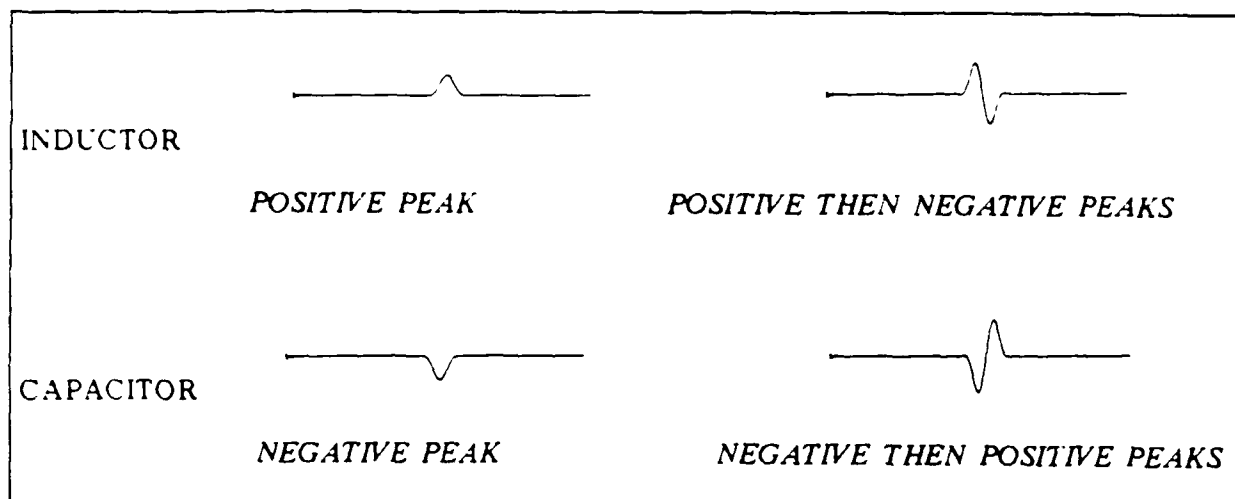


Figure 80. Low Pass Step and Impulse Response Waveforms (2 of 2)

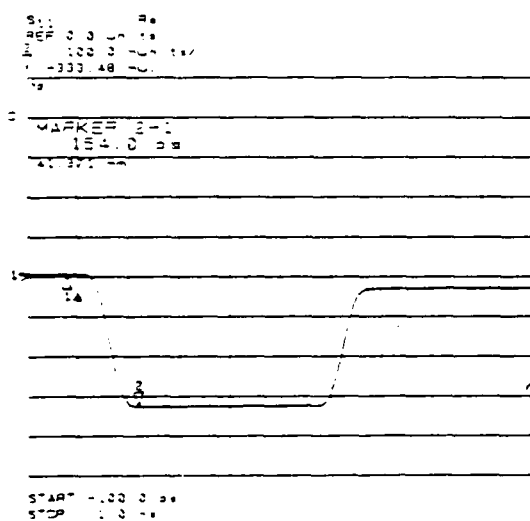
Reflection Measurements in Time Domain Low Pass

To make measurements in the Low Pass mode, use the following procedure:

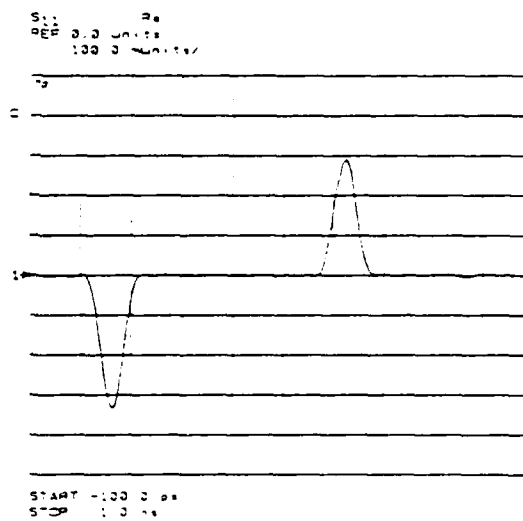
- Press **PRESET**.
- **CAL**, **CAL 1** (7 mm) or **CAL 2** (3.5 mm).

The Cal Type menu (Figure 51, p. 183) will be displayed.

- Press **SET FREQ. (LOW PASS)**.
- Perform an S_{11} 1-PORT calibration.
- Connect a 25 Ω airline and broadband load.
- Press **DOMAIN, TIME LOW PASS, SET FREQ. (LOW PASS)**.
- Press **AUTO** to view the STEP response, Figure 81.
- To view the Low Pass Impulse response of the device, press **DOMAIN, SPECIFY TIME, IMPULSE (LOW PASS)**.



STEP Response



IMPULSE Response

Figure 81 Low Pass Step Response of a 25 Ω Airline and Fixed Load

Interpreting the Low Pass Response Horizontal Axis. The horizontal axis for the Low Pass measurement is the 2-way travel time to the discontinuity, the same as for the Band Pass mode. Also, the Marker function displays both the time ($\times 2$) and electrical length ($\times 2$), obtained by multiplying the time by the velocity of light in a vacuum ($2.997925E8$ m/sec). To get the actual physical length, multiply by the relative velocity of light in the propagation medium.

Interpreting the Low Pass Response Vertical Axis. The vertical axis depends upon the format chosen. In the Low Pass mode, the most useful format is REAL, which displays the TDR response in reflection coefficient units.

This points out a key difference between the Band Pass and Low Pass modes. The Band Pass measurement is actually the response of the device to an RF pulse with an impulse shaped envelope. For Band Pass, the Inverse Fourier Transform of the (complex) Frequency Domain data gives a complex (real and imaginary parts) Time Domain response, and it is the magnitude of this response that is displayed.

In the Low Pass mode, because the Frequency Domain data is taken at harmonically related frequencies down to dc, the Inverse Fourier Transform has only a real part (the imaginary part is zero). Therefore, the most useful format for the Low Pass mode is the REAL format, which displays the response in reflection coefficient units. Other useful formats are listed in Table 15.

Table 15. Useful Time Domain Low Pass Formats

FORMAT	PARAMETER
REAL LOG MAG SWR	REFLECTION COEFFICIENT UNITS RETURN LOSS (dB) SWR UNITS

Trace Bounce. Depending on the magnitude of the response and on the test set used, the Low Pass Step response of the device may exhibit a phenomenon called display trace bounce. This is normal, and it can be improved by turning on AVERAGING (under the Response MENU). This trace bounce is caused by a loss of measurement dynamic range at low frequencies because of the roll off of the coupler-based test sets (HP 8512A and HP 8514A) below 500 MHz (down -30 dB at 45 MHz). The trace bounce is a factor of 30 times less in the bridge-based test sets (HP 8513A and HP 8515A), which have flat magnitude frequency responses down to 45 MHz.

As a second example of Low Pass reflection measurements, consider the Low Pass Step response of a 30 cm airline and fixed load, shown in Figure 82.

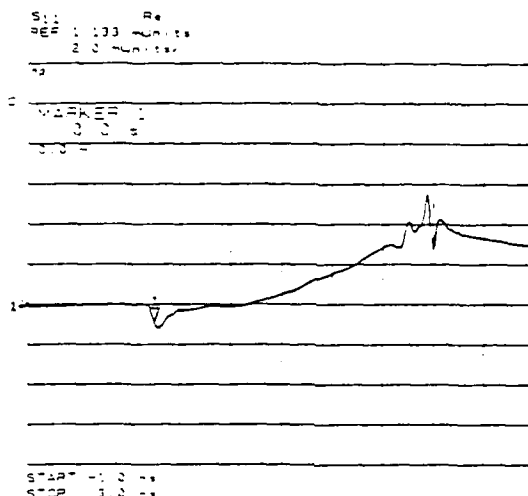


Figure 82. Step Response of a 30 cm Airline and Fixed Load

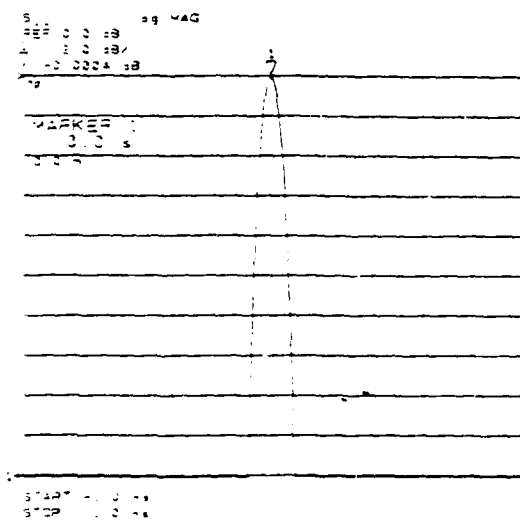
The Low Pass response at $t = 0$ is that of the airline connection. By comparing this response with the theoretical Low Pass responses, one can determine whether the mismatch present is capacitive or inductive. The discontinuity at the first connection of the airline is capacitive. The upward slope of the center section of the response is caused by the loss in the airline. The second major response is that of the fixed load.

TIME DOMAIN CONCEPTS

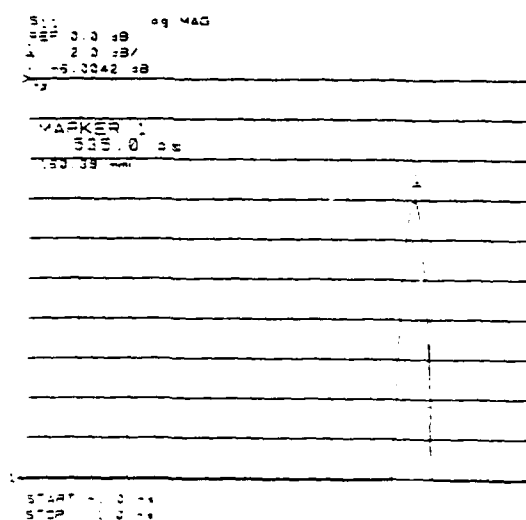
MASKING

Masking is a physical phenomenon in which the Impulse or Step response of one discontinuity affects the response of each subsequent discontinuity in the circuit. This occurs because the energy reflected from or absorbed in the first discontinuity never reaches the second. In the 25 Ω airline example (Figure 81), the Low Pass step response shows the reflection coefficient at the first discontinuity of -0.33, which is correct for an impedance of 25 Ω . However, at the end of the 25 Ω section the response does not return to zero reflection coefficient, which it should at a 50 Ω impedance. The reason is that the step incident on the second response is of less than unity amplitude because of the energy reflected in the first mismatch.

As a second example of masking, consider the Time Domain response of a 3 dB attenuator and a short circuit. The Impulse response of the short circuit alone, Figure 83, shows a return loss of 0 dB. However, the response of the short circuit placed at the end of the 3 dB attenuator displays a return loss of -6 dB. This value actually represents the forward and return path loss through the attenuator, and it illustrates how a lossy network can affect the responses that follow it.



Short Circuit



Short at End of 3dB Pad

Figure 83 Masking Example: 3 dB Pad and Short Circuit

WINDOWING



The HP 8510 has a feature called WINDOWING that is designed to enhance Time Domain measurements. The need for Windowing is due to the abrupt transitions in the Frequency Domain measurement at the START and STOP frequencies. This band limiting of the Frequency Domain response causes overshoot and ringing in the Time Domain response. It causes the (un-Windowed) Impulse stimulus to have a $\sin(kt)/kt$ shape ($k = \pi/\text{frequency span}$), which has two effects that limit the usefulness of the Time Domain measurement:

- (1) Finite Impulse Width. This limits the ability to resolve between two closely spaced responses. The effects of the finite impulse width cannot be improved without increasing the frequency span of the measurement. See Table 16.
- (2) Sidelobes. The Impulse sidelobes limit the dynamic range of the Time Domain measurement by hiding low level responses within the sidelobes of the higher level responses. The effects of sidelobes can be improved by Windowing. See Table 17.

Windowing improves the dynamic range of the Time Domain measurement by modifying (filtering) the Frequency Domain data prior to conversion to the Time Domain to produce an impulse stimulus with lower sidelobes. This greatly enhances the effectiveness in viewing Time Domain responses that are very different in magnitude. The sidelobe reduction is achieved, however, as the tradeoff with increased impulse width. The effect of Windowing on the STEP stimulus (integral of the impulse stimulus, Low Pass mode only) is a reduction of overshoot and ringing at the tradeoff with increased rise time.

Three Windows are available: MINIMUM, NORMAL, and MAXIMUM. The Window may be selected by pressing DOMAIN, SPECIFY TIME. The sidelobe levels of the Time Domain stimulus depend only on the Window that is selected (see Table 17). MINIMUM is essentially no window and therefore gives the highest sidelobes; NORMAL (selected by PRESET) gives reduced sidelobes and is normally the most useful; MAXIMUM gives the minimum sidelobes and thus provides the greatest dynamic range.

Table 16. Time Domain Window Characteristics

			
<i>Impulse Sidelobe Level</i>	WINDOW TYPE	IMPULSE SIDELOBE LEVEL	STEP SIDELOBE LEVEL
	MINIMUM	-13 dB	-21 dB
	NORMAL	-44 dB	-60 dB
<i>Step Sidelobe Level</i>	MAXIMUM	< -90 dB	< -90 dB

The sidelobe reduction due to Windowing is achieved at a tradeoff with an increase in the Step (10% - 90%) Rise Time and the Impulse (50%) width. These parameters also depend upon the frequency span of the measurement, and they can be calculated using the approximate formulas given in Table 17.

Table 17. Approximate Formulas For Step Rise Time and Impulse Width

<u>LOW PASS</u>			
STEP RISE TIME (10% - 90%)	$= \frac{0.45}{\text{FREQ SPAN}}$	x	{ 1.0 MINIMUM WINDOW { 2.2 NORMAL WINDOW { 3.3 MAXIMUM WINDOW
IMPULSE WIDTH (50%)	$= \frac{0.60}{\text{FREQ SPAN}}$	x	{ 1.0 MINIMUM WINDOW { 1.6 NORMAL WINDOW { 2.4 MAXIMUM WINDOW
<u>BAND PASS</u>			
IMPULSE WIDTH (50%)	$= \frac{1.20}{\text{FREQ SPAN}}$	x	{ 1.0 MINIMUM WINDOW { 1.6 NORMAL WINDOW { 2.4 MAXIMUM WINDOW

Multiply by the velocity of light in a vacuum (2.997925E8 m/sec) to get electrical length, and then by the relative velocity of light in the the propagation medium to get physical length.

The purpose of windowing is to make the Time Domain response more useful in isolating and identifying individual responses. The window does not affect the displayed Frequency Domain response. It is turned on only when the Time Domain response is viewed. Figure 84 shows typical effects of windowing on the Time Domain response of the reflection measurement of a short circuit.

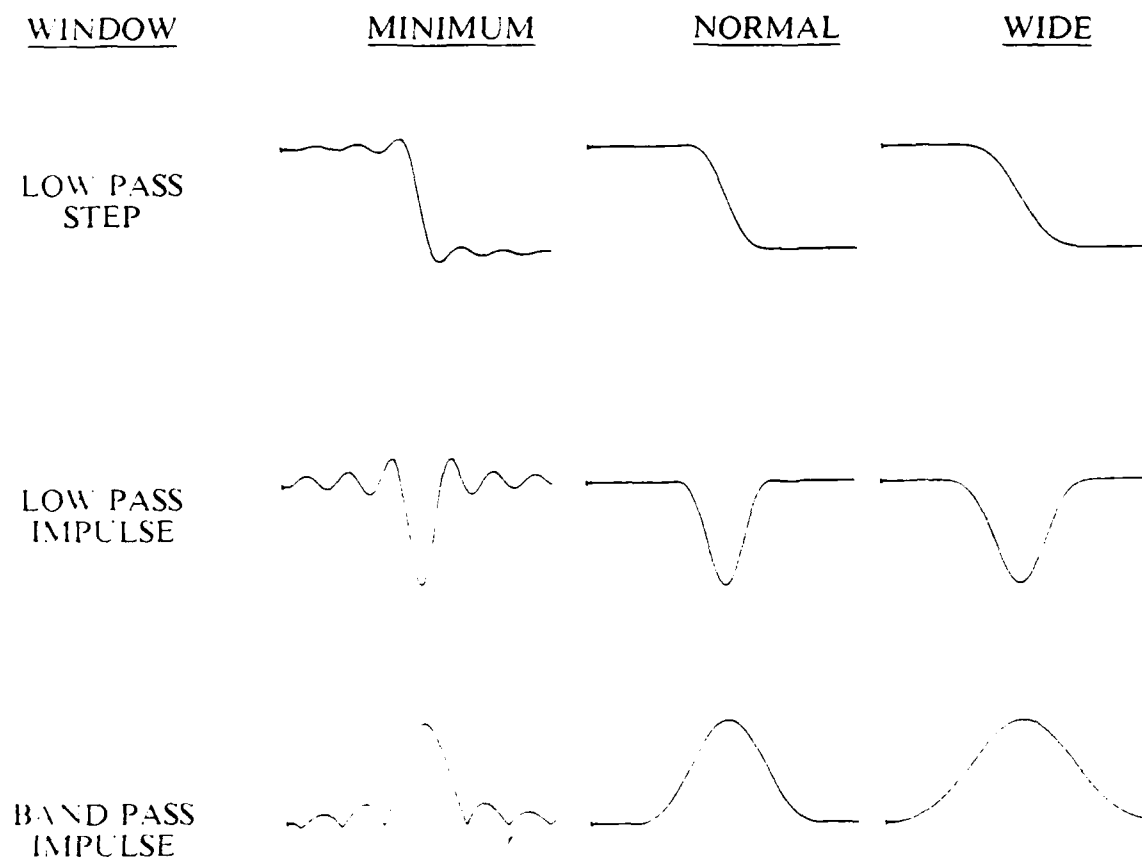


Figure 84. Effect of Windowing on Time Domain Responses of a Short Circuit

RANGE

In the Time Domain, the RANGE is defined as the length in time that a measurement can be made without encountering a repetition of the response (see Figure 85). The repetition of the Time Domain response occurs at regular intervals of time and is a consequence of the Frequency Domain data being taken at discrete frequency points rather than being continuous.

The Range of a measurement is equal to $1/\Delta F$, the spacing between frequency data points. It is therefore directly proportional to the number of points and inversely proportional to the Frequency Span (STOP - START frequency) and can be calculated using the following formula.

$$\text{RANGE} = 1/\Delta F = (\text{Number of Points} - 1)/\text{Frequency Span}$$

As a sample calculation, for a 201 point measurement from 50 MHz to 18 GHz (SPAN = 17.95 GHz), the Range is $(201 - 1) / 17.95 \text{ GHz} = 11.1 \text{ nsec}$ (3.34 m). Thus the device under test has to be 3.34 m or less in electrical length for a transmission measurement (1.67 m for a reflection measurement) or else an overlapping of the Time Domain responses (aliasing) will occur. (Remember to multiply by the relative velocity of light in the medium to get actual physical length.)

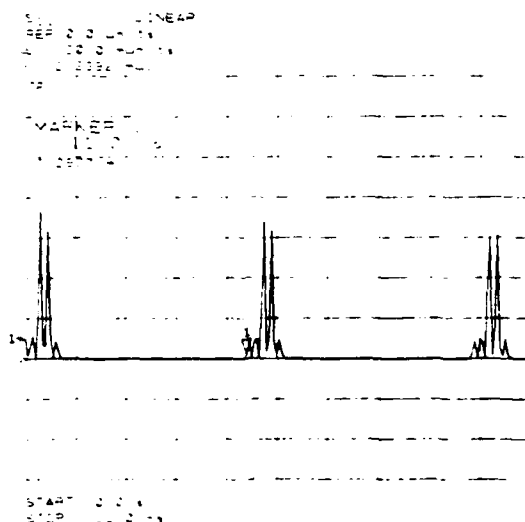


Figure 85. Time Domain Measurement Showing Response Repetitions

To increase the Time Domain measurement Range, it is usually better to first increase the number of points, because decreasing the frequency span will reduce the resolution.

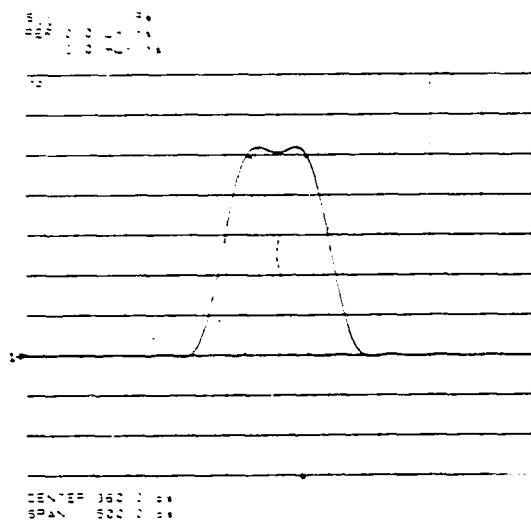
RESOLUTION

There are two different terms involving resolution in Time Domain: RESPONSE-RESOLUTION and RANGE-RESOLUTION. The Time Domain Response-Resolution is defined as the ability to resolve two closely spaced responses. In other words, if two responses are present, this is how closely they can be spaced and still be distinguished from one another. For responses of equal amplitude, the Response-Resolution is equal to the 50% (-6 dB) impulse width. It therefore is inversely proportional to the frequency span of the measurement and is also a function of the window that is used. Approximate formulas for calculating the 50% Impulse width are given in Table 17. For responses that are of different amplitudes, the Response-Resolution will be wider.

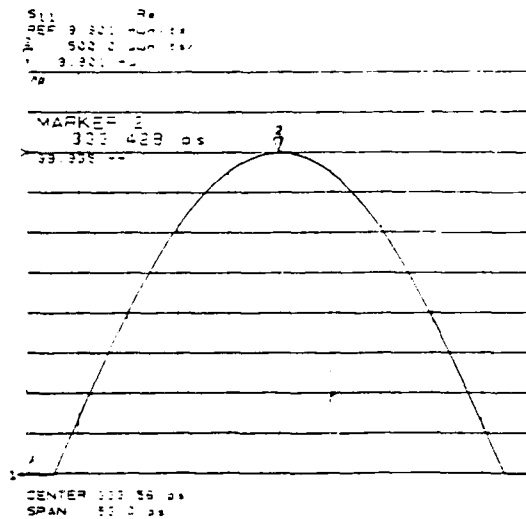
Range-Resolution is defined as the ability to locate a single response in time. In other words, if only one response is there, this is how closely you can pinpoint the peak of that response. The Range-Resolution is equal to the digital resolution of the CRT display which is the time span displayed divided by the number of points. Maximum Range-Resolution is achieved by centering the response on the display and then reducing the time span. Therefore, the Range-Resolution is always much finer than the Response-Resolution.

To illustrate the difference between these two resolution terms, consider a measurement with a frequency span of 18 GHz. For Low Pass, with a Normal Window, the Response-Resolution (Impulse width) is 53 psec ($0.6 \times (1/18 \text{ GHz}) \times 1.6$) or 16 mm in electrical length (53 psec \times 2.997925E8 m/sec). As illustrated in Figure 86, two Time Domain responses of equal amplitude separated by 16 mm could be resolved in this Time Domain measurement. (This indicates an actual discontinuity separation of 8 mm for reflection measurements.)

Now consider the case where only one response is present. By centering that response on the display and adjusting the time SPAN to equal the 50% Impulse width (53 psec, 16 mm), Figure 86, the Range-Resolution is reduced to 40 μ m (16 mm/401 points). The Range-Resolution can be further reduced by narrowing the time span.



Response-Resolution



Range-Resolution

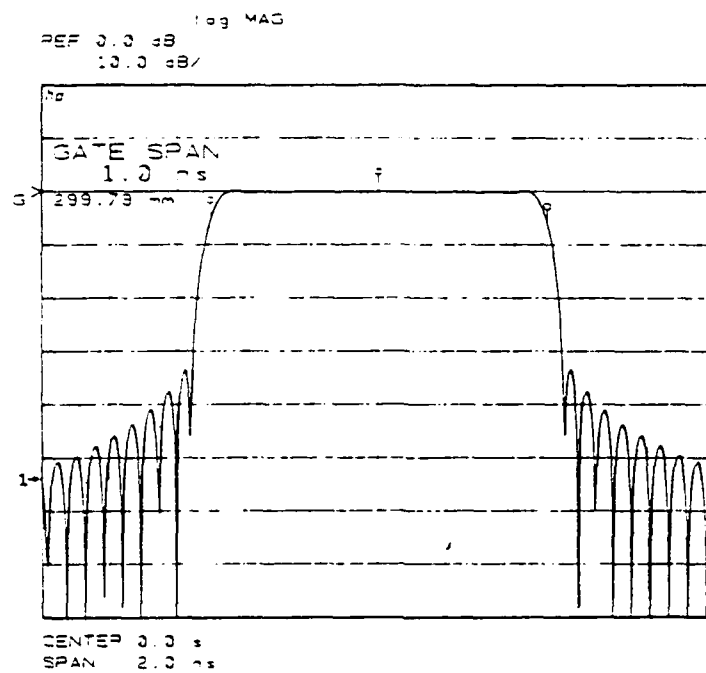
Figure 86. Resolution in Time Domain

GATING

The HP 8510 gating feature gives the user the flexibility to selectively remove reflection or transmission Time Domain responses. In converting back to the Frequency Domain, the effects of the responses outside the Gate are removed. In a reflection measurement, you can remove the effects of unwanted mismatches or else isolate and view the response of an individual mismatch. In a transmission measurement you can remove the responses of multiple transmission paths.

Setting the Gate. A Gate is a temporal band pass filter used to filter out unwanted Time Domain responses. Responses outside the selected gate are not included in the trace. There are three Gate indicators: START, CENTER, and STOP. The Gate has a bandpass filter shape, as shown in Figure 87. The GATE CENTER indicates the center time (not frequency) of this filter, and the Gate START and STOP indicate the -6 dB cutoff times. Gate SPAN = STOP - START.

Copy available to DTIC does not
permit fully legible reproduction

*Figure 87 Gate Shape*

Consider using gating to analyze the response of a 7mm-to-3.5mm adapter connected to a 3.5mm airline and a fixed load. The Frequency Domain and the Band Pass Time Domain responses of such a setup are shown in Figure 88.

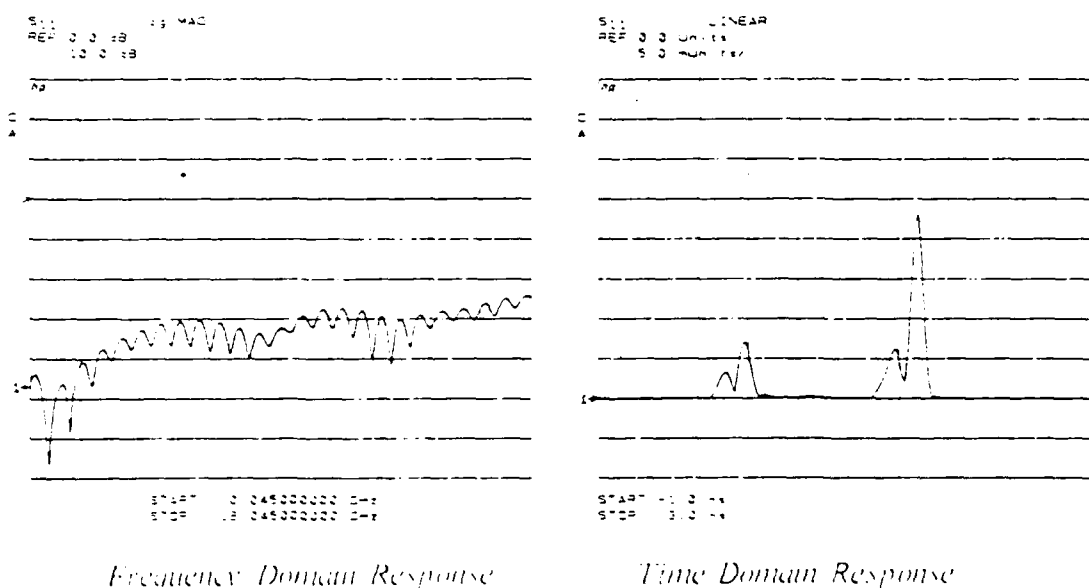


Figure 88 Reflection Measurement of 7mm-to-3.5mm Adapter, Airline, and Load

Copy available to DTIC does not
permit fully legible reproduction

We will now use gating to analyze the response of the adapter only.

- Press DOMAIN, TIME BAND PASS, SPECIFY GATE.
- The three Gate indicators will now appear on the screen. Press GATE CENTER, and use the knob or keypad to move the center indicator to $t = 0$.
In Figure 89, the time domain display shows the gate center, 86 ps, as the Active Function.
- Press GATE SPAN and use the knob or keypad to adjust the Gate Span to 0.70 ns.
- Press GATE ON to turn on the Gate.
The responses outside the Gate will be removed. See Figure 89.
- Press DOMAIN, FREQUENCY.
View the gated Frequency Domain response of the adapter. See Figure 89.

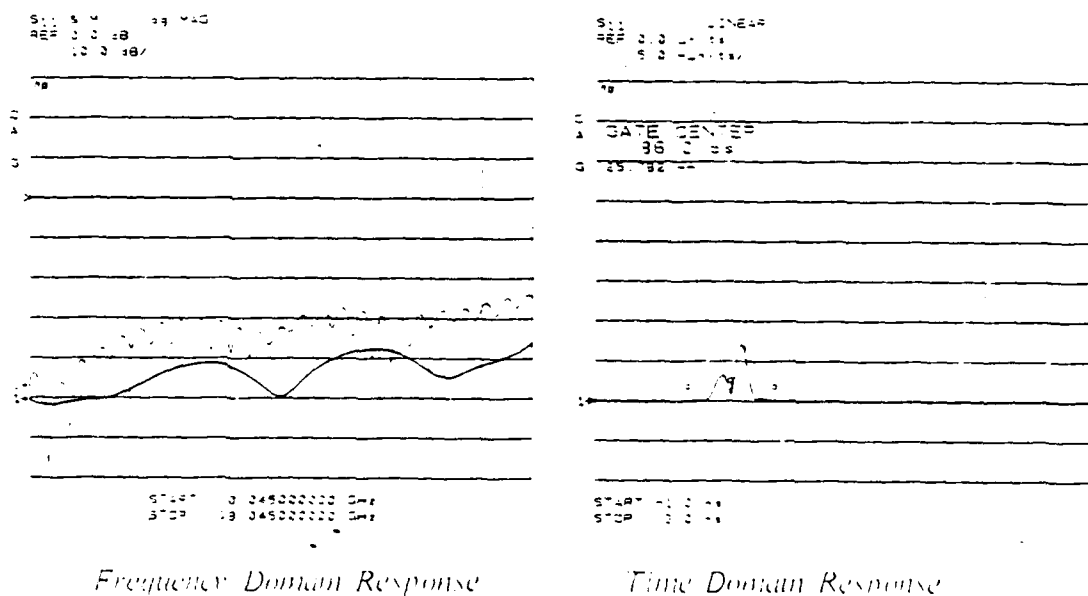


Figure 89. Gated Responses of the 7mm-to-3.5mm Adapter

The darker shaded trace in the Frequency Domain plot of Figure 89 shows the Gated Frequency Domain response, which is that of the adapter only. The effects of the fixed load on the measurement are removed.

Select Gate Shape. Four different Gate shapes are available: MINIMUM, NORMAL, WIDE, and MAXIMUM. Each of the Gates have different passband flatness, cutoff rate, and sidelobe levels. T1 indicates the Gate span which is the time between the Gate start and stop indicators. T2 is the time between the edge of the Gate passband and the -6 dB Gate stop time. T3, equal to T2, is the time between the Gate stop time and the point where the filter first reaches the level of the highest Gate sidelobe. The Gate characteristics for each Gate shape are listed in Table 18.

Table 18 Gate Characteristics

GATE SHAPE	PASSBAND RIPPLE	SIDELOBE LEVELS	CUTOFF TIME T2 = T3	MINIMUM GATE SPAN
MINIMUM	± 0.40 dB	-24 dB	0.6/ FSPAN	1.2/ FSPAN
NORMAL	± 0.04 dB	-45 dB	1.4/ FSPAN	2.8/ FSPAN
WIDE	± 0.02 dB	-52 dB	4.0/ FSPAN	8.0/ FSPAN
MAXIMUM	± 0.01 dB	-80 dB	11.2/ FSPAN	22.4/ FSPAN

The Passband Ripple and Sidelobe Levels are descriptive of the gate (filter) shape. The Cutoff Time, T2 = T3 (see Table 18), indicates how fast the gate filter rolls off. For each gate shape, there is also a Minimum Gate Span ($T1_{min} = 2 \times T2$) which gives a filter passband of zero. To enter a Gate span smaller than minimum will produce a distorted filter shape that will have no passband, will not have a narrower shape, may have higher sidelobe levels, and will give an incorrect indication of gate START and STOP times. Therefore, it is important to always select a Gate span that is higher than the minimum value. The Cutoff time and the Minimum Gate Span are inversely proportional to the frequency span of the measurement as indicated in Table 18.

For best results using Gating, it is important to always center the Gate around the (responses) that you want to retain in the measurement and to make the Gate span wide enough to include all of those responses. It is also recommended to use the widest Gate shape possible.

Copy available to DTIC does not
permit fully legible reproduction

MEASUREMENT RECOMMENDATIONS

When making Time Domain measurements, it is generally a good practice to measure the device within the frequency range that it is designed to operate. There are two reasons for this. First, the noise floor of the Time Domain response is directly related to the noise in the Frequency Domain data. Therefore, if many of the Frequency Domain data points are taken at or below the noise floor of the measurement, then the noise floor of the Time Domain measurement will be increased. A second reason to measure the device within its operating frequency range is because the in band response is normally of interest. The Time Domain measurement is an average of the response over the frequency range of the measurement, and if the Frequency Domain data is measured out of band, then the Time Domain measurement will also be the out of band response. However, since the Time Domain Response-Resolution is inversely proportional to the frequency span, it may at times be desirable (with these limitations in mind) to use a frequency span that is slightly wider than the device bandwidth to give better resolution.

Source Considerations

Although either source will work well in making Time Domain measurements, the HP 8540A synthesized sweeper has the advantage that it provides greater dynamic range than the HP 8350B sweeper. The main reason for this is the frequency stability of a synthesized source. The small nonlinearities and phase discontinuities that occur in the ramp sweep mode cause low level noise sidebands on the Time Domain Impulse or Step stimulus. These interfere in measurements requiring large dynamic range. Perform a TRIM SWEEP adjustment before calibrating to help minimize these noise sidebands. Adjusting trim sweep is explained at the end of the section of this manual titled Measurement Calibration.

In the HP 8540A (synthesized) step sweep mode, the improvement in source stability eliminates these noise sidebands and improves the Time Domain measurement dynamic range by as much as 30 dB. A second improvement is that the HP 8540A stepped sweep mode allows the use of many averages per point without greatly affecting the sweep time, and this lowers the noise floor of the Time Domain measurement. It is recommended to perform a Trim Sweep adjustment prior to calibrating when making measurements in the ramp sweep mode to minimize phase discontinuities.

*Copy available to DTIC does not
permit fully legible reproduction*

Test Set Considerations

The bridge-based test sets (HP 8513A and HP 8515A) have two advantages over the coupler-based test sets (HP 8512A and HP 8514A) when making Time Domain measurements. First, the bridge-based test sets extend in frequency to 26.5 GHz, versus 18 GHz for the coupler-based test sets. When measuring broadband devices, this extra bandwidth provides better Time Domain Response Resolution.

The second advantage is that the bridge-based test sets have a fiat response down to 45 MHz, whereas the coupler-based test sets begin to roll off (but are still usable) below 500 MHz. This coupler roll off reduces the dynamic range available at the low frequencies (-30 dB at 45 MHz) and therefore increases the Time Domain noise floor when measurements are made at those frequencies (this causes the trace bounce in the Low Pass Step response).

*Copy available for use does not
permit fully legible reproduction.*

DISTRIBUTION LIST

ARMY CERL Library, Champaign, IL
ARMY CRREL Library, Hanover, NH
ARMY EWES Library, Vicksburg MS
DTIC Alexandria, VA
GIDEP OIC, Corona, CA
NAVFACENGCOM Code 03, Alexandria, VA
NAVFACENGCOM - CHES DIV, FPO-1PL, Washington, DC
NAVFACENGCOM - LANT DIV, Library, Norfolk, VA
NAVFACENGCOM - NORTH DIV, Code 04AL, Philadelphia, PA
NAVFACENGCOM - PAC DIV, Library, Pearl Harbor, HI
NAVFACENGCOM - SOUTH DIV, Library, Charleston, SC
NAVFACENGCOM - WEST DIV, Code 04A2.2 (Lib), San Bruno, CA
PWC Code 101 (Library), Oakland, CA; Code 123-C, San Diego, CA; Code 420, Great Lakes, IL; Library
(Code 134), Pearl Harbor, HI; Library, Guam, Mariana Islands; Library, Norfolk, VA; Library, Pensacola,
FL; Library, Yokosuka, Japan; Tech Library, Subic Bay, RP